ALEXANDER E. GREEN

PHD

SEROTONIN AND BROWN ADIPOSE TISSUE

THE EFFECTS OF ELEVATED SEROTONIN (5-HT) SIGNALING ON BROWN ADIPOSE TISSUE

By ALEXANDER E. GREEN, B.SC. S.S.P. KINE., M.SC.

A Thesis Submitted to the School of Graduate Studies in Partial Fulfilment of the Requirements for the Degree of Doctor of Philosophy

1 Descriptive Note

INSTITUTION: McMaster University

LOCATION: Hamilton, Ontario (Medical Science)

DEGREE: Doctor of Philosophy (2020)

PROGRAM: Medical Sciences

TITLE: The effects of elevated serotonin (5-HT) signaling on brown adipose tissue

AUTHOR: Alexander E. Green, BSc (Queen's University), MSc (York University)

SUPERVISOR: Professor Gregory R. Steinberg

SUPERVISORY COMMITTEE: Professor Sandeep Raha and Katherine M. Morrison

NUMBER OF PAGES: 297

2 Lay Abstract

Obesity is a growing global pandemic caused by excessive energy intake over energy expenditure (EE). Some medications, such as certain selective serotonin (5-HT) reuptake inhibitor (SSRI) type antidepressants, also contribute to weight gain via reasons which are not fully understood. Currently available weight-loss medications decrease energy intake but do not affect EE. Recently, inhibiting the production of 5-HT outside the brain decreased weight gain in a model of obesity. Furthermore, this was associated with an improvement in the activity of a specialized type of adipose tissue, called brown adipose tissue (BAT). BAT is capable of expending energy in the form of thermogenesis and thus when active increases energy expenditure. We hypothesized that 5-HT impairs BAT activity and that blocking 5-HT activity may reduce weight gain in a model of antidepressant-induced weight gain. Herein, we investigated whether elevating 5-HT or increasing 5-HT downstream signaling modified BAT activity, which 5-HT receptor(s) is/are predominantly expressed in brown adipocytes (BAs), and what the effect on BAT would be if this/these receptors were eliminated. We found that in cell culture "supraphysiological" doses of 5-HT acutely impaired BA lipid mobilization and glucose metabolism; whereas, circulating concentrations of 5-HT impaired expression of select mitochondrial genes when serotonin transport was reduced. In mice, acute injections of high dose 5-HT attenuated BAT activity in response to an adrenergic stimulus. Acute treatment with an SSRI decreased EE and locomotor activity. Mice genetically lacking the serotonin transporter (the target of SSRIs) had

increased weight gain (particularly fat mass), increased food intake and reduced locomotor activity, but improved BAT functional capacity. We subsequently identified that the predominantly expressed and active receptor in BAs was the 5-HT2A receptor. Genetically eliminating the 5-HT2A receptor in BAs prevented 5-HT's reduction of a major mitochondrial gene expression regulator and improved BAT functional capacity in mice. Inhibiting 5-HT2A with a 5-HT2A brain impermeable antagonist, Xylamidine, increased BAT functional capacity in mice. Treating mice with Paroxetine (Paxil®), a SSRI known to increase weight gain, and Xylamidine did not attenuate Paroxetine-induced weight gain nor increase EE but did improve BAT functional capacity. In conclusion, we found that 1) chronic treatment with physiological levels of 5-HT impaired BAT functional capacity, 2) elimination/inhibition of adipocyte 5-HT2A improved BAT functional capacity *in vivo* and 3) inhibiting peripheral 5-HT2A alone did not attenuate Paroxetine-induced weight gain.

3 Abstract

Inhibiting peripheral serotonin (5-HT) synthesis has been shown to prevent the development of diet-induced obesity, glucose intolerance, insulin resistance and hepatic lipid deposition and to increase brown adipose tissue (BAT) thermogenic capacity. This thesis investigated 1) what effects 5-HT has on brown adipocytes (BAs), 2) if 5-HT and/or selective serotonin reuptake inhibitors (SSRIs) impair BAT function, 3) if 5-HT directly inhibits BA via a receptor-mediated mechanism, 4) which 5-HT receptor is predominantly expressed in BAT, 5) if 5-HT receptor antagonism improves BAT function and 6) if 5-HT receptor inhibition reduces SSRI induced weight gain. In murine BAs, 5-HT at concentrations ≥100 μM acutely reduced lipolysis, lipid accumulation and glycolytic flux but did not impair oxygen consumption; whereas 10 nM 5-HT reduced *Ucp1* promoter activity via an extracellular receptor-mediated mechanism. Acute injection of 5-HT or the selective serotonin reuptake inhibitor (SSRI) Paroxetine decreased BAT thermogenic capacity and energy expenditure (EE), respectively. Mice lacking the serotonin transporter gene (*Slc6a4*$^{-/-}$ mice) had increased adiposity, decreased locomotor activity and increased food intake. However, male *Slc6a4*$^{-/-}$ mice had increased BAT thermogenic capacity, in contrast to the reduced EE expenditure following acute administration of Paroxetine. Using, RNA-Seq analysis and measurements of canonical 5-HT receptor second messengers (i.e. Ca^{2+} and cAMP transients), 5-HT2A was identified as the highest expressed 5-HT receptor in murine and human BAs and the only detected active 5-HT receptor in murine BAs.

Genetic elimination of 5-HT2A prevented 5-HT induced increases in Ca^{2+} transient peaks and decreases in *Ppargc1a* mRNA expression in cultured BAs. *In vivo* ablation of 5-HT2A in adipose tissue increased BAT thermogenic capacity. Furthermore, *in silico* analyses predicted that pharmacological inhibition of 5-HT2A would induce a thermogenic program. *In vitro*, 5-HT2A receptor antagonists eliminated 5-HT induced Ca^{2+} transients and *in vivo*, a single injection of a peripherally-restricted 5-HT2A antagonist (Xylamidine) prevented 5-HT-induced impairments in BAT-mediated EE. Chronic administration of Xylamidine to chow-fed mice for 5-weeks improved BAT thermogenesis. Co-administration of Xylamidine with Paroxetine, however, did not attenuate Paroxetine-induced weight gain but did improve BAT functional capacity Therefore, 5-HT2A antagonism improves BAT thermogenic capacity but does not increase EE. This represents a novel therapeutic approach for increasing thermogenic capacity that may be used in conjunction with BAT activating strategies to increase EE and attenuate obesity.

4 Acknowledgements

The pursuit of knowledge and truth is a long arduous journey. It is filled with hurdles and hindrances. Similarly, to complete this dissertation and further my career, there was a wide variety of obstacles. The study of biology and medicine is a humbling pursuit. We are at the mercy of the engineering of evolution and must always be cognisant that there are innumerable solutions that evolution created throughout history. When we believe that we have learnt everything is the moment that we lose sight of the unknown and begin pursuing false leads from false premises, no matter how sound the logic. Nothing in my life has been more humbling and frustrating than pursuing the research topics in my doctorate. I have no doubt that, without the support of those around me, I would not have made it this far.

I would first like to thank those who believe in education and put the pursuit of student's goals and education, first and foremost. Furthermore, thank you to those that believe in the essential nature of and the practice of transparency, humility, dissemination and ethical behaviour in education and science. Thank you to those who practice integrity always and without question, even in the face of their errors. There are too few of you.

Specifically, thank you to the individuals, teams and organizations that supported me through this. Thank you to my supervisory committee, the staff and students at McMaster University. Thank you to the animal care facility technicians and administrators that support all of our research. You are not thanked enough, and your dedications allows us to pursue ever larger goals. Thank you to those scientists (undergraduates to faculty members) who have supported and contributed to all of this. Thank you especially to my laboratory colleagues with whom I have had the privilege to work. There are too many to thank by name and I owe you all a tremendous debt. Thank you to CIHR and MitoCanada for funding my scholarship. Thank you to my current workplace and those thereof that have rekindled my belief in education and science. Thank you to the McMaster University Cross-Country and Track and Field teams, you gave me much more than I was able to give you. Most importantly, thank you to my friends and family, those both with us now and those that have passed. You have given more to me than anyone should ever ask for and I owe you more than I can ever repay. Thank you again to everyone who contributed to and supported me through this. Your ears, time and effort have not been forgotten and will always be appreciated.

To those who follow, do ask for help. Do not toil in agony; do not toil alone; do not let others convince you that your concerns are false; do not let others discourage you; and most importantly do not give up. Have faith in yourself; be humble; and choose the course best for you. Follow the evidence – if it is valid, it will not deceive you. Always check the validity of evidence. Do question the premises of your experiments; do follow through; do hold others accountable; and

do believe in the outcome. Always be transparent; disseminate knowledge; be honest; and, finally, support others – they need you as you have needed others.

Science is a tedious pursuit, do not pursue it alone, learn from the mistakes of others and help others learn from yours. We all can be wrong, and we are all in this together. Thank you all.

5 Table of Contents

6 List of Illustrations, Charts, and Diagrams

7 List of Tables

8 List of Abbreviations and Symbols

3-HK	- 3-Hydroxykynurenine
5-HIAA	- 5-Hydoxyindoleacetic acid
5-HT	- 5-Hydroxytryptamine/Serotonin
5-HTP	- 5-Hydroxytryptophan
5-MIAA	- 5-Methoxyindoleacetic acid
8-Br-cAMP	- 8-Bromo-Cyclic Adenosine Monophosphate
α-MSH	- α-melanocyte-stimulating hormone
AADC	- Aromatic L-Amino Acid Decarboxylase/DOPA decarboxylase
ADMET	- Absorption, Distribution, Metabolism, Excretion and Toxicity
ADP	- Adenosine diphosphate
AFMID	- Arylformamidase
AgRP	- Agouti-related peptide
AhR	- Arylhydrocarbon Receptor
ANCOVA	- Analysis of Covariance
ANOVA	- Analysis of Variance
Ap2	- Adipocyte Protein 2
APP+	- 4-(4-Dimethylamino)phenyl-1-methylpyridinium iodide
ATGL	- Adipose Triglyceride Lipase
ATP	- Adenosine triphosphate
A.U.C.	- Area Under the Curve
BA	- Brown Adipocyte
BAT	- Brown Adipose Tissue
BBB	- Blood Brain Barrier
BCA	- Bicinchoninic Acid Assay
BeAT	- Beige Adipose Tissue
BH_2	- Dihydrobiopterin
BH_4	- Tetrahydrobiopterin
BMI	- Body Mass Index
BSA	- Bovine Serum Albumin
Ca^{2+}	- Calcium
cAMP	- Cyclic Adenosine Monophosphate
CCD	- Charge-coupled device
cDNA	- Complementary DNA
CLAMS	- Comprehensive Laboratory Animal Monitoring System
CNS	- Central nervous system
Cre	- Cre Recombinase Gene
CreERT2	- Tamoxifen Sensitive Estrogen Receptor 2 Ligated Cre Recombinase
Ct	- Cycle Threshold
D-22	- Decynium-22
DAT	- Dopamine transporter

DMEM - Dulbecco's Modified Eagle Medium
DMEM/F12 - Dulbecco's Modified Eagle Medium/Nutrient Mixture F-12
DMSO - Dimethylsulfoxide
DNP - 2,4-Dinitrophenol
DOI - 2,5-Dimethoxy-4-iodoamphetamine
dNTP - Deoxynucleoside Triphosphate
DTT - Dithiothreitol
EC - Enterochromaffin
EC_{50} - Half Maximal Excitatory Concentration
ECAR - Extracellular Acidification Rate
EDTA - Ethylenediaminetetraacetic Acid
EE - Energy Expenditure
FBS - Fetal Bovine Serum
FCCP - Carbonyl cyanide-p-trifluoromethoxyphenylhydrazone
FDA - U.S. Food and Drug Administration
FDG - Fluorodeoxyglucose
FDR - False Discovery Rate
FFA - Free fatty acids
FlpO - FLP Deleter Gene
GDP - Guanosine diphosphate
GEO - Gene Expression Omnibus
GI - Gastrointestinal
G_i - G_i protein alpha subunit
G_s - G_s protein alpha subunit
Gpr35 - G protein-coupled receptor 35
GTT - Glucose Tolerance Test
G_q - G_q protein alpha subunit
gWAT - Gonadal White Adipose Tissue
H_2O_2 - Hydrogen peroxide
HEPES - 4-(2-hydroxyethyl)-1-piperazineethanesulfonic acid
HFD - High Fat Diet
HKRB - HEPES Krebs-Ringer buffer
HIA - Human Intestinal Absorption
HSL - Hormone-Sensitive Lipase
Htr2a AdKO - Adipose Specific and Inducible 5-HT2A Gene Knockout Mice
IBMX - 3-isobutyl-1-methylxanthine
IC_{50} - Half Maximal Inhibitory Concentration
IgE - Immunoglobulin E
Ido1 - Indoleamine 2,3-dioxygenase 1
Ido2 - Indoleamine 2,3 dioxygenase 2
IP - Intraperitoneal
IV - Intravenous
Iso - Isoproterenol
ITT - Insulin Tolerance Test

iWAT - Inguinal White Adipose Tissue
KAT - Kynurenic Acid Transferases
K_m - Michaelis-Menten constant
Kyn - Kynurenine
L-Tryp - L-Tryptophan
LINCS - Library of Integrated Network-based Cellular Signatures
Lmx1b - LIM Homeobox Transcription Factor 1 Beta
LSD - Lysergic acid diethylamide
MOA - Mechanism of Action
MAOA - Monoamine Oxidase A
MAOB - Monoamine Oxidase B
$MgCl_2$ - Magnesium Chloride
MSC - Mesenchymal Stem Cells
N-FKyn - N'-Formylkynurenine
NaCl - Sodium Chloride
NaF - Sodium Fluoride
NAD - Nicotinamide adenine dinucleotide
NAFLD - Non-alcoholic Fatty Liver Disease
NE - Norepinephrine
NEFA - Nonesterified Fatty Acids
NET - Norepinephrine Transporter
NIRS - Near-infrared Spectroscopy
NPY - Neuropeptide Y
OCR - Oxygen Consumption Rate
OCT3 - Organic Cation Transporter 3
ORO - Oil Red O
PAH - Phenylalanine Hydroxylase
Par - Paroxetine
PBS - Phosphate buffered saline
PCPA - *para*-Chlorophenylalanine
PET-CT - Positron Emission Tomography–Computed Tomography
Pet1 - PC12 ETS Domain-Containing Transcription Factor 1
PFK - Phosphofructokinase
P_i - Inorganic Phosphate
PIA - R(-)N6-(2-phenylisopropyl) adenosine
PGC-1α - Peroxisome proliferator-activated receptor gamma coactivator 1-alpha
PKA - Protein Kinase A
PKC - Protein Kinase C
PLN - Perilipin
PMAT - Plasma Membrane Monamine Transporter
POMC - Proopiomelanocortin
PPAR - Peroxisome proliferator-activated receptor
Pparg - Peroxisome proliferator-activated receptor gamma gene

Ppargc1a	- Peroxisome proliferator-activated receptor gamma coactivator 1-alpha gene
PRDM16	- PR domain containing 16
qPCR	- quantitative Polymerase Chain Reaction
RER	- Respiratory Exchange Ratio
Rgs14	- Regulator of G-protein signaling 14
ROS	- Reactive Oxygen Species
RT	- Room Temperature
SERT	- Serotonin Transporter
ScAT	- Subcutaneous Adipose Tissue
scRNA	- Scramble Ribonucleic Acid
SD	- Standard Deviation
SEM	- Standard Error Mean
siRNA	- Small Interfering Ribonucleic Acid
Slc6a4	- Serotonin Transporter Gene
Slc22a3	- Organic Cation Transporter 3 Gene
Slc29a4	- Plasma Membrane Monoamine Transporter Gene
Sln	- Sarcolipin Gene
SNARE	- Soluble NSF Attachment Protein Receptor
SSRI	- Selective Serotonin Reuptake Inhibitor
T3	- Triiodothyronine
TBST	- Tris-Buffered Saline with Tween
Tdo2	- Tryptophan 2,3-dioxygenase 2
TH	- Tyrosine Hydroxylase
TM	- Thermomouse/Thermomouse Cells
TMCON	- Thermomouse Control Cells
TN	- Thermoneutrality
TNZ	- Thermoneutral Zone
TPH1	- Tryptophan Hydroxylase 1
TPH2	- Tryptophan Hydroxylase 2
TRPM8	- Transient receptor potential cation channel subfamily M (melastatin) member 8
UCP1	- Uncoupling Protein 1
VAT	- Visceral Adipose Tissue
VCO_2	- Rate of Carbon Dioxide Production
VDCC	- Voltage-Dependent Calcium Channels
VMAT2	- Vesicular Monoamine Transporter 2
VO_2	- Rate of Oxygen Consumption
WA	- White Adipocyte
WAT	- White Adipose Tissue
Xyl	- Xylamidine Tosylate

9 Declaration of Academic Achievement

Contributions:

- Alexander E. Green, MSc – Study design, method development, cell line creation, mouse line creation, etc.
- Gregory R. Steinberg, PhD – Initial conception, financial support and document editing
- Eulaine Ma, BSc – Adipocyte culture, daily injections, western blotting, etc.
- Elizabeth Kim, BSc – Acute *in vivo* awake 5-HT thermography, western blotting, etc.
- Sam D. Chorlton, MD – LINCS Bioinformatics Analysis
- Naja Z. Jespersen, MD – Human adipocyte culture and RNA-Sequencing
- Camilla Scheele, PhD – Human adipocyte culture and RNA-Sequencing
- Soren Nielsen, PhD – Human adipocyte culture and RNA-Sequencing
- Rhokhsana Mortuza, PhD – Preliminary *Slc6a4*$^{-/-}$ *in vivo thermography*
- Sonal Patel, PhD – *Htr2a AdKO* breeding, western blotting
- Andrea Llanos, MSc – cAMP measurements
- Ryan D. Pitt, BSc – *Ucp1* mRNA qPCR and daily injections
- Emilio P. Mottillo, MSc PhD – Adipocyte culture training and preliminary data
- Justin D. Crane, MSc, PhD – Initial *in vivo* thermography training
- Emily A. Day, PhD – Tissue harvesting and daily injections
- Eric M. Desjardins, MSc – Tissue harvesting and daily injections
- Julian M. Yabut, BSc – Tissue harvesting and daily injections
- Brennan K. Smith, PhD – Tissue harvesting

10 Academic Contributions

10.1 Published/Accepted Manuscripts

1. Bujak, A.L., Crane, J.D., Lally, J.S., Ford, R.J., Kang, S.J., Rebalka, I.A., Green, A.E., Kemp, B.E., Hawke, T.J., Schertzer, J.D., et al. (2015). AMPK activation of muscle autophagy prevents fasting-induced hypoglycemia and myopathy during aging. Cell Metab. 21, 883–890.
2. Percival, M.E., Martin, B.J., Gillen, J.B., Skelly, L.E., MacInnis, M.J., **Green, A.E.,** Tarnopolsky, M.A., and Gibala, M.J. (2015). Sodium bicarbonate ingestion augments the increase in PGC-1α mRNA expression during recovery from intense interval exercise in human skeletal muscle. J. Appl. Physiol. 119, 1303–1312.
3. Villani, L.A., Smith, B.K., Marcinko, K., Ford, R.J., Broadfield, L.A., **Green, A.E.,** Houde, V.P., Muti, P., Tsakiridis, T., and Steinberg, G.R. (2016). The diabetes medication Canagliflozin reduces cancer cell proliferation by inhibiting mitochondrial complex-I supported respiration. Mol. Metab. 5, 1048–1056.
4. Smith, B.K., Ford, R.J., Desjardins, E.M., **Green, A.E.,** Hughes, M.C., Houde, V.P., Day, E.A., Marcinko, K., Crane, J.D., Mottillo, E.P., et al. (2016). Salsalate (salicylate) uncouples mitochondria, improves glucose homeostasis, and reduces liver lipids independent of AMPK-β1. Diabetes 65, 3352–3361.
5. Mottillo, E.P., Desjardins, E.M., Crane, J.D., Smith, B.K., **Green, A.E.,** Ducommun, S., Henriksen, T.I., Rebalka, I.A., Razi, A., Sakamoto, K., et al. (2016). Lack of Adipocyte AMPK Exacerbates Insulin Resistance and Hepatic Steatosis through Brown and Beige Adipose Tissue Function. Cell Metab. 24, 118–129.
6. Rondini, E.A., Mladenovic-Lucas, L., Roush, W.R., Halvorsen, G.T., **Green, A.E.,** and Granneman, J.G. (2017). Novel pharmacological probes reveal ABHD5 as locus of lipolysis control in white and brown adipocytes. J. Pharmacol. Exp. Ther. 363, 367–376.
7. Yabut, J.M., Crane, J.D., **Green, A.E.,** Keating, D.J., Khan, W.I., and Steinberg, G.R. (2019). Emerging Roles for Serotonin in Regulating Metabolism: New Implications for an Ancient Molecule. Endocr. Rev. *40*, 1092–1107.

10.2 Patent Applications

1. Steinberg, G.R., and **Green, A.E.** (2017). Treatment for obesity, non-alcoholic fatty liver disease and type 2 diabetes using inhibitors of the peripheral 5-hydroxytryptamine receptor 2A (HTR2a).

2. Steinberg, G.R., and **Green, A.E.** (2018). A method of treating obesity.

11 Introduction

11.1 Literature Review

11.1.1 *Obesity*

Each year the obesity epidemic worsens. In 2013, globally, an estimated 36.9% and 38.0% of adult men and women, respectively, were diagnosed with obesity, an increase from 28.8% and 29.8% of men and women, respectively, in 1980 (Ng et al., 2014). Furthermore, in the U.S. the percentage of adults suffering obesity is predicted to rise to 48.9% (Ward et al., 2019). Not only is the prevalence of obesity rising but concurrently the risk of contracting co-morbidities including, type 2 diabetes (Whiting et al., 2011), non-alcoholic fatty liver disease (NAFLD; Cohen et al., 2011) and cardiovascular disease (Yusuf et al., 2004). Of particular note recently is the increasing rate of hepatocellular carcinoma (El-Serag, 2011; Ryerson et al., 2016) which is partially associated with obesity (Welzel et al., 2013). Thus, obesity and its co-morbidities continue to pose a major health risk that continues to worsen.

Excessive accumulation of adiposity defines obesity. This accrual is a result of prolonged disproportionate consumption of nutritional energy (caloric intake) versus that which is expended (caloric expenditure). Calories that are consumed and not expended, are consequently stored as fat within adipose tissue and if prolonged and excessive (as in obesity) eventually in other tissues – termed ectopic lipid deposition. Genetics, toxicants, and medications can all modify the risk for

developing obesity by changing an individual's caloric intake or their energy expenditure (EE), adding a complexity to the natural history of the disease (McAllister et al., 2009). However, the increase in adiposity is nonetheless due to a net positive intake of energy. Consequently, all treatments, whether behavioural or pharmaceutical, for obesity are predicated on altering the caloric balance to facilitate weight loss.

11.1.1.1 Treatments

11.1.1.1.1 Behavioural Interventions

Behavioural interventions, such as increasing EE through exercise or decreasing caloric intake via "dieting", are used to achieve a negative energy balance. Increasing physical activity has a plethora of beneficial effects, including but not limited to: increased caloric expenditure, improved glucose homeostasis (Shaw et al., 2006), improved affect (Cooney et al., 2013), resistance to cancer (Kampert et al., 1996), etc. However, as a weight-loss intervention it can have limited effectiveness for a variety of reasons (Thorogood et al., 2011). These include exercise intolerance in individuals with type 2 diabetes (Lewis et al., 2019), lack of adherence (Lemstra et al., 2016), and consequent increases in appetite (Thomas et al., 2012), all of which can undermine the utility of exercise to induce weight loss. Reducing dietary caloric intake, to induce a negative energy balance, is a very popular method of weight reduction (Bray et al., 2016). However, as with exercise, limitations also exist. Short-term weight loss can be quite profound, but maintenance can be difficult and might be because of numerous factors, including

the body's natural response to reduce caloric expenditure in response to caloric restriction (Leibel et al., 1995) and adherence (Lemstra et al., 2016). While reductions in weight are often greater with caloric restriction than with exercise, adverse effects of reduced caloric intake include loss of lean body mass (Weiss et al., 2007). Combination interventions of exercise and dietary restriction are the most effective means of behavioural interventions (Miller et al., 1997; Wu et al., 2009) but as mentioned above are limited by individual's adherence to often a strict and at times unpleasant lifestyle intervention. Because of this lack of utility there is interest to improve these strategies in the future and find other strategies that may be useful in the meantime and for those unable to adhere to the improved lifestyle.

11.1.1.1.2 Surgical Interventions

Alternative treatment strategies also include surgical interventions that remove excess adiposity or alter an individual's energy balance. Lipectomy, the removal of adipose tissue from the body, can yield temporary weight loss (Seretis et al., 2015a) but does not rectify the underlying energy surplus or metabolic disease (Seretis et al., 2015b). Alternatively, procedures including insertion of an intragastric balloon (Tate and Geliebter, 2017) and bariatric surgery are designed to reduce caloric intake by artificially reducing the physical capacity of the stomach to hold food. Bariatric surgeries include gastric banding, vertical sleeve gastrectomy, and Roux-en-Y gastric bypass. Together these are highly effective in reducing weight and attenuating symptoms of type 2 diabetes (Buchwald et al., 2004, 2009). Because of the invasiveness of these surgeries and partial weight

regain there still remains a desire to find alternative treatment modalities to induce weight-loss (Bray et al., 2016).

11.1.1.1.3 Pharmaceutical Interventions

Pharmaceutical interventions are another method to induce weight loss that have been used widely. However, many past weight-loss drugs have had toxic adverse effects and current medications have limited effectiveness. Notable weight-loss drugs that are no longer approved include 2,4-dinitrophenol (DNP) and fenfluramine (and its derivatives). DNP is a chemical "uncoupler" that can increase the body's EE by increasing the consumption of energy substrates in cells by inducing a futile cycle within the cells mitochondria whereby energetic substrate catabolism does not lead to ATP production. As such, DNP was widely used in the early 20th century for weight loss. However due to its very narrow therapeutic index, numerous reports of deaths due to hyperthermia and acute cardiac toxicities from acute overdosing rendered it unsafe for use (Grundlingh et al., 2011). Fenfluramine, a serotonin releasing drug, was paired with Phentermine, a norepinephrine releasing drug, to form an appetite suppressant, colloquially known as "Fen-Phen." Although highly effective, Fenfluramine-Phentermine was removed from the market after it was found Fenfluramine caused cardiac valvulopathy (Connolly et al., 1997). Later, a metabolite of fenfluramine (norfenfluramine) was found to act as a 5-HT2B receptor agonist and postulated to cause the adverse cardiac effects (Roth, 2007; Rothman et al., 2000). Other anti-obesity drugs (including sibutramine and aminorex; Table 1; Ioannides-Demos et al., 2006) also elicited adverse

cardiovascular effects that prevented further use. Thus, effective novel pharmaceuticals for weight-loss with wider safety margins and little or no adverse cardiac effects were required.

Today, there are 5 approved anti-obesity medications in the USA and only 2 in Canada (Table 1). These include: topiramate/phentermine (U.S.A.: Qsymia®; Canada: not approved), lorcaserin (U.S.A: Belviq®; Canada: not approved), bupropion/naltrexone (U.S.A.: Contrave®; Canada: not approved), liraglutide (U.S.A. and Canada: Victoza® or Saxenda®) and orlistat (U.S.A and Canada: Xenical® and Alli®). Topiramate/phentermine is a combination treatment consisting of Topiramate – an anti-epileptic drug with multiple cellular targets – and phentermine – the norepinephrine releasing drug. Lorcaserin is a 5-HT2C receptor agonist that suppresses appetite by activating 5-HT2C receptors in the Pro-opiomelanocortin (POMC) neurons of the hypothalamus (Martin et al., 2011; Smith et al., 2009; Thomsen et al., 2008). Although Lorcaserin demonstrated efficacy in clinical trials, only 7.2% of individuals administered Lorcaserin for 60 days were still receiving Lorcaserin at 12 months (Ganguly et al., 2018). Due to its similar mechanism of action (MOA) to fenfluramine, Lorcaserin was and continues to be heavily investigated for adverse cardiovascular effects (Bohula et al., 2018). Notably, the U.S. Food and Drug Administration (FDA) has recently requested the voluntary withdrawal of lorcaserin following a follow up review of a previous clinical study that showed an increased cancer risk (U.S. Food and Drug Administration, 2020) with lorcaserin treatment. Bupropion/Naltrexone decrease

appetite by activating hypothalamic Proopiomelanocortin (POMC) neurons through decreased reuptake/increased release of dopamine and norepinephrine by Bupropion and antagonism of endogenous POMC opioid inhibitors by Naltrexone (Coulter et al., 2018). Unlike the above medications, Orlistat, instead of reducing appetite, inhibits intestinal absorption of lipids by inhibiting pancreatic lipase (Borgström, 1988). Unfortunately, due to this MOA, it has some undesired gastrointestinal effects. All of these medications have associated adverse events and varying degrees of effectiveness including limited weight loss (Khera et al., 2016). Because all of these drugs restrict caloric intake, it is conceivable that the limitations of caloric expenditure also apply to them, such as reduced lean mass, reduced basal EE, etc. In all, these caloric intake restricting agents, all struggle with patients' adherence (Ganguly et al., 2018) and rely on the body to remove lipid via a normal (or reduced; Leibel et al., 1995) metabolic rate. As such new therapies safely eliciting enhanced energy expenditure may maximize weight loss. New pharmaceutical agents that induce weight-loss by increasing the body's metabolic rate to eliminate adipocyte hypertrophy and ectopic lipid deposition, without inducing adverse cardiovascular events, remains a promising therapeutic avenue and goal.

Table 1 Current and previously weight-loss medications

Anti-Obesity Medication	Brand Name(s)	General MOA	Specific MOA	Approval/Removal	Reason for Disuse/ Contraindications
2,4-DNP		Increased caloric expenditure	Mitochondrial Uncoupler	N/A	Pathological hyperthermia,
Fenfluramine	Pondimin®	Decreased caloric intake	Central Serotonin Releasing Agents. Adverse effects due to metabolite (norfenfluramine) acting as agonist at 5-HT2B	Canada Approved: 1991-12-31/1996-09-23 Removed: 1997-08-15/1998-08-13[1] U.S.A. Approved: Removal: 1997-09-15[2]	Cardiac valvulopathy Pulmonary hypertension
Phentermine	Ionamine® (Discontinued)	Decreased caloric intake	Norepinephrine releasing agent	Canada Approved: 1958-12-31[3] U.S.A. Approved: 1959-05-04[4]	
Dexfenfluramine	Redux®	Decreased caloric intake	Central serotonin releasing agent	Canada N/A U.S.A. Approved: Removal: 1997-09-15[5]	Cardiac valvulopathy

Anti-Obesity Medication	Brand Name(s)	General MOA	Specific MOA	Approval/Removal	Reason for Disuse/ Contraindications
Liraglutide	Victoza® (Treatment for Type 2 diabetes) Saxenda® (Treatment for Obesity)	Decreased caloric intake	GLP-1 Receptor agonist	Canada Approved: Victoza®: 2010-05-27[6] Saxenda®: 2015-05-27[7] U.S.A. Approved: Victoza®: 2010-01-25[8] Saxenda®: 2014-12-23[9]	
Lorcaserin	Belviq®	Decreased caloric intake	Central 5-HT2C receptor agonist	U.S.A. Approved: 2012-06-27[10] Discontinued: 2020-02-13[11]	Potential carcinogenic effect
Orlistat	Xenical® Alli®	Decreased caloric intake	Pancreatic lipase inhibitor	Canada Approved: 1999-06-03[12] U.S.A. Approved: 1999-04-23[13]	
Bupropion/naltrexone	Contrave®	Decreased caloric intake	POMC neuron activator	Canada N/A U.S.A.	

Anti-Obesity Medication	Brand Name(s)	General MOA	Specific MOA	Approval/Removal	Reason for Disuse/ Contraindications
				Approved: 2014-09-10[14]	
Topiramate/ phentermine	Qsymia®	Decreased caloric intake	Many/undefined and norepinephrine releasing agent	Canada N/A U.S.A. Approved: 2012-07-17[15]	
Sibutramine	Meridia®	Decreased caloric intake	Norepinephrine and serotonin reuptake inhibitor	Canada Approved: 2001-02-28[16] Removed: 2010-10-12[16] U.S.A. Approved: 1997-11-22[17] Removed: 2010-10-08[18]	Increased risk for heart attack and stroke (SCOUT Trial – Sibutramine Cardiovascular Outcomes Trial)
Aminorex	Menocil	Decreased caloric intake	Norepinephrine releasing agent	N/A	Pulmonary hypertension

1. https://health-products.canada.ca/dpd-bdpp/info.do?lang=en&code=12678 and https://health-products.canada.ca/dpd-bdpp/info.do?lang=en&code=26974
2. https://wayback.archive-it.org/7993/20170723090512/https://www.fda.gov/Drugs/DrugSafety/PostmarketDrugSafetyInformationforPatientsandProviders/ucm179871.htm
3. https://health-products.canada.ca/dpd-bdpp/info.do?lang=en&code=11201

4. https://www.accessdata.fda.gov/scripts/cder/daf/index.cfm?event=overview.process&ApplNo=011613
5. https://wayback.archive-it.org/7993/20170723090512/https://www.fda.gov/Drugs/DrugSafety/PostmarketDrugSafetyInformationforPatientsandProviders/ucm179871.htm
6. https://health-products.canada.ca/dpd-bdpp/info.do?lang=en&code=83627
7. https://health-products.canada.ca/dpd-bdpp/info.do?lang=en&code=92226
8. https://www.accessdata.fda.gov/scripts/cder/daf/index.cfm?event=overview.process&ApplNo=022341
9. https://www.accessdata.fda.gov/scripts/cder/daf/index.cfm?event=overview.process&ApplNo=206321
10. https://www.accessdata.fda.gov/scripts/cder/daf/index.cfm?event=overview.process&ApplNo=022529
11. https://www.fda.gov/drugs/fda-drug-safety-podcasts/fda-requests-withdrawal-weight-loss-drug-belviq-belviq-xr-lorcaserin-market
12. Search Orlistat at https://health-products.canada.ca/dpd-bdpp/newSearch-nouvelleRecherche.do?lang=
13. https://www.accessdata.fda.gov/scripts/cder/daf/index.cfm?event=overview.process&ApplNo=020766 and https://www.accessdata.fda.gov/scripts/cder/daf/index.cfm?event=overview.process&ApplNo=021887
14. https://www.accessdata.fda.gov/scripts/cder/daf/index.cfm?event=overview.process&ApplNo=200063
15. https://www.accessdata.fda.gov/scripts/cder/daf/index.cfm?event=overview.process&ApplNo=022580
16. https://health-products.canada.ca/dpd-bdpp/info.do?lang=en&code=67038
17. https://www.accessdata.fda.gov/scripts/cder/daf/index.cfm?event=overview.process&ApplNo=020632
18. https://wayback.archive-it.org/7993/20170112004434/http://www.fda.gov/Safety/MedWatch/SafetyInformation/SafetyAlertsforHumanMedicalProducts/ucm228830.htm
19. N/A – Not applicable/available

11.1.2 *Brown Adipose Tissue (BAT)*

Endothermic organisms maintain a high core-body temperature via highly-conserved and energy costly mechanisms of heat generation, including muscular shivering thermogenesis and BAT derived non-shivering thermogenesis. Although long-known to exist in rodents (Smith and Horwitz, 1969), human infants (Aherne and Hull, 1966; Dawkins and Scopes, 1965), and outdoor workers (Huttunen et al., 1981) - BAT garnered renewed attention in the last decade when inadvertently rediscovered in adult humans undergoing cancer screening (Cypess et al., 2009; Hany et al., 2002; Van Marken Lichtenbelt et al., 2009; Saito et al., 2009; Virtanen et al., 2009; Zingaretti et al., 2009). Consequently, with the increasing epidemic of obesity and metabolic diseases in adults, there is renewed interest in exploiting human adult BAT to increase EE to treat metabolic diseases.

Unlike the more commonly known white adipose tissue (WAT), BAT functions not to store energy in the form of lipid within its adipocytes, but to utilize stored and circulating substrates to generate heat in response to cold. Large depots of BAT exist in the intrascapular region of rodents and human infants (Cannon and Nedergaard, 2004). Using cold-exposure and a glucose tracer (fluorodeoxyglucose – FDG) in Positron emission tomography–computed tomography (PET-CT) scans BAT depots were identified in the supraclavicular, perirenal and mediastinal regions of adult humans (Hany et al., 2002), and were later confirmed to contain Uncoupling Protein 1 (UCP1; Cypess et al., 2009; Saito et al., 2009; Virtanen et al., 2009; Zingaretti et al., 2009). Histologically BAT possesses multilocular lipid

droplets (contrasting unilocular in WAT), a reddish-brown appearance (due to high levels of mitochondria) and much greater vascularization than WAT (Rosen and Spiegelman, 2014). Biochemically, unlike WAT, BAT expresses a unique protein within its mitochondria called UCP1. In non-BAT mitochondria, protons from the intermembrane space flow through ATP-Synthase to drive ATP synthesis from ADP and P_i. However, when active, UCP1 in BAT allows protons to freely flow into the matrix of the mitochondria from the intermembrane space bypassing ATP-Synthase in a process termed "uncoupling". Alleviation of the membrane potential induces maximal activity of the electron transport chain and the upstream catabolic processes. The inefficiencies of all these processes produce large amounts of heat and cumulatively defines non-shivering thermogenesis. Under optimal conditions non-shivering thermogenesis from BAT consumes 75% of whole-body glucose disposal and 50% of whole-body lipid disposal in rodents (Bartelt et al., 2011; Nedergaard et al., 2011). In humans, it is estimated that BAT can consume ~203 kcal per day (Cypess et al., 2015). Furthermore, under certain stimuli, WAT acquires brown-like phenotypes, including increased mitochondrial content and UCP1 expression, in a process termed, "browning" (Rosen and Spiegelman, 2014). This occurs through either adaptation of existing white adipocytes or production of new brown-like adipocytes termed beige adipocytes. These brown like WAT depots are also known as beige adipose tissue (BeAT) and can also perform thermogenesis, but contain ~20% of total body UCP1 mRNA in rodents at 4ºC and <10% at 30ºC (Kalinovich et al., 2017; Nedergaard and Cannon, 2013). Therefore, because of the

high capacity for consuming substrate, activation of BAT and conversion of WAT to brown-like adipose tissue is of great interest to the therapeutic community.

11.1.2.1 BAT Activation Pathway

Canonical activation of BAT occurs in response to sympathetic neuron released NE (Figure 1). NE binds to the G_s-coupled, β-adrenergic receptors on BAs and induces an adrenergic signalling cascade (Cannon and Nedergaard, 2004). Intracellular cyclic AMP (cAMP) levels increase activating protein kinase A (PKA) and leading to phosphorylation of downstream substrates including ABHD5, perilipins (PLNs), and hormone-sensitive lipase (HSL; Braun et al., 2018). This coordinated response allows for increased access to the lipid droplet via displacement of PLNs and increased activity of ATGL (via stimulation of its coactivator ABHD5) and HSL. Free fatty acids (FFAs) flood the intracellular milieu providing substrate for β-oxidation and in BAT allosterically bind and activate UCP1 (Fedorenko et al., 2012). Additionally, systemic glucose and FFA (released by tissues including WAT) increase and provide additional substrate for non-shivering thermogenesis and activation of UCP1 (in the case of FFAs; Schreiber et al., 2017; Shin et al., 2017). In addition to acute activation of metabolism, PKA induces a signal cascade that can activate transcription factors through post-translational modifications and signalling FFAs that activate transcriptional co-activators PGC-1α and PRDM16 (via stimulation of PPAR transcription factors; Mottillo et al., 2012) to enhance the expression of thermogenic-related genes.

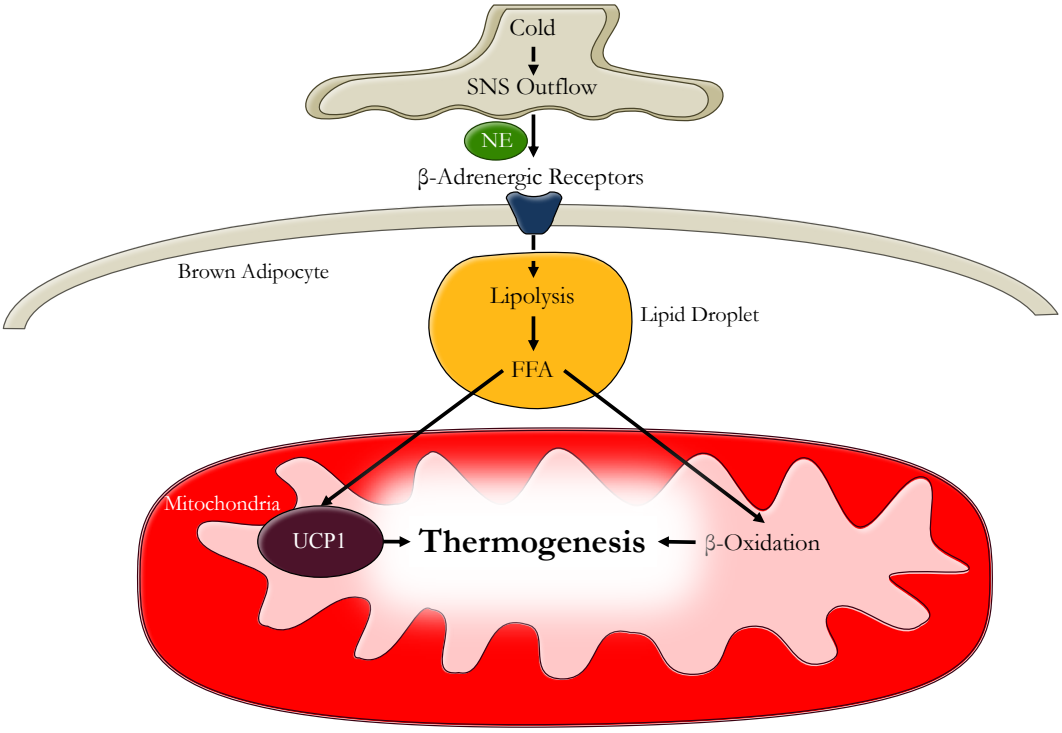

Figure 1 General depiction of BAT thermogenesis pathway.

11.1.2.2 Extracellular Regulators of BAT Function

Canonical physiology research implies that BAT acts as a thermogenic organ to defend core-body temperature against environmental cold to maintain homeostasis (Cannon and Nedergaard, 2004). Additional research suggests that brown adipocyte EE may also play a role in other processes, such as defending against weight gain, and respond to non-temperature related stimuli, including hormonal and metabolic signals. As such, there is an ever-expanding list of extracellular regulators of BAT that pose novel targets for therapeutic intervention.

11.1.2.2.1 Cold Stimulus

Cold exposure robustly activates BAT and has been extensively studied. Exposure to environments outside the thermoneutral zone (TNZ), defined as the

temperature region where no additional energy is required to maintain core body temperature (typically 28-33ºC for mice and unclothed humans), requires an endotherm to generate or dissipate heat (Kingma et al., 2012; Virtue and Vidal-Puig, 2013). Any exposure to environments below 27ºC activates thermogenesis, acutely, via an increase in shivering and non-shivering thermogenesis, and chronically, via increasing BAT activity and functional capacity (Golozoubova et al., 2001; Kalinovich et al., 2017). Mechanistically, cold activates TRPM8 receptors in afferent neurons on the skin and transduces the signal to the hypothalamus (Bautista et al., 2007; Colburn et al., 2007; Dhaka et al., 2007). Whereby central circuits increase sympathetic outflow to efferent neurons including those in BAT and WAT (Morrison et al., 2014; Nakamura and Morrison, 2007). These neurons possess high levels of tyrosine hydroxylase (TH) and consequently contain large amounts of norepinephrine (NE) in their synaptic vesicles. Upon depolarization, efferent neurons release NE that binds and activates G_s-coupled β-adrenergic receptors on adipocytes (Cannon and Nedergaard, 2004). The consequent adrenergic cascade increases FFAs for oxidation and direct activation of UCP1 and induces the thermogenic gene program. Although a study has suggested that some adipocytes in WAT depots may directly sense changes in temperature and trigger adaptation, this mechanism remains sparsely studied (Ye et al., 2013). Thus, cold-stimulus, via adrenergic signalling, not only activates non-shivering thermogenesis but promotes adaptation of BAT and WAT to enhance non-shivering thermogenesis capacity in the future.

11.1.2.2.2 Dietary Influences on Thermogenesis

A more controversial, but long investigated, regulator of BAT is caloric and macronutrient intake. Acutely, food consumption increases caloric expenditure, known as the "thermic effect of food." Many investigations implicate BAT as the source or a contributor to this acute increase in EE. Early research indicated BAT to partially contribute to an acute increase in energy expenditure due to facultative food intake (Rothwell and Stock, 1979). Although, the increase in EE in response to caloric intake and BAT's involvement has been debated (Kozak, 2010), recently, when housed at thermoneutrality, mice have elevated EE during their feeding period but this was absent in mice genetically lacking *Ucp1* (*Ucp1*$^{-/-}$; (von Essen et al., 2017). Furthermore, not only can an acute caloric intake increase EE, but chronic dietary macronutrient composition can influence expression of thermogenic genes in adipose tissue. As reviewed in Fromme and Klingenspoor (2011) chronic high fat diet (HFD) increases the expression of UCP1 in BAT. This increase in UCP1 is dependent upon the innervation of BAT (Fischer et al., 2019).

However, this is in contrast to the often argued, but potentially incorrect, notion that obese individuals have impaired BAT functional capacity. In mice, this was supported by early research in leptin deficient mice (i.e. *Ob/Ob* mice) which suggested their obesity was associated with impaired BAT activity. However, it has since become apparent that this was not the case (Fischer et al., 2016) and is an example of the incorrect practice of correcting energy expenditure to body mass. In humans, basal EE clearly increases with increasing body mass, thus suggesting that

obesity is not a result of reduced BMR (Carneiro et al., 2016). Although this does not exclude the possibility of a lower BMR than expected for the amount of tissue acquired during obesity. To this point, in the rejuvenation of the human BAT field quite a bit of excitement was generated with the observation that obese individuals had reduced BAT (Van Marken Lichtenbelt et al., 2009). However, this finding is confounded by the use of FDG (a glucose analog) to measure human BAT. In patients with type 2 diabetes, uptake of glucose in to BAT may be inhibited but fatty acid tracers are not (Blondin et al., 2015). Although, to our knowledge, this has yet to be completed in obese individuals, presumably since obesity is associated with glucose intolerance the reduction in glucose-tracer uptake might simply indicate a change in BAT substrate preference. Regardless additional experiments need to be completed with new methods to investigate if BAT is impaired in obese individuals.

11.1.2.2.3 Circulating Factors

Although NE mediated neuronal activation of BAT is the established route of BAT activation, recently there have been a plethora of circulating factors identified that may regulate BAT. These include positive regulators of BAT function, including but not limited to thyroid hormone (particularly T3; Golozoubova et al., 2004) and atrial natriuretic peptides (Bordicchia et al., 2012). There are also proposed negative regulators of BAT function/activity including but not limited to serotonin (Crane et al., 2015; Oh et al., 2015). This provides an

interesting avenue for investigation of molecules that might be blood-borne and easily manipulated to change and alter the activity BAT.

11.1.3 *Potential for Activation of BAT to Treat Obesity*

As discussed above, net caloric balance determines weight gain or weight loss and current approved anti-obesity treatments focus exclusively on decreasing caloric intake, either through pharmacological inhibition of appetite or macronutrient absorption, or through surgical interventions. However, BAT as a thermogenic organ capable of consuming energetic substrates and dissipating their potential energy in the form of heat has drawn much attention as a potential target to treat obesity. Although as discussed before whether BAT is truly reduced in obese mice or humans is still to be determined, it does not prevent BAT from being a potential target for anti-obesity medications.

Many studies have explored the therapeutic potential of BAT to treat obesity using genetically engineered mice. Experiments eliminated BAT using diphtheria toxin and found mice had greater weight gain (Lowell et al., 1993). This was also confirmed in mice lacking all three β-adrenergic receptors (Bachman et al., 2002; Jimenez et al., 2002), but only mildly in mice lacking β3 alone (the receptor most commonly associated with BAT; Susulic et al., 1995). In contrast, whole body germline elimination of UCP1 did not recapitulate these results at room temperature (Liu et al., 2003) but only at thermoneutrality (Feldmann et al., 2009) or with age (Kontani et al., 2005). This discrepancy may be due to compensatory increases in less substrate efficient thermogenic processes and since diphtheria toxin induced

elimination of BAT yielded obesity, part of the compensatory pathway is likely within BAT and may be β-adrenergic-receptor dependent. One potential compensatory pathway that has recently been described is phosphocreatine cycling which occurs in BAT/WAT of *Ucp1*$^{-/-}$ mice and thus does not require UCP1 (Kazak et al., 2015). Interestingly, overexpression of *Ucp1* using the *Ap2*-promoter caused BA cytotoxicity and consequently elicited only a modest (~20%) overall increase in UCP1 in BAT. This resulted in BAT atrophy in male mice and reduced thermogenesis in response to adrenergic stimuli. Furthermore, *Ucp1* overexpression did not change weight gain in mice fed regular chow diet. However, overexpression of *Ucp1* reduced white adipose tissue depots in mice fed a HFD or *Ob/Ob* mice (Kopecky et al., 1995; Kopecký et al., 1996). Furthermore, mice overexpressing the β1-adrenergic receptor under the control of the *Ap2*-promoter are resistant to obesity (Soloveva et al., 1997). The absence of *Ucp1* (at thermoneutrality), elimination of BAT and expression of all three β-adrenergic receptors suggests that the lack of BAT-mediated thermogenesis/BAT increases susceptibility to obesity while the overexpression of *Ucp1* or increased adipose adrenergic signalling suggests BAT could be a potential therapeutic target for treating excessive adiposity.

Prior investigations using pharmaceuticals activating BAT to treat obesity have proven successful in rodent models of obesity but have yet to successfully translate to humans. One of the earliest approaches was the activation of β_3-adrenergic receptors using agonists such as CL-316,243. In mice CL-316,243,

robustly increases EE in mice, elicits expression of BA like gene expression in WAT, and induces weight loss (Collins et al., 1997; Crane et al., 2014; Guerra et al., 1998). However, in humans it does not increase EE (Weyer et al., 1998). This has previously been explained to the relative differences in β_3-adrenergic receptor expression in humans (Granneman and Lahners, 1994; Krief et al., 1993). More recently, Mirabegron, an FDA approved β_3-adrenergic receptor agonist, increased ^{18}F-FDG uptake into supraclavicular BAT depot in humans (Cypess et al., 2015). Unfortunately, at doses that activate BAT, Mirabegron also increased systolic blood pressure, thereby limiting its therapeutic potential due to potential increase risk of cardiac events. Therefore, β-adrenergic agonists although effective in activating BAT in rodents, may have limited applicability in humans and elicit undesirable adverse cardiovascular disease indicators.

Alternatively, the antidiabetic drug class, thiazolidinediones, have been explored for their ability to activate BAT to treat metabolic disease. *In vitro* TZDs, such as rosiglitazone, are known inducers of the thermogenic gene program in adipose tissue (Digby et al., 1998; Tai et al., 1996). Recent, studies found pioglitazone, a PPARϒ agonist, increased UCP1 levels in cultured BAs but reduced BAT activity in humans (Loh et al., 2018). Consistent with this, TZDs have been found to actually attenuate thermogenic capacity *in vitro* (Paulik et al., 1998), which may be related to their known ability to inhibit the mitochondrial pyruvate carrier (Divakaruni et al., 2013). It also might suggest that increasing the thermogenic gene program alone is insufficient to increase EE; however, the inhibition of

mitochondrial substrate supply may confound this conclusion. Furthermore, contrary to the desired effect of increasing the thermogenic gene program in adipose tissue – TZDs, including pioglitazone – increase weight gain in patients (Cariou et al., 2012). Therefore, although TZDs have been found effective to upregulate the thermogenic gene program they lack efficacy to elicit BAT thermogenesis and increase weight gain.

A non-pharmaceutical approach that has been explored to increase BAT thermogenesis is through modifying the living environment. In mice, it has long been known that keeping mice at standard RT (i.e. below the TNZ) activates the thermogenic response. This is often exploited to test if cold-induced thermogenesis mediates a suspected BAT phenotype (Melnyk et al., 1997). As ambient temperature decreases there is a proportional increase in energy expenditure (Fischer et al., 2018). Notably one example of the importance of housing temperature, Tian et al. (2016) demonstrated that mice housed at TNZ suffered increased atherosclerosis, thus suggesting that ambient temperature not only affects EE but also other metabolic phenotypes. Proof of principle for the translatability of ambient temperature effects on adipose tissue was found early on in the association of increased BAT like adipose tissue in outdoor Scandinavian workers in 1981 (Huttunen et al., 1981). In humans, EE expended by BAT in response to BAT activators is estimated to be ~200 kcal/day (Cypess et al., 2015). Furthermore, chronic exposure to cold temperatures can recruit human BAT (Van Der Lans et al., 2013). Trials reduced night time ambient temperature and demonstrated

improved insulin sensitivity but no changes in body mass (Lee et al., 2014). Further work would be required to see what amount of exposure to temperatures below the TNZ in humans would be required to induce sufficient EE to cause weight loss and how they may efficaciously be implemented in the human population.

Although above we have discussed some of the trialed therapies for activating BAT to combat obesity in humans, many more potential therapeutic targets have been identified in rodents. These include adenosine (Gnad et al., 2014), and natriuretic peptides (Bordicchia et al., 2012), and non-adrenergic targets are reviewed in Villarroya and Vidal-Puig (2013). Future work will be required to examine which of these targets are robust, reproducible and translatable to human BAT for therapeutic potential and use.

11.1.4 *Tryptophan and Metabolism*

Tryptophan is an essential amino acid critical to many cellular processes. It is a precursor for not only protein synthesis but also important signalling molecules, including serotonin, kynurenine, melatonin, NAD, etc. (Figure 2). Directly or through these metabolites, tryptophan regulates aspects of physiology including metabolism. In mammals, tryptophan cannot be *de novo* synthesized but must be obtained directly from the diet or recycling of degraded proteins.

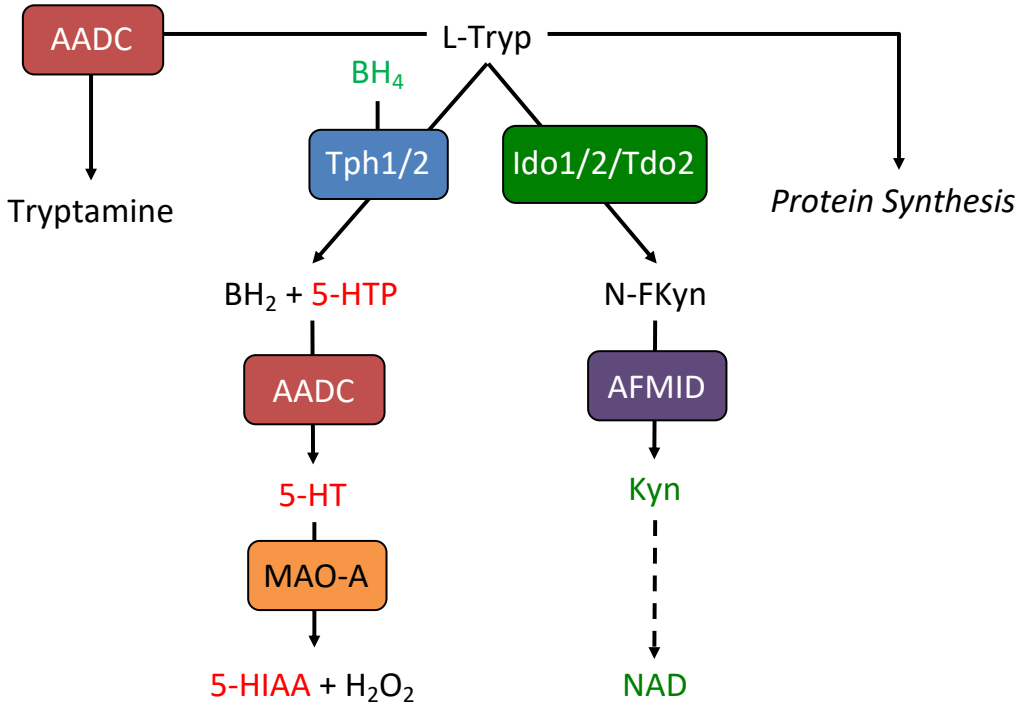

Figure 2 Diagram of major fates of L-Tryptophan. AADC, Aromatic L-amino acid decarboxylase; BH_4, Tetrahydrobiopterin; Tph1, Tryptophan hydroxylase 1; Tph2, Tryptophan hydroxylase 2; Ido1, Indoleamine 2,3-dioxygenase 1; Ido2, Indoleamine 2,3-dioxygenase 2; Tdo2, Tryptophan 2,3-dioxygenase 2; BH_2, Dihydrobiopterin; 5-HTP, 5-hydroxytryptophan; N-FKyn, N′-Formylkynurenine; AFMID, Arylformamidase; MAO-A, Monoamine oxidase-A; 5-HT, 5-Hydroxytryptamine/Serotonin; Kyn, Kynurenine; 5-HIAA, 5-Hydroxyindoleacetic acid; NAD, Nicotinamide adenine dinucleotide.

11.1.4.1 Fates of Tryptophan

The majority of the effects of tryptophan are via its downstream metabolites. Upon ingestion tryptophan can be directly metabolized by the gut microbiota to form tryptophan metabolites (e.g. Tryptamine and indole-3-acetate; Jin et al., 2014). Studies have found that these metabolites have agonist activity for the Aryl-hydrocarbon Receptor (AhR) and consequently regulate hepatocyte and macrophage immune responses (Krishnan et al., 2018). Tryptophan that escapes

this fate enters the intestinal lining where it undergoes metabolism via mammalian cells.

Aside from protein synthesis, within mammalian tissues the two major early metabolites of tryptophan are kynurenine and serotonin. The first and rate limiting step into kynurenine is deoxygenation via Ido1/Ido2/Tdo2 or into serotonin via hydroxylation via Tph1/Tph2, respectively (Palego et al., 2016). Additionally, these pathways feed into the synthesis of important active metabolites including melatonin and nicotinamide adenine dinucleotide (NAD). Although it is not clear what signals determine the fate of tryptophan numerous studies have examined the major downstream metabolites individually.

11.1.5 *Kynurenine and Metabolism*

Kynurenine is an active metabolite of tryptophan (Rossi et al., 2019). Entry into the kynurenine pathway occurs via catabolism of tryptophan by Indoleamine 2,3-Dioxyegenase 1 and 2 (Ido1 and 2) or Tryptophan 2,3-Dioxygenase (Tdo2) to form N-formyl-L-kynurenine. Subsequently, Kynurenine Formamidase converts N-formyl-L-kynurenine to kynurenine where it can either 1) form kynurenic acid via kynurenine aminotransferases or 2) continue to be metabolized into picolinic acid, quinolinic acid and eventually NAD via a series of enzymatic mediated and spontaneous steps.

Kynurenine synthesis occurs primarily in the liver, brain and immune cells. This is chiefly determined by the tissue specific distribution of Ido1, Ido2, and the predominantly liver expressed Tdo2. Additionally, mass action also plays a role. *In*

vitro assays reveal K_ms of Ido1, Ido2 and Tdo2 as ~20 μM, ~55 mM and ~100 μM (Yuasa et al., 2009). The circulating concentration of Tryptophan is 46 μM (Liu et al., 2018) suggesting that not all of these enzymes are saturated. This is further supported by evidence that infusions of tryptophan increase kynurenine and 5-hydroxy-tryptophan levels in plasma (Huether et al., 1992). Furthermore, inhibition of other fates of tryptophan lead to increased kynurenine levels. Tph2 and Tph1 elimination increases kynurenine levels ~2-fold (Sibon et al., 2019; Weng et al., 2015). Additionally, metabolites of serotonin also regulate the kynurenine pathway. Reports suggest melatonin regulates activity through the kynurenine pathway through transcriptional upregulation of Ido1 (Li et al., 2017). Thus, this suggests a reciprocal balance between the major fates of tryptophan, kynurenine and serotonin, and linking their effects.

Kynurenine is actively taken up across the Blood Brain Barrier (BBB; Fukui et al., 1991) and modulates neuronal function. It has been suggested to be a regulator of depression (Müller and Schwarz, 2007). Additionally, kynurenine can be metabolized into kynurenic acid via kynurenic acid transferases (KATs). Kynurenic acid only passively diffuses across the BBB (Fukui et al., 1991) and this conversion is thought to prevent kynurenine's influence on mood (Agudelo et al., 2014). Furthermore, tissues such as muscle express KATs in response to exercise and PGC-1α overexpression, leading to reduced kynurenine and greater kynurenic acid levels (Agudelo et al., 2014).

Kynurenine and its metabolites have also been identified as metabolic regulators. Patients with obesity have elevated levels of kynurenine (Favennec et al., 2015). Furthermore, genetic ablation of *Ido*1 prevents weight gain in response to an HFD (Nagano et al., 2013). Kynurenic acid has also been identified as a modulator of BAT (Agudelo et al., 2018). Specifically, kynurenic acid supplementation increases the sensitivity of BAT to sympathetic nervous system activity by upregulating the G_i modifying enzyme Rgs14 via activation of Gpr35. Additionally, a further downstream metabolite of kynurenine is NAD. Supplementation with precursors of NAD, such as nicotinamide riboside, increase metabolism in mice and attenuated HFD-induced weight gain (Cantó et al., 2012). These data suggest that kynurenine is an important regulator of metabolism.

11.1.6 *Serotonin (5-Hydroxytryptamine; 5-HT)*

Alternatively, tryptophan can become serotonin, also known as 5-hydroxytryptamine (5-HT). 5-HT was first identified as a smooth muscle contraction inducer derived from the gut (known as enteramine) and later found to regulate vascular tone and renamed serotonin (Whitaker-Azmitia, 1999). Subsequently 5-HT has been implicated in a variety of regulatory processes. 5-HT is formed via 2 enzymatic steps. First Tryptophan Hydroxylase 1 (TPH1) or Tryptophan Hydroxylase 2 (TPH2) hydroxylates tryptophan to produce 5-hydroxytrophan (5-HTP). Subsequently, Aromatic L-Amino Acid Decarboxylase (AADC; a.k.a. DOPA decarboxylase – DDC) converts 5-HTP to 5-HT via decarboxylation. Upon metabolism by monoamine oxidases (MAOA or MAOB)

and other enzymes 5-HT can also form other active metabolites including 5-HIAA and melatonin.

11.1.6.1 5-HT Synthesis, Excretion and Regulation

The initial step of 5-HT metabolism is catalyzed by tryptophan hydroxylases. These enzymes belong to the biopterin-dependent aromatic amino acid hydroxylase enzyme family that evolved from a shared enzyme (Grenett et al., 1987) and in mammals consist of Phenylalanine Hydroxylase (PAH; the rate limiting step in phenylalanine metabolism), Tyrosine Hydroxylase (TH; the rate limiting step in catecholamine synthesis) and the Tryptophan Hydroxylases (TPH1 and TPH2; the rate limiting enzyme in 5-HT synthesis). Each sharing ~48-53% sequence homology. Conversion of tryptophan to 5-hydroxytryptophan (5-HTP) by TPH1/TPH2 requires the co-substrate tetrahydrobiopterin (BH4).

For many years, 5-HT was thought to be synthesized by a sole tryptophan hydroxylase. However in 2003, it was discovered that two isoforms of Tryptophan Hydroxylase exist, TPH1 and TPH2 (Côté et al., 2003; Walther et al., 2003a). TPH1 was the isoform previously annotated in the literature and is primarily expressed in enterochromaffin cells of the small intestine (Walther et al., 2003a), the pineal gland (Côté et al., 2003) and mast cells (Schindler, 1959; Yabut et al., 2020), and at lower levels in a variety of tissues including the pancreas (Paulmann et al., 2009) and adipose tissue (Oh et al., 2015; Stunes et al., 2011). In contrast, TPH2 is primarily expressed in serotonergic neurons of the central nervous system and enteric nervous system (Walther et al., 2003a; Zhang et al., 2004). AADC is

expressed in the intestine, pineal gland, and also other tissues (Rahman et al., 1981). *In vitro*, TPH2 has a *Km* of ~40 μM (McKinney et al., 2005) and administration of tryptophan *in vivo* increases the levels of 5-HT in the central nervous system (Quay, 1963). In contrast, in purified enzymatic preparations TPH1 has a *Km* of ~23 μM (McKinney et al., 2005). Interestingly, dietary supplementation with tryptophan increases 5-HT in the pineal gland (a tissue with predominantly *Tph1* expression; Quay, 1963) and intravenous infusion of tryptophan increases peripheral 5-HT (Huether et al., 1992). *para*-Chlorophenylalanine (PCPA) was the first TPH1/TPH2 competitive inhibitor developed and is still widely used in preclinical models (Koe and Weissman, 1966). Given the gastrointestinal (GI) effects of 5-HT, efforts to develop additional inhibitors of 5-HT synthesis lead to the development of LP-533401 for treatment of chemotherapy induced emesis (Liu et al., 2008) and approval of LX-1032 (Telotristat) for treatment of carcinoid syndrome associated diarrhea. Additionally, non-competitive allosteric inhibitors of TPH1 have now been developed (Petrassi et al., 2017).

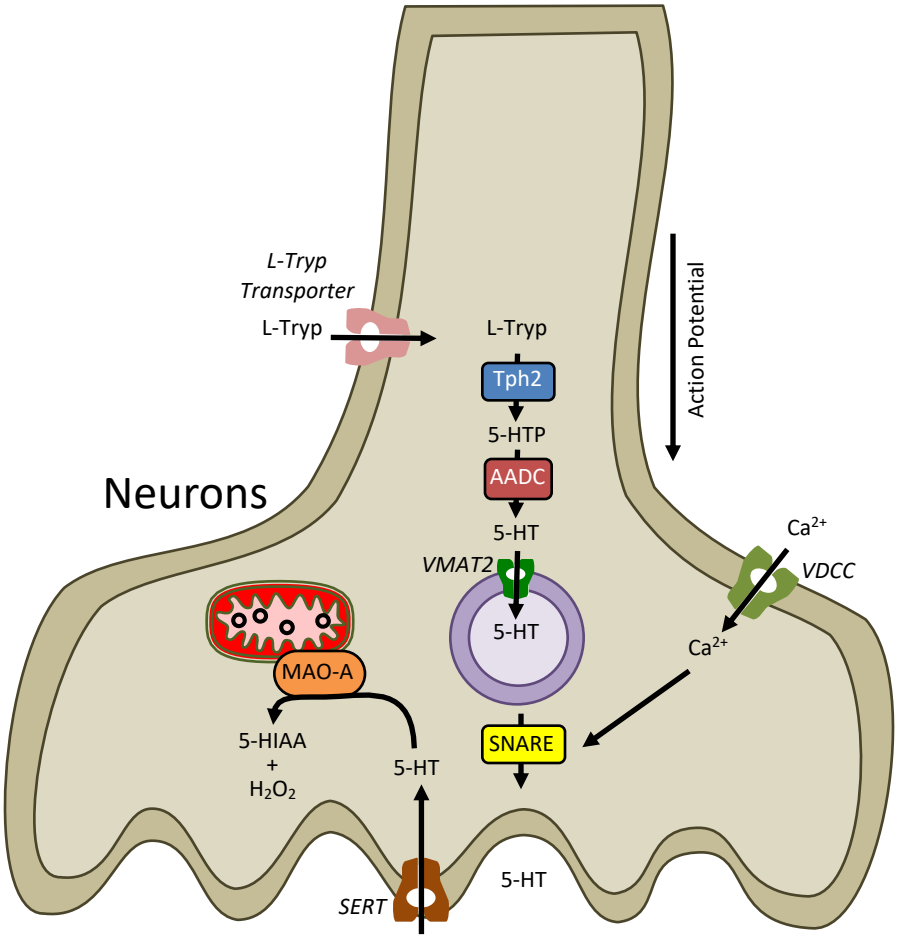

Figure 3 General pathway of 5-HT synthesis, secretion and metabolism in neurons. L-Tryp, L-tryptophan; Tph2, Tryptophan hydroxylase 2; AADC, Aromatic L-amino acid decarboxylase; 5-HT, 5-hydroxytryptamine; VDCC, voltage-dependent calcium channels; SNARE, soluble NSF attachment Protein Receptor; VMAT2, vesicular monoamine transporter 2; MAO-A, monoamine oxidase A; 5-HIAA, 5-hydroxyindoleacetic acid; H_2O_2, hydrogen peroxide; SERT, serotonin transporter

Consistent with the tissue distribution of the synthetic enzymes (i.e. Tph1), early studies using radiolabelled 5-HTP identified 5-HT to be primarily contained within the intestine (Gershon and Ross, 1966). Estimates suggests that the majority of 5-HT is contained within the enterochromaffin cells. Other major 5-HT depots include synaptic end bulbs in serotonergic neurons, mast cells, and blood platelets.

Notably, 5-HT itself is relatively impermeable across the BBB compared to other amino acid metabolites (Oldendorf, 1971). Although some reports contradict this and suggest that 5-HT is permeable across the BBB (Bulat and Supek, 1968). Inhibition of TPH1 or TPH2 reduce 5-HT in their respective compartments with little or no effect on the level of 5-HT in the complementary compartment (Côté et al., 2003). Thus, the segmented distribution of TPH1 and TPH2, in the peripheral tissues versus the central tissues, respectively, generally creates 2 pools of 5-HT that are physically separated from each other.

Following synthesis, the most well-described actions of 5-HT require 5-HT to be released into the extracellular space. In serotonergic neurons, *de novo* synthesized 5-HT, and 5-HT absorbed from the extracellular space via the Serotonin Transporter (SERT; Gene name: *Slc6a4*) and other transporters, is repacked into vesicles via VMAT2 (Henry et al., 1998; Narboux-Nême et al., 2011). Upon depolarization of the neuronal membrane by an action potential, the influx of extracellular Ca^{2+} stimulates SNARE-dependent fusion of serotonin vesicles to the presynaptic end-plate and subsequent release of 5-HT into the synaptic cleft (Müller et al., 2014). In mast cells, 5-HT is stored in granules and released in response to antigen-bound IgE exposure and Ca^{2+} influx (Siraganian, 2003). 5-HT from the enterochromaffin cells of the intestine is thought to be released in response to stimuli, such as glucose (Drapanas et al., 1962; Zelkas et al., 2015). Obesity and free fatty acids (FFA) exposure increase the quantity of 5-HT released from enterochromaffin (EC) cells in response to glucose (Bertrand et al.,

2011; Young et al., 2018). Although platelets do not synthesize 5-HT, they take up large amounts of 5-HT via SERT (Chen et al., 2001). Upon platelet aggregation, 5-HT is released from platelets (de Clerck et al., 1982; Lindblad et al., 1984). Through a variety of regulated mechanisms 5-HT release into the extracellular compartment is regulated.

To regulate extracellular 5-HT following release, a mechanism exists to counteract 5-HT release. SERT, the serotonin transporter, is expressed in a variety of tissues where SERT transports 5-HT from the extracellular space across the cell membrane into the cytoplasm. In neurons, SERT removes 5-HT from the synaptic cleft to terminate 5-HT signalling in the post-synaptic tissue (Sangkuhl et al., 2009). Furthermore, Selective Serotonin Reuptake Inhibitors (SSRIs) are drugs that inhibit SERT to increase/prolong the 5-HT-induced signalling in neuronal tissue to yield antidepressant effects. Platelets contain SERT to take up plasma 5-HT and transport 5-HT systemically (Chen et al., 2001). Other tissues, including the lung and the intestine, also contain high levels of SERT (Gill et al., 2007).

Although SERT is the most well described transporter of 5-HT, other proteins capable of transporting 5-HT exist. These include promiscuous activity by the Dopamine Transporter (DAT; Gene name: *Slc6a3*; Mössner et al., 2006; Pan et al., 2001), the Plasma Membrane Monoamine Transporter (PMAT; Gene name: *Slc29a4*; Engel et al., 2004) and Organic Cation Transporter 3 (OCT3; Gene name: *Slc22a3*; Wu et al., 1998). The activity of PMAT and OCT3 has previously been termed non-neuronal uptake or "uptake2". Unlike SERT, multiple substrates are

transported through PMAT and OCT3 and these transporters express relatively low specificity but higher capacity for 5-HT transport versus SERT (Hagan et al., 2011). Further, upon inactivation of SERT, expression of OCT3 increases in neurons suggesting potential compensatory mechanisms to maintain 5-HT transport (Baganz et al., 2008; Schmitt et al., 2003).

Upon uptake/reuptake of 5-HT from the extracellular space, 5-HT can either be metabolized or repackaged into vesicles for subsequent release. 5-HT is metabolized by Monoamine Oxidases (MAOA or MAOB), with MAOA having greater affinity for 5-HT (Shih et al., 1999; Sjoerdsma et al., 1955). Oxidation of 5-HT produces 5-HIAA and subsequently 5-MIAA which has PPARɣ agonist activity (Waku et al., 2010). Additionally, 5-HT can be metabolized into other active metabolites, including melatonin.

11.1.6.2 Mechanisms of 5-HT Action

Following release from 5-HT synthesizing tissues and prior to reuptake/degradation, 5-HT regulates numerous tissues primarily via 5-HT receptors and to a lesser extent post-translational modification. By sequence homology, there are 7 classes of 5-HT receptors in mammals as outlined in Hoyer et al. (1994) and summarized below and in Table 2. All 5-HT receptor classes except the 5-HT3 class are G-protein coupled and are described by their canonical signalling pathways. The 5-HT1 and 5-HT5 receptor classes are coupled to G_i-proteins and decrease cAMP levels. The 5-HT4, 5-HT6 and 5-HT7 receptors are coupled to G_s-proteins and increase cAMP levels. The 5-HT2 class receptors are

coupled to G_q-proteins and signal via IP_3 and DAG, and subsequently intracellular Ca^{2+}. In contrast, the 5-HT3 receptor class is a ligand-gated cation channel. These receptors are expressed in a tissue-specific manner to confer unique activities within target tissues.

In contrast to 5-HT receptor-mediated signalling, intracellular 5-HT can be ligated to proteins as a post-translational modification termed serotonylation (Dale et al., 2002). Transglutaminases catalyze the addition of 5-HT to proteins, such as small GTPases, to induce constitutive activity (Walther et al., 2003b). Although less well described, serotonylation has been implicated in platelet (Dale et al., 2002; Szasz and Dale, 2002; Walther et al., 2003b) and pancreatic function (Paulmann et al., 2009).

Table 2 Murine 5-HT Receptor family and associated G-proteins

Receptor Family	G-Protein (if applicable)	Subfamily Receptors
5-HT1	Gi	A, B, D, E and F
5-HT2	Gq	A, B and C
5-HT3	Ion channel	
5-HT4	Gs	
5-HT5	Gi	A and B
5-HT6	Gs	
5-HT7	Gs	

11.1.6.3 Effects of 5-HT

Through the 5-HT receptors and serotonylation, 5-HT mediates regulation of a large number of cellular processes both in the nervous system and in other peripheral tissues.

11.1.6.3.1 5-HT in the Central Nervous System

The central effects of 5-HT are diverse and encompass regulation of mood, appetite, thermogenesis, and many others. The discovery that 5-HT positively regulates mood has led to the wide use of SSRIs to increase 5-HT signalling centrally and treat chronic depression. In rodent models of depression, SSRIs acutely improve measurements of despair and acute depression (Holmes et al., 2002). However, in contrast, SSRIs in humans require chronic usage to achieve antidepressant effects (Pérez et al., 1997). The mechanism underlying this adaptive improvement is still debated but often believed to be due to activation of 5-HT1A autoreceptors (Richardson-Jones et al., 2010). Additionally, the synthetic psychotropic molecule, lysergic acid diethylamide (LSD), activates central 5-HT2A receptors to elicit hallucinations (Fiorella et al., 1995; González-Maeso et al., 2007). These receptors are also targets for atypical antipsychotics, such as Pimavanserin (Brand Name: Nuplazid; Abbas and Roth, 2008; Vanover et al., 2006). Reciprocally to enhancing the effects of 5-HT via inhibition of its reuptake, simultaneous elimination of *Tph2* and *Tph1* in mice demonstrate altered behavioural phenotypes including depression-like behaviour and thus provides

evidence for 5-HT/5-HT-synthesis as a regulator of affect (Fiorella et al., 1995). The specific neural networks mediated by 5-HT signalling are wide and diverse.

Central regulation of appetite is partially modulated by 5-HT. Early studies demonstrated that depletion of central 5-HT induced hyperphagia and obesity (Breisch et al., 1976). As discussed previously, the 5-HT-releasing agent, Fenfluramine, was previously used as an appetite suppressant before discovery of adverse effects likely due to the active metabolite norfenfluramine. Subsequently, elimination of the 5-HT2C receptor in mice induced dramatic hyperphagia and thus the 5-HT2C has been suggested to be the target of Fenfluramine's anorexigenic behaviour (Nonogaki et al., 1998). After the removal of Fenfluramine from the market because of its off-target effects and the elucidation the role of 5-HT2C in appetite regulation, this led to the development of the more specific 5-HT2C agonist, Lorcaserin, for suppressing appetite and promoting satiety to treat obesity (Smith et al., 2008, 2009; Thomsen et al., 2008). In addition to 5-HT2C, some evidence suggests that the 5-HT1B receptor may also inhibit appetite (Nonogaki et al., 2007). It has been proposed that within the arcuate nucleus of the hypothalamus 5-HT activates 5-HT2C receptors on the anorexigenic proopiomelanocortin (POMC) neurons which leads to the release of the anorexigenic factor – α-melanocyte-stimulating hormone (α-MSH; Tecott, 2007; Xu et al., 2008). Simultaneously, 5-HT via the 5-HT1B receptor inhibits the release of the orexigenic hormone AgRP from NPY/AgRP neurons (Tecott, 2007). Thus, activation of these two appetite suppressing receptors additively reduces appetite and increases satiety.

Complementary to the anorexigenic effects of 5-HT, central 5-HT also regulates body temperature regulation and thermogenesis. A series of studies implicated 5-HT in regulating thermal response. Elimination of *Lmx1b*, a transcription factor required for serotonergic neuron development, resulted in mice with altered thermal homeostasis and decreased interscapular surface temperature in response to cold exposure (Hodges et al., 2008). Additionally, a study in whole-body *Tph2* ablated mice also revealed an altered thermogenic cold-stress response (Alenina et al., 2009). Furthermore, a third study expressed the Diphtheria toxin receptor under the control of the serotonergic-neuron specific promoter of the *Pet1* gene (McGlashon et al., 2015). Upon treatment with Diphtheria toxin, these mice experienced a decrease in BAT temperature. Although elimination of central serotonin synthesis or elimination of serotonergic neurons implicates 5-HT in thermal regulation, the specific neural pathways cannot be elicited from these experiments. Numerous studies have revealed a complex regulatory network of neurons that control thermogenesis and BAT (Morrison et al., 2014). Administration of 5-HT to different regions of the brain result in different effects on sympathetic outflow to BAT. Therefore, although complete or near-complete loss of 5-HT within the central nervous system (CNS) causes dysregulated thermogenic responses, the specific location of 5-HT in the CNS has differential effects on BAT function.

Herein we presented a brief description of some of the 5-HT mediated mechanisms in the CNS including modulation of affect, appetite and

thermogenesis, but it should be noted that 5-HT occupies numerous additional mediator roles in the CNS that have not been discussed.

11.1.6.3.2 Tissue-Specific Effects of Peripheral 5-HT

Although the role of 5-HT in the nervous system is most often discussed, 5-HT was originally identified in the periphery as a blood borne factor. Furthermore, the vast majority of the 5-HT in the body resides in the periphery and primarily in the intestine. The peripheral effects of 5-HT are as wide and diverse as the variety of tissues in the body. They span from the initially identified regulatory roles of vascular tone and gut motility to more recently identified effects on BAT.

Initial identification of 5-HT was elicited from its vasoactive properties and are the origin of the term "serotonin" (Whitaker-Azmitia, 1999). Early research described 5-HT as a vasoconstrictive compound that induces a pressor response. Acutely, 5-HT induces vasoconstriction of numerous blood vessels throughout the body primarily through activation of the 5-HT2A receptor on smooth muscle (Watts et al., 2012). Although, pharmaceuticals, such as Ketanserin (a 5-HT2A antagonist), have been developed with the intention to treat hypertension (de Cree et al., 1981), no drug has yet to be approved in North America. In the UK, the 5-HT2 pan-antagonist, Naftidrofuryl, is marketed as a vasodilator for peripheral artery disease (de Backer et al., 2012).

In addition to regulating vascular tone, 5-HT also regulates thrombus formation. Platelets carry large amounts of 5-HT throughout the circulation (Humphrey and Jaques, 1954; Zucker et al., 1954). Upon activation, 5-HT is

released from platelets and stimulates additional aggregation, activation of nearby platelets and local vasoconstriction, again via 5-HT2A receptors (de Clerck et al., 1982; Lindblad et al., 1984). In Japan, Sarpogrelate, a 5-HT2A receptor antagonist is approved for treating poor blood perfusion by inhibiting platelet activity and vasoconstriction (Tanabe and Corporation, 2012). Thus, complementary to the vasoconstrictive effects of 5-HT, 5-HT also promotes thrombus formation at wounds to reduce blood loss.

5-HT also plays a crucial but complicated role in the heart. As mentioned above, Fenfluramine, was removed from the market due to severe cardiac valvulopathy (Connolly et al., 1997). This was subsequently attributed to adverse agonist activity of the fenfluramine metabolite, norfenfluramine, on the 5-HT2B receptors on heart valves (Roth, 2007; Rothman et al., 2000). Additionally, *Tph1*$^{-/-}$ mice experience hypertrophic cardiomyopathy and eventual heart failure (Côté et al., 2003). Therefore, in addition to its effects on vascular tone and hemostasis, 5-HT/5-HT synthesis also regulates cardiac tissue.

Prior to the structural determination of 5-HT, there was a parallel discovery of a gut hormone that regulated gut-motility, termed “enteramine”. This hormone was later confirmed to be 5-HT and is consistent with the high abundance of 5-HT within the intestinal epithelium. Surprisingly, mice lacking *Tph1* have dramatically lower 5-HT levels within the intestine (Walther et al., 2003a) but had no observed effect on gut motility (Li et al., 2011). Using *Tph2* ablated mice, TPH2-dervied 5-HT was found to reduce gut motility. Additionally, to treat carcinoid syndrome-

induced diarrhea LX-1032, a peripherally-restricted TPH1/TPH2 inhibitor, was developed and approved for clinical use (Kulke et al., 2014; Liu et al., 2008).

Further, 5-HT also plays an important role in regulating liver homeostasis and regeneration. Mice lacking *Slc6a4* preferentially accumulate lipid compared to control mice in response to an HFD and high sucrose diets (Chen et al., 2012). Consistent with this, 5-HT3 receptor antagonists (Oh et al., 2015), *Htr2a* ablation (Choi et al., 2018) and TPH1 inhibitors (Crane et al., 2015; Namkung et al., 2018) decrease hepatic lipid accumulation in mouse models. Additionally, through the use of 5-HT2A and 5-HT2B agonists/antagonists and genetic ablation of *Tph1,* Lesuertel et al. (2006) demonstrated that 5-HT receptors facilitate liver regeneration in response to liver injury and that genetic ablation of *Tph1* decreases platelet 5-HT and impairs liver regeneration. As such, 5-HT appears to regulate both liver metabolism and regeneration.

In addition to regulating liver metabolism, 5-HT modulates glucose metabolism in muscle. Acute treatment with 5-HT increases glucose uptake into both cultured myotubes and skeletal muscle via the 5-HT2A receptor (Hajduch et al., 1999). Furthermore, the 5-HT2A receptor activates Phosphofructokinase (PFK) in skeletal muscle (Coelho et al., 2007). Others have suggested this might also contribute to anti-obesogenic effect of extremely high doses of 5-HT (Watanabe et al., 2016). Albeit, the intermittent (2x/week) and high single doses of 5-HT (~30-40 mg/kg) likely led to large quantities of 5-HT metabolites. As a whole, this

suggests that high concentrations of 5-HT might positively regulate glucose disposal into muscle.

Consistent with the regulation of liver lipid metabolism and muscle glucose disposal, 5-HT directly regulates insulin secretion from pancreatic β-cells. During pregnancy, 5-HT3 is required for maintenance of glycemic control and glucose stimulated insulin secretion (GSIS; Ohara-Imaizumi et al., 2013). Additionally, other groups have demonstrated that 5-HT via intracellular serotonylation is required in infantile mice for insulin secretion capacity and glucose tolerance (Paulmann et al., 2009). Notably, this is in contrast to adult *Tph1*$^{-/-}$ mice, which have improved glucose tolerance (Crane et al., 2015).

11.1.6.4 5-HT and Obesity

Numerous studies have investigated the effect of 5-HT or 5-HT receptor modulators on obesity. Early studies quickly identified a regulatory role of 5-HT on appetite and obesity (Kruk, 1973). Subsequently, investigations into the use of 5-HT modulating drugs to treat obesity through reducing appetite commenced.

These included the use of SSRIs which had mixed results on obesity. Some SSRIs such as Fluoxetine were found to suppress appetite (Wurtman and Wurtman, 1977) while others have since proven to increase weight gain in preclinical and clinical trials (Serretti and Mandelli, 2010). Additionally, post-approval studies confirmed these findings and showed weight loss initially but subsequent weight gain depending on the SSRI and duration of treatment (Serretti and Mandelli, 2010). Numerous studies have also associated polymorphisms in 5-HT transport and

degradation genes with obesity (Hinney et al., 1997; Sookoian et al., 2008). Consistent with this, mice lacking *Slc6a4* (encoding SERT, the target of SSRIs) are prone to obesity (Chen et al., 2012; Murphy and Lesch, 2008; Üçeyler et al., 2010; Zha et al., 2017). However, the mechanism underlying this sensitivity is currently unknown.

In addition to SSRIs, as discussed above, 5-HT receptor agonists have been used to treat obesity. The central 5-HT2C receptor agonist, Fenfluramine, was approved as an anti-obesity medication in the early 1990s (Connolly et al., 1997). However, as discussed above was removed from the U.S. and Canadian markets after severe cardiac affects (Connolly et al., 1997). A new 5-HT2C agonist, Lorcaserin, was approved in the U.S.A. to reduce appetite and obesity; however, has recently been removed from the market (U.S. Food and Drug Administration, 2020). Both 5-HT2C agonist and SSRIs, share a similar mechanism of action of increasing central 5-HT signalling to reduce appetite.

In contrast to this mechanism, recent work suggests that peripheral 5-HT may both be affected in obesity and regulate obesity. An early study in patients with Type 1 diabetes demonstrated elevated circulating levels of 5-HT (Malyszko et al., 1994). Recent studies have shown that lifestyle interventions in obese children reduce circulating 5-HT levels (Ojeda-Rodríguez et al., 2018). In one study in rodents, systemic plasma 5-HT increased 7.5-fold in response to a 60% HFD (Kim et al., 2011). Another study showed elevated 5-HT in the portal vein of mice fed a HFD (Choi et al., 2018) and is consistent with observations that the release of 5-

HT from the intestine appears to be augmented in high cholesterol diet fed animals (Bertrand et al., 2011) and obese humans (Young et al., 2018). Additionally, some studies have shown that murine adipose tissue 5-HT increases in response to HFD feeding (Crane et al., 2015; Oh et al., 2015). Notably, this increase appears much greater in WAT than BAT (Oh et al., 2015). However, in contrast to the above studies, there are many studies that show 5-HT not changing or decreasing with obesity or HFD-feeding. A study in humans found reduced platelet-poor plasma 5-HT in obese versus lean humans (Blum et al., 1993) and a more recent study found similar findings in obese women (Cussotto et al., 2020). Similar to these findings, other studies with mice found decreased 5-HT in platelet poor plasma (Rami et al., 2018) and in BAT (Ikegami et al., 2018) with HFD-feeding and are consistent with additional unpublished findings from the Steinberg laboratory where BAT or platelet poor plasma 5-HT either does not change or decreases in response to HFD in mice. Some of this variability in 5-HT correlations with obesity may be due to the known variability in isolating platelet poor plasma (Brand and Anderson, 2011); however, the majority of the current rodent evidence suggests that systemic platelet-poor plasma and BAT 5-HT decrease in response to a HFD feeding in contrast to previously published results (Crane et al., 2015).

In addition, or in replace, of measuring 5-HT some studies have measured 5-HIAA – a major metabolite of 5-HT – in patients with obesity. This seems likely based off of the clinical practice of diagnosing patients with carcinoid tumors (neuroendocrine tumors that primarily secrete 5-HT) by measuring 5-HIAA in urine

which parallels changes in serum 5-HT and severity of clinical outcomes - particularly diarrhea (Feldman, 1978). Similar to 5-HT, there is contradicting reports of 5-HIAA levels in patients with obesity. Circulating 5-HIAA positively correlates with obesity (Afarideh et al., 2015) whereas urinary 5-HIAA is decreased in children with obesity (Popa et al., 1989). Furthermore, the pro-adipogenic properties of metabolites down stream of 5-HIAA may be related to their known PPARɣ agonist activity and complicate its use as a marker for 5-HT levels (Waku et al., 2010). Despite the contradictory evidence of the effect of obesity on 5-HT levels both in circulation and adipose tissue, the effects of peripheral 5-HT on obesity are still of interest and actively explored.

Similar to the contradictory evidence of 5-HT levels during obesity, the effects of peripheral 5-HT on weight gain and/or adipose tissues have not always been consistent. Early research demonstrated that administration of 5-HT peripherally reduced food intake (Edwards and Stevens, 1989; Fletcher and Burton, 1984; Kanarek and Dushkin, 1988; Pollock and Rowland, 1981). Furthermore, administration of 5-HT has led to increased metabolism via bile acid turnover (Watanabe et al., 2010) and weight loss via muscle (Watanabe et al., 2016). However, in contrast to this, reducing 5-HT via genetic ablation or inhibition of the rate limiting step in serotonin synthesis, TPH1, rendered mice resistant to HFD-induced weight gain (Crane et al., 2015; Oh et al., 2015). Although these studies demonstrated that the absence of peripheral serotonin synthesis reduced weight gain, they did not show a causative effect of peripheral 5-HT administration on

weight gain. Therefore, additional research is required to reconcile the contrasting effects of peripheral 5-HT administration promoting weight gain and the inhibition of peripheral 5-HT synthesis on attenuation of obesity.

Although 5-HT has been well studied in obesity and central serotonin is an active target of pharmacological strategies to reduce appetite in obese patients, the roles of 5-HT in other compartments, such as the periphery, remain to be clearly elucidated.

11.1.6.5 Effects of Peripheral 5-HT on WAT

The generation 5-HT within WAT and the effects of 5-HT therein are an active area of investigation. Some studies have suggested that *in vitro* differentiated WAs express *Tph1*, synthesize and store 5-HT (Stunes et al., 2011). Furthermore, loss of *Tph1* in 3T3-L1 pre-adipocytes prevent differentiation and 5-HT-treatment promotes adipogenesis (Kinoshita et al., 2010). 5-HT2A is expressed in WAs and high concentrations (≥ 10 μM) of 5-HT and 5-HT2A agonists impair WA lipolysis (Hansson et al., 2016). Furthermore, metabolites of amine oxidase (e.g. MAO) substrates reduce WA lipolysis (Visentin et al., 2003). Similarly, 5-MIAA, a major 5-HT metabolite promotes WA adipogenesis via activation of PPARɣ (Waku et al., 2010). In contrast, one study, using mice lacking *Tph1* in enterochromaffin cells, suggested that, during fasting, 5-HT is released from the intestine and stimulates lipolysis in WAT (Sumara et al., 2012). However, it is noteworthy that many of these experiments had not been repeated in BAs. While the *in vitro* data suggests

that 5-HT increases adipogenesis and impairs lipolysis, indirect *in vivo* data might suggest that 5-HT promotes lipolysis and therefore requires further investigation.

11.1.6.1 Effect of Peripheral 5-HT on BAT

While many studies have investigated the effects of central 5-HT on BAT, recent revelations in the field have reignited interest in the effects of peripheral 5-HT on BAT. An early study found detectable amounts of 5-HT in BAT (Stock and Westermann, 1963). One study found 5-HT to be primarily stored in mast cells, released in response to acute cold stimulus and accumulates in response to chronic cold stimulus (Mory et al., 1984). Another study demonstrated that administration of 5-HT to BAT increased FFA production (Steiner and Evans, 1976). However, this was due to a direct effect of 5-HT on efferent neurons in BAT, promoting their release of norepinephrine and consequently stimulating the release of FFAs. In contrast, recent studies found that direct treatment of cultured BAs with high concentration of 5-HT (100 μM) impaired cAMP and *Ucp1* mRNA levels in response to adrenergic stimuli (Crane et al., 2015) and others have found that 5-HT activation of 5-HT2A on BAs impairs differentiation (Rozenblit-Susan et al., 2018). Therefore, it appears that high dose 5-HT might directly impair BA substrate mobilization (i.e. lipolysis) and differentiation in cell culture, but in intact tissue increases local NE release from neurons.

Despite the contradictory evidence *in vitro* of the effects of 5-HT, two studies in short succession identified that mice lacking *Tph1* or treated with TPH1/2 inhibitors were resistant to high-fat diet induced weight gain (Crane et al., 2015;

Oh et al., 2015). These mice contained BAT with high levels of UCP1 and had elevated oxygen consumption when corrected to body mass. Furthermore, *Tph1* in mast cells was identified as a regulator of beige adipocytes in WAT (Yabut et al., 2020; Zhang et al., 2019). In one study, 5-HT was reintroduced into *Tph1*$^{-/-}$ mice by implanting 5-HT slow release pellets in the intrascapular region and found that BAT thermogenic capacity was reduced (Crane et al., 2015). This suggested that local 5-HT in *Tph1*$^{-/-}$ mice was an inhibitor of BAT function. Notably, despite this reduced BAT activity, these mice did not gain more weight versus control animals as expected, suggesting that although local 5-HT may impair BAT function, this did not result in increased weight gain. Another recent study found that intravenous administration of 5-HT to the periphery decreases sympathetic nerve activity to BAT (Mota et al., 2020), thus suggesting that peripheral 5-HT can inhibit CNS circuits that activate BAT. This evidence suggests that peripheral 5-HT synthesis is an inhibitor of BAT but the direct effects of physiological levels of 5-HT on BAs and the mechanisms/receptors that mediate these effects on BAs remain to be elucidated.

12 Aims and Objectives

Based upon the previous evidence, we hypothesized that 1) 5-HT inhibited BAT-mediated EE, 2) this was mediated by a 5-HT receptor or receptors, 3) inhibiting this mechanism would increase EE and 4) inhibiting this mechanism would also prevent SSRI-induced weight gain. The overall aims of this thesis were thus 1) to describe the effects of 5-HT on BAs and mouse EE, 2) to identify which 5-HT receptor or receptors may mediate these effects and 3) to investigate if blocking these receptors could increase BAT thermogenesis and attenuate SSRI-induced weight gain. The ultimate objective being the identification of a 5-HT receptor antagonist that might reproduce the effects of TPH1 inhibitors on BAT and subsequently EE.

13 Methods

13.1 Origin/Generation of Cell Lines

All experiments were performed in cultured adipocytes differentiated from immortalized adipocyte progenitors. Progenitor cell lines were either a generous gift from Dr. James Granneman (Uldry et al., 2006; SpBAT cells) or newly generated within the laboratory. New cell lines were created from wild type FVB/N-Tg (female; hereafter called TMCON cells), ThermoMouse (FVB/N-Tg$^{(Ucp1\text{-}Luc2\text{-}tdTomato)1Kajim}$; Galmozzi et al., 2014; male; TM cells), wild type C57Bl/6 (littermates of B6.129(Cg)-Slc6a4^{tm1Kpl}/J – i.e. *Slc6a4*$^{-/-}$ mice; *Slc6a4*$^{+/+}$ cells), *Slc6a4*$^{-/-}$ (Bengel et al., 1998; *Slc6a4*$^{-/-}$ cells), wild type C56Bl/6;129 (littermates of *Htr2a*$^{-/-}$ mice; *Htr2a*$^{+/+}$ cells), and *Htr2a*$^{-/-}$ (C57Bl/6;129-5-HT2A$^{tm1a/Nju}$; *Htr2a*$^{-/-}$ cells) mice.

Briefly, BAT was excised from 4-day-old pups, minced and digested with collagenase II (2 mg/mL in HKRB - HEPES Krebs-Ringer buffer containing: 10 mM HEPES, 1 mM $CaCl_2$ - with 4% BSA and 1% Anti-Anti) at 37ºC until well dissociated. The slurry was filtered through a 100 μm cell strainer and plated in 1 mL of high glucose DMEM supplemented with 20% FBS and 1% Anti-Anti. Following 12 hours, cells were infected with a pBABE-puro-SV40 LT (a gift from Thomas Roberts - Addgene plasmid # 13970; http://n2t.net/addgene:13970; RRID:Addgene_13970) containing retrovirus derived from the Phoenix-ECO packaging cell line (Pear et al., 1993). The initial infection media was supplemented with Polybrene. Subsequently, cells were selected for SV40LT integration for 7

days with puromycin. Cells were treated for an additional 14 days with ciprofloxacin to remove potential mycoplasma contamination and passaged as necessary to avoid ≥ ~80% confluence.

Following immortalization, all cell cultures were maintained in DMEM supplemented with 10% fetal bovine serum (FBS) and 1% Anti-Anti. Pre-adipocytes were differentiated as per Uldry et al. (2006). Cells were seeded at either 5,000 or 10,000 cells/cm^2 (based on success of differentiation as per oil red o staining). Subsequently, 2 days later cells were induced to differentiate (day 0) by treating cells for 2 days with 125 μM indomethacin, 0.5 μM dexamethasone, 500 μM 3-isobutyl-1-methylxanthine (IBMX), 20 nM insulin and 1 nM triiodothyronine (T3). Adipocytes were then allowed to mature in the presence of 20 nM insulin and 1 nM T3 for an additional 5 days (SpBAT) or longer (TM and TMCON cells; 7-10 days). Unless noted, all cultured adipocytes were used at 7-12 days after initiation of induction.

Unless otherwise noted, SpBAT cells were used for NEFA release assays. TM cells were used for Ucp1 promoter activity assays and TMCON cells were used for ECAR, *Ucp1* mRNA and UCP1 protein experiments because they expressed much greater levels of *Ucp1* mRNA than SpBAT cells.

13.2 Human Primary Adipocyte Progenitor Culture

Human brown and white adipocyte progenitors were cultured in the laboratory of Dr. Camilla Scheele according to their previous methods (Jespersen

et al., 2013). Briefly, biopsies from supraclavicular and abdominal subcutaneous adipose tissue depots were obtained, digested in a DMEM/F12 solution supplemented with 1 mg/mL collagenase II and fatty acid-free BSA (15 mg/mL), strained, pelleted and seeded in DMEM/F12 supplemented with 1% penicillin-streptomycin and 10% FBS.

Before inducing differentiation, cells were cultured in DMEM/F12 supplemented with 10% FBS, 1% penicillin-streptomycin and 1 nM Fibroblast Growth Factor-Acidic (FGF-1). After cells reached confluence to induce differentiation, cells were cultured in DMEM/F12 augmented with 0.1 µM dexamethasone, 100 nm insulin, 200 nm rosiglitazone, 540 µM IBMX, 2 nM T3 and 10 µg/mL transferrin for 3 days. After induction, cells were maintained in the same medium but without IBMX for an additional 12 days.

13.3 Mouse Lines and Experiments

All mice were housed under standard housing conditions at the McMaster University Central Animal Facility and all experiments were approved by the McMaster University Animal Research Ethics Board. Unless otherwise stated all mice were housed at ~22ºC and fed *ad libitum* a standard chow diet (17% kcal fat; Diet 8640, Harlan Teklad, Madison, WI). Lighting was under the control of a 12-hour light/dark cycle beginning with lights on at 7:00 am and lights turning off at 7:00 pm. Xylamidine was delivered IP at 3 mg/kg for acute treatments. For chronic treatments, Xylamidine was initially delivered at 3 mg/kg for ~3 weeks and

subsequently reduced to 1.5 mg/kg for the remainder of treatment. For acute treatments, Paroxetine was administered via IP injection at dose of 10 mg/kg. For chronic treatment, Paroxetine was administered via the drinking water at a dose of 10 mg/kg/day.

For chronic injection experiments, C57Bl/6J mice from The Jackson Laboratory were used. *Slc6a4*$^{-/-}$ (B6.129(Cg)-Slc6a4^{tm1Kpl}/J; Bengel et al., 1998) and ThermoMouse (FVB/N-Tg$^{(Ucp1\text{-}Luc2\text{-}tdTomato)1Kajim}$; Galmozzi et al., 2014) mice were purchased from The Jackson Laboratory. Heterozygous *Slc6a4*$^{+/-}$ parents were bred together to generate homozygous *Slc6a4*$^{+/+}$ and *Slc6a4*$^{-/-}$ mice. At all times littermate controls of the same age were used. *Htr2a*$^{-/-}$ and *Htr2a* AdKO mice were rederived/generated as describe below.

13.4 *Htr2a*$^{-/-}$ (C57Bl/6;129-5-HT2A$^{tm1a/}$Nju) Mouse Rederivation

Female *Htr2a*$^{+/-}$ mice (C57Bl/6;129-5-HT2A$^{tm1a/}$Nju) were rederived from frozen sperm at the NBRI (Nanjing Biomedical Research Institute of Nanjing University) and received at the Central Animal Facility of McMaster University. Following quarantine, health checks and acclimatization, female *Htr2a*$^{+/-}$ mice were bred with male C57Bl/6J mice from The Jackson Laboratory or used to generate *Htr2a* AdKO animals (see below). Non-littermate pups, from the *Htr2a*$^{+/-}$ x C57Bl/6J cross, heterozygous for *Htr2a* were then bred together. The consequent offspring were either used to generate *Htr2a*$^{-/-}$ cell lines or pilot experiments with

whole body *Htr2a*$^{-/-}$ mice. All mice were checked for genotype before using. Genotyping primers were as follows: Forward – 5'-CAATAACTCGCTGCTTTCTC-3' and Reverse – 5'-TTACCTGATAACTGTCAATATGA-3'. The expected amplicon sizes were 339 base pairs and 451 base pairs for *Htr2a*$^{+/+}$ and *Htr2a*$^{-/-}$ mice, respectively.

13.5 *Htr2a* AdKO Mouse Generation

To generate mice that lacked *Htr2a* selectively in adipose tissue and under temporal control, first *Htr2a*$^{+/-}$ mice were bred with FLPo expressing mice (B6.129S4-Gt(ROSA)26Sor$^{tm2(FLP*)Sor}$/J purchased from The Jackson Laboratory; Raymond and Soriano, 2007). This excised both an interrupting *lacZ* and interrupting neomycin resistance (*Neo*) gene sequence from the integrated targeting vector and thus generated C57Bl/6;129-5-HT2A$^{tm1c/}$Nju mice (according to the IMPC standard nomenclature - https://www.mousephenotype.org/about-impc/targeting-strategies/; herein termed *Htr2a LoxP* mice). *Htr2a LoxP* mice were then bred with *AdipoQ-CreERT2* mice from Dr. James Granneman (Mottillo et al., 2014). Offspring negative for *Neo*, positive/negative for *Cre* and positive for *LoxP* were then used for future breeding. Experiments were performed in *LoxP*$^{+/+}$ and *Cre*$^{-/-}$ (herein WT) or *LoxP*$^{+/+}$ and *Cre*$^{+/-}$ (herein *Htr2a* AdKO) littermate animals. All mice were checked for genotype before using. Genotyping primers were as follows: *FlpO* – Forward – 5'-AAAGTCGCTCTGAGTTGTTAT-3', Null Reverse – 5'- GGAGCGGGAGAAATGGATATG-3', and Mutant Reverse – 5'-

GCGAAGAGTTTGTCCTCAACC-3'; *LoxP* – Forward – 5'-CAATAACTCGCTGCTTTCTC-3' and Reverse – 5'-TTACCTGATAACTGTCAATATGA-3'; *Cre* – Forward – 5'-ATGTCCAATTTACTGACCG-3' and Reverse – 5'-CGCCGCATAACCAGTGAAAC; *Cre*-Control – Forward – 5'-CAATCCTGGAGAAAACGCAC-3' and Reverse – 5'-CAGAACACAGCACGGAAAGA-3'; *Neo* – Forward – 5'-CTTGGGTGGAGAGGCTATTC-3' and Reverse – 5'-AGGTGAGATGACAGGAGATC-3'; *Neo*-Control – Forward – 5'-CAAATGTTGCTTGTCTGGTG-3' and Reverse – 5'-GTCAGTCGAGTGCACAGTTT-3'. The expected amplicon lengths are as follows: *FlpO* positive – 340 and 650 base pairs; *FlpO* negative – 650 base pairs; *LoxP* positive – 339 base pairs; *LoxP* negative – 451 base pairs; *Cre* – 350 base pairs; *Cre*-Control – 800 base pairs; *Neo* – 280 base pairs; and *Neo*-Control 210 base pairs. To induce deletion mice were administered 100 mg/kg tamoxifen daily (dissolved in a solution of 10% EtOH in sunflower oil) via oral gavage for 5 consecutive days.

13.1 *In vivo* Thermogenesis Assays

BAT capacity was assessed as per Crane et al. (2014). Briefly, mice were anaesthetized using Avertin (tribromoethyl alcohol in tert-amyl alcohol) and on two different days (separated by a minimum of two days) received, two minutes later,

either saline or CL-316,243. Mice were then placed in an enclosed treadmill connected to a metabolic cage assessment tool (Comprehensive Laboratory Animal Monitoring System; CLAMS – Columbus Instruments; Columbus, Ohio, USA) to collect VO_2 values from 17-19 minutes following anaesthetization. Immediately following VO_2 measurements, an infrared image was obtained using a FLIR T650sc camera (FLIR Systems; Wilsonville, Oregon, USA) at 20 minutes following Avertin administration. Unless otherwise noted, each mouse received both saline and CL-316,243 on separate days. Mice with VO_2 measurements after CL-316,243 administration of less than ~500 mL/kg/hr above saline elicited levels were repeated on a subsequent day to confirm the accuracy of the result.

13.2 Metabolic Cage Assessments

Whole body free moving metabolism was measured in a comprehensive laboratory animal monitoring system as previously described (O'Neill et al., 2011). Briefly, mice were placed individually in metabolic cages with *ad libitum* access to food and water at an approximate temperature of 24ºC unless otherwise noted. Mice were allowed to acclimatize for a minimum of 12 hours. Oxygen consumption rates (VO_2), CO_2 production rates (VCO_2), activity (ambulatory and total) in the X-axis, feeding amount and drinking volume were measured for a minimum of 48 hours after acclimation. To reduce potential noise from instrument measurement errors, readings from the first 24 hours were averaged with the corresponding time point during the second 24 hours.

13.3 Body Composition Measurements

Mice were weighed weekly with a standard laboratory balance. A 3-component measurement of body composition was obtained from using a Bruker MiniSpec LF90II Body Composition Analyzer (Billerica, Massachusetts, USA). Fluid, fat and lean mass were then analyzed individually and as a percentage of total body mass.

13.4 Glucose (GTT) / Insulin Tolerance Tests (ITT)

All mice began fasting for 6 hours between 7:00 and 9:00 am. Using a OneTouch® Blood Glucose monitor (LifeScan Canada; Burnaby, BC, Canada), baseline blood glucose measurements (0 minutes) were taken immediately after a small incision was made on the tail. Subsequently mice received an intraperitoneal injection of either glucose (for GTTs) or insulin (NovoRapid – Novo Nordisk A/S, Bagsvaerd, for ITTs) at the indicated doses. Blood glucose was measured at 20, 40, 60, 90 and 120 minutes after glucose/insulin injection. For each animal, individual glucose tolerance/insulin tolerance was calculated by approximating the integral for each animal's individual glucose response using Prism 8 (GraphPad Software, San Diego, California, USA).

13.5 Oil Red O (ORO) Staining

Following treatment, cells were rapidly rinsed with PBS and fixed in room-temperature 10% formalin for 30 minutes. Subsequently, cells were washed with PBS and 60% isopropanol. Fresh Oil Red O staining solution was made by diluting a 5 mg/mL Oil Red O solution (in 100% isopropanol) 3:2 with ddH_2O. Following 20 minutes of rest, the solution was filtered through a 0.2 μm filter. Immediately, staining solution was added to cells for 10 minutes at room temperature. Cells were then washed with 60% isopropanol once and 4 times with PBS. For imaging, cells were maintained in PBS. For quantification all PBS was removed, cells were dried and the ORO eluted by adding 100% isopropanol with gentle shaking. The subsequent eluent was transferred to a microtiter plate and the optical density at 500 nm measured.

13.6 Origin of Compounds for Experiments

5-HT HCl was purchased from Cayman Chemical (Ann Arbor, Michigan, USA). All 5-HT receptor antagonists and agonists were obtained from Tocris Bioscience (Bristol, UK) except for xylamidine tosylate (herein Xylamidine or Xyl) which was purchased from Kemprotec Limited (Cumbria, UK). Paroxetine HCl (herein Paroxetine) was purchased from Ark Pharma Inc. (Libertyville, IL, USA).

Table 3. List of investigative compounds used herein and their respective targets of interest.

Pharmaceutical Agent	Abbreviation	Intended/Presumed Target
4-(4-Dimethylamino)phenyl-1-methylpyridinium iodide	APP+	Fluorescent Serotonin Transporter Substrate
A23187		Calcium Ionophore
Altanserin		5-HT2A Antagonist
Antimycin A	Anti A	Mitochondrial Complex III Inhibitor
Avertin		Anaesthetic
BRL-54443		5-HT1E/F Agonist
Carbonyl cyanide-p-trifluoromethoxyphenylhydrazone	FCCP	Mitochondrial Uncoupler
Citalopram		Serotonin Transporter Inhibitor
CL-316,243	CL	β3-Adrenergic Receptor Agonist
Corticosterone		Investigated as potential OCT3 and PMAT Inhibitor
Decynium-22	D-22	OCT3 and PMAT Inhibitor
EMD-281014	EMD	5-HT2A Antagonist
Fluoxetine		Serotonin Transporter Inhibitor
GR-113808		5-HT4 Antagonist
GR-127935		5-HT1D Antagonist
Hydrocortisone		Investigated as potential OCT3 and PMAT Inhibitor
Isoproterenol	Iso	β-Adrenergic Receptors Agonist
Ketanserin		5-HT2A Antagonist
LY-344865		5-HT1F Agonist
MDL-100907	MDL	5-HT2A Antagonist
Methylphenidate		Dopamine and Norepinephrine Transporter Inhibitor

Pharmaceutical Agent	Abbreviation	Intended/Presumed Target
N-acetylcysteine	NAC	Glutathione precursor and subsequent ROS scavenger
NBOH-2C-CN	NBOH	5-HT2A Agonist
Oligomycin	Oligo	ATP-Synthase Inhibitor
Ondansetron		5-HT3 Antagonist
Paroxetine	Par	Serotonin Transporter Inhibitor
R(-)N6-(2-phenylisopropyl) adenosine	PIA	A_1 Adenosine Receptor Agonist
Rotenone	Rot	NADH Dehydrogenase Inhibitor
RS-56812		5-HT3 Agonist
Sarpogrelate		5-HT2A/B Antagonist
SB-204741		5-HT2B Antagonist
SB-242084		5-HT2C Antagonist
SB-258719		5-HT7 Antagonist
SB-399885		5-HT6 Antagonist
Serotonin	5-HT	5-HT Receptors Agonist
TCB-2		5-HT2A Agonist
Tropisetron		5-HT3 Antagonist
Xylamidine	Xyl	Peripherally-restricted 5-HT2A Antagonist

13.7 Non-Esterified Fatty Acid (NEFA) Assay

Unless otherwise noted, NEFA assays were completed on SpBAT cells 7 days post initiation of differentiation. To do so, cells were washed with PBS and then incubated in HKRB supplemented with 1% fatty acid free bovine serum albumin (BSA). For non-adrenergic agonist experiments, compounds (e.g. 5-HT) were added 30 minutes prior to the addition of either a vehicle (DMSO) or adrenergic agonist (isoproterenol – Iso; norepinephrine – NE, etc. as indicated). For

antagonist experiments, antagonists were added 30 minutes prior to agonist addition. Unless otherwise indicated, media was immediately collected 60 minutes after adrenergic agonist addition. Media was then assayed using the HR Series NEFA-HR(2) kit from Wako Diagnostics (Mountain View, California, USA).

13.8 Extracellular Acidification Rate (ECAR) Assay

ECAR was assessed using a method modified from Yang and Balcarcel (2003). Differentiated cells were changed into bicarbonate-free, pyruvate-free DMEM supplemented with 11 mM D-glucose, 2 mM L-glutamine and 25 mg/L phenol red at a pH of 7.8. Cell culture plates were then interrogated for optical density at 560 nm and 480 nm in a SpectraMax M5 microplate reader heated to 37ºC. Following an initial settling period, readings for basal ECAR were collected. 5-HT and Iso were sequentially injected with corresponding 30-minute periods of data collection. Each absorption value at 480 nm (control) were subtracted from absorption values at 560 nm to obtain corrected values. Rates were calculated by taking the average slope over each incubation time period and corrected for potential drift to values from cell-free wells.

13.9 Oxygen Consumption Assays

Oxygen consumption from cell cultures was measured using PreSens Oxoplates (Regensburg, Germany) with chemical stimuli similar to Seahorse MitoStress Tests (Santa Clara, California, USA). Briefly, differentiated cells were

transferred from culture flasks to Oxoplates (excluding outer wells) ensuring to maintain similar cell density in the smaller surface area. The following day, media was removed and replaced with respiration media (DMEM supplemented with 4% fatty-acid free BSA and bubbled with 100% oxygen; 100 µL/well). For each plate, a 0% oxygen control created from a ddH_2O solution with 10 mg/mL sodium sulfite and a cell-free 100% oxygen control consisting of respiration medium was placed in the outer wells and used for calibration. Following ≥ 45 minutes of adaptation, wells were then sealed with 75 µL of mineral oil to prevent oxygen egress or entry. Measurement of fluorescence emission at 645 nm and 590 nm in response to excitation at 530 nm were then obtained with a SpectraMax M5 plate reader. Following detection of a steady state baseline measurement of decreasing dissolved O_2 concentrations, injections of solutions of DMSO/5-HT, oligomycin A (2.5 µM), isoproterenol (1 nM – 1 µM), FCCP (1 µM), and rotenone (2 µM) with antimycin A (2 µM) were sequentially injected. Data measurements were obtained in between injections. Experiments were continued only if sufficient dissolved O_2 remained for respiration.

13.10 Western Blotting

Upon completion of treatment, adherent cells were rapidly rinsed with RT PBS and flash frozen in liquid nitrogen. Cells were then thawed in lysis buffer consisting of 50 mM HEPES, 150 mM NaCl, 100 mM NaF, 10 mM Na-Pyrophosphate, 5 mM EDTA, 25 mM sucrose, 1 mM DTT, 1% Triton-X, 1 mM

sodium orthovanadate, 1% protease inhibitor solution (Roche cOmplete, mini protease inhibitor cocktail tablets) under gentle agitation in an orbital plate shaker. After transferring the cells to a microcentrifuge tube, cells were vigorously vortexed and spun at 16,000 x g for 10 minutes at 4ºC. The supernatant was transferred into a new microcentrifuge tube and stored at -80ºC.

Protein quantification was performed using a BCA™ Protein Assay Kit from Fisher Scientific (Ottawa, Ontario, Canada). Standards were supplemented with equal volumes of lysis buffer to correct for any interference by lysis components (i.e. DTT). Subsequently, lysates were diluted in Laemmli buffer and then boiled for 5 minutes at 95ºC.

Samples were separated by size by loading 1-25 μg, unless otherwise indicated, in a 10% SDS-PAGE gel and separating using a Bio-Rad™ Mini Protean Tetra System (Bio-Rad Laboratories; Hercules, California, USA). To compare samples separated on multiple gels, a common vehicle/control sample was loaded on all gels from the same experiment and further loaded at a diluted ratio of 1:4 to confirm that no reagents or saturation of camera exposure limited detection. Following separation, protein was transferred to a nitrocellulose cell membrane using a BioRad™ Mini Trans-Blot (Hercules, California, USA).

Following protein transfer to the nitrocellulose membrane and to prevent further protein binding, the membrane was blocked using a 5% BSA in TBST solution for 60 minutes at RT. Membranes were interrogated with primary antibodies (1:1000 anti-UCP1 – UCP11-A – ADI Technologies – San Antonio,

Texas, USA; 1:500 anti-5-HT2A – 24288 – Immunostar – Hudson, Wisconsin, USA; 1:1000 anti-PKA P-Substrates – 9624 – Cell Signalling Technologies; 1:1000 anti-PKC P-Substrates – 6967 – Cell Signalling Technologies; and 1:5000 anti-β-Actin – 5125 – Cell Signalling Technologies – Danvers, Massachusetts, USA) diluted in 5% BSA in TBST overnight at 4ºC. Subsequently, membranes were rinsed for 5 minutes with TBST and then probed with an HRP-conjugated (horseradish peroxidase) secondary antibody (1:10000 anti-Rabbit IgG – 7074 – Cell Signalling Technologies – Danvers, Massachusetts, USA) in 5% BSA in TBST for 60 minutes at RT. Membranes were washed 3 times with TBST.

For detection, membranes were incubated with SuperSignal West Femto Chemiluminescent Substrate (PI34096 – ThermoFisher Scientific – Waltham, Massachusetts, USA) and detected with a standard Charge-coupled device (CCD) camera imaging system. Multiple exposures were obtained, and image exposure histograms were examined to ensure the CCD was not saturated. Quantification of band size and intensity were performed using FIJI software following rolling ball background correction.

13.11 Quantitative Polymerase Chain Reaction (qPCR) Assays

Cells were rapidly rinsed with RT PBS and flash frozen in liquid nitrogen. Cells were lysed with Qiagen RLT buffer with gentle agitation on an orbital plate shaker. RNA extraction from lysates was performed using a Roche High Pure RNA

Isolation kit as per the manufacturer's recommended protocol (excluding the lysis step). RNA yield (absorption at 260 nm) and quality (ratio of absorption at 260/280 nm and 260/230 nm) were quantified on a spectrophotometer (Implen NanoPhotometer – Munich, Germany).

Creation of complementary DNA (cDNA) was performed using 3 µL of 10 mM/µL dNTPs, 12 µL of First Strand Buffer, 3 µL of 0.1 M DTT, 0.9 µL of 200 U/µL of SuperScript III Reverse Transcriptase (18080044 – ThermoFisher Scientific), 1.5 µL of 50 ng/µL random hexamers (N8080127 – Applied Biosystems) and the remaining RNAse/DNase Free H_2O to a total of 60 µL. Prior to cDNA creation, DNAse inactivation is completed with a 5 minute incubation at 70ºC. First strand synthesis was completed with a cycling profile of 65ºC for 5 minutes, 25ºC for 5 minutes, 50ºC for 60 minutes, and 70ºC for 15 minutes.

For qPCR, 25 ng of cDNA was loaded into each reaction mixture consisting of 1.7 µL RNAse/DNase Free H_2O, 1 µL AmpliTaq Gold Buffer without $MgCl_2$, 1 µL of 25 mM $MgCl_2$, 1 µL of 2 mM dNTPs, 0.05 µL of 5 U/µL AmpliTaq Gold and 0.25 µL of TaqMan probe per 10 µL reaction. Probes used were as follows: *Ucp1* (Mm01244861_m1), *Pparg* (Mm00440940_m1), *Ppargc1a* (Mm00447183_m1), *Htr2a* (exons 1-2: Mm00555764_m1 or exons 2-3: Mm01321887_m1), *Htr2b* (Mm00434123_m1), *Htr2c* (Mm00434127_m1), or *Ppia* (Mm02342430_g1). Temperature cycling and detection was performed with a Qiagen Rotor-Gene thermocycler. Cycle threshold (Ct) values were determined with a fixed threshold of 0.5 and quantification was calculated via the ΔΔCt method

using *Ppia* as a housekeeping gene and the corresponding control/vehicle for the experiment.

13.12 APP+ Uptake Assays

Following differentiation, cultured adipocytes were transferred to collagen coated 96-well clear-bottom black-walled plates using trypsin-EDTA. The next day media was gently removed and cells rinsed with PBS to eliminate all phenol red containing media. Test compounds in HKRB were added to each well at 100 µL/well. Basal readings were obtained by exciting at 440 nm reading at 520 nm on a SpectraMax M5 microplate reader heated to 37ºC for 30 minutes. Subsequently, APP+ (IDT307 Sigma Aldrich – Oakville, Ontario, Canada) was added at the indicated concentrations and readings were obtained for an additional 60 minutes.

13.13 RNA-Sequencing

For data from differentiated murine adipocyte progenitors, RNA was extracted as described above for qPCR assays. RNA from technical replicates of high purity (i.e. those with a high 260 nm/280 nm absorbance ratio) samples were pooled, yielding 4 merged replicates representing 4 independent experiments. Samples were then further checked for quality (RNA Integrity Number of > 7) by the McMaster Genomics Facility using an Agilent RNA BioAnalyzer RNA Nano Kit. Samples were enriched for mRNA using a NEBNext Poly(A) mRNA Magnetic Isolation Module. cDNA libraries were created using an Illumina NEBNext Ultra

II Directional RNA Library Prep Kit. cDNA libraries were sequenced with a HiSeq Rapid v2 flow cell kit at a depth of approximately 14-million paired-end reads in a 2x51 bp configuration with onboard cluster generation. Analysis of sequencing data was performed using the Galaxy platform. Briefly, raw sequences were processed with the following software tools: Trimmomatic for removal of invalid reads/adapter sequences, FASTQC for quality control, HISAT2 to map sequence reads to gene transcripts, htseq-count to count reads per transcript, and DESeq2 for non-linear normalization of counts per transcript.

For differentiated human adipocyte progenitor data, RNA was extracted using Trizol in Dr. Camilla Scheele's laboratory. Briefly, BGI (Hong Kong) created a TruSeq cDNA library (Illumina) from 1 μg of RNA and subsequently sequenced the cDNA using a HiSeq 2000 sequencer (Illumina) and obtaining 3Gb per sample from a 91-bp paired end sequencing strategy.

13.14 *Ucp1* Promoter Activity Assay

Cells grown in 24-well plates were treated as indicated and then harvested. Briefly, cells were rinsed with PBS and snap frozen in liquid nitrogen. Cells were lysed using 75 μL/well of Promega Passive Lysis Buffer (Madison, Wisconsin, USA) and gentle shaking on an orbital plate shaker. Cell lysates were then transferred to 1.5 mL centrifuge tubes and flash frozen in liquid nitrogen and allowed to thaw on ice. Supernatant was collected following 10-min centrifugation at 16,0000 x g and 4ºC. Samples were analyzed in duplicate by adding 20 μL of

each sample to 2 wells of a white 96-well plate. Immediately before detection, 50 µL of luciferin reagent was added to 8 wells per detection round. Detection was performed on a SpectraMax M5 microplate reader.

13.15 Calcium Transient Assays

Calcium transient assays were completed as per a method modified from (Roth, 2012). After differentiation, adipocytes were transferred to collagen coated black-walled clear bottom 96-well microtiter cell culture plates. The following day cells were incubated in 5 µM Fluo-4 AM (dissolved in 20% pluronic acid; ThermoFisher, Waltham, Massachusetts, USA) and 2 mM sulfinpyrazone in HKRB for 60 minutes at 37ºC and protected from light. Cells were then incubated for an additional 30 minutes in a solution of 2 mM sulfinpyrazone in HKRB and then washed an additional 3 times. Antagonists were added to each well 9 minutes before baseline readings. Baseline readings (1 min) were obtained before the injection of an agonist and an additional 2-minute reading. Final values were obtained by correcting the maximal post-agonist reading to the average value of the last 30 second readings of the baseline data collection. To calculate EC_{50}/IC_{50}, data was first normalized using the smallest and largest values obtained in the 5-HT dose response. Subsequently, nonlinear regression was performed to fit the Hill equation with a fixed Hill slope of 1.0 and calculate an EC_{50}/IC_{50}.

13.16 Cyclic-AMP (cAMP) Assays

cAMP was measured through a modified method from (Roth, 2012). Briefly, BA progenitors were stably transfected with a Promega pGloSensor™-22F (Madison, Wisconsin, USA) using Lipofectamine 2000 (ThermoFisher, Waltham, Massachusetts, USA). Cells were selected in culturing media supplemented with 0.4 mg/mL Hygromycin B (Sigma-Aldrich, Oakville, Ontario, Canada). Individual clones were selected via limiting dilution into two 96-well cell culture plates. Following clonal expansion of the cells, all clones were tested for cells expressing high activity of the pGloSensor™-22F plasmid. Clones were incubated each in an HKRB solution supplemented with 4 mM D-Luciferin Potassium Salt (Cayman Chemical, Ann Arbor, Michigan, USA) at RT for 30 minutes. Baseline measurements were obtained in a SpectraMax M5 plate reader and then 8-Br-cAMP was injected at a final concentration of 1 mM and additional readings were obtained. The clone with highest response was used for future experiments.

To test if 5-HT affected cAMP levels in BAs, cells were incubated with luciferin as above. Baseline measurements were obtained. Subsequently, 5-HT (1 nM to 100 μM) or 1 μM PIA (A_1 adenosine receptor agonist; positive control for G_i-coupled receptors) was added and additional measurements made. Finally, to activate the β_1-β_3-adrenergic receptors (G_s-coupled receptors), isoproterenol (100 pM to 1 μM; used as a stimuli and positive control for G_s-coupled receptors) was added and readings obtained immediately. The difference in luminescence from before to after isoproterenol was normalized and used for analysis.

13.17 *In silico* Receptor–Gene Expression Correlation Analyses

Using GeneNetwork (http://www.genenetwork.org/), the expression levels of *Htr2a* mRNA in human subcutaneous and visceral (omental) adipose tissue (from the GTEX v5 database) was determined and correlated to expression of other mRNA species within those tissues. Briefly, mRNA expression levels were determined from 368 and 234 biopsies obtained from subcutaneous and visceral (omental) human adipose tissue, respectively. RNA extraction and RNA-Sequencing were as per Lonsdale et al (2013). Raw data is available within the GTExPortal database (version 5; subcutaneous - GTEXv5 Human Adipose Subcutaneous RefSeq (Sep15) RPKM log2; visceral - GTEXv5 Human Adipose Visceral Omentum RefSeq (Sep15) RPKM log2). GeneNetwork calculated Pearson's correlation coefficient for expression levels of *Htr2a* mRNA in each depot to mRNA of all genes within the corresponding depot. Genes with mRNA expression levels that were positively correlated in both subcutaneous and visceral to *Htr2a* mRNA levels were submitted to the DAVID (version 6.8; Huang et al., 2009b, 2009a) analysis tool to perform gene ontology analysis. This was also repeated for negatively correlated genes. Herein gene groups categorized by cellular component (i.e. the location where the gene product is active) are reported.

13.18 *In silico* Receptor–Phenotype Correlation Analyses

Correlation of BAT 5-HT receptor mRNA expression from mice with mixed genetic backgrounds (i.e. recombinant inbred mouse strains derived from crosses of C57Bl/6 mice with DBA/2 mice – termed BXD mice) with various phenotypes was performed using GeneNetwork. Specifically, BAT gene expression from multiple BXD mice lines (EPFL/LISP BXD CD Brown Adipose Affy Mouse Gene 2.0 ST Gene Level (Oct13) RMA) was used and compared to phenotypes assessed within those same mouse lines.

13.19 *In silico* Pharmaceutical Property Predictions

To assess the pharmaceutical promise of 5-HT2A antagonist compounds, we utilized a variety of computational tools to predict binding, structure activity relationships (SAR) and ADMET properties. For docking experiments, a homology-based model of the mouse 5-HT2A receptor was retrieved from the GPCR-Sequence-Structure-Feature-Extractor 2.0 (GPCR-SSFE 2.0; http://www.ssfa-7tmr.de/ssfe2/index.php; Worth et al., 2017) in July 2017. Docking simulations using the mouse 5-HT2A model and structures of 5-HT, MDL-100,907 and xylamidine were performed using SwissDock (http://www.swissdock.ch/; Grosdidier et al., 2011b, 2011a). Results of the simulations were visualized using UCSF Chimera (version 1.13.1). Only the top result from each simulation is displayed.

To confirm on-target and ascertain potential off-target effects of 5-HT2A antagonists and other related-/anti-obesity compounds, we submitted the chemical structure of each compound to the Way2Drug PASS Online analysis tool (http://www.way2drug.com/PASSOnline/index.php). Where agonist and antagonist activities for each compound were predicted against the 5-HT2/5-HT2A receptor they were reported as such. The top off-target/adverse effects for each compound were also reported.

To predict absorption, distribution, metabolism, excretion and toxicity (ADMET) properties, compound structures were submitted to PreADMET (https://preadmet.bmdrc.kr/) and activity in a variety of computational assays testing BBB permeability, intestinal absorption (HIA), protein plasma binding etc. was obtained. Furthermore, xylamidine's structure was submitted to ACD Labs Percepta as well for additional testing with a particular focus on BBB permeability.

13.20 Gene Expression Knockdown Assay

siRNA against the murine *Htr2a* gene (Silencer® Select Pre-Designed siRNA ID: s67937) and scRNA (Silencer® Select Negative Control No. 1 siRNA) was purchased from (ThermoFisher, Waltham, Massachusetts, USA). As per the method from Isidor et al. (2016), cells were transfected on day 6 of differentiation via reverse transfection using Lipofectamine 2000 (ThermoFisher, Waltham, Massachusetts, USA). Cells were then allowed to continue to differentiate. On day 10 of differentiation, cells were treated with 100 µM 5-HT. A sample of media was

collected at 1 hour for NEFA analysis and cells were collected at 4 hours for confirmation of knockdown and analyses of genes of interest.

13.21 In silico Compound-Gene Signature Correlation Analysis

Data from immortalized human mesenchymal stem cells (MSC) was obtained from the Gene Expression Omnibus (GEO) Database (https://www.ncbi.nlm.nih.gov/geo/query/acc.cgi?acc=GSE19643) by Sam Chorlton. Subsequently, data was normalized using frozen Robust Multiarray Analysis and confounders detected with Surrogate Variable Analysis. Differentially expressed genes were determined using a limma model after considering identified confounders with thresholds of ≥ 2-fold change and false discovery rate (FDR) of 0.05. Data was further restricted to genes with a fold of change of ≥ 2.58 to achieve a gene signature containing the most equal balance of up- and down-regulated genes. Subsequently, these gene lists were submitted to the Library of Integrated Network-based Cellular Signatures (LINCS) L1000 dataset analysis tool to obtain a list of compounds that elicited similar gene signatures.

13.22 Statistical Analyses

Inferential statistical tests were performed on all experiments where sample sizes exceeded three and were performed in GraphPad Prism 8 (San Diego,

California, USA). Unless otherwise noted, samples for animal experiments were defined as individual animals. Sick mice and values that were greater than 2 S.D. away from the mean were omitted from analysis. For cell culture experiments, a sample was defined as a single experiment (comprised of the mean of the number of technical replicates as indicated). Experiments with sample sizes less than three are reported simply as means and considered preliminary. For single comparisons between two treatments, student's t-tests were performed. For comparisons between greater than two treatments, analysis of variances (ANOVA) were used with Bonferroni *post-hoc* tests. Where comparisons were made in experiments with 2x2 group designs, 2-way ANOVAs were used. Comparisons resulting in a p-value of < 0.05 were considered statistically significant and results with a p-value ≤ 0.10 were indicated as such.

14 Results

14.1 Identification and Description of the Effects of 5-HT on BAT

Previous studies described the effects of inhibiting peripheral 5-HT synthesis (using *Tph1*$^{-/-}$ mice or a Tph1 inhibitor: LP-533401 and PCPA) on brown adipose tissue related phenotypes (Crane et al., 2015; Oh et al., 2015). However, these studies examined the effects of increasing 5-HT levels only in mouse models with an abnormal serotonergic system (i.e. not producing peripheral 5-HT; Crane et al., 2014b) or limited cell culture conditions (Oh et al., 2015, i.e. no 5-HT in the presence of receptor antagonists). Therefore, we examined the effects of a wide-range of 5-HT concentrations directly on brown adipocytes or *in vivo* with 5-HT injections and 5-HT signalling manipulations (i.e. *Slc6a4*$^{-/-}$ mice or SSRI treatment).

14.1.1 *Direct Effects of 5-HT on Brown Adipocytes*

Firstly, we examined direct effects of 5-HT on brown adipocytes in cell culture. To begin, because a function of all adipocytes is the storage of lipid, we examined the accumulation of lipid during differentiation in response to a high concentration of 5-HT (100 μM), as had been used previously (Crane et al., 2015). High dose 5-HT supplementation attenuated the accumulation of lipid in cultured brown adipocytes (Figure 4a). Therefore, storage of lipid in brown adipocytes seems to be compromised in response to high levels of 5-HT.

Stored lipid must be mobilized by adipocytes via lipolysis to fuel other organs and/or thermogenesis in brown adipocytes. Lipolysis occurs primarily in response to adrenergic stimuli. Therefore, we tested the effects of various doses of 5-HT on both basal lipolysis and adrenergic stimulated lipolysis. Using the β-adrenergic receptor pan-agonist – isoproterenol (Iso), in multiple preliminary experiments we found low doses of 5-HT (< 10 μM) had little or no effect on reducing FFA production whereas higher doses of 5-HT (≥ 100 μM) reduced FFA (Figure 4b and Figure S4- 1a and c) and glycerol production (data not shown). Furthermore, the effect only persisted at doses of Iso less than or equal to 1 nM (Figure 4c and Figure S4- 1b). Therefore, the liberation of fatty acids is only inhibited by high doses of 5-HT in the absence or under sub-maximal adrenergic stimulation.

Although fatty acids, released by lipolysis, have traditionally been thought to be the primary energetic substrate for brown adipocyte thermogenesis (Li et al., 2014), many findings also suggest that glucose is also a substrate for BAs and thermogenesis (Ma and Foster, 1986; Vallerand et al., 1990; Weir et al., 2018) where it increases TCA cycle intermediate content via pyruvate carboxylase and anapleurosis (Cannon and Nedergaard, 1979). Additionally, glucose uptake and glycolysis is activated in response to adrenergic stimulus (Olsen et al., 2014). Therefore, we examined if 5-HT inhibited extracellular acidification rate (ECAR), a marker of glycolytic flux, basally and in response to Iso. Similar to its anti-lipolytic activity, preliminary results show high dose 5-HT inhibited basal but not

maximal adrenergic-stimulated ECAR (Figure 4d and Figure S4- 1d). Consequently, high dose 5-HT might reduce basal glycolytic rates, but adrenergic stimulus can overcome this inhibition.

Finally, because our focus was on the ability of brown adipocytes to consume energetic substrates and expend the resultant energy, we examined if 5-HT altered BA thermogenesis. Initial attempts to measure direct heat production from BAs using an IR-camera in culture proved unreliable. Therefore, we measured rates of oxygen consumption as a surrogate for BA thermogenesis. In preliminary experiments, only a very high dose of 5-HT (1 mM) inhibited oxygen consumption rates (OCR) basally (Figure 4e), without minimizing ATP-synthase dependent respiration (Figure 4f) and thus reducing mitochondrial leak respiration (a measure of mitochondrial uncoupling; Figure 4g). Since UCP1 is directly activated by FFA (Fedorenko et al., 2012), we also measured the effect of 5-HT on Iso-stimulated (to induce lipolysis as above) respiration and found little to no effect (Figure S4- 1e to g). Further, we found 5-HT had no effect on maximal respiration induced by FCCP (a chemical mitochondrial respiration uncoupler; Figure S4- 1e, f and h). Therefore, with the exception of extremely high doses, *in vitro* 5-HT does not acutely impair BA oxygen consumption and therefore presumably thermogenesis.

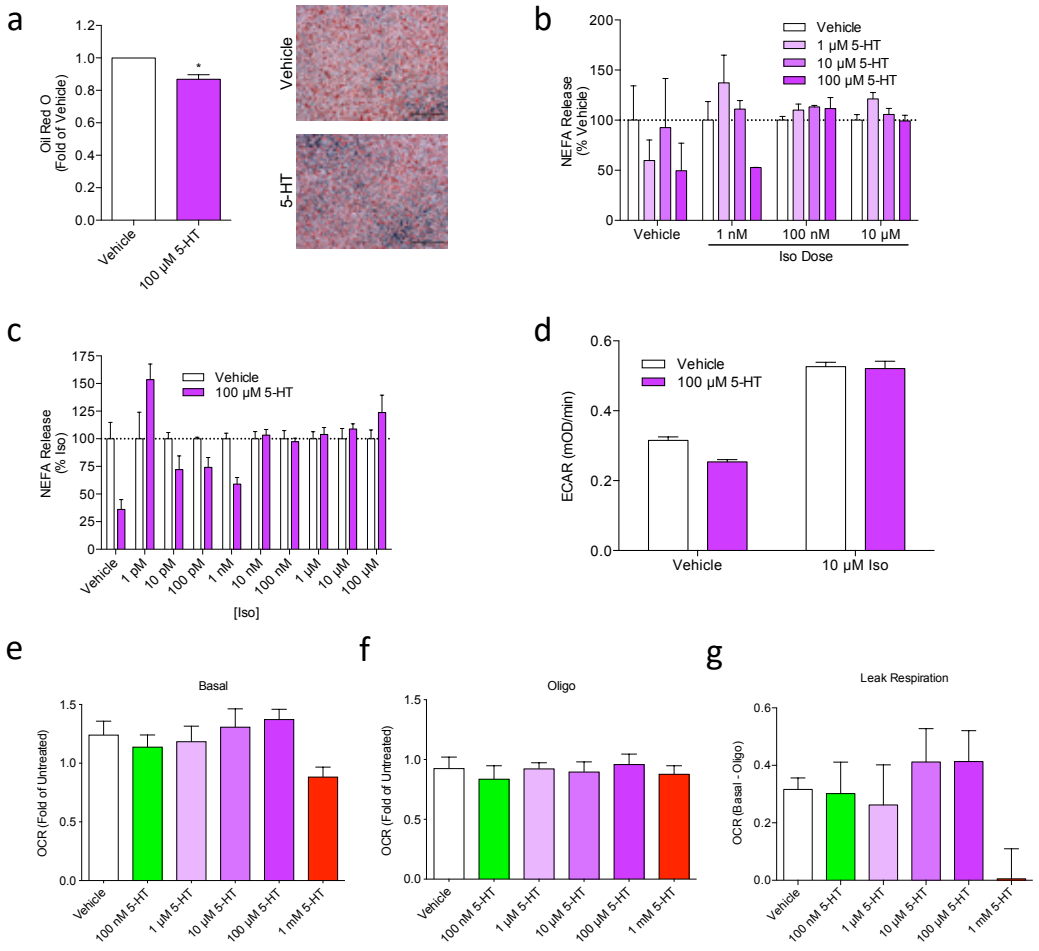

Figure 4. 5-HT has dose dependent direct effects on BA functions – lipid accumulation, lipolysis and ECAR. a, Lipid content by ORO in BAs after 7-day treatment during differentiation with 100 µM 5-HT (replenished every 2 days; n = 3 independent experiments performed in triplicate). * indicates statistically significant difference from vehicle by t-test. b and c, NEFA release from BAs after acute treatment with various doses of 5-HT or Iso (Isoproterenol; n = 1 independent experiment performed in triplicate – error bars represent within experiment error). d, Extracellular acidification rate (ECAR) of BAs acutely treated with 5-HT and/or Iso (n = 1 independent experiment performed in 5 replicates – error bars represent within experiment error). e-g, Basal, oligomycin and leak respiration in response to various doses of 5-HT, respectively (n = 1 independent experiment performed in 5 replicates – error bars represent within experiment error). Additional data is available in Figure S4- 1, Figure S4- 2 and Figure S4- 3.

Subsequently, we investigated if exposure to 5-HT after differentiation might change expression of thermogenic gene products. First, using immortalized

BAs derived from a *Ucp1-Luciferase* mouse (ThermoMouse; Galmozzi et al., 2014), we tested if 5-HT affects the activity of the *Ucp1* promoter. Preliminary experiments with 100 μM 5-HT (high dose) revealed that following 18 hours of treatment, 5-HT did not inhibit the increase in activity of the *Ucp1* promoter in response to various adrenergic stimuli (Iso; CL-316,243 – β3 receptor agonist; 8-Br-cAMP – a PKA agonist), but generally augmented the response (Figure S4- 2a to c) despite inhibiting NEFA release (Figure S4- 2d to f), in direct contrast to previous studies looking at *Ucp1* mRNA (Crane et al., 2015). A similar pattern was observed in preliminary data from another BA cell line (TMCON) where *Ucp1* mRNA measurements were reduced with 100 μM 5-HT alone but additively increased *Ucp1* mRNA expression with co-treatment with Iso (Figure S4- 3a to c). UCP1 protein expression was also increased with high doses of 5-HT (Figure S6-1a). Additional experiments revealed that this increase may be due to the known PPARγ agonist activity of the major 5-HT metabolite, 5-HIAA (Grès et al., 2013; Waku et al., 2010; Figure S4- 2g and h).

In culture, direct, acute inhibitory effects of 5-HT on BA metabolism and functions appear to be limited to only high concentrations of 5-HT not commonly found in plasma (Brand and Anderson, 2011). Additionally, high levels of 5-HT may enhance the transcription of *Ucp1* through downstream metabolites of 5-HT.

14.1.2 *Expression and Activity of Serotonin Transporting Genes*

The serotonergic system consists of regulatory mechanisms to control 5-HT release, duration of activity and degradation. The most commonly discussed

negative regulator of receptor-mediated 5-HT activity is the 5-HT specific transporter, SERT (gene: *Slc6a4*). Since only high doses of 5-HT had effects in culture, we hypothesized that transport and/or degradation of 5-HT would be present in BAs.

Subsequently, we found that *Slc6a4* mRNA is expressed in mouse BAs from multiple mouse strains (Figure 5a to b and Figure S5- 1a), human BAs (Figure 5c), and human WAs (Figure S5- 1b). Furthermore, mouse BAs actively uptake APP+ – a fluorescent analog of 5-HT commonly used to measure transport (Figure S5- 1c to f).

Consistent with previous papers describing the mechanism of transport of 5-HT to be concentration dependent (Hagan et al., 2011), we observed a non-linear increase in transportation kinetics with increasing 5-HT concentrations (Figure S5- 1c). Furthermore, at clinical doses of Paroxetine (Par) – a highly-potent and relatively-specific SERT inhibitor (SSRI) – there was only modest inhibitory effects on low [APP+] transport in BAs (Figure S5- 1c to e). Additionally, other SSRIs (i.e. Citalopram and Fluoxetine) and DAT/NET inhibitors (i.e. Methylphenidate) had no effect on APP+ uptake (Figure S5- 2a to e and Figure S5- 4a to e). Notably, *Slc6a4*$^{-/-}$ BAs still transported APP+ but supraclinical doses of Paroxetine inhibited this transport (Figure S5- 3b to c), suggesting some non-specific activity of Paroxetine at high doses as has previously been reported (Zhu et al., 2012).

In addition to expression of *Slc6a4*, we also found mRNA expression of the organic cation transporter 3 (OCT3; gene: *Slc22a3*) and plasma membrane monoamine transporter (PMAT; gene: *Slc29a4*) in BAs (Figure 5b and c and Figure S5- 1a and b). OCT3, PMAT and others (i.e. DAT/NET) are also known to transport 5-HT. The OCT3/PMAT transporter inhibitor decynium-22 (D-22) attenuated transport across all doses of APP+ (Figure S5- 1c and Figure S5- 4b). Additionally, other known OCT3 transporter inhibitors (i.e. corticosterone and hydrocortisone; Hill et al., 2011) exhibited moderate inhibition of APP+ uptake (Figure S5- 4d and h). Combinations of D-22 with SSRIs only revealed modest additional inhibition of APP+ transport by SSRIs (Figure S5- 5). A summary of conditions and pharmacological values for inhibitors of 5-HT transport in BAs are included in Table S5- 1. Finally, BAs express high levels of mRNA for 5-HT degradation enzymes (i.e. *Maoa* and *Maob*). Thus, this evidence suggests that BAs transport 5-HT at high levels, transport occurs primarily via a non-SERT-mediated mechanism, and BAs express mRNA transcripts for genes known to degrade 5-HT.

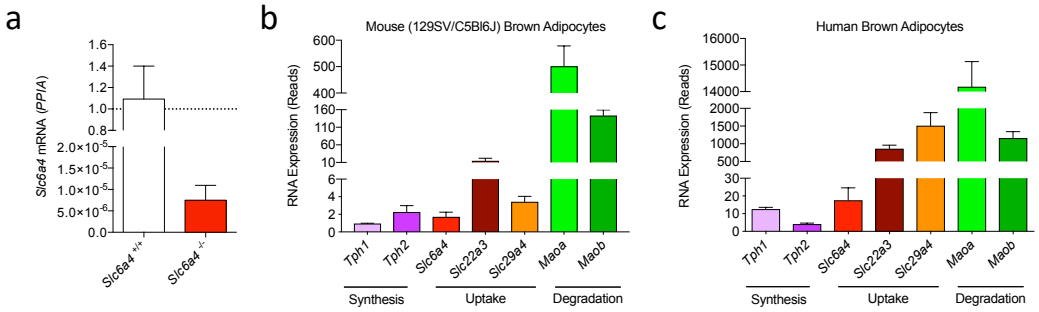

Figure 5. 5-HT transporter and metabolism genes are expressed in mouse and human brown adipocytes. a, *Slc6a4* mRNA expression in immortalized *Slc6a4*$^{+/+}$ *and Sl6a4*$^{-/-}$ BA progenitors after differentiation (n = 1 independent experiment performed in triplicate – error bars represent within experiment error). b and c,

Expression of 5-HT synthesis, uptake/transport and degradation gene mRNAs in mouse BAs. (n = 1 independent experiment performed in triplicate – error bars represent within experiment error) and human BAs (data is obtained from BAs from 5 different subjects), respectively. Bars represent mean ± S.E.M. Additional data is included in Figure S5- 1, Figure S5- 2, Figure S5- 3, Figure S5- 4, Figure S5- 5 and Table S5- 1.

14.1.3 *The Effects of Inhibiting 5-HT Transport Proteins on BA Genes*

Because in neurons uptake of 5-HT into the pre-synaptic membrane reduces 5-HT signalling, we tested if blocking or reducing cellular 5-HT uptake might exacerbate the effects of 5-HT on BAs and induce adaptive changes. Attempts to block 5-HT uptake with D-22 (100 nM) resulted in cell detachment (data not shown) and high dose Paroxetine (20 μM) dramatically decreased lipid accumulation (Figure S6- 2). In contrast, the absence of *Slc6a4* alone did not impair lipid accumulation (Figure S5- 3). However, in combination with lower doses of Paroxetine (250 nM) *Ucp1* promoter activity tended to be reduced by 5-HT (Figure 6a and b). Similar results were observed in BAs from *Slc6a4*$^{-/-}$ mice (Figure 6c). Notably, this reduction in *Ucp1* occurred at 5-HT doses similar to those found in circulating plasma (~1-10 nM). Preliminary findings suggest the decrease in *Ucp1* promoter activity may translate to lower UCP1 protein levels (Figure S6- 1a to c). These data suggest that inhibiting 5-HT uptake in BAs either pharmacologically

(Paroxetine) or genetically (*Slc6a4*$^{-/-}$) enhances the effects of 5-HT to reduce *Ucp1* expression.

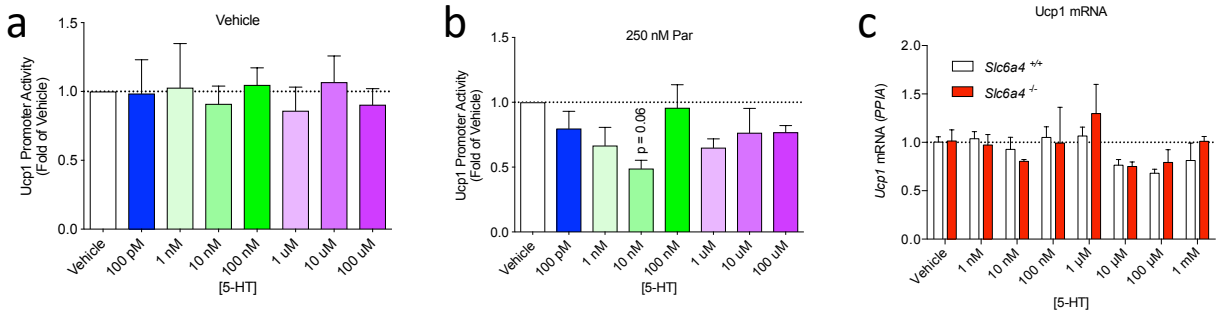

Figure 6. Low dose 5-HT directly reduces BA *Ucp1* transcription via a cell membrane receptor. a and b, *Ucp1* promoter activity in response to a dose response of 5-HT in the absence or presence of an SSRI (Par), respectively (n = 3 independent experiments performed in 2-3 replicates). Trend indicated is from 1-way ANOVA with Bonferroni post-hoc analysis. c, *Ucp1* mRNA expression in response to a dose response of 5-HT in BA having intact (*Slc6a4*$^{+/+}$) or inactivated 5-HT receptor (*Slc6a4*$^{-/-}$; n = 1 performed in in 3 replicates; bars represent within experiment error). Additional data is in Figure S6- 1 and Figure S6- 2.

14.1.4 *Acute Effects of 5-HT on Thermogenesis*

To determine if 5-HT may reduce whole body energy expenditure, we examined the effects of exogenous 5-HT *in vivo*. Based upon preliminary experiments performed by Dr. Justin Crane to find the lowest effective dose, anaesthetized male C57Bl/6J mice were injected IV with 0.1 mg/kg 5-HT (Figure 7a to d) at RT. 5-HT reduced oxygen consumption and interscapular surface temperature in response to CL-316,243 under both conditions. Similar results were found with awake female FVB mice at thermoneutrality (TN) and injected IP with 5-HT (Figure 15d to h) and with anaesthetized male C57Bl/6J mice at RT injected IP with 5-HT (Figure S15- 7), suggesting that 5-HT reduced adrenergic-induced

thermogenesis *in vivo*. This suggests that unlike direct treatment of 5-HT on cultured BAs (Figure 4e-g and Figure S4- 1e-h), *in vivo* 5-HT acutely impairs BAT thermogenesis.

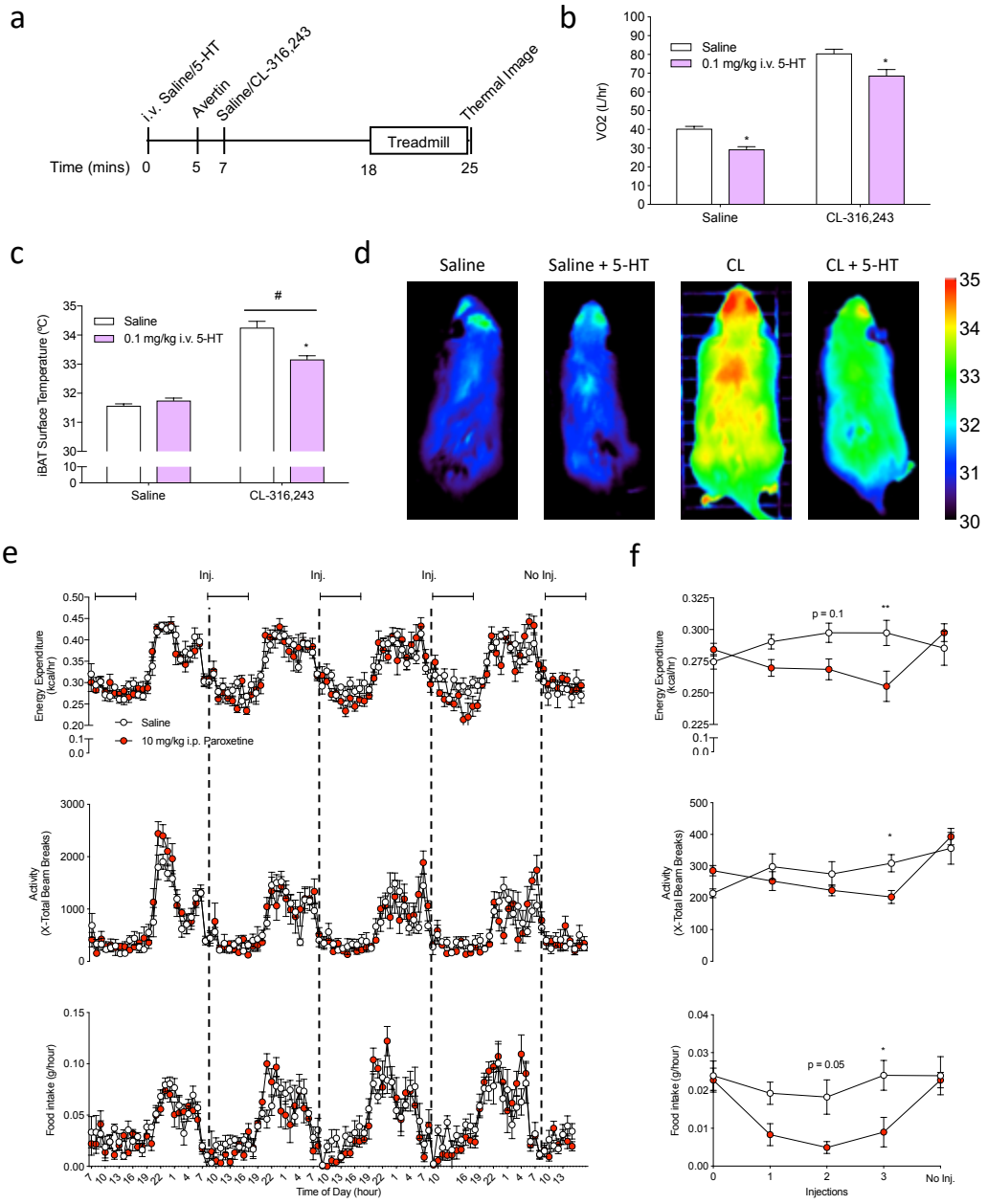

Figure 7. 5-HT acutely reduces EE. a, Timeline of administration of 5-HT for b-d. b and c, VO2 and iBAT surface temperature of mice anaesthetized and treated

according to a, respectively (n = 8 mice). # indicates interaction overall effect by 2-way ANOVA and * indicates significant difference from saline via Bonferroni *post-hoc* analysis. d, Representative images used for calculation in c. e, EE, activity and feeding timeline in mice treated daily with par (n = 6 mice). f, average of EE, activity and feeding amounts 6 hours post-injection with Par. * indicates significant difference by Bonferroni post-hoc analysis following 2-way ANOVA. All data is presented as mean ± S.E.M.

A single IP injection of 10 mg/kg Paroxetine increases platelet poor plasma 5-HT levels by ~350%, 0.5 hours after IP injection in rats (Ortiz and Artigas, 1992) and was used as a more clinically relevant model to enhance circulating serotonin levels. We injected male C57Bl/6J mice daily for 3 days with Paroxetine and measured their energy expenditure, physical activity and food intake (Figure 7e and f). The post-injection (0-6 hours) mean EE was reduced following each injection and reversed following cessation of treatment. This coincided with reduced physical activity and feeding behaviour. Therefore, acute Paroxetine (presumably increasing 5-HT relatively modestly) reduced energy expenditure but it is unclear if this was due to a reduction in BAT mediated thermogenesis or may have been due to reductions in physical activity and feeding.

14.1.5 *Chronic Effects of Elevated 5-HT on in vivo Thermogenesis*

Given the observations linking reduction of 5-HT transport in combination with low 5-HT to reducing *Ucp1* expression and the reduced energy expenditure in mice acutely injected with 5-HT and Paroxetine, we examined the metabolic consequences of chronically elevating 5-HT signalling in mice lacking SERT (gene: *Slc6a4*). Since previous papers suggested that *Slc6a4*$^{-/-}$ mice and rats were obese despite no changes in food intake (Chen et al., 2012; Homberg et al., 2010;

Üçeyler et al., 2010) and reduced *Ucp1* mRNA expression in BAT (Zha et al., 2017), we particularly focused on EE. *Slc6a4*$^{-/-}$ mice, housed under standard conditions with *ad libitum* standard chow diet, were monitored for ~30 weeks for weight and metabolic changes (Figure 8a). Both male and female *Slc6a4*$^{-/-}$ mice gained more weight than littermate *Slc6a4*$^{+/+}$ mice (Figure 8b and c; Figure S8- 1e and f). In particular, this additional mass was comprised of fat mass (Figure 8d and e; Figure S8- 1g to j) and not lean mass (Figure S8- 1a, b, k and l). Fluid mass was elevated but to a lesser degree than fat mass (Figure S8- 1c, d, m and n). Furthermore, this was paralleled in the size of the white adipose tissue depots in both sexes at sacrifice (Figure 8g and h; Figure S8- 1b and d). These results suggest a net positive energy balance.

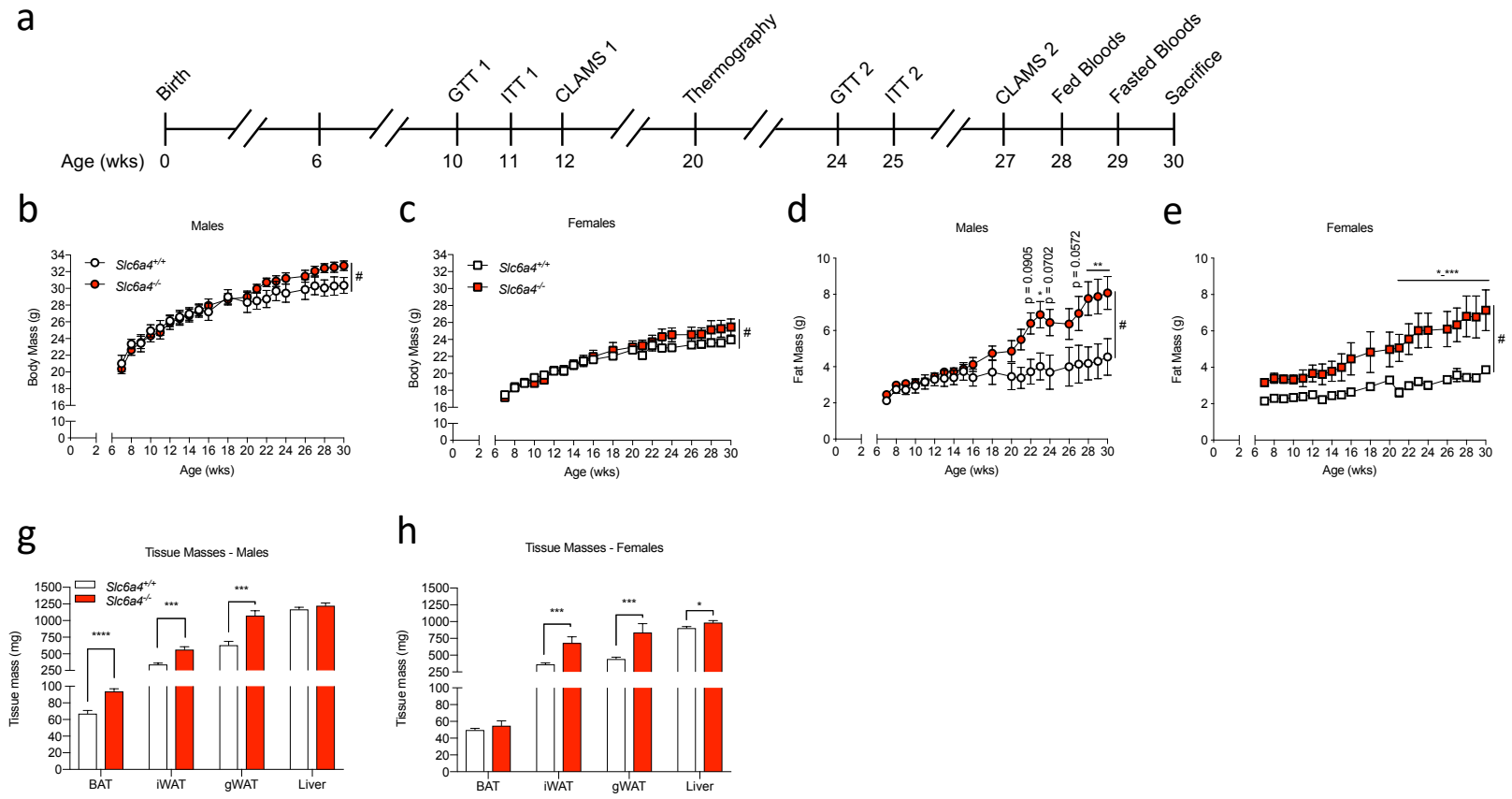

Figure 8. Inactivation of the Slc6a4 gene induces obesity in mice. a, Experimental timeline for metabolic analysis of mice. b and c, growth curves of male (b; n = 5-9 mice) and female (c; n = 6-8 mice) *Slc6a4*$^{+/+}$ and *Slc6a4*$^{-/-}$ mice. # indicates interaction effect by 2-way ANOVA and * indicates significant difference by Bonferroni post-hoc analysis. d and e, Fat mass for the mice

included in b and c. g and h, Tissue masses at sacrifice from male (g; n = 13-20) and female (h; n = 6-15) *Slc6a4*$^{+/+}$ and *Slc6a4*$^{-/-}$ mice. * = $p < 0.05$, ** = $p < 0.01$, *** = $p < 0.001$ and **** = $p < 0.0001$ by t-test. Additional data is included in Figure S8- 1 and Figure S8- 2

We next investigated energy balance both before (~12 weeks of age) and after (~27 weeks of age) divergence in body mass. Although at both ages there were similar or slight reductions in VO_2 when corrected to body weight (Figure S9- 1a to f; Figure S9- 2a to f), no differences in absolute energy expenditure were found in male *Slc6a4*$^{-/-}$ mice and only small elevations in female mice at individual hourly points (Figure 9a to f). Notably, both male and female *Slc6a4*$^{-/-}$ mice consumed more food (Figure 9g to l) and had reduced activity levels at 12 weeks (Figure 9m to r; Figure S9- 1g to l). Because there were no large differences in EE between genotypes, despite reduced activity levels in *Slc6a4*$^{-/-}$ mice, we analyzed EE across different levels of activity. Contrary to our hypothesis that elevating 5-HT might decrease EE, we found that male and female *Sl6a4*$^{-/-}$ mice had elevated EE independent of physical activity levels at both time points (Figure 9s to v; Figure S9- 3s to v). This suggests that the net positive energy balance in *Slc6a4*$^{-/-}$ mice is due to excessive caloric intake, not reduced EE, and these mice have improved, not impaired, locomotive-independent EE.

Additionally, we investigated which macronutrient is used for energy expenditure in *Slc6a4*$^{-/-}$ and if glucose homeostasis is dysregulated in these mice. According to their elevated RER, male and female *Slc6a4*$^{-/-}$ mice oxidise relatively more carbohydrates versus lipid and this is particularly exacerbated with age (Figure 10a to f; Figure S10- 1). Consistent with this, we observed few differences in glucose or insulin tolerance (Figure 10g to n; Figure S10- 2a to l). Although, in

aged *Slc6a4*$^{-/-}$ mice, females have greater 6 hour fasted blood glucose and a small reduction in glucose tolerance (Figure S10- 2k). Thus, despite relatively greater body mass, *Slc6a4*$^{-/-}$ do not appear to have major deficits in glucose homeostasis at the time points investigated.

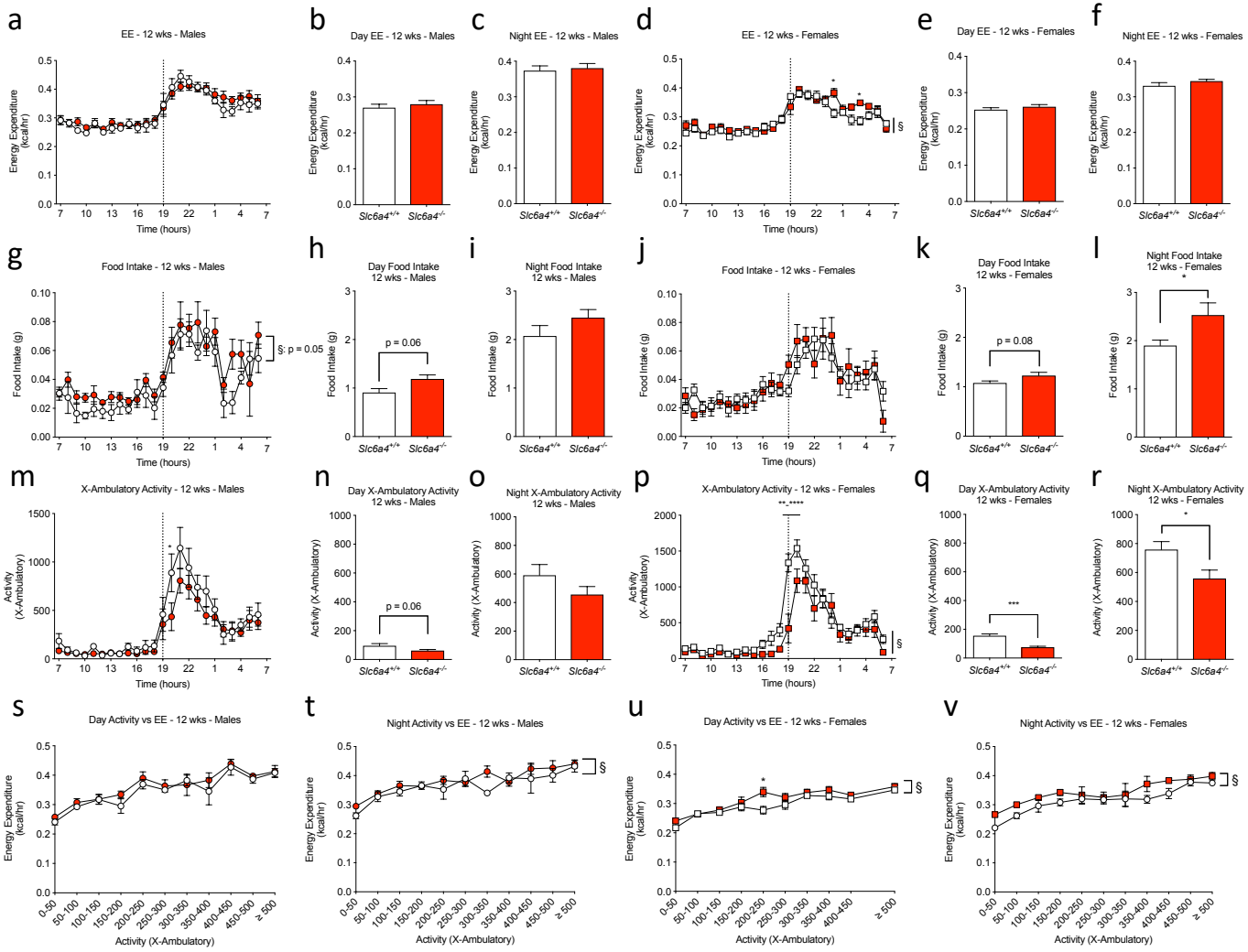
a
EE - 12 wks - Males
Energy Expenditure (kcal/hr)
Time (hours)
b
Day EE - 12 wks - Males
c
Night EE - 12 wks - Males
d
EE - 12 wks - Females
§
e
Day EE - 12 wks - Females
f
Night EE - 12 wks - Females
Slc6a4+/+
Slc6a4-/-
g
Food Intake - 12 wks - Males
Food Intake (g)
§: p = 0.05
h
Day Food Intake 12 wks - Males
p = 0.06
i
Night Food Intake 12 wks - Males
j
Food Intake - 12 wks - Females
k
Day Food Intake 12 wks - Females
p = 0.08
l
Night Food Intake 12 wks - Females
*
m
X-Ambulatory Activity - 12 wks - Males
Activity (X-Ambulatory)
n
Day X-Ambulatory Activity 12 wks - Males
p = 0.06
o
Night X-Ambulatory Activity 12 wks - Males
p
X-Ambulatory Activity - 12 wks - Females
,**
q
Day X-Ambulatory Activity 12 wks - Females
***
r
Night X-Ambulatory Activity 12 wks - Females
s
Day Activity vs EE - 12 wks - Males
Activity (X-Ambulatory)
t
Night Activity vs EE - 12 wks - Males
u
Day Activity vs EE - 12 wks - Females
v
Night Activity vs EE - 12 wks - Females

Figure 9. *Slc6a4*$^{-/-}$ mice have greater food intake, lower physical activity and greater EE per level of activity than *Slc6a4*$^{+/+}$ littermates. a-c, EE of male mice throughout an entire 24-hour period and the average over inactive (light) and active (dark) periods, respectively (n = 6-11). d-f, same as a-c except in female mice (n = 5-9). g-i, Food intake of male *Sl6a4*$^{-/-}$ and *Slc6a4*$^{+/+}$ mice throughout an entire 24-hour period (g), average for the light phase (h) and average for the dark phase (I; n = 6-11). j-l, Same as g-i except for female mice (n = 5-9). m-o, Physical activity levels of male mice throughout a 24-hour period (m), average for the light phase (n) and average for the dark phase (o; n = 6-11). p-r, Same as m-o except for female mice instead of males (n = 5-9). s-t, average EE in *Slc6a4*$^{+/+}$ and *Slc6a4*$^{-/-}$ mice at different levels of activity (n = 6-11). u-v, Same as s-t except for female mice (n =5-9). All points and bars are means and error bars represent S.E.M. § = overall statistically significant effect of genotype as assessed by 2-way ANOVA. * = $p < 0.05$, ** = $p < 0.01$, *** = $p < 0.001$ and **** = $p < 0.0001$ by Bonferroni post-hoc test for time courses and t-test for average comparisons, respectively. Additional data is included in Figure S9- 1, Figure S9- 2, and Figure S9- 3.

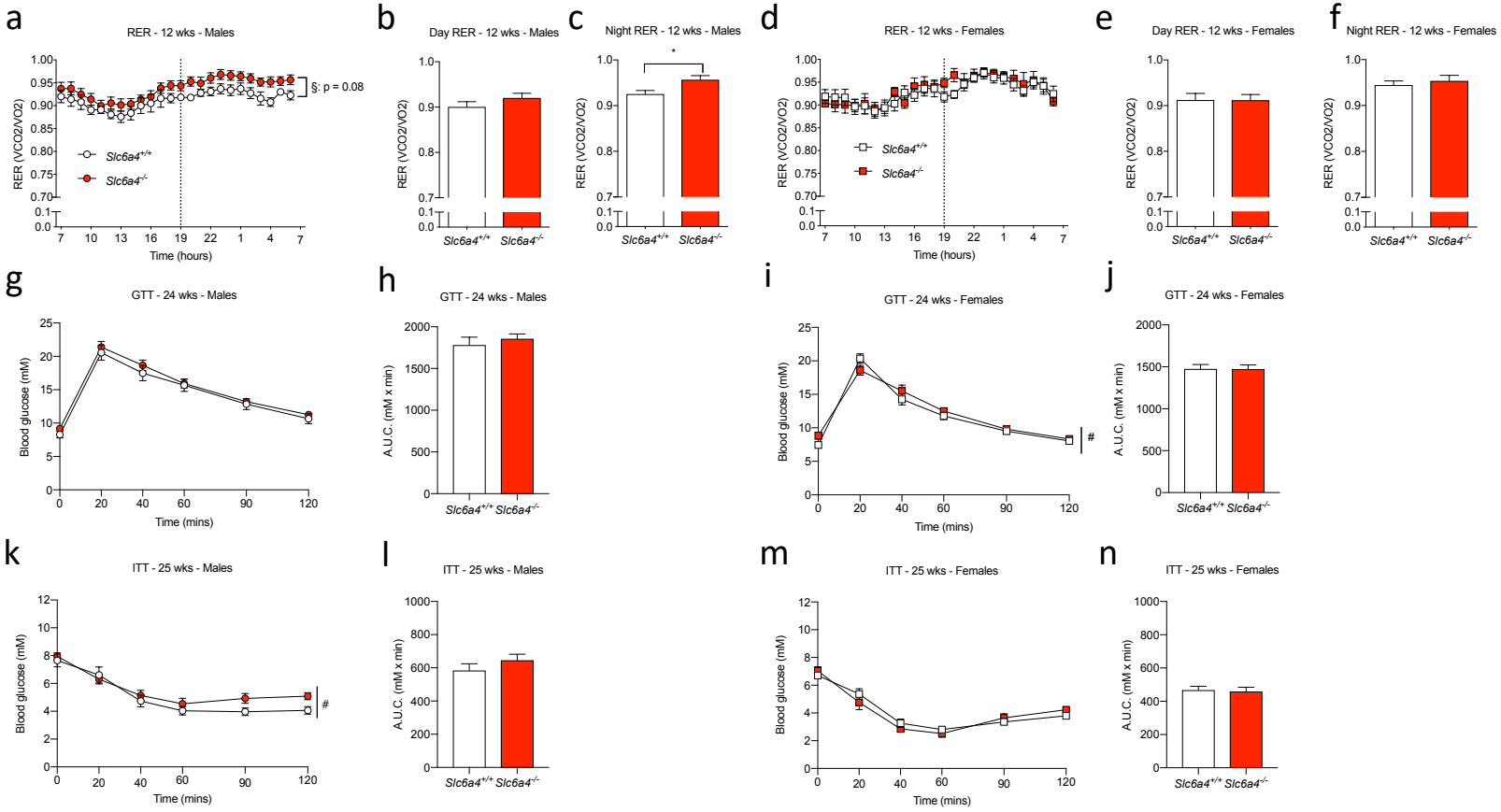

Figure 10. Male, but not young female, *Sl6a4*$^{-/-}$ mice preferentially oxidize glucose with few differences in glucose homeostasis. a-c, RER of male *Slc6a4*$^{-/-}$ and *Sl6a4*$^{+/+}$ mice throughout the day (a), averaged over the light period (b) and averaged over the dark period (c; n = 6-11). d-f, RER as presented in a-c except for female mice (n = 5-8). g and h, Time course of blood

glucose response to acute IP bolus of D-glucose in male mice (g) and corresponding A.U.C. (h; n = 15-21). i and j, Same as g and h except in female mice (n = 9-16). k and l, Time course of blood glucose measurements following acute IP injection of insulin (k) and corresponding A.U.C. (l; n = 16-21). m and n, Same as k and l except in female mice (n = 9-15). All points and bars are means and error bars represent S.E.M. § = overall statistically significant effect of genotype and # = overall interaction effect as assessed by 2-way ANOVA. * = $p < 0.05$ by t-test. Additional data is included in Figure S10- 1, Figure S10- 2 and Figure S10- **2**3.

To further investigate the origin of the differences in non-locomotive EE, we assessed the maximal BAT capacity of *Slc6a4*$^{-/-}$ mice. Under mild anaesthetization and saline injection, no differences in VO_2 or interscapular surface temperature were found between *Slc6a4*$^{-/-}$ and *Slc6a4*$^{+/+}$ mice (Figure 11a and d; Figure S11- 1a and e). However following administration of CL-316,243, we found that male *Slc6a4*$^{-/-}$ had greater adrenergic induced VO_2 and interscapular surface temperature (Figure 11b, c, e, and f; Figure S11- 1a and e). Furthermore, these differences persisted when correcting for individual mouse differences in basal (i.e. saline) induced thermogenesis (Figure S11- 1b to d). However, these effects were not observed in female *Slc6a4*$^{-/-}$ mice (Figure S11- 1f to h). Therefore, it appears that male but not female *Slc6a4*$^{-/-}$ mice have elevated BAT capacity.

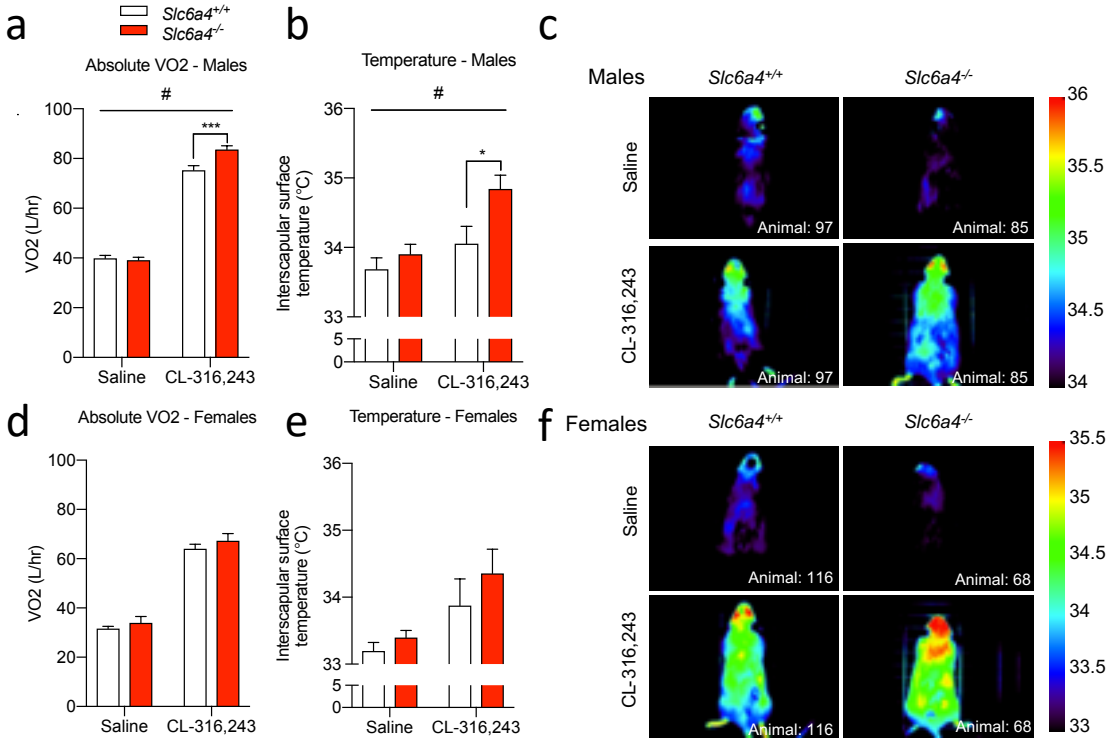

Figure 11. *Slc6a4*$^{-/-}$ have greater functional BAT capacity versus *Slc6a4*$^{+/+}$ littermates. a-c, VO2 (a), interscapular surface temperature (b) and representative IR images (c) in male *Slc6a4*$^{+/+}$ and *Slc6a4*$^{-/-}$ mice (n = 17-20). d-f, Same as a-c except in female mice (n = 10-17). All points and bars are means and error bars represent S.E.M. # = overall interaction effect as assessed by 2-way ANOVA. * = $p < 0.05$ by Bonferroni *post-hoc* test. Additional data is included in Figure S11- 1.

To summarize, whole-body germline elimination of *Slc6a4*, which would be anticipated to increase tissue 5-HT signaling, leads to increased weight gain (primarily adiposity) due to elevated caloric intake and not decreased energy expenditure. Furthermore, non-locomotive EE and thermogenic capacity of *Slc6a4*$^{-/-}$ BAT is intact or elevated *in vivo*.

14.2 Investigation of the predominant 5-HT receptor(s) on BAs

14.2.1 *Identifying the predominant 5-HT receptor(s) on BAs*

The observation that 5-HT decreases *Ucp1* promoter activity and mRNA expression with direct 5-HT treatment on BAs indicate a potential cell-autonomous role for 5-HT. The exacerbation of the effects of low dose 5-HT by inhibition of 5-HT transport suggests a cell membrane mediated mechanism, such as a 5-HT receptor. We, therefore, sought to identify which 5-HT receptor or receptors are present and active in BAs.

To begin, we performed RNA-sequencing of BAs to quantify mRNA species for each of the 5-HT receptors. Results from human BAs and WAs, and murine BAs all revealed *Htr2a* mRNA to be predominantly expressed (Figure 12a and b; Figure S12- 1a and b) versus all other 5-HT receptors. Additionally, for corroboration, we retrieved receptor mRNA expression data (as Ct values) for undifferentiated and differentiated murine preadipocytes/BAs from another study (Klepac et al., 2016) and upon analysis found *Htr2a* to be the predominant 5-HT receptor expressed in both BAs and preadipocytes (Figure S12- 1c and d). Furthermore, to assess if *Htr2a* was expressed in whole adipose tissue from humans, we extracted white adipose tissue RNA-Sequencing data from the GTExPortal (Lonsdale et al., 2013) and found detectable levels of *Htr2a* mRNA (Figure S12- 1e and f). These data suggested that *Htr2a* is the predominant 5-HT

receptor mRNA expressed in adipocytes and present in adipose tissue of mice and humans.

Because RNA-sequencing has been shown to not always agree with protein expression levels (Vogel and Marcotte, 2012) and attempts to use an anti-5-HT2A antibody failed to provide conclusive results (Figure S12- 1g), we corroborated the RNA-sequencing findings by assessing second messengers of the major 5-HT receptor classes. We first examined cAMP, the major second messenger of G_i- and G_s-coupled 5-HT receptors, by measuring cAMP levels using BAs stably expressing the pGloSensor-22F cAMP reporter. In BAs, treated acutely with 5-HT alone and in combination with Iso we observed no significant effects of 5-HT below 10 μM (Figure 12c; Figure S12- 2a). This is consistent with our lipolysis data (Figure 4b and c; Figure S4- 1a and b) and previous reports (Crane et al., 2015; Hansson et al., 2016) where we observed inhibition of Iso-induced cAMP production by 5-HT above 10 μM (supraphysiological). We also did not observe any activation of canonical downstream G_s- or G_i-coupled pathways (i.e. PKA substrate phosphorylation; Figure S9- 2b - d). Furthermore, no 5-HT receptor/transporters antagonists/siRNAs tested herein rescued the decreased lipolysis effect nor did any agonist class consistently recapitulate the inhibitory effect of 5-HT on isoproterenol-stimulated lipolysis (Figure S12- 3 to Figure S12- 7 and unpublished data from Dr. Emilio Mottillo). Therefore, at physiological levels of 5-HT, our data suggests that G_i- or G_s-coupled 5-HT receptors are not active in BAs, consistent with the lack of non-*Htr2a* 5-HT receptor mRNA expression.

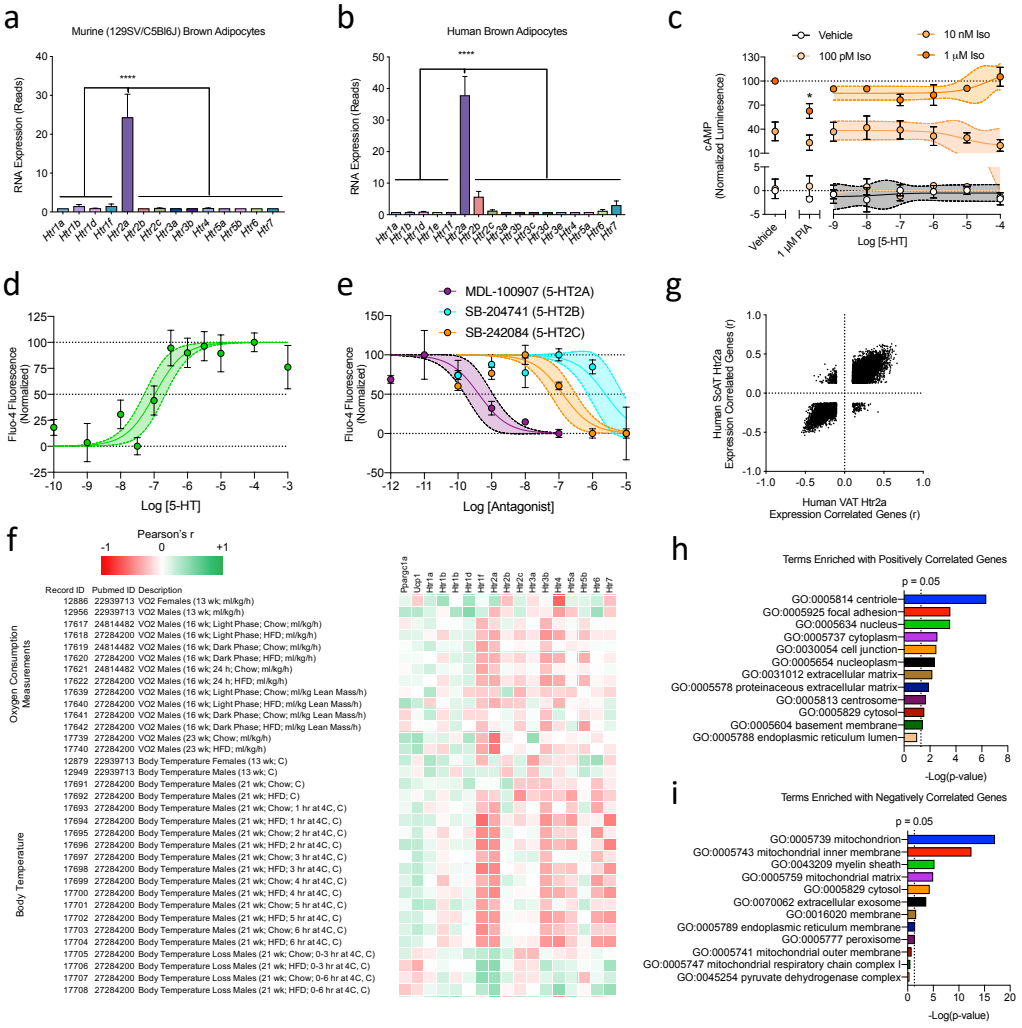

Figure 12. 5-HT2A is expressed and active in BAs and *Htr2a* expression is correlated with BAT-related genes and phenotypes. a and b, RNA-sequencing data of all known 5-HT2A receptors in cultured mouse (a; n = 3 independent experiments performed in 2-3 replicates) and human (b; n = 5 subjects) BAs. **** indicates statistically significant difference ($p < 0.0001$) of *Htr2a* expression versus each of the other 5-HT receptor mRNA levels via Bonferroni post-hoc test. c, cAMP levels in response to 5-HT, Iso (positive control) and PIA (negative control; A1 adenosine agonist) measured using differentiated BAs stably expressing the pGloSensor™-22F transgene (n = 3 independent experiments performed in triplicate). * = statistically significant difference by Bonferroni post-hoc test ($p < 0.05$). d, Dose response of Ca^{2+} transients in response a dose response of 5-HT (n = 3 independent experiment performed in triplicate). e, Ca^{2+} transient peak in response to 316 nM 5-HT and dose responses of MDL-100907 (5-HT2A antagonist), SB-204741 (5-HT2B antagonist) and SB-242084 (5-HT2C; n = 3 independent experiments performed in triplicate). f, GeneNetwork correlation

heatmap of indirect calorimetry and body temperature phenotypes in BXD mice strains with various 5-HT receptor genes. g, Scatter plot of correlation coefficients (r) of mRNA species correlated with *Htr2a* mRNA levels in human VAT and human ScAT. h-i, Cellular component gene ontology terms containing disproportionate numbers of genes positively (h) or negatively (i) correlated with *Htr2a* mRNA levels in both human VAT and ScAT. Additional data is included in Figure S12- 1, Figure S12- 2, Figure S12- 3, Figure S12- 4, Figure S12- 5, Table S12- 1, Table S12- 2, Table S12- 3, Table S12- 4, Table S12- 5, Table S12- 6, Table S12- 7, Table S12- 8, Table S12- 9 and Table S12- 10.

To examine the activity of the G_q-coupled 5-HT receptors, we examined the induction of intracellular Ca^{2+} transients using the Ca^{2+} sensitive fluorescent dye, Flou-4. 5-HT dose-dependently increased the magnitude of Ca^{2+} transients at 10 nM and above (Figure 12d and Figure S12- 8). Furthermore, these 5-HT-induced transients were blocked by the 5-HT2A antagonist, MDL-100907 (Figure 12e and Figure S12- 8b). Additionally, SB-204741 (5-HT2B antagonist) and SB-242084 (5-HT2C antagonist) failed to do so at doses known to be specific to their respective targets but did inhibit transients at doses consistent with their known affinity for the 5-HT2A receptor (Figure 12e and Figure S12- 8b). The 5-HT3 antagonist – Ondansetron – also failed to block transients (Figure S12- 8c). Furthermore, other 5-HT2A antagonists (i.e. Altanserin) dose-dependently inhibited 5-HT-induced Ca2+ transients (Figure S12- 10a to c) and across a wide range of 5-HT concentrations (Figure S12- 10d and e). Additionally, the effects of 5-HT were recapitulated by 5-HT2A agonists (Figure S12- 9a to d). However, activation of the canonical downstream pathway (i.e. Protein Kinase C; PKC substrate phosphorylation) of the 5-HT2A receptor was not detected under our conditions (Figure S12- 2b-d). These data suggest that 5-HT2A is the predominant 5-HT

receptor expressed in BAs, is activated at physiological concentrations of 5-HT and can be respectively activated or inhibited by existing pharmacological agonists and antagonists.

To ascertain what metabolic phenotypes the 5-HT2A receptor might mediate, we leveraged available data from the recombinant inbred BXD mice strains (Williams and Auwerx, 2015; Williams et al., 2014). BAT mRNA expression levels of all the murine 5-HT receptors, other 5-HT related gene mRNAs, and circulating 5-HT related measures from numerous BXD mouse lines were correlated with metabolic phenotypes associated with BAT, including VO_2 and body temperature, from the same mouse lines. This analysis identified numerous 5-HT receptors that are present in whole brown adipose tissue that to varying degrees correlated negatively with BAT influenced phenotypes (Figure 12f; others in Table S12- 5 to Table S12- 10). Notably, *Htr2a* was amongst the receptors that correlated with multiple of the above phenotypes. However, in comparison to *Htr2a* and *Tph1/2* mRNA expression, circulating 5-HT levels had relatively weak and variable correlations to VO_2 and body temperature (Table S12- 5 and Table S12- 6). However, compared to VO_2 and body temperature 5-HT levels correlated relatively stronger with RER and glucose tolerance, suggesting circulating 5-HT might have more influence over substrate selection or vice-versa. Therefore, it seems that BAT *Htr2a* mRNA negatively correlates with BAT-related phenotypes, but circulating 5-HT may not.

Since 5-HT did not acutely affect cAMP levels, the most well described BAT regulatory pathway, and BAT *Htr2a* mRNA correlated with metabolic phenotypes, we investigated what genes and functionally annotated gene families correlated with human adipose *Htr2a* mRNA levels. By correlating *Htr2a* mRNA expression from RNA-sequencing of human adipose tissue (subcutaneous and visceral; from the GTExPortal - Lonsdale et al., 2013) with all other mRNA species, we identified 2 lists of genes with mRNA expression either negatively or positively correlated with *Htr2a* mRNA in both depots (Figure 12g, Table S12- 1, and Table S12- 2). Transcripts common in both depots were used to define a general adipose tissue signature since BAT data was not available. Each list was then submitted for cellular component gene ontology analysis using the gene ontology tool (DAVID version 6.8; Huang et al., 2009b, 2009a). We found that positively correlated mRNA species were enriched in genes belonging to centriole, focal adhesion, nucleus, and other components. (Figure 12h and Table S12- 3) Interestingly and with greater statistical significance, mitochondrial components contained of many of the negatively correlated genes (Figure 12i and Table S12- 4). Since BAT-mediated thermogenesis is heavily reliant on mitochondrial function, these results suggest that the 5-HT2A receptor might regulate mitochondrial-related gene expression and consequently affect BAT phenotypes.

14.2.2 *Examining the effects of genetic inactivation/ablation of the 5-HT2A receptor*

To fully eliminate and evaluate 5-HT2A function, we rederived and obtained mice from frozen sperm at the NBRI-NJU with genetically inactivated *Htr2a* (C57Bl/6;129-5-HT2A$^{tm1a/Nju}$ herein termed *Htr2a*$^{-/-}$). Using a targeting vector, developed as part of the International Mouse Phenotyping Consortium, a gene trap cassette was introduced into chromosome 14. These mice have a *LacZ* and *Neo* interruption gene inserted before the *Htr2a* exon 2 (Figure 13a) and can be differentiated from *Htr2a*$^{+/+}$ via identification of an elongated PCR product due to the insertion (Figure 13b). We isolated, immortalized and confirmed the differentiation capacity (Figure S13- 1) of adipocyte progenitors from *Htr2a*$^{-/-}$ and *Htr2a*$^{+/+}$ littermate mice. Confirming the results from 5-HT2A antagonists, cultured *Htr2a*$^{-/-}$ brown adipocytes did not experience a 5-HT-induced Ca^{2+} transient and had reduced *Htr2a*$^{-/-}$ mRNA (Figure 13c and Figure S13- 2a). Although *Htr2b* and *Htr2c* mRNA appears to be lower in the *Htr2a*$^{-/-}$ versus *Htr2a*$^{+/+}$ cell line (Figure 13d), these differences were not statistically significant (*Htr2b:* $p = 0.17$ and *Htr2c:* $p = 0.37$). The apparent differences are likely due to the low abundance of these transcripts in the *Htr2a*$^{+/+}$ cell line as assessed by RNA-seq (Figure 12a) which may have led to inefficient/unpredictable amplification during qPCR and large variability. Low expression of *Htr2b* and *Htr2c* mRNA is also consistent with the RNA-Seq from other BA cell lines where *Htr2b* and *Htr2c* mRNA is significantly lower than *Htr2a* mRNA levels (Figure 12b and Figure S12-

1a to d). Furthermore, decreasing *Htr2a* levels in BAs using siRNA does not affect the expression of *Htr2b* or *Htr2c* thus suggesting the absence of linked or compensatory gene expression control of the 3 receptors (data not shown).

To examine the potential downstream effects of 5-HT2a, we treated *Htr2a*$^{+/+}$ and *Htr2a*$^{-/-}$ BAs acutely (4 hours) with 10 nM 5-HT. 5-HT reduced *Ucp1* mRNA in both BA lines (Figure 13e and f) and no changes in *Pparg* mRNA levels (Figure S13- 2b and c). However, in *Htr2a*$^{+/+}$ BAs 5-HT reduced *Ppargc1a* mRNA but not *Htr2a*$^{-/-}$ (Figure 13g and h). Therefore, consistent with correlations with mitochondrial genes, 5-HT appears to acutely impair expression of *Ppargc1a* – a major transcriptional co-regulator of mitochondrial-related genes. However, the mechanism mediating the decrease in *Ucp1* mRNA at this time point remains unknown.

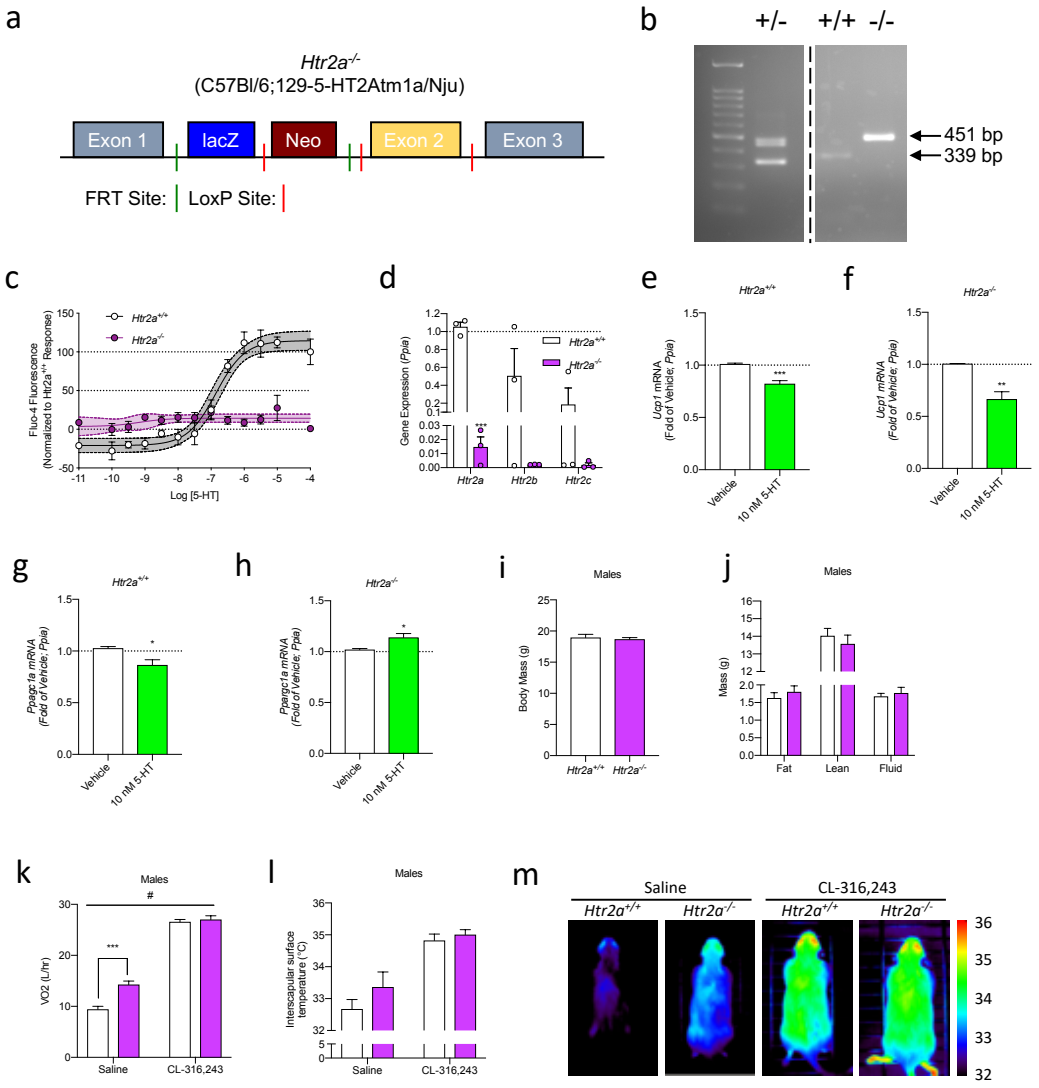

Figure 13. *Htr2a*$^{-/-}$ BAs are resistant to 5-HT induced reductions in *Ppargc1a* mRNA but do not have elevated BAT thermogenic capacity. a, Diagram of targetting vector for *Htr2a* inactivation in *Htr2a*$^{-/-}$ mice. b, example of genotyping result of *Htr2a*$^{-/-}$ showing that *Htr2a*$^{-/-}$ have a large amplicon from the *LacZ/Neo* gene interruption. c, Fluo-4 fluoresence (Ca^{2+}) of immortalized BAs from *Htr2a*$^{-/-}$ and *Htr2a*$^{+/+}$ littermates treated with different doses of 5-HT (n = 3 independent experiments performed in triplicate). d, mRNA expression levels of *Htr2a*, *Htr2b*, and *Htr2c* in BAs from *Htr2a*$^{-/-}$ and *Htr2a*$^{+/+}$ (n = 3 independent experiments performed in triplicate). e, *Ucp1* mRNA in *Htr2a*$^{+/+}$ BAs treated with 10 nM 5-HT for 4 hours (n = 3 performed in 2-3 replicates). f, Same as in e but with *Htr2a*$^{-/-}$ BAs (n = 4 performed in 2-3 replicates). g, *Ppargc1a* mRNA in *Htr2a*$^{+/+}$ BAs treated as in e (n = 4 performed in 2-3 replicates). h, Same as in g but in *Htr2a*$^{-/-}$ BAs (n = 4 performed in 2-3 replicates). i, Body mass in male *Htr2a*$^{+/+}$ and *Htr2a*$^{-/-}$ mice (n =

3-4 mice). j, Tissue type masses in male *Htr2a*$^{+/+}$ and *Htr2a*$^{-/-}$ mice (n = 3-4 mice). k, Absolute oxygen consumption rate in male *Htr2a*$^{+/+}$ and *Htr2a*$^{-/-}$ mice in response to CL-316,243 (n = 3-4). l, Interscapular surface temperature in mice from k. m, Representative images for l. All bars and points represent means and bars represent S.E.M. # = overall statistically significant interaction effect as assessed by 2-way ANOVA. * = $p < 0.05$, ** = $p < 0.01$, *** = $p < 0.001$ and **** = $p < 0.0001$ by Bonferroni post-hoc test for j. For d-h, * indicates $p < 0.05$ on from t-test. Additional data is included in Figure S13- 1, Figure S13- 2 and Figure S13- 3.

Subsequently, we collected preliminary metabolic information from young chow-fed *Htr2a*$^{-/-}$ and *Htr2a*$^{+/+}$ littermate mice (Males: N = 3-4; Females: N = 1-3; age: 5-6 weeks of age). We found no statistically significant differences in body mass or body composition in male (Figure 13i and j and Figure S13- 3a) or female mice (Figure S13- 3b to d). Under anaesthesia VO_2 was significantly higher in male *Htr2a*$^{-/-}$ mice compared to controls (Figure 13k to m; Figure S13- 3e to o). Activation of BAT with CL-316,243 increased VO_2 and intrascapular surface temperature to similar levels in both genotypes. These preliminary results suggest that germline inactivation of the *Htr2a* gene does not affect body composition or maximal BAT activity.

14.2.3 *Analysis of adipose-specific deletion of Htr2a*

Since 5-HT2A is expressed in numerous tissues, including neuronal tissues, and previous evidence for the contradictory regulatory roles of central (potentially positive) versus peripheral (potentially negative) 5-HT on BAT, we developed an adipose-tissue and temporally inducible conditional *Htr2a* KO mouse (herein termed the *Htr2a* AdKO; Figure 14a and Figure S14- 1). To induce deletion of exon 2 of *Htr2a* mice were dosed with tamoxifen (as per Mottillo et al., 2014) to activate

the translocation of the Cre-ERT2 fusion protein to the nucleus to perform its excision activity. However, confirmation of the deletion of *Htr2a* from BAT in this particular animal model remains to be completed and measurement of *Htr2a* mRNA in WAT has proven ambiguous; therefore, the extent of *Htr2a* deletion remains to be elucidated.

An initial cohort of induced male *Htr2a* AdKO (*LoxP*$^{+/+}$; *Cre*$^{+/+}$) and WT (*LoxP*$^{+/+}$; *Cre*$^{-/-}$) mice both received dosages of tamoxifen to induce deletion/act as a control. Following a 4-week washout, we assessed the BAT thermogenic capacity of these mice. We found that *Htr2a* AdKO mice consumed more oxygen and had elevated interscapular surface temperature in response to CL-316,243 (Figure 14b to f; Figure S14- 2). Therefore, *Htr2a* AdKO animals have elevated BAT thermogenic capacity and confirm the validity of targeting the 5-HT2A receptor on BAT to improve BAT capacity.

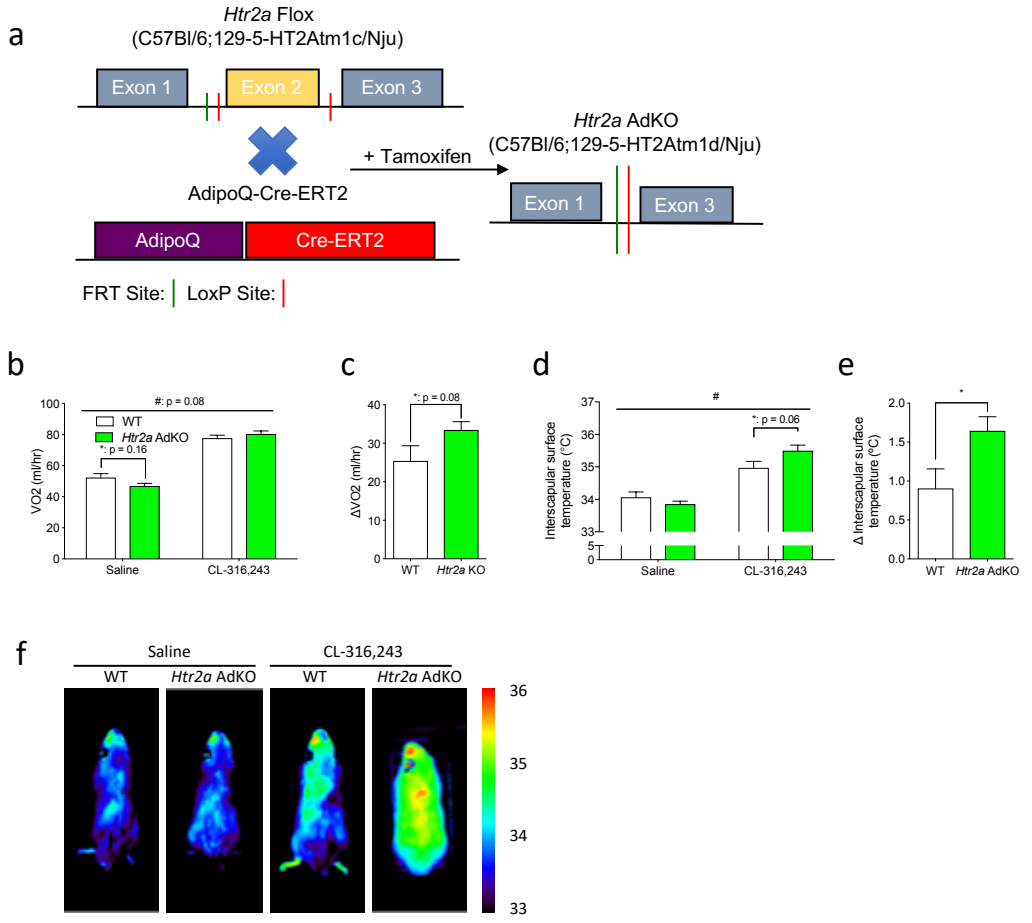

Figure 14. *Htr2a* AdKO mice have elevated BAT thermogenic capacity. a, Schematic of induction of adipose-specific *Htr2a* gene inactivation. b, Absolute rate of oxygen consumption in male *Htr2a* AdKO mice in response to CL-316,243 (n = 6-8 mice). c, Difference between saline and CL-316,243 induced VO2 from b. d, Interscapular surface temperature from same mice as b. e, Change in interscapular surface temperature of mice from b. f, representative images for d and e. Bars represent means with error bars represent S.E.M. # = overall statistically significant interaction effect as assessed by 2-way ANOVA. * = $p < 0.05$ by Bonferroni *post-hoc* test. Additional related data and information is included in Figure S14- 1 and Figure S14- 2.

14.2.4 *Examination of the effect of pharmacological inhibition of 5-HT2A on BAT thermogenic capacity*

Since *Htr2a* AdKO demonstrated increased BAT capacity versus littermate controls, we investigated if a pharmaceutical antagonist of the 5-HT2A receptor might yield similar results. With the help of Sam Chorlton, we identified a gene signature distinguishing MSCs from MSCs overexpressing *Ppargc1a*. This gene signature was then submitted to the LINCS tool to compare it to gene signatures similar to those elicited by known pharmaceutical agents (Figure 15a). Consequently, this produced a list of compounds that elicited adaptations similar to the overexpression of *Ppargc1a* in BAs (Figure 15b; Table S15- 1). Amongst these compounds of interest, numerous compounds were found to have activity against the 5-HT2A receptor or some of its known downstream pathways (Figure 15b). We found that the highest-ranking compound (Altanserin) blocked Ca^{2+} transients in BAs (Figure S12- 10a to c). This thereby suggested that available 5-HT2A antagonists indeed block 5-HT2A activity in BAs and consequently might directly convey a beneficial mitochondrial gene expression program in BAs similar to genetic ablation.

a

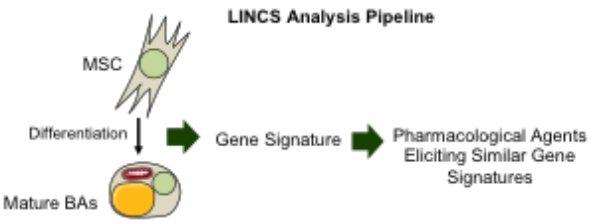

b

COMPOUND	CONNECTIVITY SCORE	COMPOUND	MECHANISM OF ACTION
I	0.4873	Altanserin	Htr2a antagonist
II	0.4856	Lysergol	Weak Htr2a agonist
III	0.485	Pimozide	Htr2a, Htr7, D2, D3 and D4 antagonist
IV	0.4845	Midostaurin	Ca^{2+} /DAG-dependent PKC isoform inhibitor
V	0.4672	Isoxicam	COX1 and COX2 Inhibitor
VI	0.4647	Nortriptyline	NET and Htr2a antagonist

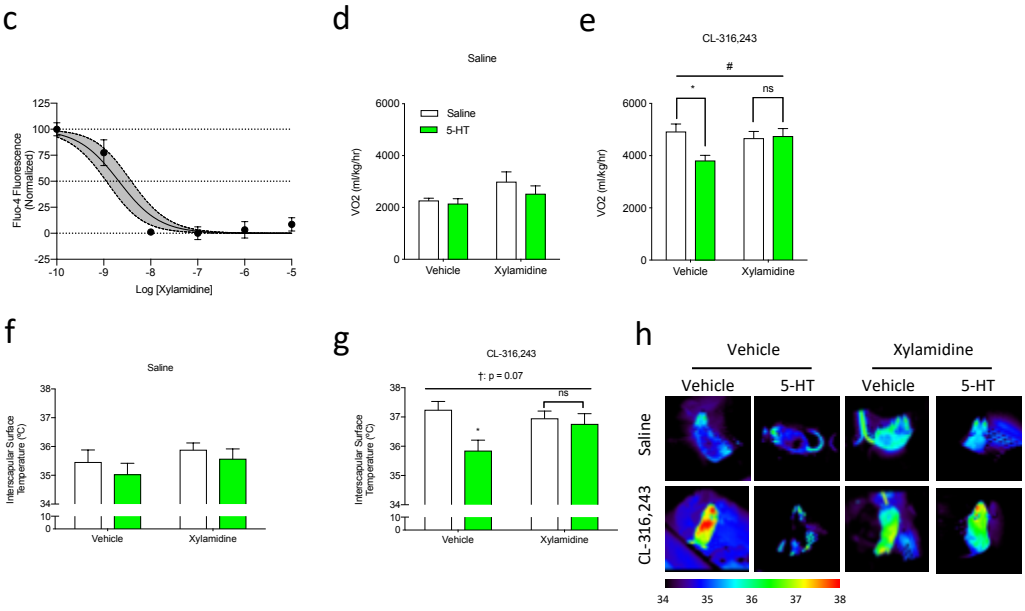

Figure 15. 5-HT2A antagonists are predicted to increase BAT differentiation gene program and Xylamidine, a peripherally-restricted 5-HT2A antagonist, blocks 5-HT induced Ca^{2+} transients and improves BAT thermogenic capacity. a, Schematic of Connectivity-Map analysis. b, List of hit compounds from a that are affect 5-HT2A or downstream pathways. c, Dose resposne of Xylamidine on 5-HT induced Ca^{2+} transients (n = 3 independent experiments performed in triplicate). d-h, Analysis of BAT functional thermogeneic capacity following acute Xylamidine injection followed by 5-HT administration and CL-316,243 by measuring VO2 (d – saline; e – CL-316,243) and interscapualr surface temperature (f – saline; g – CL-316,243; h – representative IR images; n = 4-6 mice). All bars and points represent means and error bars represent SEM. † = overall statistically significant effect of treatment and # = overall statistically significant interaction

effect as assessed by 2-way ANOVA. * = $p < 0.05$, ** = $p < 0.01$, *** = $p < 0.001$ and **** = $p < 0.0001$ by Bonferroni post-hoc test. Additional information is included in Table S15- 1, Table S15- 2, Table S15- 3, Figure S15- 1, Figure S15- 2, Figure S15- 3, Figure S15- 4, Figure S15- 5, Figure S15- 6 and Figure S15- 7.

Because preliminary whole-body *Htr2a* inactivation experiments yielded no significant differences in BAT activity but *Htr2a* AdKO mice did, we focused on 5-HT2A antagonists that did not cross the blood brain barrier (BBB). The compound we selected was Xylamidine. *In vitro*, it effectively attenuated 5-HT-induced Ca^{2+} transients with an IC_{50} of 7.53 ± 5.69 nM (Figure 15c and Figure S15-1a) and at 10 nM ablated 5-HT-induced Ca^{2+} transients at all doses of 5-HT tested (100 pM – 100 μM Figure S15- 1b). Notably, in confirmation that only high doses of 5-HT impair lipolysis and presumably via receptor-independent mechanisms, we found that Xylamidine did not block 5-HT induced attenuations of lipolysis (Figure S15- 4a to c) nor did siRNA against *Htr2a*, any other 5-HT receptor antagonist, 5-HT transporter inhibitors or reactive oxygen species (ROS) scavenger used (Figure S12- 3 to Figure S12- 7 and unpublished data from Dr. Emilio Mottillo; note that H_2O_2 is produced during 5-HT degradation by MAOs). Because this compound was discovered in 1967 without any specific application and relatively little knowledge of 5-HT receptors (Copp et al., 1967), we performed a variety of *in silico* analyses to predict its pharmacological properties and effects. Firstly, we used a model 5-HT2A receptor protein structure model (constructed from structures from homologous G-coupled receptors) and performed fixed structure docking simulations of 5-HT, MDL-100,907 and Xylamidine. Indeed, we confirmed that –

despite the inconsistency in pharmacological behaviour (i.e. inability of 5-HT to out-compete Xylamidine in Ca^{2+} assays; Figure S15- 1b) – that Xylamidine is predicted to occupy the same binding pocket as 5-HT and other 5-HT2A competitive antagonists (Figure S15- 1c-i). Next, we used predictive structure-activity/ADMET tools to analyze the potential effectiveness and complications of using this drug *in vivo*. Xylamidine was predicted to have the greatest activity for antagonizing 5-HT2A versus a variety of other 5-HT2A antagonists (Table S15- 2a and c). Conversely, it was not predicted to have 5-HT2A agonist activity (Table S15- 2b and d). Furthermore, when compared against other 5-HT2A antagonists and anti-obesity/diabetes medications, Xylamidine ranked lowest for predicted toxicological effects (Table S15- 2e). Consistent with previous reports of poor CNS effects (Copp et al., 1967; Dave et al., 2004), Xylamidine was either predicted to have low-moderate BBB permeability (relative to the centrally-targeted 5-HT2A antagonists MDL-100907 and Pruvanserin; Table S15- 3) or near BBB impermeability (Figure S15- 3). Additionally, Xylamidine was predicted to have moderate to high intestinal absorption and moderate plasma protein binding (Table S15- 3). Therefore, Xylamidine is an effective inhibitor of 5-HT2A with favourable pharmacological properties including relatively poor BBB permeability.

Xylamidine and other 5-HT2A antagonists are known to attenuate acute drops in body temperature induced by high levels of 5-HT (Carter and Leander, 1980; Osuide et al., 1984; Sugimoto et al., 1991). As shown in Figure 7b to d, we demonstrated acute 5-HT injection reduced BAT-induced thermogenesis. We

consequently repeated the previously published experiments (Carter and Leander, 1980; Osuide et al., 1984; Sugimoto et al., 1991) in non-anaesthetized male FVB/NJ mice at thermoneutrality with or without CL-316,243. Consistent with our previous findings in anaesthetized animals, we found that acute IP injection of 5-HT decreased VO_2 and interscapular surface temperature only under CL-316,243 stimulation (Figure 15d to h). This effect was quite transient (~ < 2 hours), consistent with a rapid clearance/metabolism of 5-HT from circulation (Figure S15-5a to d). Notably, following a 1-hour pre-treatment with Xylamidine these effects were attenuated (Figure 15d to h). We repeated these experiments in anaesthetized mice and observed similar results (Figure S15- 7). Although a single dose administered 3 hours before was found to be less effective at rescuing the 5-HT-induced decrease in interscapular surface temperature (data not shown), repeated daily administration of Xylamidine followed by a 24-hour washout period also partially rescued the attenuated VO_2 (data not shown). Thus, suggesting that Xylamidine can attenuate acute high dose 5-HT inhibition of BAT mediated energy expenditure.

Following the finding that Xylamidine can restore BAT thermogenesis following acute 5-HT treatment, we examined whether chronic administration of Xylamidine might increase BAT thermogenesis similar to that observed in the *Htr2a* AdKO. To do so, we IP injected RT housed, chow-fed C57Bl/6J mice daily with Xylamidine for ~5 weeks (Figure 16a). We observed no statistically significant differences in body mass, body composition, fat masses or tissue masses (Figure

16b to d and Figure S16- 1). Subsequently, we analyzed BAT thermogenic capacity by injecting anaesthetized mice with CL-316,243. Similar to *Htr2a* AdKO, Xylamidine-treated mice consumed more oxygen compared to vehicle (saline) controls (Figure 16e to I and Figure S16- 2). Therefore, it appears that Xylamidine represents a novel pharmaceutical that can improve BAT thermogenic capacity. Thereby indicating its potential therapeutic use in conditions where obesity may be induced by elevations of extracellular 5-HT levels.

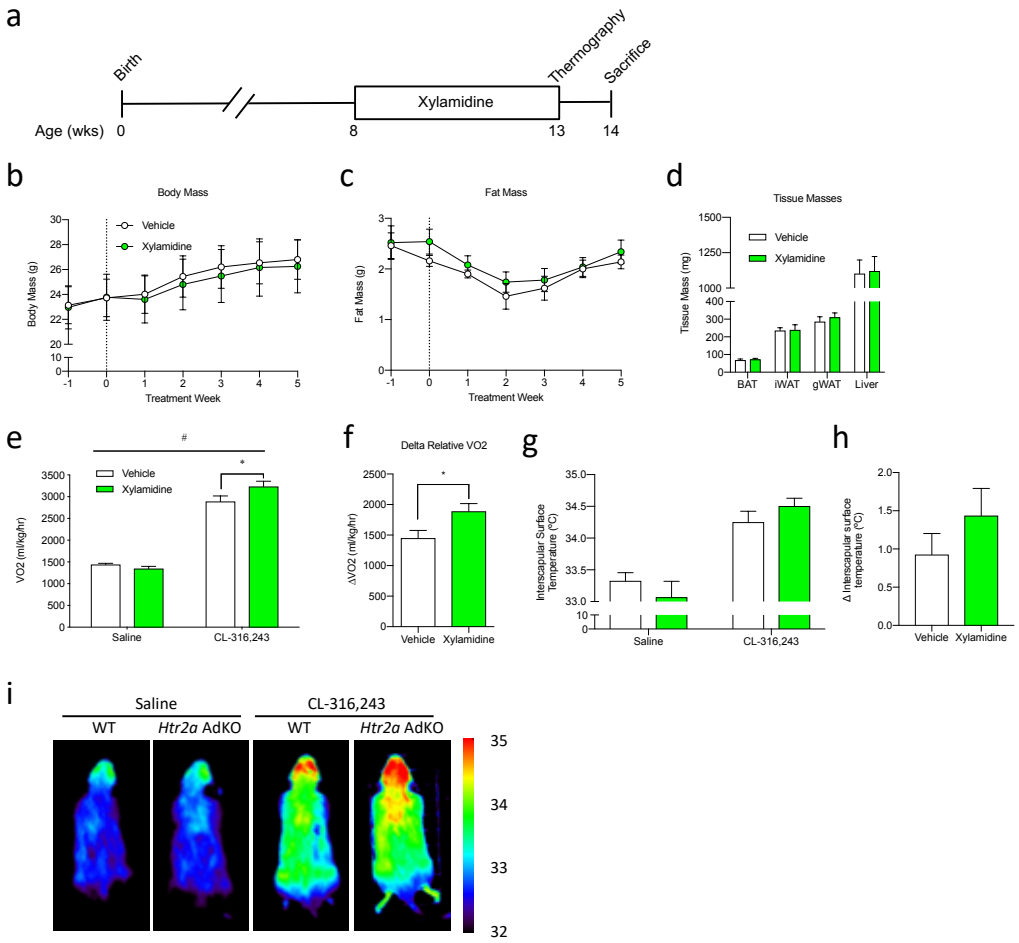

Figure 16. Chronic administration of Xylamidine improves BAT thermogenic capacity but does not affect body mass. a, Time course of treatment administration. b, Growth curve of male C57Bl/6J mice treated with Xylamidine (n = 5 mice). c, Fat mass during duration of Xylamidine treatment (n = 5 mice). d,

Select tissue masses at sacrifice of mice in b and c (n = 5). e-i, Analysis of the effect of chronic xylamidine administration on thermogenic capacity of BAT by measuring VO2 (e) the change in VO2 from saline to CL-316,243-induced (f), interscapular surface temperature (g) and change in tnerscapular surface temperature (h; i - representative images; n = 5 mice). # = overall statistically significant interaction effect as assessed by 2-way ANOVA. * = $p < 0.05$ by Bonferroni *post-hoc* test for e and by t-test for f. Additional data is included in Figure S16- 1 and Figure S16- 2.

14.3 The effect(s) of inhibiting 5-HT2A receptor activity in a model of SSRI-induced obesity

Having demonstrated that both eliminating adipose tissue 5-HT2A and that a peripherally-restricted 5-HT2A antagonist (Xylamidine) can improve BAT thermogenic capacity, we explored if Xylamidine could rescue SSRI-induced obesity. Not all SSRIs are associated with weight gain; however, Paroxetine (Par; tradename: Paxil®) is associated with weight gain with chronic treatment (Serretti and Mandelli, 2010) and Paroxetine has been previously suggested to impair BAT thermogenic capacity (Zha et al., 2017). Although, we demonstrated that *Slc6a4*$^{-/-}$ mice have elevated BAT thermogenic capacity (Figure 11 and Figure S11- 1), they still had increased adiposity suggesting that the elevated BAT capacity and EE was insufficient to counter the obesogenic processes induced by whole body deletion of *Slc6a4* (Figure 8, Figure S8- 1 and Figure S8- 2). Given we found Xylamidine increased BAT thermogenic capacity, we administered Paroxetine in the drinking water to chow-fed, RT-housed male C57Bl/6J mice with or without daily IP injections of Xylamidine for 15 weeks with the hypothesis that Xylamidine would counteract Paroxetine-induced weight gain by further enhancing BAT thermogenesis (Figure 17).

Paralleling our previous results with *Slc6a4*$^{-/-}$ mice and consistent with previous studies (Zha et al., 2017), Paroxetine treatment caused a modest but statistically significant increase in body mass at sacrifice (~1-2 g; Figure S17- 2a and Figure 17b and c). In particular, there was expanded fat mass ($p = 0.001$ versus

saline controls via 2-way ANOVA; Figure 17d and e and Figure S17- 1d) and white adipose tissue depots, with (Figure S17- 2c and d) or without correction (Figure 17g and h) for body mass. Furthermore, this was paralleled by an increase in fluid mass but not lean mass (Figure S17- 1a, b f and g). However, in contrast to our hypothesis, Xylamidine did not attenuate increases in body mass or fat mass derived from Paroxetine-treatment (Figure 17c and e and Figure S17- 1d).

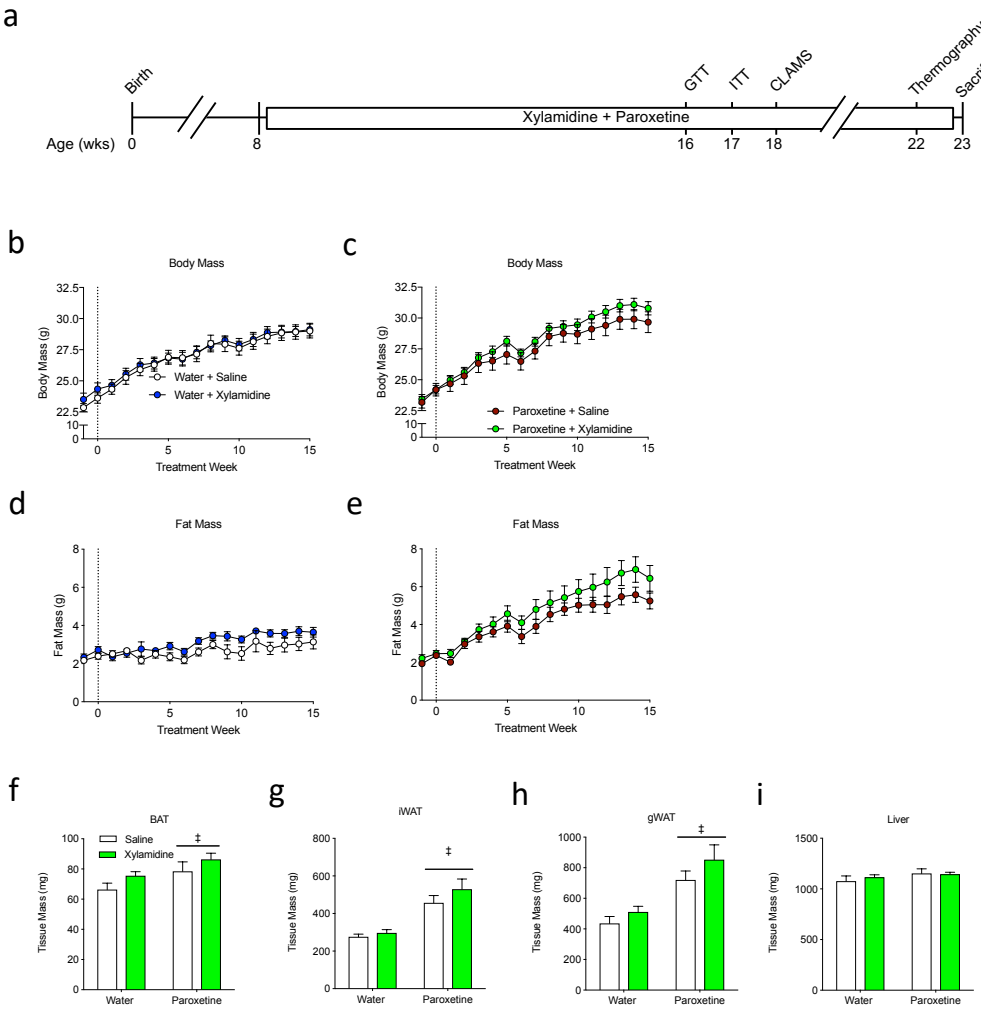

Figure 17. Paroxetine-induced increases in body mass and adiposity is not blocked by Xylamidine. a, Time course of treatment administration and experimental data collection. Body mass overtime of mice treated with saline or

xylamidine alone (b; n = 9-10 mice) or in combination with paroxetine (c; n = 9-10 mice). Fat mass for water (d; n = 9-10 mice) or paroxetine-treated (e; n = 9-10 mice) mice treated with or without xylamidine. BAT (f; n = 9-10 mice), iWAT (g; n = 9-10 mice), gWAT (h; n = 9-10 mice) and Liver (i; n = 8-10 mice) masses at sacrifice of mice treated with water or paroxetine in combination with saline or xylamidine. ‡ = overall statistical significance elicited by Paroxetine as determined by 2-way ANOVA. Additional data is included in Figure S17- 1 and Figure S17- 2.

To investigate the cause of increase in adiposity with Paroxetine and Xylamidine, we used metabolic cages to assess energy expenditure and caloric intake. Consistent with our results in *Slc6a4*$^{-/-}$ mice, Paroxetine elevated EE during the day (Figure 18a to d). Xylamidine did not have a statistically significant effect on total EE in either the vehicle or Paroxetine-treated mice. However, surprisingly at this time point, Paroxetine-treated mice appeared to have reduced dark phase food intake (Figure 18e to h) and reduced physical activity (Figure 18i to l and Figure S18- 1d to f). Interestingly, Xylamidine did increase EE in Paroxetine - treated mice when accounting for differences in physical activity (Figure 18m to p); however, as noted above, this was insufficient to alter overall caloric expenditure. We observed no significant differences in RER with either Paroxetine, Xylamidine or the combination of the two (Figure 19a to d). However, Paroxetine impaired glucose tolerance (Figure 19e to g and Figure S19- 1a and b) and increased insulin resistance (Figure 19h to j and Figure S19- 1c and d), an effect which was unaltered by Xylamidine. These data indicate that Paroxetine promotes obesity and insulin resistance and that the peripherally restricted 5-HT2A antagonist Xylamidine is unable to prevent these effects.

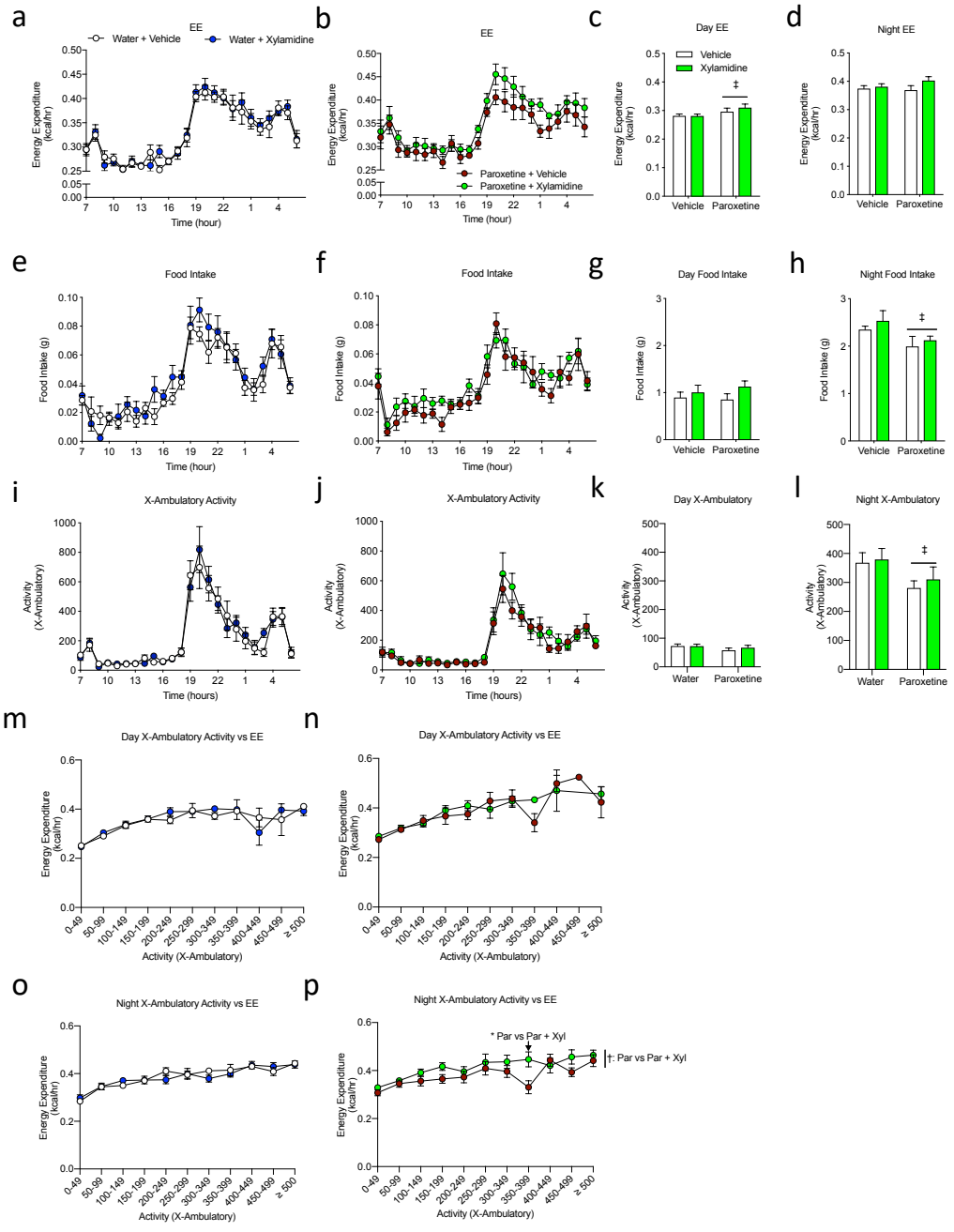

Figure 18. Xylamidine does not alter EE or caloric intake in paroxetine treated mice. Energy expenditure of mice treated with water (a; n = 7-9 mice) or Paroxetine (b; n = 8 mice) in combination with vehicle (saline) or Xylamidine over 24 hours.

Average energy expenditure during light- (c; n = 7-9 mice) or dark-period (d; n = 7-9 mice). Food intake over 24-hours in water- (e; n = 7-9 mice) or paroxetine-treated (f; n = 8 mice) mice. Total food intake during light- (g; n = 7-9 mice) or dark-period (h; n = 7-9 mice). Ambulatory activity in the x-axis as treated above (i: water-treated; n = 7-9 mice j: paroxetine-treated; n = 8 mice). Average ambulatory activity in the x-axis during the light-(k; n = 7-9 mice) or dark-period (l; n= 7-9 mice). Energy expenditure as a function of ambulatory activity for water-(m and o; n = 7-9 mice) or paroxetine-treated mice (n and p; n = 8 mice) in the light-phase (m and n) and dark-phase (o and p). † = overall effect of Xylamidine and ‡ = overall statistical significance elicited by Paroxetine as determined by 2-way ANOVA. * indicates significant effect as assessed by Bonferroni *post-hoc* test. Figure S18- 1.

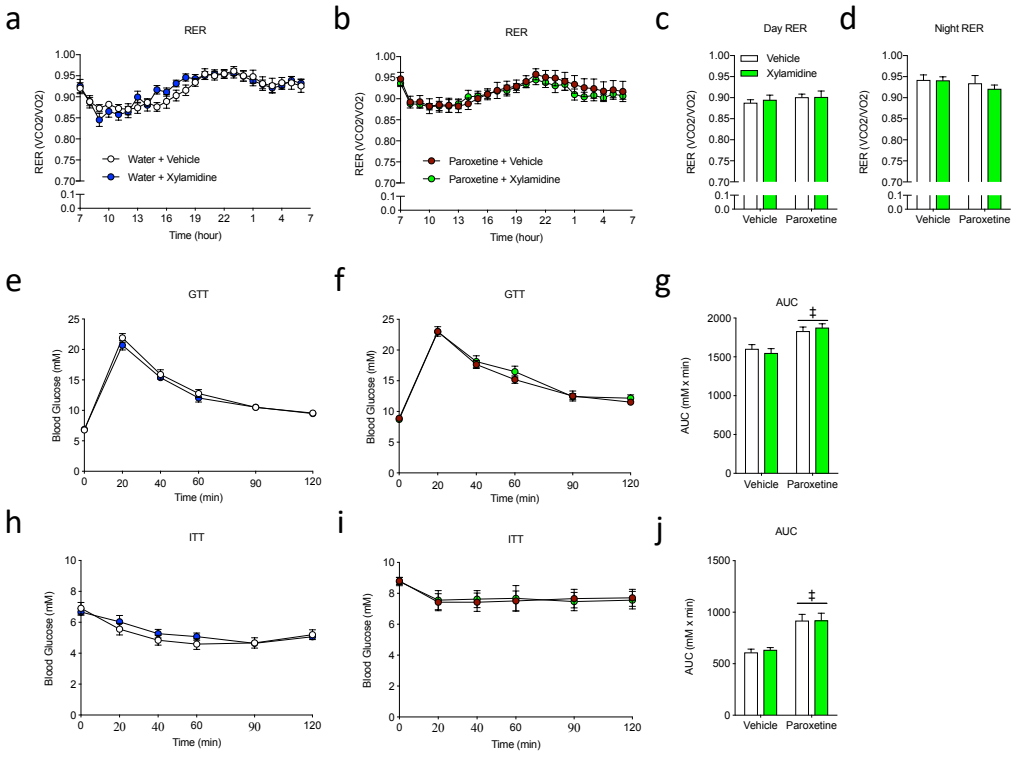

Figure 19. Chronic Xylamidine does not improve SSRI induced changes in glucose homeostasis. Respiratory exchange ratio (RER) of mice treated with water (a; n = 7-9 mice) or paroxetine (b; n = 8 mice) in combination with vehicle or Xylamidine over a 24 hour period. RER during the light-(c; n = 7-9 mice) and dark-period (d; n = 7-9 mice). Blood glucose levels throughout a glucose tolerance test (GTT) in water-(e; n = 8-10 mice) or paroxetine-treated (f; n = 10 mice), and AUC (g; n = 8-10 mice). Blood glucose levels throughout an insulin tolerance test (ITT) in water-(e; n = 9-10 mice) or paroxetine-treated (f; n = 10 mice), and AUC (g; n =

9-10 mice). ‡ = overall statistical significance elicited by Paroxetine as determined by 2-way ANOVA. Additional data is included in Figure S19- 1.

We hypothesized that Xylamidine might further enhance BAT thermogenesis in mice treated with Paroxetine; therefore, we examined if BAT thermogenic capacity was improved in these animals. Using CL-316,243 to activate β3-receptors on BAT, we measured maximal BAT thermogenic capacity. In water-treated mice, Xylamidine did not increase VO_2 (Figure 20a and Figure S20- 1a) or interscapular surface temperature (Figure 20d and g) in response to CL-316,243. Paroxetine-treatment alone increased CL-316,243 induced VO_2 (Figure 20c) and interscapular surface temperature (Figure 20f). In combination with Paroxetine-treatment, Xylamidine further increased CL-316,243 induced interscapular surface temperature (Figure 20e to g) and tended to increase VO_2 (Figure 20b and c and Figure S20- 1b and c). This finding is consistent with the hypothesis that Paroxetine increases 5-HT signalling systemically and increases BAT thermogenic capacity, and Xylamidine inhibition of peripheral 5-HT2A receptor activity enhances this effect.

In conclusion, although Xylamidine improves BAT capacity in mice treated with Paroxetine, it is insufficient to attenuate the energy surplus that causes increased fat mass in these animals.

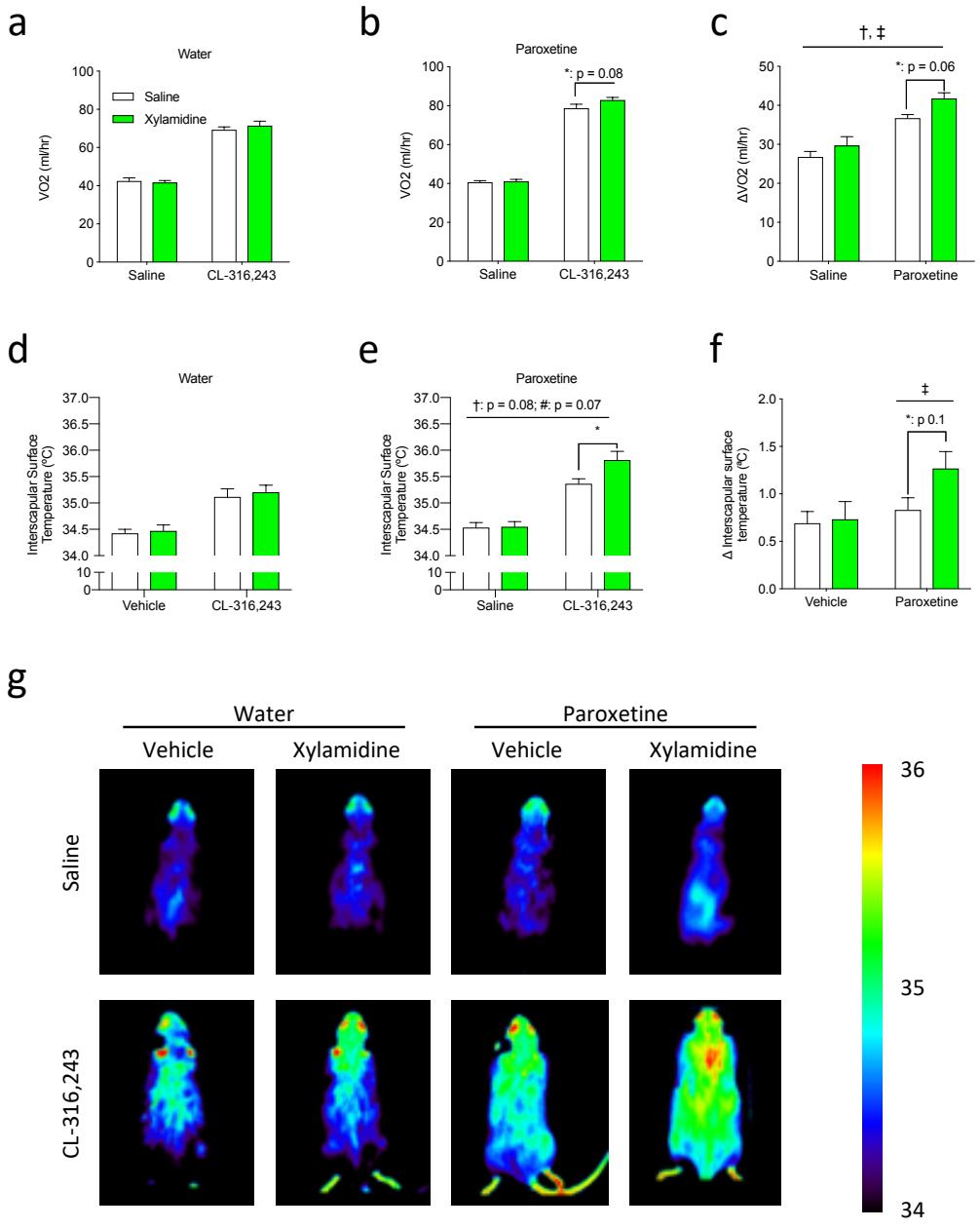

Figure 20. Xylamidine improves BAT thermogenic capacity in Paroxetine treated mice. Oxygen consumption rates (VO_2: a-c) and interscapular surface temperature (d-f) in mice chronically treated with water (a; n = 9-10 mice) or Paroxetine (b; n = 10 mice) in combination with saline or Xylamidine and acutely challenged with saline or CL-316,243. Difference in VO_2 (c; n = 9-10 mice) and interscapular surface temperature (f; n = 9-10 mice) elicited under CL-316,243- and

saline-treatment. g, Representative infrared images of mice assayed in d-f. † = overall effect of Xylamidine, ‡ = overall statistical significance effect of Paroxetine, and # = overall interaction effect as determined by 2-way ANOVA. * indicates significant effect as assessed by Bonferroni *post-hoc* test. Additional data in Figure S20- 1.

15 Discussion

As detailed in the results section the primary findings of the thesis: 1) described the effects of 5-HT on BAT *in vitro* and *in vivo*; 2) identified 5-HT2A as the predominant 5-HT receptor expressed in BAT; 3) showed that pharmacological and genetic inhibition of 5-HT2A blocks 5-HT signaling in BAT; and 4) established that Xylamidine, a peripherally restricted 5-HT2A antagonist, enhances BAT thermogenesis and EE. The following will discuss how these main findings contributed to the field.

15.1 *In vitro,* direct effects of 5-HT on BAT

With the recent papers demonstrating that inhibiting peripheral serotonin synthesis prevents obesity (Crane et al., 2015; Oh et al., 2015), there has been a surge of interest in the area of peripheral serotonin as a potential therapeutic target. However, few studies have investigated the effects of elevated 5-HT on BAs and the potential metabolic outcomes. Furthermore, in the few studies that have investigated the effects of 5-HT on BAs the results were often limited by experimental design (i.e. high doses of 5-HT) and lack of functional outcomes (i.e. thermogenesis/oxygen consumption; Crane et al., 2014b; Oh et al., 2016; Rozenblit-Susan et al., 2018). To further elucidate the effects of elevated 5-HT on BAs, we conducted experiments on both BAs *in vitro* and BAT function *in vivo*.

Firstly, we demonstrated that 5-HT has direct effects on BAs *in vitro*. We found that a high dose of 5-HT (100 μM) inhibits BA lipid accumulation, free-fatty acid mobilization and extracellular acidification rate. These data indicate that BA

fuel storage during differentiation and fuel mobilization after differentiation might be compromised by high dose 5-HT. High dose 5-HT (100 μM) reduced BA lipid accumulation, an indicator of impaired differentiation. This is consistent with recent work showing reductions in differentiated BA mRNA markers (including *Ucp1*) in an immortalized BA cell line treated with 10 μM 5-HT during differentiation (Rozenblit-Susan et al., 2018). However, we later found that treating BAs after differentiation with high dose 5-HT resulted in increased *Ucp1* promoter activity, increased *Ucp1* mRNA (in combination with adrenergic and PKA agonists) and tended to increase UCP1 protein, indicating potential contrasting effects of 5-HT during differentiation of BAs and post-differentiation.

FFAs are endogenous direct activators of UCP1 and supply fuel for oxidation during thermogenesis. Early research demonstrated that treatment of freshly isolated BAT with 5-HT increased BAT lipolysis (Yoshimura et al., 1969a) and thermogenesis (Yoshimura et al., 1969b). This effect was explained by increased activation of afferent nerve terminals by the administered 5-HT (Steiner and Evans, 1976). Using *in vitro* differentiated BAs we found that high doses of 5-HT impaired BA lipolysis, consistent with recent observations that cultured WAs treated with 10 μM 5-HT have attenuated lipolysis (Hansson et al., 2016) and that BAs treated with 100 μM 5-HT have decreased cAMP levels (Crane et al., 2015). In addition to FFAs, glucose has also been shown to be a substrate for BAT during thermogenesis (Ma and Foster, 1986; Vallerand et al., 1990; Weir et al., 2018) and we found ECAR (an indicator of glycolytic flux) was also reduced by high doses

of 5-HT (100 μM). However, the high dose 5-HT induced reductions of lipolysis and glycolysis were not sufficient to limit oxygen consumption rates in vitro. Furthermore, concentrations of isoproterenol above 1 nM appeared to overcome 5-HT-induced reductions in lipolysis and ECAR. In addition to these acute effects of 5-HT on BAT metabolism, the combination of high dose 5-HT and adrenergic stimuli appeared to increase BAT *Ucp1* promoter activity and consequently *Ucp1* mRNA levels. These are in stark contrast to observations previously made in our laboratory/group where acute 5-HT administration attenuates *Ucp1* mRNA levels in response to mild adrenergic stimuli (Crane et al., 2015). Although we repeated the inhibitory effect of high dose 5-HT with no/low adrenergic stimuli (i.e. ≤ 1 nM), we did not find that adrenergic stimuli at this concentration induced a similar increase in *Ucp1* mRNA (no change but 3-fold increase with 10 μM Iso versus ~40 fold with 1 nM Iso; Crane et al., 2015). However, the 10 μM isoproterenol induced increase in *Ucp1* mRNA is consistent with other previous reports treating BAs in culture with CL-316,243 (Cao et al., 2001) but might represent a unique effect of the cell line used previously by our group which had low basal levels of *Ucp1* mRNA expression (data not shown) compared to the BAs used in the current study.

Our findings of increased *Ucp1* mRNA levels in response to high dose 5-HT with typical adrenergic stimuli concentrations (≥ 10 nM) can be explained by the known PPARɣ agonist activity of 5-HT metabolites (formed during oxidation of 5-HT by MAOs) in WAs (Waku et al., 2010). In preliminary experiments, when BAs were treated with high dose 5-HT or 5-HIAA, GW-9662 - a PPARɣ antagonist

– blocked the increase in *Ucp1* promoter activity. Furthermore, we found active transportation of 5-HT via high-capacity low-affinity transporters (PMAT and OCT3) and high expression of MAOs in BAs, consistent with early reports of monoamine oxidase activity in BAs (Masters, 1972; Yoshimura et al., 1969a) and recent findings in WAs (Bour et al., 2007). These findings suggest that BAs maintain molecular machinery to degrade high amounts of 5-HT. Notably metabolites of 5-HT (i.e. 5-HIAA, 5-HTP, Melatonin and L-Tryptophan from Crane et al., 2015) do not appear to impair lipolysis signaling, nor does antagonists of 5-HT receptors/5-HT transporters or a ROS scavenger (to scavenge H_2O_2 produced by MAOs) rescue the attenuation of lipolysis by 100 μM 5-HT. In fact, this 5-HT concentration exceeds binding affinities of 5-HT receptors (≤ ~1 μM; Watts, 2016) and far exceeds circulating levels of 5-HT (i.e. ~1-10 nm; Brand and Anderson, 2011), thereby suggesting that high dose 5-HT impairs lipolysis via an unknown noncanonical mechanism.

The physiological relevance of the high doses of 5-HT used above are unknown. Although previous studies have speculated that HFD-feeding and obesity increases 5-HT pathologically (potentially to sufficiently high levels to elicit the effects discussed above) and suggested that this leads to impairment of EE and consequent weight gain (Crane et al., 2015), there have been conflicting results. Some studies have found that HFD-feeding increases 5-HT in BAT (Crane et al., 2015), plasma/serum (Crane et al., 2015; Kim et al., 2011), while data from within the Steinberg lab and more recent studies have shown unchanged (Oh et al., 2015;

Crane, J., unpublished), reduced levels (Mortuza, R., unpublished; Yabut, J., unpublished; Rami et al., 2018) or undetectable levels of 5-HT (Ikegami et al., 2018) within BAT and the circulation. Therefore, whether 5-HT is elevated in BAT/plasma during HFD appears to be absent and thus, even under pathological conditions – such as obesity, unlikely to reach the high doses required to inhibit lipolysis, ECAR, and cAMP generation. Furthermore, the combination of the high concentration for 5-HT (high ≥ 100 μM) and low adrenergic stimuli (relatively low; i.e. ≤ 1 nM) required to observe impairment by 5-HT *in vitro* suggests that these conditions likely have poor translatability to *in vivo* physiology. Additional studies will be required to quantitatively assess extracellular 5-HT in BAT *in vivo*.

Because of the high concentrations required to elicit deleterious effects of 5-HT on BAs and the abundance of non-specific 5-HT transporter and 5-HT catabolism genes, it can be postulated that 5-HT transport and metabolism in cultured BAs might mask the effect of low dose 5-HT on BAs that would occur *in vivo* with a constant blood supply. WAs express SERT (*Slc6a4*; Stunes et al., 2011) and OCT3 (Song et al., 2019), BeAs express OCT3 (Breining et al., 2017) and resident non-adipocyte cells in adipose tissue also express MAO and OCT3 (Camell et al., 2017; Pirzgalska et al., 2017), enzymes important for the breakdown and uptake of 5-HT. Our findings suggest that BAs express low levels of *Slc6a4* (compared to other 5-HT related genes, i.e. the 5-HT2A receptor) with low transport activity (as determined by poor sensitivity to SERT inhibitors). However, genetic inactivation of *Slc6a4* and treatment with 250 nM Paroxetine (SERT

inhibitor) both revealed greater effects of 5-HT on *Ucp1* promoter activity, *Ucp1* mRNA expression, and UCP1 protein levels in response to low levels of 5-HT (~1-10 nM). Therefore, presumably impeding the intracellular import of 5-HT allows for greater extracellular receptor activation. This suggests that SERT and other 5-HT transporters might block the inhibitory effects of 5-HT on *Ucp1* gene transcription by reducing extracellular 5-HT available to activate 5-HT receptors (similar to that observed in pre-synaptic membranes of synaptic clefts).

In conclusion, although 5-HT has many acute effects on BAs including reducing triglyceride hydrolysis and glycolysis, the 5-HT concentrations required to elicit these responses are likely supraphysiological and unlikely to be mediated by canonical (i.e. 5-HT receptor or 5-HT transporter) mechanisms. Furthermore, high doses of 5-HT results in increases in *Ucp1* promoter activity and mRNA – presumably due to production of downstream metabolites by MAOs and consequent PPARɣ agonism. However, more physiological doses of 5-HT in combination with SSRIs revealed transcriptionally regulated processes in *Ucp1* promoter activity and mRNA that subsequently could impair BA function.

15.2 Effects of acute *in vivo* manipulations of 5-HT on BAT-mediated Energy Expenditure

Because previous work has implicated peripheral serotonin synthesis in energy balance/EE, this required the investigation of the effects of elevated 5-HT *in vivo*. Both IV and IP administration of 5-HT acutely impaired VO_2/EE under cold stress and adrenergic stimuli (CL-316,243). This is consistent with prior

literature showing acute 5-HT administration decreases core body temperature (Carter and Leander, 1980; Sugimoto et al., 1991) and chronic administration of 5-HT (with slow release 5-HT pellets) reduces BAT functional capacity (Crane et al., 2015). However, whether these effects were due to direct inhibition of BAT thermogenesis or may have been due to alterations in blood flow or other mechanisms was not understood. In order to elicit a more physiological and small increase in extracellular 5-HT (~350% increase), we administered Paroxetine to mice at RT and measured acute changes in EE. Consistent with the administration of 5-HT, this also reduced EE. However, this reduction in EE may have been related to reduced physical activity and feeding behaviour – a known 5-HT regulated behaviour (Tecott, 2007). Notably, this effect was also reversed upon cessation of Paroxetine treatment, suggesting an acute effect of the reduction in 5-HT transport and consequent presumed elevated extracellular 5-HT on EE. Together with the fact that, *in vitro*, preliminary data with physiological concentrations of 5-HT failed to reduce BA oxygen consumption rates or lipolysis, this suggests that 5-HT impairs adrenergic induced EE (presumably mainly BAT-mediated) via indirect effects on BAs. These effects might be due to the known vasoconstrictive (typically mediated by 5-HT2A receptors; Watts et al., 2012), the hypoxic effect of 5-HT (Cater et al., 1961) and the recently identified peripheral 5-HT inhibition of sympathetic outflow to BAT (Mota et al., 2020). Upon cold-exposure, to defend core body temperature against decreasing, NE is released from nerves and binds to α-adrenergic receptors in cutaneous vessels causing vasoconstriction (Ekenvall et al., 1988). NE

additionally activates BAT with a concurrent rapid increase in local blood flow (Heim and Hull, 1966) that might be attributed to the increase blood flow mediated by β-adrenergic receptors (Kondo et al., 1992) and is independent of UCP1-mediated thermogenesis (Abreu-Vieira et al., 2015). Although no study, to our knowledge, has demonstrated that selective vasoconstrictive agents reduce BAT function, the increased shunting of blood flow to BAT during cold/adrenergic-stimulus presumably makes it susceptible to inhibition by vasoconstrictive agents, such as 5-HT. Furthermore, hypoxia – a presumed consequence of vasoconstriction and known effect of 5-HT (Dawkins and Hull, 1964) – inhibits BAT thermogenesis, presumably by limiting O_2 supply for mitochondrial respiration – and is not limiting in typical cell culture conditions (Ast and Mootha, 2019). Additionally, the hypothesized acute vasoconstriction response in our model is consistent with our casual observations of difficulty initiating blood draws and subsequent short bleeding times in animals treated with 5-HT; however, these observations may be partially attributed to 5-HT-induced platelet aggregation and subsequent coagulation (Lopez-Vilchez et al., 2009), notably, a process also thought to be regulated by 5-HT2A (Ogawa et al., 2002; Stott et al., 1988). Acutely, injecting 5-HT or Paroxetine with CL-316,243 in the *Htr2a* AdKO would test if 5-HT acutely regulates thermogenesis *in vivo* via the predominant 5-HT receptor in adipocytes. Future studies are needed to investigate the contribution of reduced blood flow/hypoxia and physical activity to mediating the suppression of EE by 5-HT.

15.3 Effects of chronic *in vivo* manipulations of 5-HT on BAT-related phenotypes

Some SSRI drugs are known to cause obesity. In particular, Paroxetine appears to be highly obesogenic with chronic treatment in clinical populations (Serretti and Mandelli, 2010). Recently, studies have investigated if SSRIs inhibit or activate BAT to modify body mass. These results however have been contradictory. Fluoxetine (Prozac) administration during the neonatal period in mice decreased body mass, increased EE and increased GDP-sensitive oxygen consumption in BAT, thereby suggesting a positive effect on BAT (Braz et al., 2020). However, in contrast to this, Paroxetine (Paxil) induced weight gain and hypertrophy in WAT and BAT (Zha et al., 2017). Furthermore, this was recapitulated in *Slc6a4*$^{-/-}$ mice which have a known propensity for obesity (Chen et al., 2012; Murphy and Lesch, 2008; Üçeyler et al., 2010) as do *Slc6a4*$^{-/-}$ rats (Homberg et al., 2010). However, notably, no functional measurements of EE were made in *Slc6a4*$^{-/-}$ or Paroxetine-treated mice (Zha et al., 2017) and the EE decrease was simply implied from increased body mass without changes in caloric intake. Therefore, the origin of the net positive caloric balance remained unknown.

In our experiments, we confirmed earlier studies describing a propensity for obesity in *Slc6a4*$^{-/-}$ mice (Chen et al., 2012; Murphy and Lesch, 2008; Üçeyler et al., 2010; Zha et al., 2017). Surprisingly, when measuring absolute (i.e. not corrected to body mass) EE using indirect calorimetry, we found that *Slc6a4*$^{-/-}$ mice had similar and not reduced EE both before (12 weeks) and after (27 weeks)

detectable differences in body mass. We found reduced physical activity as per previous reports (Üçeyler et al., 2010). However, when correcting for physical activity levels, in contrast to suggestions from previous studies (Zha et al., 2017), we found that these mice had increased EE at rest and each level of activity, indicative of excess energy expenditure at each physical activity level, potentially caused by a form of mitochondrial uncoupling. Thus, reduced EE did not explain the observed weight gain.

To ascertain the source of the net positive energy balance, we examined caloric intake. We observed that *Slc6a4*$^{-/-}$ mice had elevated food intake. In contrast, previous studies of *Slc6a4*$^{-/-}$ mice found no differences in caloric intake but corrected their values to body mass (Chen et al., 2012; Üçeyler et al., 2010; Zha et al., 2017). Although this is often used to describe nutritional requirements, it neglects to appreciate the first law of thermodynamics - the conservation of energy. Weight gain/loss is determined by the net number of calories absorbed minus the calories expended. Correcting to body mass does not allow for correct comparisons to energy expenditure (when not corrected for body mass) and thus previous studies thereby masked the greater caloric intake in the heavier *Slc6a4*$^{-/-}$ mice and its positive contribution to caloric balance. This is in contrast to the anti-obesity effects of the 5-HT2C receptor centrally (Nonogaki et al., 1998) and the acute effects of some SSRIs in humans but is consistent with the chronic obesogenic effect of SSRIs like Paroxetine (Serretti and Mandelli, 2010). Because our model elevates 5-HT signalling systemically, the increase in appetite may represent an increase in central

5-HT signaling affecting behaviour. This contradicts both our observation that acute Paroxetine reduces caloric intake and the anorexigenic effect of activating the 5-HT2C receptor in the hypothalamus (Martin et al., 2011). However, it may represent an adaptive response to the elevated 5-HT signalling as SSRIs are known clinically to cause adaptive responses to produce their antidepressant effects.

In contrast to previous studies in both chow-fed and HFD mice, we found that our chow-fed *Slc6a4*$^{-/-}$ mice did not have significant reductions in glucose tolerance (Chen et al., 2012; Zha et al., 2017). Given the increased adiposity of the *Slc6a4*$^{-/-}$ mice, the lack of a difference in glucose tolerance is surprising. However, we did observe a greater rate of glucose oxidation in male *Slc6a4*$^{-/-}$ mice which might suggest that these mice are preferentially oxidizing glucose. Therefore, although there may be glucose intolerance in some tissues (such as the hypertrophic WAT) other tissues may be oxidizing more glucose than normal and thus masking an overall glucose intolerant phenotype. Alternatively, as HFD-feeding has been shown to exacerbate the reduced glucose tolerance in *Slc6a4*$^{-/-}$ mice (Chen et al., 2012), the adiposity observed in our experiments may have not been sufficient to decrease whole body glucose tolerance. Further investigation would be required to determine glucose oxidation in a tissue specific manner in *Slc6a4*$^{-/-}$ mice.

As other papers have had conflicting findings about whether SSRIs affect BAT, we analyzed the energy expenditure of *Slc6a4*$^{-/-}$ mice under conditions known to inactivate and activate BAT. Under anaesthetic at ~30ºC, there were no differences in VO_2 between *Slc6a4*$^{+/+}$ and *Slc6a4*$^{-/-}$ mice. Consistent with the

increased EE (independent of physical activity) in free living mice at RT, stimulation of anaesthetized mice with CL-316,243 at ~30ºC revealed that male *Slc6a4*$^{-/-}$ mice had greater VO_2 than male *Slc6a4*$^{+/+}$ mice, suggesting that male mice have greater BAT functional capacity. This is in direct contrast to our *in vitro* experiments with Paroxetine that demonstrated reductions in *Ucp1* promoter activity in combination with 5-HT and a previous paper suggesting that *Slc6a4*$^{-/-}$ or Paroxetine-treated mice had reduced BAT capacity based upon gene and protein expression (Zha et al., 2017). However, as noted above, these papers failed to make any measurements of EE. Furthermore, as central serotonin in select areas are known to increase adrenergic stimulation to BAT (Morrison et al., 2014), this might explain this elevated BAT capacity and the elevated EE. Since the *Slc6a4*$^{-/-}$ mice have a germline inactivation of *Slc6a4*, this might more accurately reflect the effects observed in fluoxetine-treated neonatal mice (Braz et al., 2020). Interestingly, despite elevated EE independent of activity, we did not detect elevated BAT thermogenic capacity in female *Slc6a4*$^{-/-}$ mice.

The absence of impaired EE in *Slc6a4*$^{-/-}$ mice and associated obesity was surprising. It is in contrast to the anticipated results based upon previous studies reporting elevated EE in mice with reduced 5-HT levels, using whole body Tph inhibitors (PCPA; Oh et al., 2015), peripherally restricted pan-Tph inhibitors (i.e. LP-533,401) and *Tph1*$^{-/-}$ mice (Crane et al., 2015). *Slc6a4*$^{-/-}$ mice would be expected to have elevations in 5-HT signalling both peripherally and centrally. This suggests, that upon global elevation, certain 5-HT-regulated central pathways may positively

regulate BAT thermogenesis and override peripheral 5-HT's effects but in the absence of peripheral 5-HT the central 5-HT is not required for improved BAT thermogenesis. Further studies are required to elucidate the intricacies of this regulation and investigate the potential cross-talk between the two (or more) mechanisms.

15.4 5-HT2A is the predominant 5-HT Receptor in BAT

Because of the apparent beneficial metabolic effects from previous research of reducing peripheral 5-HT synthesis and the known adverse cardiac (Côté et al., 2003) and liver effects (Lesurtel et al., 2006) of Tph1 inhibition, identification of potential 5-HT receptors that are on BAs may lead to novel therapies that are specific and avoid the adverse effects of Tph1 inhibition. Some studies have already identified components of the 5-HT pathway in adipose tissue (i.e. *Tph1*, *Slc6a4* and *Htr2a;* Stunes et al., 2011). Furthermore, whole body inactivation of the *Htr3a* confers beneficial BAT phenotypes (Oh et al., 2015). However, quantification and a thorough characterization of 5-HT receptor activities in BAs had not been completed. Therefore, we investigated which 5-HT receptor(s) are present and active in BAs, and their effects on BAT-related phenotypes.

We identified *Htr2a* mRNA to be predominantly expressed versus other 5-HT receptors in cultured BAs from 129SV/C57Bl6J and FVB mice, and in cultured WAs and BAs from humans. This is consistent with data from a study that, as part of a GPCR qPCR array, quantified *Htr2a* mRNA in cultured adipocytes (Klepac et

al., 2016; raw supplemental data analyzed and graphed in Figure S12- 1c and d) but distinct from measurements in whole adipose tissue (Hansson et al., 2016; Figure S12- 1e and f) where multiple receptors are expressed and likely due to the other cell types present in adipose tissue (such as immune cells and blood vessels). Subsequently, we found 5-HT induced Ca^{2+} transients but not changes in cAMP at near physiological levels of 5-HT (EC_{50} of Ca^{2+} transients: 230 nM) and the Ca^{2+} transients were mediated by the 5-HT2A receptor. This was surprising as the primary regulatory pathway in BAs is the cAMP-PKA axis (Cannon and Nedergaard, 2004) and, in adipocytes, cAMP and lipolysis (important for mitochondrial substrate provision and activation of UCP1 in BAT) has previously been reported to be regulated by high concentrations of 5-HT (Crane et al., 2015; Hansson et al., 2016). However, recently the Gq-Ca^{2+} pathway has been found in high levels in BAs and inhibit BA thermogenic gene expression (Klepac et al., 2016). In contrast, Oh et al. (2015) postulated that 5-HT3 (the only non-GPCR 5-HT receptor) mediated the inhibitory effects of 5-HT on BAs. We were unable to develop a specific assay for testing the activity of 5-HT3 in BAs using Sodium Green to measure sodium influx via the 5-HT3 receptor (data not shown). Alternatively, because some reports suggest that 5-HT3 might transport Ca^{2+}, we tested if Ondansetron (a 5-HT3 antagonist) could block 5-HT-induced Ca^{2+} transients but found no effect. Furthermore, Oh et al. (2015) suggested that 5-HT3 receptors mediate cAMP levels and PKA activity in BAs. However, this does not agree with our findings on cAMP or PKA substrate phosphorylation in response to

5-HT. Surprisingly, Oh et al. (2015) demonstrated this only using antagonists/specific-agonists of 5-HT3 and not in the presence of 5-HT. Thus, these effects may be due to non-specific effects of these pharmaceutical agents. Further, they suggested that 5-HT2A might promote lipogenesis in WAs. We did not test this in WAs and in fact found that high doses of 5-HT inhibited lipid accumulation in BAs. In conclusion from our data, using both gene expression data and functional activity assays, it appears that 5-HT2A is the predominantly expressed and active 5-HT receptor in BAs, and we found little evidence to suggest other 5-HT receptors are active in BAs.

Because our initial findings into the effects of 5-HT on BAs investigated only select pathways of interest, after discovering the prevalent activity of 5-HT2A, we revisited potential pathways that might be altered by BA 5-HT2A. We correlated metabolic phenotypes in recombinant-inbred BXD mouse lines to the expression level of each 5-HT receptor mRNA in BAs. *Htr2a* mRNA was amongst the receptors whose expression level negatively correlated with both VO_2 and body temperature. Notably the *Htr3a* expression in BA correlated poorly with these phenotypes thus suggesting that the superior BAT phenotype observed by Oh et al. (2015) in *Htr3a*$^{-/-}$ mice might not be due to BAT *Htr3a* but *Htr3a* expression in other tissues. Additionally, although our initial efforts focused primarily on regulation of *Ucp1* gene expression and UCP1 protein content, we subsequently found, through gene ontology analysis, that the list of genes negatively correlated with 5-HT2A in human WAT were preferentially enriched in mitochondrial related

genes. In summary, these data suggest that the 5-HT2A receptor is the most prevalent and active receptor within BAs and its expression is correlated to both BAT-related metabolic phenotypes and adipose tissue mitochondrial gene expression.

15.5 5-HT2A negatively affects BA gene expression and function

Using whole body *Htr2a*$^{-/-}$ mice, we created BA progenitor cell lines lacking *Htr2a* and, through subsequent breeding with mice expressing FlpO and subsequently mice expressing CreERT2 under the control of the *AdipoQ* promoter, developed a novel adipose-specific inducible *Htr2a* ablated mouse (*Htr2a* AdKO). With the BA progenitors we demonstrated that 5-HT-induced Ca^{2+} transients were mediated by 5-HT2A and that *Htr2a* was required for the deleterious effects of physiological levels (10 nM) of 5-HT on *Ppargc1a* - the major co-activator of mitochondrial gene expression. Thus, providing causal evidence for our previous findings where human WAT *Htr2a* mRNA expression was negatively correlated with mitochondrial gene transcript expression. This contrasts findings in the kidney and cortical neurons where 5-HT via 5-HT2A positively regulates mitochondrial gene expression (Fanibunda et al., 2019; Harmon et al., 2016) and may represent tissue specific regulation of mitochondrial content. It is noteworthy that *Ucp1* mRNA was also decreased in *Htr2a*$^{-/-}$ BAs, suggesting 5-HT2A independent mechanisms might be present. *Ucp1* is a downstream target of PGC-1α, suggesting some overlap between the 5-HT2A mediated mechanism and the unknown

mechanism affecting *Ucp1* mRNA. These data suggest that 5-HT2A may regulate BA mitochondrial gene expression via modulating PGC-1α.

Previous studies have implicated central 5-HT synthesis and specifically 5-HT2A receptors in thermogenesis. Mice lacking *Tph2* (Alenina et al., 2009), *Lmx1b* in *Pet1* expressing neurons (Hodges et al., 2008), and Diphtheria toxin induced chemotoxicity in *Pet1* positive neurons (McGlashon et al., 2015), all suffer from dysregulated thermoregulation and suggest that central 5-HT in general positively regulates thermogenesis. A detailed review of which areas in the brain where 5-HT promotes or inhibits BAT thermogenesis is available from Morrison et al. (2014). Additional studies have investigated the involvement of specific 5-HT receptors in these effects. For example, administration of 2,5-Dimethoxy-4-iodoamphetamine (DOI; a centrally acting 5-HT2A agonist) increased BAT thermogenesis in rats via increasing sympathetic neural activity (Ootsuka and Blessing, 2006). Furthermore, both thermogenesis from restraint stress (Ootsuka et al., 2008) and intruder-induced stress (Sinh and Ootsuka, 2019) were attenuated by acute treatment with the 5-HT2A receptor antagonist – Epilvanserin. However, in preliminary experiments using whole body *Htr2a*$^{-/-}$ mice we did not observe any differences in thermogenic capacity following administration of CL-316,243. Thus, the basal level of 5-HT under unstressed conditions does not appear to elicit elevated thermogenic capacity. Further, we observed elevated VO_2 under saline conditions in male mice, which may represent differences in non-BAT mediated thermogenesis. This did not alter the body composition of these mice though. Other groups have demonstrated higher

elevated LDL and glucose levels in female *Htr2a*$^{-/-}$ mice (Jaggar et al., 2017). However, to our knowledge no study has investigated the EE in *Htr2a*$^{-/-}$ mice. Additional experiments will be required to: 1) test the robustness of our preliminary findings in *Htr2a*$^{-/-}$ mice, and 2) identify the discrepancy between previous experiments using 5-HT2A agonists (i.e. DOI) eliciting increased BAT temperature and the elevated basal VO_2 in whole body *Htr2a* ablated animals.

Because of the previous evidence suggesting that central 5-HT2A receptors and 5-HT promote BAT thermogenesis and our identification of 5-HT2A receptors on BAs, we developed the inducible *Htr2a* AdKO mice. These mice permitted the elucidation of the role of 5-HT2A in mature adipocytes *in vivo* with temporal specificity. As failure to validate pharmaceutical targets and subsequent treatment efficacy has resulted in many drug/treatment failures (Harrison, 2016; Jones, 2016) the temporal control of the model is invaluable for potential therapeutic development. We found that male *Htr2a* AdKO mice had similar VO_2 under saline conditions at TN, suggesting similar EE when no thermal stress was present. However, upon activation of BAT with CL-316,243, we observed a greater increase in thermogenesis in *Htr2a* AdKO mice compared to WT animals – similar to mice housed at RT versus TN (Crane et al., 2014). Therefore, *Htr2a* AdKO have elevated functional BAT thermogenic capacity. It remains to be seen if these mice have elevated EE in metabolic cages and standard housing conditions. Together with our *in vitro* data, this suggests that 5-HT2A inhibits thermogenic capacity of BAs. Thus,

inactivating *Htr2a* specifically in adipocytes after early development appears to be a potential target for enhancing BAT thermogenic capacity.

15.6 Xylamidine represents a promising molecule for antagonizing peripheral 5-HT2A *in vivo*

Following identification of 5-HT2A in BAs and validation that BA 5-HT2A is a therapeutic target using inducible *Htr2a* AdKO, we identified 5-HT2A antagonists that were viable pharmaceutical agents. Using an untargeted approach, Sam Chorlton identified a list of pharmaceuticals known to elicit similar gene signatures to that of MSCs overexpressing *Ppargc1a*. This method has previously been used to identify numerous compounds yielding functional benefit in a variety of models of disease, including attenuation of muscle atrophy (Dyle et al., 2014). Included within this list were numerous compounds affecting 5-HT2A or related to known downstream pathways (Masson et al., 2012). Of these compounds, we tested and confirmed Altanserin as a compound effective at attenuating 5-HT induced Ca^{2+} transients. Upon examination of pharmacological properties (including adherence to Lipinski's rule of five, BBB permeability, predicted toxicities, etc.), we settled on the use of the peripherally-restricted 5-HT2A antagonist, Xylamidine. Xylamidine was first created in 1967 and found to attenuate peripheral (e.g. acute pressor response to 5-HT and bronchoconstriction; Copp et al., 1967) but not central effects of 5-HT2 agonists. Notably, at that time, only 2 of the 14 5-HT receptors had been identified and we presume that, because no direct application for Xylamidine was noted at the time, the specificity of Xylamidine was never tested.

We found that like other newer generation 5-HT2A antagonists, Xylamidine blocked 5-HT-induced Ca^{2+} transients (IC_{50}: 7.53 nM) but had no effects on high dose 5-HT inhibited lipolysis. Notably, Sarpogrelate a newer 5-HT2A/5-HT2B antagonist with proposed peripheral effects was not found in our hands to block the 5-HT-induced Ca^{2+} transients. Interestingly, Xylamidine, despite being predicted to occupy the same binding pocket as 5-HT and other competitive 5-HT2A antagonists, cannot be outcompeted with 5-HT in Ca^{2+} assays. This effect might be attributed to unusual leaving kinetics of agonists from 5-HT2 class receptors as seen with the 5-HT2A and 5-HT2B receptors (Wacker et al., 2017). Therefore, 5-HT2A antagonists are predicted to positively regulate BA gene transcription and appear to be active and potent inhibitors of 5-HT-induced Ca^{2+} transients in BAs.

Additionally, Xylamidine has previously been shown to attenuate acute 5-HT induced drops in core body temperature (Carter and Leander, 1980; Sugimoto et al., 1991). We found that acute administration of Xylamidine *in vivo* attenuated 5-HT-induced reductions in CL-316,243 elicited VO2 and interscapular surface temperature increases. As discussed above, this effect might be due to vasoconstrictive effects of 5-HT, which are known to be partially mediated by the 5-HT2A receptor. However, the effects of acute vasoconstriction on BAT needs to be fully elucidated. If it exists, Xylamidine appears to be able to protect BAT from indirect inhibition as well. Experiments using 5-CT (5-Carboxamidotryptamine; a non-specific 5-HT agonist with activity at multiple receptors including 5-HT7) and *Htr7*$^{-/-}$ mice have suggested the drop in core body temperature is mediated by the

5-HT7 receptor (Hedlund et al., 2003). Additional experiments using whole body or vasculature specific *Htr2a*$^{-/-}$ are also required to confirm that this effect is mediated by 5-HT2A receptors and the specificity of Xylamidine as it is untested. Regardless, the ability of Xylamidine to block this effect can also serve as a quantifiable acute pharmacodynamic effect for optimization of dose and administration *in vivo*. In conclusion, Xylamidine appears to be a viable 5-HT2A antagonist to block 5-HT2A activity in BAs with promising additional *in vivo* effects.

15.7 Chronic Xylamidine treatment improves BAT thermogenic capacity but not activity

Given the positive effect of acute Xylamidine on blocking 5-HT inhibition of BAT thermogenesis, we began treating mice repeatedly with Xylamidine. Although chronic administration of Xylamidine has been completed before to assess toxicity (Copp et al., 1967), no data to our knowledge has been presented on any physiological outcomes. Following a 5-week treatment we found that Xylamidine treated mice had elevated BAT thermogenic capacity but no differences in body mass or body composition. This finding is consistent with our *in vitro* evidence that suggested 5-HT at plasma concentrations inhibit transcription of thermogenic genes. However, the lack of change in body mass and/or body composition suggested that under these conditions this increase in thermogenic capacity alone was not sufficient to reduce the net caloric balance. Because these mice were housed below TN, there is a constant demand for thermogenesis.

However, BAT is recruited proportionally to the environmental cold insult to maintain core body temperature – as demonstrated by the ability to further activate BAT with acute CL-316,243 administration (Crane et al., 2014). The additional BAT capacity gained with Xylamidine treatment therefore may have not been activated under the mild cold stress experienced by mice at RT and therefore did not elucidate changes in free living EE and consequently body mass. This is in contrast to *Tph1*$^{-/-}$ animals or mice treated with Tph1 inhibitors, where EE is elevated in animals housed at RT and even at TN, where there is minimal to no thermogenic drive, suggesting that with Tph1 ablation or inhibition there is an increase in activation of BAT (Crane et al., 2015; Oh et al., 2015). Therefore, Xylamidine alone does not recapitulate the effect of Tph1 inhibitors. However, under conditions where peripheral 5-HT is elevated and may limit BAT functional capacity, we hypothesized that differences in EE and adiposity with Xylamidine treatment may become apparent.

15.8 Xylamidine improves BAT functional capacity further in SSRI-treated mice but does not prevent obesity

As herein we and others have shown before (Chen et al., 2012; Murphy and Lesch, 2008; Üçeyler et al., 2010; Zha et al., 2017), genetic ablation of *Slc6a4* (SERT) and chronic treatment with some SSRIs (i.e. Paroxetine) results in expansion of white adipose tissue mass and weight gain. In theory, these interventions elevated the levels of extracellular 5-HT and result in increased 5-HT

receptor mediated signalling in tissues. Therefore, this might represent a condition whereby elevated 5-HT reduces EE by reducing BAT functional capacity enough to become limiting. However, as discussed above, *Slc6a4*$^{-/-}$ mice appear to have elevated BAT capacity and EE, which might be due to increased sympathetic outflow via central circuits. This does not preclude the possibility that peripheral 5-HT still limits the BAT functional capacity. In fact, *Slc6a4* ablation or SSRI-treatment may represent a model where central 5-HT might increase adrenergic stimulation to further activate BAT while local levels of 5-HT might limit BAT transcriptionally. Therefore, with SSRI-treatment, 5-HT2A inhibition might not only increase BAT thermogenic capacity but this additional capacity might also be realized with increased BAT activation from central circuits and yield a superior EE phenotype.

Subsequently, we treated mice with Xylamidine in combination with Paroxetine. As expected, Paroxetine-treated mice had increased body mass and fat mass gain. This was accompanied by elevated BAT, iWAT and gWAT mass. Additionally, Paroxetine increased daytime EE and decreased physical activity. However, Paroxetine-treated mice did not have increased food intake as seen in the *Slc6a4*$^{-/-}$ mice at this time point. Therefore, the origin for Paroxetine-induced weight gain remains unknown at this timepoint. Xylamidine had a non-significant ($p = 0.16$ by Bonferroni post-hoc test) increase in EE at night in Paroxetine-treated mice. There was, however, a significant difference between EE versus activity level in Paroxetine- vs Paroxetine with Xylamidine-treated mice. As the body masses

and adiposity were not different between Paroxetine- and Paroxetine with Xylamidine-treated mice, this would suggest that the Xylamidine-induced increase EE was insufficient to alter body composition.

Consistent with our findings in *Slc6a4*$^{-/-}$ mice, CL-316,243 induced respiration appears higher in Paroxetine-treated mice. Furthermore, concurrent with our hypothesis that SSRI-treatment would enhance 5-HT receptor activity and subsequently exacerbate the differences between the vehicle and the inhibitory effects of Xylamidine, we observed Xylamidine treatment to enhance BAT thermogenic capacity in Paroxetine-treated animals. Unfortunately, it appears that this enhancement in BAT functional capacity is insufficient to shift EE high enough to battle SSRI-induced obesity alone.

Obesity is a multifaceted disease predicated by a net positive energy intake, elicited by many stimuli including SSRI treatment and nutrient excess – such as HFD. Therefore, although we investigated inhibiting BAT 5-HT receptor activity as a method to battle SSRI-treatment, one might propose that blocking 5-HT2A in other models of obesity could be useful. Not included herein were attempts with 5 cohorts of animals to treat HFD-induced obesity with Xylamidine or genetic ablation of *Htr2a* AdKO. These treatments were ineffective to prevent obesity-induction and genetically ablated *Htr2a* AdKO gained more weight than controls in response to an HFD. Furthermore, the did not have elevated BA thermogenic capacity when fed a HFD. This might be explained by findings from recent studies (Ikegami et al., 2018; Rami et al., 2018) and unpublished data from the Steinberg

laboratory (Mortuza, R.; Yabut, J; Crane, J), that found decreased levels of 5-HT in plasma and BAT following HFD-feeding in mice, in contrast to earlier studies showing increases (Crane et al., 2015; Kim et al., 2011). Therefore, attenuating 5-HT receptor activity in BAT may be ineffective to increase BAT functional capacity under HFD-conditions because the low levels of 5-HT in BAT may not sufficiently activate 5-HT receptors and lead to adverse effects. This is consistent with the observation that under HFD-conditions, BAT *Ucp1* mRNA levels are increased, not decreased (von Essen et al., 2017; Fromme and Klingenspor, 2011). Therefore, the effects of peripheral 5-HT on BAT and the potential causative/contributing role of 5-HT in obesity remains uncertain and requires further investigation.

15.1 5-HT levels may not regulate EE via BAT

Revisiting previous studies on 5-HT and BAT reveal caveats to the conclusions made from research derived from the inhibition of peripheral 5-HT synthesis. Previously, two groups had demonstrated that inhibition of TPH1 (either genetically or pharmacologically) yielded a lean phenotype under HFD feeding and attributed this to enhanced BAT-mediated EE (Crane et al., 2015; Oh et al., 2015). Although the molecular measurements of BAT machinery appear elevated in *Tph1*$^{-/-}$ mice and are reciprocal to our findings *in vitro* with 5-HT, the functional measurements in *Tph1*$^{-/-}$ mice contradict the anticipated results of a true BAT phenotype and/or may represent a unique BAT presentation. For example, *Ucp1*$^{-/-}$ and TN-housed mice demonstrate no differences in VO_2 when compared to *Ucp1*$^{+/+}$ or RT-hosued mice, respectively (Crane et al., 2014) – consistent with a lack of

cold-stress and subsequent insufficient adrenergic drive to activate BAT-mediated EE. The difference in the thermogenic capacity is only evident following administration of a β3-adrenergic agonist (CL-316,243), where upon treatment *Ucp1*$^{-/-}$ and TN-housed mice have reduced VO_2 and a reduction in the difference in VO_2 between CL-316,243 and saline conditions. Reciprocal to the phenotypes of *Ucp1*$^{-/-}$ and TN-housed mice, we see elevated absolute VO_2 in *Slc6a4*$^{-/-}$ mice only in response to CL-316,243 at TN – suggesting elevated BAT functional capacity. However, in contrast, in *Tph1*$^{-/-}$ mice the relative VO_2 is elevated not only under CL-316,243 but also under saline conditions (Crane et al., 2015), and the difference in the elicited VO_2 is not significantly different. This would suggest 1) another tissue has elevated VO_2 basally that is masked with adrenergic stimulus, 2) that BAT is activated even under saline-conditions (for example via increased sympathetic outflow), or 3) that the dramatically lower body mass in *Tph1*$^{-/-}$ mice mathematically raises the VO_2 under both saline and CL-316,243-stimulated conditions without differences in actual EE.

To date we have little evidence to suggest that other tissues in *Tph1*$^{-/-}$ mice have elevated metabolism. Crane et al (2014) measured *in vivo* glucose uptake into muscle, heart, liver and BAT of *Tph1*$^{-/-}$ mice using radiolabelled FDG, only BAT appeared to be elevated. Interestingly, administration of the presumed peripherally restricted pan-Tph inhibitor – LP-533,401 – did reveal differences in FDG uptake into the liver and recent studies have suggested that changes in the liver precede morphological changes in adipose tissue with LP-533,401 treatment (Namkung et

al., 2018). Although FDG uptake is useful in regard to glucose uptake, it neglects to inform on the state of other macronutrient metabolism nor the successful oxidation of glucose. Recently groups have shown that in individuals with type 2 diabetes, an apparent reduction in glucose tracer uptake suggested impaired BAT function; however, the use of lipid tracers revealed their BAT to be functional and thus suggesting a change in substrate preference and questioning the pervasive use of glucose tracers to quantify BAT function (Blondin et al., 2015). Other methods that might reveal increased spatial resolution of metabolism include thermal imaging (Crane et al., 2014), near-infrared spectroscopy (Nirengi et al., 2015) and the use of hyperpolarized chemical probes (Ntziachristos et al., 2019). Furthermore, expression of proteins in other tissues (such as *Sln* in skeletal muscle; Bal et al., 2012) are known contributors to EE. Thus, further research would be required to suggest that tissue other than BAT is contributing to the increased VO_2 in Tph1 inhibited mice.

Considering that little evidence exists to suggests another tissue has elevated VO_2, a thorough examination of BAT was warranted and completed. The increased VO_2 might be explained by elevation in endogenous adrenergic receptor ligands. In Crane et al. (2015), *Tph1*$^{-/-}$ mice did not have any differences in levels of endogenous adrenergic ligands (e.g. norepinephrine) within BAT and serum. However, a recent study has shown that, upon administration of 5-HT via IV, sympathetic nervous activity is decreased to BAT (Mota et al., 2020). Together, this would suggest that the same amount of NE might be present in *Tph1*$^{-/-}$ mice but

in these mice more NE may be released into the extracellular space to activate BAs. Interestingly, this is in contrast to reports suggesting that 5-HT directly activates adrenergic neurons in BAT sections and increases lipolytic rates (Steiner and Evans, 1976). An alternative hypothesis might be that the *Tph1*$^{-/-}$ mice might be sensitized to adrenergic stimulation as was postulated and supported by demonstrating higher PKA substrate phosphorylation in *Tph1*$^{-/-}$ mice serum (Crane et al., 2015). This was further supported with the observed inhibition of NEFA release using low concentrations of adrenergic agonists (e.g. isoproterenol) and very high doses of 5-HT (100 μM) *in vitro*. However, if this was the case a rightward shift of the isoproterenol dose response curve would be expected, and, with our experiments, we demonstrated that 100 μM 5-HT impairs NEFA release even in the absence of adrenergic stimuli, thus not suggesting a desensitization. Furthermore, the physiological validity of the 100 μM dose of 5-HT used is unproven and ≥ 1000x higher than circulating levels as discussed above. Alternatively, kynurenic acid, another tryptophan metabolite, has been shown to increase adrenergic sensitivity in BAT potentially via upregulation of an endogenous G_i-coupled receptor activity modulator Rgs14 (Agudelo et al., 2018). The kynurenine pathway is widely thought to consume the majority of ingested tryptophan and thus competes with the 5-HT synthetic pathway for tryptophan. Therefore, it is unsurprising to know that upon elimination of *Tph2*$^{-/-}$ and *Tph1*$^{-/-}$, kynurenine levels increase ~2-3 fold (Sibon et al., 2019; Weng et al., 2015). We also found that a metabolite of kynurenine (3-HK) alone increased *Ucp1* promoter

activity, albeit at a 100 μM dose. Notably supplementation with BH_4, a co-substrate in the Tph1 and TH enzymatic reactions, also increases BAT activity (Oguri et al., 2017). Therefore, in the absence of no change in total norepinephrine levels it appears there may be increased release of NE and/or sensitization of BAT to adrenergic stimuli either via the absence of 5-HT or an increase in Tph1 substrates/other tryptophan metabolites (such as kynurenine and consequently kynurenic acid) and this might contribute to increased BAT VO_2 and potentially other effects mediated by adrenergic stimuli.

Alternatively, a long-debated but more simplistic explanation perhaps is the confounding variable of the ~15-25% lower body weight in *Tph1*$^{-/-}$ mice versus *Tph1*$^{+/+}$ mice. As discussed above regarding the use of correcting to body mass for measures of caloric intake, the same bias occurs when measuring VO_2 and EE. With regards to the regulation of body mass the total number of calories expended regardless of body mass in relation to the total number of calories absorbed is important. This debate has enthralled one of the highest echelons of the scientific literature (Himms-Hagen et al., 1997). Most groups recognize that differences in body mass are potential confounders in analysis of EE and that it is important to determine if EE is greater due to differences in the metabolic processes of an organism or simply due to the greater amount of tissue (particularly adipose tissue; Tschöp et al., 2012b). Consequently, new tools have even been created to assist in the proper analysis of metabolic cage data (Mina et al., 2018). It is, however. well recognized that analyzing EE corrected to total body mass is incorrect (Tschöp et

al., 2012). Crane et al. (2014b) and Oh et al. (2015), both correct VO_2 to body mass for *Tph1*$^{-/-}$ and Tph-inhibitor treated mice and either do not report EE or report EE also corrected to body mass. Presumably if not correcting for the ~15-25% differences in body mass observed, the approximate ~10-15% difference in body mass corrected VO_2 and EE observed in both awake and anaesthetized mice in these studies would be nullified. A caveat to this is dose of CL-316,243 administered in the quantification of BAT functional capacity in anaesthetized animals. Because administration was based on body mass, the heavier *Tph1*$^{+/+}$ mice would have received a ~15-25% higher dose of CL-316,243. If this dose elicits a maximal VO_2 response by saturation of β3-receptors on BAs the higher dose should be inconsequential with this acute measurement – as is supported by the similar fold-increase (~3 fold) in VO_2 in anaesthetized mice receiving ~0.015 mg/kg as awake mice receiving 1 mg/kg; however, more investigations would be needed to confirm this. Alternative methods to help accurately measure the EE and caloric intake in these mice may include performing an analysis of covariance (ANCOVA) analysis of energy expenditure as a function of body mass (Tschöp et al., 2012), doubly-labelled water experiments (Westerterp, 2017) and energy balance techniques (Ravussin et al., 2013). In conclusion, the EE phenotype of *Tph1*$^{-/-}$ and Tph1 inhibitor-treated mice should be revisited with the new analytical tools available to assist in explaining the discrepancies found herein with previous studies.

However, since Tph1 is a biosynthetic enzyme and as noted above this results in increased synthesis of other tryptophan metabolites, this leaves the

possibility that other non-5-HT metabolites may be mediating some of the beneficial effects observed with Tph1 inhibition. The authors correctly investigated if restoring 5-HT levels in *Tph1*$^{-/-}$ mice would reverse the obesity phenotype (Crane et al., 2015). To do so, slow-release 5-HT pellets were implanted subcutaneous in the interscapular region of *Tph1*$^{-/-}$ mice. Consequently, *Tph1*$^{-/-}$ mice had reduced BAT functional capacity as measured by VO_2 and interscapular surface temperature; however, no measures of BAT molecular componentry were completed, such as mitochondrial content, thermogenic gene signatures or UCP1 protein levels. Surprisingly, the 5-HT pellet did not elicit a change in body mass. Although 5-HT did not elevate circulating 5-HT levels to *Tph1*$^{+/+}$ levels, because BAT is still impaired, this experiment suggests that restoring 5-HT levels to BAT in *Tph1*$^{-/-}$ mice does not reverse the lean phenotype and subsequently the reduced levels of 5-HT in BAT do not explain the obesity-resistant phenotype in whole body. This is further supported by our findings from BXD mice that revealed that circulating 5-HT is not highly correlated with body mass. Therefore, it appears that another mechanism must explain the differences in body mass observed.

Although the EE in *Tph1*$^{-/-}$ and Tph1-inhibitor treated mice needs revisiting, the molecular changes observed in the BAT componentry is uncontested. Our findings with treating BAs with 5-HT yield similar but far less dramatic effects than expected from the *Tph1*$^{-/-}$ phenotype. With the current understanding that other tryptophan metabolites (e.g. kynurenine metabolites) can increase BAT activity and are increased in *Tph1*$^{-/-}$, this might suggest an additional mechanism by which BAT

and body mass is altered in these animals that would agree with the findings from 5-HT-elevating interventions.

16 Limitations

Although this work utilized numerous corroborating techniques and models, there still remain multiple limitations. These include, but are not limited to, the use of immortalized cell lines, undetermined extracellular concentrations of 5-HT in BAT, absence of genetic model confirmation, unknown specificity of Xylamidine, and the unknown translatability to female mice and humans.

All experiments in mouse BAs were completed using immortalized cell lines. Although common, the use of immortalized cell lines comes with multiple caveats. All mouse BA progenitor cells used in the above experiments were created via transduction with SV40T, a viral gene known to reduce the activity of numerous tumor suppressor proteins involved in cell cycle progression (Ahuja et al., 2005). These proteins, such as p53, have known metabolic roles in adipose tissue that may consequently be affected by the expression of SV40T (Krstic et al., 2018). Furthermore, the integration of SV40T into the mouse genome of these cells occurs spontaneously and as with any transgene insertion (including the insertion of the AdipoQ-CreERT2 and GloSensor-22F constructs) can interrupt or interfere with the expression of genes in the mouse genome. Additionally, adipocyte progenitors are comprised of numerous cell populations. Immortalization and the subsequent selection of these cells may favour certain progenitors over others and subsequently

yield a population of cells *in vitro* that does not reflect those observed *in vivo*. Further to this point, continual culturing of immortalized cell lines can lead to the acquisition of genetic mutations that can affect the phenotype of these cells. However, since we completed many of these experiments in multiple cell lines from different mouse strains (i.e. both C7Bl/6J and FVB) and also had similar observations in human BAs (i.e. for 5-HT receptor expression), it appears the majority of the phenotypes appear to not be affected by the limitations of cell immortalization.

A key barrier and limitation in this work surrounded the correct 5-HT concentration to be used *in vitro*. The concentration of 5-HT within platelet poor plasma is ≤ 10 nM (Brand and Anderson, 2011). However, previous research observing reduced cAMP and FFA mobilization by 5-HT on BAs and WAs was performed with ≥ 10 μM 5-HT (Crane et al., 2015; Hansson et al., 2016). The 100 μM dose used far exceeds the dose required for maximal activation of the 5-HT2A receptor. We found effects of 5-HT on *Ucp1* promoter activity at low doses (i.e. 10 nM) which were attenuated at moderate doses (~1 μM) and then apparent again at high doses, suggestive of a triphasic response of cells to 5-HT. We presumed that the effects at the lowest doses of 5-HT are receptor mediated and confirmed some effects to be 5-HT2A dependent. Further, we have shown data suggesting that the mechanism activated by high doses of 5-HT appears to be independent of canonical 5-HT receptor or 5-HT transporter pathways, thus suggesting a non-specific effect of 5-HT. Despite this, we cannot exclude for certain that moderate (~ 1 μM) or high

concentrations (i.e. 100 μM) of 5-HT do not occur in BAT due to local production or release (e.g. from mast cells) and thus why the use of wide dose responses of 5-HT were employed in many assays. To ascertain the basal extracellular concentration of 5-HT, one could use microdialysis in BAT *in vivo*. This has previously been used to resolve the unexpected decrease in circulating 5-HT levels with SSRI treatment, whereby extracellular tissue (specifically neuronal tissue) levels of 5-HT do rise as expected (Gartside et al., 1995). Therefore, although we have found some effects of 5-HT at low doses and even more at high doses of 5-HT, without accurate measurement of extracellular 5-HT *in vivo* we cannot be sure which *in vitro* effects are physiologically relevant.

Another limitation of this work is the limited validation of 5-HT2A inhibitors and *Htr2a* gene ablation in the conditional *Htr2a AdKO* animals. At the time that Xylamidine was discovered, only two 5-HT receptors had been identified and the inhibitory action of Xylamidine against the 5-HT2 was inferred via from its physiological effects. We now know that there are at least fourteen 5-HT receptors, and the previously named 5-HT2 receptor became what is now known as the 5-HT2A receptor. Presently, to our knowledge, no investigation of the binding specificity or affinity of Xylamidine has been completed nor an empirical measurement of its tissue distribution and blood brain barrier permeability. Although we did not complete these experiments, we attempted to use predictive ADMET tools to confirm the previously inferred activity of Xylamidine and found it to be consistent with the previous claims. However, this does not eliminate the

need for empirical testing of Xylamidine's specificity and tissue distribution in the future.

Further to the need for validation of 5-HT2A inhibitors used in this study, the novel genetic mouse models used herein, require confirmation of the target gene inactivation. Neither the *Htr2a*$^{-/-}$ nor the *Htr2a AdKO* mice used in this study have been used in previously published papers. Although we demonstrated that immortalized and differentiated BA progenitors isolated from *Htr2a*$^{-/-}$ mice express low levels of *Htr2a* mRNA and that 5-HT-induced Ca^{2+} transients were absent, we did not examine the effectiveness of the gene targeting strategy *in vivo* by analysis of tissue expression levels of *Htr2a* mRNA or 5-HT2A protein. As discussed above, the absence of a specific 5-HT2A antibody limits the completion of this task. Further to this point, the inducible *Htr2a AdKO* mice also did not undergo confirmation of gene inactivation. Due to the tamoxifen inducible nature of the CreERT2 protein, there is additional variability in the activation of CreERT2 and subsequent excision of exon 2 of *Htr2a* because of not only the efficiency of the Cre itself but also the administration, distribution and metabolism of tamoxifen. Notably while the induction protocol used herein has previously been used to induce deletion of other genes using the same *AdipoQ-CreERT2* construct with high efficiency (Mottillo et al., 2014), within our model this still requires empirical validation, preferably using a 5-HT2A specific antibody but from our experience most likely by quantification of *Htr2a* mRNA. Therefore, like the lack of empirical

evidence for Xylamidine there also remains a requirement for the validation of the inducible *Htr2a AdKO* efficiency.

Another limitation of these experiments is the primarily male murine model use. Although experiments in *Slc6a4*$^{-/-}$ mice were completed in both male and females and some cell lines, all experiments in FVB, C57Bl/6J, *Htr2a*$^{-/-}$ and *Htr2a AdKO* mice were completed only in male mice. This not only may limit the translatability of these findings to female subjects but also may have limited the weight gain with paroxetine treatment in C57Bl/6J mice as female *Slc6a4*$^{-/-}$ gained more weight than male mice. Furthermore, with the exception of RNA-Seq data from human adipocytes obtained from Dr. Camilla Scheele's laboratory (Jespersen et al., 2013) and other openly available data sources (i.e. the GTExPortal) all cell culture experiments were completed in murine adipocyte progenitors. Quantification of the activity of 5-HT2A activity via analysis of downstream second messengers, such as Ca^{2+} transients, from primary human adipocytes would assist in confirming that 5-HT2A activity in adipose tissue is conserved between species. Therefore, although some experiments were performed in mice and murine cell lines derived from both sexes, additional work confirming the efficacy of Xylamidine and the presence of 5-HT2A activity in human adipocytes would confirm the conserved nature of this pathway in both sexes and across species.

17 Future Directions

To further extend this line of inquiry and expand our understanding of the regulation of BAT by 5-HT and the 5-HT2A receptor, there are a variety of avenues that invite exploration beyond those addressing the limitations above. These range from revisiting the mechanism of the obesity-resistant phenotype of *Tph1*$^{-/-}$ mice, exploring systemic factors regulated by 5-HT that affect BAT, further examination of the effects of 5-HT on BAT, and examining the potential additive/synergistic effect of 5-HT2A antagonism and β-adrenergic agonism.

As discussed above, there are outstanding questions regarding the phenotype of *Tph1*$^{-/-}$ animals and consequently the theoretical model of the inhibitory effect of peripheral 5-HT on EE. For example, our findings that male *Slc6a4*$^{-/-}$ mice have greater BAT thermogenic capacity and that Xylamidine-treatment to block the predominant 5-HT receptor expressed on BAT might suggest that peripheral 5-HT is not a major inhibitor of BAT-mediated EE. To attempt to refine our understanding of peripheral 5-HT and obesity, a re-examination of the anti-obesity mechanism(s) in *Tph1*$^{-/-}$ mice might include: 1) chronically housing *Tph1*$^{-/-}$ mice at thermoneutrality, to reduce cold-induced BAT activity, and monitoring weight gain; 2) monitoring *Tph1*$^{-/-}$ mouse caloric intake throughout HFD-feeding as unpublished data revealed strong trends for reduced food intake in *Tph1*$^{-/-}$ mice and LP-533,401 treatment did not attenuate weight gain in *Ob/Ob* mice (an orexigenic obesity model; unpublished data from Dr. Rengasamy Palanivel); and 3) since LP-533,401 and PCPA have recently been shown to affect liver

morphology prior to changes in adipose tissue (Namkung et al., 2018) and kynurenine is known to increase with TPH inhibition, an examination of indirect effects on BAT in *Tph1*$^{-/-}$ mice might reveal additional mechanisms by which inhibition of peripheral 5-HT synthesis may contribute to the obesity resistance. Performing the above experiments might reveal additional mechanisms that occur in *Tph1*$^{-/-}$ mice that confer their anti-obesity phenotype and refine our understanding of the regulation of EE by peripheral 5-HT.

To further our understanding of the effects of 5-HT on BAs, there remain additional experiments of interest that should be explored with a particular focus on the chronic effects of physiological doses of 5-HT on BAs. Many of the experiments completed herein used high concentrations of 5-HT and should likely be repeated with more appropriate concentrations. These include the acute effects on glycolysis. Preliminary analysis of RNA-Seq data obtained from BA treated with 10 nM 5-HT, suggest that the mitochondrial gene transcription is down regulated by 5-HT (as is consistent with our *in silico* analyses) and thus suggests a chronic regulation of BA thermogenic capacity. Therefore, analysis of the chronic effects of 5-HT on BA gene transcription by analyzing mitochondrial content and activity (i.e. respiration) following 7 days of treatment with a range of appropriate concentrations of 5-HT (e.g. 1 nM – 1 μM) is of particular interest. Additionally, to confirm which phenotypes are mediated by the 5-HT2A receptor these experiments should be completed in BAs from *Htr2a*$^{+/+}$ and *Htr2a*$^{-/-}$ animals. These experiments could be complemented by implantation of *Htr2a*$^{+/+}$ and *Htr2a*$^{-/-}$

animals with 5-HT pellets to elevate peripheral 5-HT and examine if peripheral 5-HT is obesogenic and mediated by 5-HT2A. These additional experiments could further elucidate if 5-HT directly impairs mitochondrial gene expression and may explain the improved BAT thermogenic capacity in *Htr2a*$^{-/-}$ animals.

As adrenergic-stimuli are major activators of BAT and increased adrenergic-stimuli might be needed to activate BAT mediated-EE maximally, investigating the combination of 5-HT2A receptor antagonists and adrenergic-stimuli might be superior to either alone. Unfortunately, adrenergic agonists (such as CL-316,243 or Mirabegron) alone have adverse cardiovascular effects (Cypess et al., 2015) and have proven only moderately effective in humans (Weyer et al., 1998) . Given that we have shown that acute 5-HT desensitization of adrenergic stimuli appears to primarily occur at doses of 5-HT that are above those that maximally activate 5-HT receptors (more than 10,000x plasma levels) and in the absence of/low levels of adrenergic stimuli, we concluded that, *in vivo*, 5-HT likely does not impair adrenergic signalling. However, as 10 nM 5-HT appears to impair a gene that regulates mitochondrial gene transcription (i.e. *Ppargc1a*), without an observed effect on second messengers of β-adrenergic-receptors (i.e. cAMP), this would suggest that 5-HT regulates mitochondrial content independent of adrenergic-stimuli in BA. Additionally, we found that administering Xylamidine chronically *in vivo* increases BAT thermogenic capacity but does not alter basal EE, suggesting that this new additional capacity is not being activated at RT (i.e. mild adrenergic stimulation). This might suggest that the combination of a 5-HT2A

receptor antagonist and a BAT-targeted adrenergic ligand, might serve as a combination therapy yielding additive effects to both enhance (via 5-HT2A receptor inhibition and β-adrenergic agonists) and further activate (via β-adrenergic agonists) the thermogenic capacity of BAT. Consequently, this combination might be able to combat weight gain and requires further investigation.

19 Conclusion

There are a variety of conclusions that can be made from the evidence presented about the role 5-HT has in regulating BAT and the mechanisms therein. From the current experiments presented above it appears that: 1) 5-HT can alter BA mitochondrial gene expression, 2) BAs are protected from 5-HT effects by large amounts of 5-HT uptake and degradation machinery, 3) *in vivo* acute 5-HT stimulus decreases EE, 4) chronic administration of Paroxetine does not decrease BAT thermogenic capacity, 5) 5-HT2A is the predominant 5-HT receptor expressed in BAs, 6) inhibition of the 5-HT2A receptor increases thermogenic capacity and 7) inhibition of 5-HT2A does not further enhance BAT function in Paroxetine-treated mice nor does it prevent excess adiposity. Overall, we concluded that local 5-HT may play a role in negatively regulating the mitochondrial transcriptional program in BAT and may attenuate BAT thermogenesis but inhibiting 5-HT2A receptor activity alone is not sufficient to combat Paroxetine-induced obesity.

20 References

- Abbas, A., and Roth, B.L. (2008). Pimavanserin tartrate: A 5-HT2A inverse agonist with potential for treating various neuropsychiatric disorders. Expert Opin. Pharmacother. *9*, 3251–3259.
- Abreu-Vieira, G., Hagberg, C.E., Spalding, K.L., Cannon, B., and Nedergaard, J. (2015). Adrenergically stimulated blood flow in brown adipose tissue is not dependent on thermogenesis. Am. J. Physiol. - Endocrinol. Metab. *308*, E822–E829.
- Afarideh, M., Behdadnia, A., Noshad, S., Mirmiranpour, H., Mousavizadeh, M., Khajeh, E., Rad, M.V. ahid., Mazaheri, T., Nakhjavani, M., and Esteghamati, A. (2015). Association of Peripheral 5-Hydroxyindole-3-Acetic Acid, a Serotonin Derivative, With Metabolic Syndrome and Low-Grade Inflammation. Endocr. Pract. *21*, 711–718.
- Agudelo, L.Z., Femenía, T., Orhan, F., Porsmyr-Palmertz, M., Goiny, M., Martinez-Redondo, V., Correia, J.C., Izadi, M., Bhat, M., Schuppe-Koistinen, I., et al. (2014). Skeletal muscle PGC-1α1 modulates kynurenine metabolism and mediates resilience to stress-induced depression. Cell *159*, 33–45.
- Agudelo, L.Z., Ferreira, D.M.S., Cervenka, I., Bryzgalova, G., Dadvar, S., Jannig, P.R., Pettersson-Klein, A.T., Lakshmikanth, T., Sustarsic, E.G., Porsmyr-Palmertz, M., et al. (2018). Kynurenic Acid and Gpr35 Regulate Adipose Tissue Energy Homeostasis and Inflammation. Cell Metab. *27*, 378-392.e5.
- Aherne, W., and Hull, D. (1966). Brown adipose tissue and heat production in the newborn infant. J. Pathol. Bacteriol. *91*, 223–234.
- Ahuja, D., Sáenz-Robles, M.T., and Pipas, J.M. (2005). SV40 large T antigen targets multiple cellular pathways to elicit cellular transformation. Oncogene *24*, 7729–7745.
- Alenina, N., Kikic, D., Todiras, M., Mosienko, V., Qadri, F., Plehm, R., Boyé, P., Vilianovitch, L., Sohr, R., Tenner, K., et al. (2009). Growth retardation and altered autonomic control in mice lacking brain serotonin. Proc. Natl. Acad. Sci. U. S. A. *106*, 10332–10337.
- Ast, T., and Mootha, V.K. (2019). Oxygen and mammalian cell culture: are we repeating the experiment of Dr. Ox? Nat. Metab. *1*, 858–860.
- Bachman, E.S., Dhillon, H., Zhang, C.-Y., Cinti, S., Bianco, A.C., Kobilka, B.K., and Lowell, B.B. (2002). betaAR signaling required for diet-induced thermogenesis and obesity resistance. Science (80-.). *297*, 843–845.
- de Backer, T.L., Vander Stichele, R., Lehert, P., and Van Bortel, L. (2012). Naftidrofuryl for intermittent claudication. Cochrane Database Syst. Rev.
- Baganz, N.L., Hortona, R.E., Calderon, A.S., Owens, W.A., Munn, J.L., Watts, L.T., Koldzic-Zivanovic, N., Jeske, N.A., Koek, W., Toney, G.M., et al. (2008). Organic cation transporter 3: Keeping the brake on

extracellular serotonin in serotonin-transporter-deficient mice. Proc. Natl. Acad. Sci. U. S. A. *105*, 18976–18981.

- Bal, N.C., Maurya, S.K., Sopariwala, D.H., Sahoo, S.K., Gupta, S.C., Shaikh, S.A., Pant, M., Rowland, L.A., Goonasekera, S.A., Molkentin, J.D., et al. (2012). Sarcolipin is a newly identified regulator of muscle-based thermogenesis in mammals. Nat. Med. *18*, 1575–1579.
- Bartelt, A., Bruns, O.T., Reimer, R., Hohenberg, H., Ittrich, H., Peldschus, K., Kaul, M.G., Tromsdorf, U.I., Weller, H., Waurisch, C., et al. (2011). Brown adipose tissue activity controls triglyceride clearance. Nat. Med. *17*, 200–206.
- Bautista, D.M., Siemens, J., Glazer, J.M., Tsuruda, P.R., Basbaum, A.I., Stucky, C.L., Jordt, S.E., and Julius, D. (2007). The menthol receptor TRPM8 is the principal detector of environmental cold. Nature *448*, 204–208.
- Bengel, D., Murphy, D.L., Andrews, A.M., Wichems, C.H., Feltner, D., Heils, A., Mössner, R., Westphal, H., and Lesch, K.P. (1998). Altered brain serotonin homeostasis and locomotor insensitivity to 3,4-methylenedioxymethamphetamine ('ecstasy') in serotonin transporter-deficient mice. Mol. Pharmacol. *53*, 649–655.
- Bertrand, R.L., Senadheera, S., Markus, I., Liu, L., Howitt, L., Chen, H., Murphy, T. V., Sandow, S.L., and Bertrand, P.P. (2011). A western diet increases serotonin availability in rat small intestine. Endocrinology *152*, 36–47.
- Blondin, D.P., Labbé, S.M., Noll, C., Kunach, M., Phoenix, S., Guérin, B., Turcotte, É.E., Haman, F., Richard, D., and Carpentier, A.C. (2015). Selective impairment of glucose but not fatty acid or oxidative metabolism in brown adipose tissue of subjects with type 2 diabetes. Diabetes *64*, 2388–2397.
- Blum, I., Nessiel, L., Graff, E., Harsat, A., Gabbay, U., Sulkes, J., Raz, O., and Vered, Y. (1993). Food preferences, body weight, and platelet-poor plasma serotonin and catecholamines. Am. J. Clin. Nutr. *57*, 486–489.
- Bohula, E.A., Wiviott, S.D., McGuire, D.K., Inzucchi, S.E., Kuder, J., Im, K.A., Fanola, C.L., Qamar, A., Brown, C., Budaj, A., et al. (2018). Cardiovascular safety of lorcaserin in overweight or obese patients. N. Engl. J. Med. *379*, 1107–1117.
- Bordicchia, M., Liu, D., Amri, E.Z., Ailhaud, G., Dessì-Fulgheri, P., Zhang, C., Takahashi, N., Sarzani, R., and Collins, S. (2012). Cardiac natriuretic peptides act via p38 MAPK to induce the brown fat thermogenic program in mouse and human adipocytes. J. Clin. Invest. *122*, 1022–1036.
- Borgström, B. (1988). Mode of action of tetrahydrolipstatin: a derivative of the naturally occurring lipase inhibitor lipstatin. Biochim. Biophys. Acta (BBA)/Lipids Lipid Metab. *962*, 308–316.
- Bour, S., Daviaud, D., Gres, S., Lefort, C., Prévot, D., Zorzano, A.,

Wabitsch, M., Saulnier-Blache, J.S., Valet, P., and Carpéné, C. (2007). Adipogenesis-related increase of semicarbazide-sensitive amine oxidase and monoamine oxidase in human adipocytes. Biochimie *89*, 916–925.

- Brand, T., and Anderson, G.M. (2011). The measurement of platelet-poor plasma serotonin: A systematic review of prior reports and recommendations for improved analysis. Clin. Chem. *57*, 1376–1386.
- Braun, K., Oeckl, J., Westermeier, J., Li, Y., and Klingenspor, M. (2018). Non-adrenergic control of lipolysis and thermogenesis in adipose tissues. J. Exp. Biol. *121*.
- Bray, G.A., Frühbeck, G., Ryan, D.H., and Wilding, J.P.H. (2016). Management of obesity. Lancet *387*, 1947–1956.
- Braz, G.R.F., da Silva, A.I., Silva, S.C.A., Pedroza, A.A.S., de Lemos, M.D.T.B., de Lima, F.A.S., Silva, T.L.A., and Lagranha, C.J. (2020). Chronic serotonin reuptake inhibition uncouples brown fat mitochondria and induces beiging/browning process of white fat in overfed rats. Life Sci. *245*, 117307.
- Breining, P., Pedersen, S.B., Pikelis, A., Rolighed, L., Sundelin, E.I.O., Jessen, N., and Richelsen, B. (2017). High expression of organic cation transporter 3 in human BAT-like adipocytes. Implications for extraneuronal norepinephrine uptake. Mol. Cell. Endocrinol. *443*, 15–22.
- Breisch, S., Zemlan, F., and Hoebel, B. (1976). Hyperphagia and obesity following serotonin depletion by intraventricular p-chlorophenylalanine. Science (80-.). *192*, 382–385.
- Buchwald, H., Avidor, Y., Braunwald, E., Jensen, M.D., Pories, W., Fahrbach, K., and Schoelles, K. (2004). Bariatric surgery: A systematic review and meta-analysis. J. Am. Med. Assoc. *292*, 1724–1737.
- Buchwald, H., Estok, R., Fahrbach, K., Banel, D., Jensen, M.D., Pories, W.J., Bantle, J.P., and Sledge, I. (2009). Weight and Type 2 Diabetes after Bariatric Surgery: Systematic Review and Meta-analysis. Am. J. Med. *122*.
- Bulat, M., and Supek, Z. (1968). Passage of 5-Hydroxytryptamine Through the Blood-Brain Barrier, Its Metabolism in the Brain and Elimination of 5-Hydroxyindo-Leacetic Acid From the Brain Tissue. J. Neurochem. *15*, 383–389.
- Camell, C.D., Sander, J., Spadaro, O., Lee, A., Nguyen, K.Y., Wing, A., Goldberg, E.L., Youm, Y.-H., Brown, C.W., Elsworth, J., et al. (2017). Inflammasome-driven catecholamine catabolism in macrophages blunts lipolysis during ageing. Nature *550*, 119–123.
- Cannon, B., and Nedergaard, J. (2004). Brown Adipose Tissue: Function and Physiological Significance. Physiol. Rev. *84*, 277–359.
- CANNON, B., and NEDERGAARD, J. (1979). The Physiological Role of Pyruvate Carboxylation in Hamster Brown Adipose Tissue. Eur. J. Biochem. *94*, 419–426.
- Cantó, C., Houtkooper, R.H., Pirinen, E., Youn, D.Y., Oosterveer, M.H.,

Cen, Y., Fernandez-Marcos, P.J., Yamamoto, H., Andreux, P.A., Cettour-Rose, P., et al. (2012). The NAD+ precursor nicotinamide riboside enhances oxidative metabolism and protects against high-fat diet-induced obesity. Cell Metab. *15*, 838–847.

- Cao, W., Medvedev, A. V., Daniel, K.W., and Collins, S. (2001). β-adrenergic activation of p38 MAP kinase in adipocytes: cAMP induction of the uncoupling protein 1 (UCP1) gene requires p38 map kinase. J. Biol. Chem. *276*, 27077–27082.
- Cariou, B., Charbonnel, B., and Staels, B. (2012). Thiazolidinediones and PPARγ agonists: Time for a reassessment. Trends Endocrinol. Metab. *23*, 205–215.
- Carneiro, I.P., Elliott, S.A., Siervo, M., Padwal, R., Bertoli, S., Battezzati, A., and Prado, C.M. (2016). Is Obesity Associated with Altered Energy Expenditure? Adv. Nutr. *7*, 476–487.
- Carter, R.B., and Leander, J.D. (1980). Evidence for a peripheral effect of serotonin or metabolites in 5-hydroxytryptophan-induced hypothermia. Neuropharmacology *19*, 777–784.
- Cater, D.B., Garattini, S., Marina, F., and Silver, I.A. (1961). Changes of oxygen tension in brain and somatic tissues induced by vasodilator and vasoconstrictor drugs. Proc. R. Soc. London. Ser. B. Biol. Sci. *155*, 136–157.
- Chen, J.J., Li, Z., Pan, H., Murphy, D.L., Tamir, H., Koepsell, H., and Gershon, M.D. (2001). Maintenance of serotonin in the intestinal mucosa and ganglia of mice that lack the high-affinity serotonin transporter: Abnormal intestinal motility and the expression of cation transporters. J. Neurosci. *21*, 6348–6361.
- Chen, X., Margolis, K.J., Gershon, M.D., Schwartz, G.J., and Sze, J.Y. (2012). Reduced serotonin reuptake transporter (SERT) function causes insulin resistance and hepatic steatosis independent of food intake. PLoS One *7*, e32511.
- Choi, W., Namkung, J., Hwang, I., Kim, H., Lim, A., Park, H.J., Lee, H.W., Han, K.H., Park, S., Jeong, J.S., et al. (2018). Serotonin signals through a gut-liver axis to regulate hepatic steatosis. Nat. Commun. *9*.
- de Clerck, F., David, J.L., and Janssen, P.A.J. (1982). Inhibition of 5-hydroxytryptamine-induced and-amplified human platelet aggregation by ketanserin (R 41 468), a selective 5-HT2-receptor antagonist. Agents Actions *12*, 388–397.
- Coelho, W.S., Costa, K.C., and Sola-Penna, M. (2007). Serotonin stimulates mouse skeletal muscle 6-phosphofructo-1-kinase through tyrosine-phosphorylation of the enzyme altering its intracellular localization. Mol. Genet. Metab. *92*, 364–370.
- Cohen, J.C., Horton, J.D., and Hobbs, H.H. (2011). Human fatty liver disease: Old questions and new insights. Science (80-.). *332*, 1519–1523.

- Colburn, R.W., Lubin, M. Lou, Stone, D.J., Wang, Y., Lawrence, D., D'Andrea, M.R.R., Brandt, M.R., Liu, Y., Flores, C.M., and Qin, N. (2007). Attenuated Cold Sensitivity in TRPM8 Null Mice. Neuron *54*, 379–386.
- Collins, S., Daniel, K.W., Petro, A.E., and Surwit, R.S. (1997). Strain-specific response to β3-adrenergic receptor agonist treatment of diet-induced obesity in mice. Endocrinology *138*, 405–413.
- Connolly, H.M., Crary, J.L., McGoon, M.D., Hensrud, D.D., Edwards, B.S., Edwards, W.D., and Schaff, H. V. (1997). Valvular heart disease associated with fenfluramine phentermine. N. Engl. J. Med. *337*, 581–588.
- Cooney, G.M., Dwan, K., Greig, C.A., Lawlor, D.A., Rimer, J., Waugh, F.R., McMurdo, M., and Mead, G.E. (2013). Exercise for depression. Cochrane Database Syst. Rev.
- Copp, F.C., Green, A.F., Hodson, H.F., Randall, A.W., and Sim, M.F. (1967). New peripheral antagonists of 5-hydroxytryptamine. Nature *214*, 200–201.
- Côté, F., Thévenot, E., Fligny, C., Fromes, Y., Darmon, M., Ripoche, M.A., Bayard, E., Hanoun, N., Saurini, F., Lechat, P., et al. (2003). Disruption of the nonneuronal tph1 gene demonstrates the importance of peripheral serotonin in cardiac function. Proc. Natl. Acad. Sci. U. S. A. *100*, 13525–13530.
- Coulter, A.A., Rebello, C.J., and Greenway, F.L. (2018). Centrally Acting Agents for Obesity: Past, Present, and Future. Drugs *78*, 1113–1132.
- Crane, J.D., Mottillo, E.P., Farncombe, T.H., Morrison, K.M., and Steinberg, G.R. (2014). A standardized infrared imaging technique that specifically detects UCP1-mediated thermogenesis in vivo. Mol. Metab. *3*, 490–494.
- Crane, J.D., Palanivel, R., Mottillo, E.P., Bujak, A.L., Wang, H., Ford, R.J., Collins, A., Blümer, R.M., Fullerton, M.D., Yabut, J.M., et al. (2015). Inhibiting peripheral serotonin synthesis reduces obesity and metabolic dysfunction by promoting brown adipose tissue thermogenesis. Nat. Med. *21*, 166–172.
- de Cree, J., Leempoels, J., de Cock, W., Geukens, H., and Verhaegen, H. (1981). The Antihypertensive Effects of a Pure and Selective Serotonin-Receptor Blocking Agent (R 41 468) in Elderly Patients. Angiology *32*, 137–144.
- Cussotto, S., Delgado, I., Anesi, A., Dexpert, S., Aubert, A., Beau, C., Forestier, D., Ledaguenel, P., Magne, E., Mattivi, F., et al. (2020). Tryptophan Metabolic Pathways Are Altered in Obesity and Are Associated With Systemic Inflammation. Front. Immunol. *11*, 557.
- Cypess, A.M., Lehman, S., Williams, G., Tal, I., Rodman, D., Goldfine, A.B., Kuo, F.C., Palmer, E.L., Tseng, Y.H., Doria, A., et al. (2009). Identification and importance of brown adipose tissue in adult humans. N. Engl. J. Med. *360*, 1509–1517.

- Cypess, A.M., Weiner, L.S., Roberts-Toler, C., Elía, E.F., Kessler, S.H., Kahn, P.A., English, J., Chatman, K., Trauger, S.A., Doria, A., et al. (2015). Activation of human brown adipose tissue by a β3-adrenergic receptor agonist. Cell Metab. *21*, 33–38.
- Dale, G.L., Friese, P., Batar, P., Hamilton, S.F., Reed, G.L., Jackson, K.W., Clemetson, K.J., and Alberio, L. (2002). Stimulated platelets use serotonin to enhance their retention of procoagulant proteins on the cell surface. Nature *415*, 175–179.
- Dave, K.D., Quinn, J.L., Harvey, J.A., and Aloyo, V.J. (2004). Role of central 5-HT2 receptors in mediating head bobs and body shakes in the rabbit. Pharmacol. Biochem. Behav. *77*, 623–629.
- Dawkins, M.J.R., and Hull, D. (1964). Brown adipose tissue and the response of new-born rabbits to cold. J. Physiol. *172*, 216–238.
- Dawkins, M.J.R., and Scopes, J.W. (1965). Non-shivering thermogenesis and brown adipose tissue in the human new-born infant [33]. Nature *206*, 201–202.
- Dhaka, A., Murray, A.N., Mathur, J., Earley, T.J., Petrus, M.J., and Patapoutian, A. (2007). TRPM8 Is Required for Cold Sensation in Mice. Neuron *54*, 371–378.
- Digby, J.E., Montague, C.T., Sewter, C.P., Sanders, L., Wilkison, W.O., O'Rahilly, S., and Prins, J.B. (1998). Thiazolidinedione exposure increases the expression of uncoupling protein 1 in cultured human preadipocytes. Diabetes *47*, 138–141.
- Divakaruni, A.S., Wiley, S.E., Rogers, G.W., Andreyev, A.Y., Petrosyan, S., Loviscach, M., Wall, E.A., Yadava, N., Heuck, A.P., Ferrick, D.A., et al. (2013). Thiazolidinediones are acute, specific inhibitors of the mitochondrial pyruvate carrier. Proc. Natl. Acad. Sci. U. S. A. *110*, 5422–5427.
- Drapanas, T., McDonald, J.C., and Steward, J.D. (1962). Serotonin Release Following Instillation of Hypertonic Glucose into the Proximal Intestine. Ann. Surg. *156*, 528–536.
- Dyle, M.C., Ebert, S.M., Cook, D.P., Kunkel, S.D., Fox, D.K., Bongers, K.S., Bullard, S.A., Dierdorff, J.M., and Adams, C.M. (2014). Systems-based discovery of tomatidine as a natural small molecule inhibitor of skeletal muscle atrophy. J. Biol. Chem. *289*, 14913–14924.
- Edwards, S., and Stevens, R.G. (1989). Effects of xylamidine on peripheral 5-hydroxytryptamine-induced anorexia. Pharmacol. Biochem. Behav. *34*, 717–720.
- Ekenvall, L., Lindblad, L.E., Norbeck, O., and Etzell, B.M. (1988). α-Adrenoceptors and cold-induced vasoconstriction in human finger skin. Am. J. Physiol. - Hear. Circ. Physiol. *255*.
- El-Serag, H.B. (2011). Hepatocellular carcinoma. N. Engl. J. Med. *365*, 1118–1127.

- Engel, K., Zhou, M., and Wang, J. (2004). Identification and characterization of a novel monoamine transporter in the human brain. J. Biol. Chem. *279*, 50042–50049.
- von Essen, G., Lindsund, E., Cannon, B., and Nedergaard, J. (2017). Adaptive facultative diet-induced thermogenesis in wild-type but not in UCP1-ablated mice. Am. J. Physiol. - Endocrinol. Metab. *313*, E515–E527.
- Fanibunda, S.E., Deb, S., Maniyadath, B., Tiwari, P., Ghai, U., Gupta, S., Figueiredo, D., Weisstaub, N., Gingrich, J.A., Vaidya, A.D.B., et al. (2019). Serotonin regulates mitochondrial biogenesis and function in rodent cortical neurons via the 5-HT2A receptor and SIRT1–PGC-1α axis. Proc. Natl. Acad. Sci. U. S. A. *166*, 11028–11037.
- Favennec, M., Hennart, B., Caiazzo, R., Leloire, A., Yengo, L., Verbanck, M., Arredouani, A., Marre, M., Pigeyre, M., Bessede, A., et al. (2015). The kynurenine pathway is activated in human obesity and shifted toward kynurenine monooxygenase activation. Obesity *23*, 2066–2074.
- Fedorenko, A., Lishko, P. V., and Kirichok, Y. (2012). Mechanism of fatty-acid-dependent UCP1 uncoupling in brown fat mitochondria. Cell *151*, 400–413.
- Feldman, J.M. (1978). Serotonin metabolism in patients with carcinoid tumors: Incidence of 5-hydroxytryptophan-secreting tumors. Gastroenterology *75*, 1109–1114.
- Feldmann, H.M., Golozoubova, V., Cannon, B., and Nedergaard, J. (2009). UCP1 Ablation Induces Obesity and Abolishes Diet-Induced Thermogenesis in Mice Exempt from Thermal Stress by Living at Thermoneutrality. Cell Metab. *9*, 203–209.
- Fiorella, D., Rabin, R.A., and Winter, J.C. (1995). The role of the 5-HT2A and 5-HT2C receptors in the stimulus effects of hallucinogenic drugs I: Antagonist correlation analysis. Psychopharmacology (Berl). *121*, 347–356.
- Fischer, A.W., Hoefig, C.S., Abreu-Vieira, G., de Jong, J.M.A., Petrovic, N., Mittag, J., Cannon, B., and Nedergaard, J. (2016). Leptin Raises Defended Body Temperature without Activating Thermogenesis. Cell Rep. *14*, 1621–1631.
- Fischer, A.W., Cannon, B., and Nedergaard, J. (2018). Optimal housing temperatures for mice to mimic the thermal environment of humans: An experimental study. Mol. Metab. *7*, 161–170.
- Fischer, A.W., Schlein, C., Cannon, B., Heeren, J., and Nedergaard, J. (2019). Intact innervation is essential for diet-induced recruitment of brown adipose tissue. Am. J. Physiol. - Endocrinol. Metab. *316*, E487–E503.
- Fletcher, P.J., and Burton, M.J. (1984). Effects of manipulations of peripheral serotonin on feeding and drinking in the rat. Pharmacol. Biochem. Behav. *20*, 835–840.
- Fromme, T., and Klingenspor, M. (2011). Uncoupling protein 1 expression

and high-fat diets. Am. J. Physiol. - Regul. Integr. Comp. Physiol. *300*, R1--8.

- Fukui, S., Schwarcz, R., Rapoport, S.I., Takada, Y., and Smith, Q.R. (1991). Blood–Brain Barrier Transport of Kynurenines: Implications for Brain Synthesis and Metabolism. J. Neurochem. *56*, 2007–2017.
- Galmozzi, A., Sonne, S.B., Altshuler-Keylin, S., Hasegawa, Y., Shinoda, K., Luijten, I.H.N., Chang, J.W., Sharp, L.Z., Cravatt, B.F., Saez, E., et al. (2014). ThermoMouse: An In Vivo Model to Identify Modulators of UCP1 Expression in Brown Adipose Tissue. Cell Rep. *9*, 1584–1593.
- Ganguly, R., Tian, Y., Kong, S.X., Hersloev, M., Hobbs, T., Smolarz, B.G., Ramasamy, A., Haase, C.L., and Weng, W. (2018). Persistence of newer anti-obesity medications in a real-world setting. Diabetes Res. Clin. Pract. *143*, 348–356.
- Gartside, S.E., Umbers, V., Hajós, M., and Sharp, T. (1995). Interaction between a selective 5-HT1A receptor antagonist and an SSRI in vivo: effects on 5-HT cell firing and extracellular 5-HT. Br. J. Pharmacol. *115*, 1064–1070.
- Gershon, M.D., and Ross, L.L. (1966). Location of sites of 5-hydroxytryptamine storage and metabolism by radioautography. J. Physiol. *186*, 477–492.
- Gill, R.K., Pant, N., Saksena, S., Singla, A., Nazir, T.M., Vohwinkel, L., Turner, J.R., Goldstein, J., Alrefai, W.A., and Dudeja, P.K. (2007). Function, expression, and characterization of the serotonin transporter in the native human intestine. Am. J. Physiol. - Gastrointest. Liver Physiol. *294*.
- Gnad, T., Scheibler, S., Kugelgen, I. Von, Scheele, C., Kilic, A., Glode, A., Hoffmann, L.S., Reverte-Salisa, L., Horn, P., Mutlu, S., et al. (2014). Adenosine activates brown adipose tissue and recruits beige adipocytes via A2A receptors. Nature *516*, 395–399.
- Golozoubova, V., Hohtola, E., Matthias, A., Jacobsson, A., Cannon, B., and Nedergaard, J. (2001). Only UCP1 can mediate adaptive nonshivering thermogenesis in the cold. FASEB J. *15*, 2048–2050.
- Golozoubova, V., Gullberg, H., Matthias, A., Cannon, B., Vennström, B., and Nedergaard, J. (2004). Depressed Thermogenesis but Competent Brown Adipose Tissue Recruitment in Mice Devoid of All Hormone-Binding Thyroid Hormone Receptors. Mol. Endocrinol. *18*, 384–401.
- González-Maeso, J., Weisstaub, N. V., Zhou, M., Chan, P., Ivic, L., Ang, R., Lira, A., Bradley-Moore, M., Ge, Y., Zhou, Q., et al. (2007). Hallucinogens Recruit Specific Cortical 5-HT2A Receptor-Mediated Signaling Pathways to Affect Behavior. Neuron *53*, 439–452.
- Granneman, J.G., and Lahners, K.N. (1994). Analysis of human and rodent β3-adrenergic receptormessenger ribonucleic acids. Endocrinology *135*, 1025–1031.
- Grenett, H.E., Ledley, F.D., Reed, L.L., and Woo, S.L. (1987). Full-length

cDNA for rabbit tryptophan hydroxylase: functional domains and evolution of aromatic amino acid hydroxylases. Proc. Natl. Acad. Sci. U. S. A. *84*, 5530–5534.

- Grès, S., Gomez-Zorita, S., Gomez-Ruiz, A., and Carpéné, C. (2013). 5-hydroxytryptamine actions in adipocytes: Involvement of monoamine oxidase-dependent oxidation and subsequent PPARγ activation. J. Neural Transm. *120*, 919–926.
- Grosdidier, A., Zoete, V., and Michielin, O. (2011a). SwissDock, a protein-small molecule docking web service based on EADock DSS. Nucleic Acids Res. *39*, W270–W277.
- Grosdidier, A., Zoete, V., and Michielin, O. (2011b). Fast docking using the CHARMM force field with EADock DSS. J. Comput. Chem. *32*, 2149–2159.
- Grundlingh, J., Dargan, P.I., El-Zanfaly, M., and Wood, D.M. (2011). 2,4-Dinitrophenol (DNP): A Weight Loss Agent with Significant Acute Toxicity and Risk of Death. J. Med. Toxicol. *7*, 205–212.
- Guerra, C., Koza, R.A., Yamashita, H., Walsh, K., and Kozak, L.P. (1998). Emergence of brown adipocytes in white fat in mice is under genetic control effects on body weight and adiposity. J. Clin. Invest. *102*, 412–420.
- Hagan, C.E., Schenk, J.O., and Neumaier, J.F. (2011). The contribution of low-affinity transport mechanisms to serotonin clearance in synaptosomes. Synapse *65*, 1015–1023.
- Hajduch, E., Rencurel, F., Balendran, A., Batty, I.H., Downes, C.P., and Hundal, H.S. (1999). Serotonin (5-Hydroxytryptamine), a novel regulator of glucose transport in rat skeletal muscle. J. Biol. Chem. *274*, 13563–13568.
- Hansson, B., Medina, A., Fryklund, C., Fex, M., and Stenkula, K.G. (2016). Serotonin (5-HT) and 5-HT2A receptor agonists suppress lipolysis in primary rat adipose cells. Biochem. Biophys. Res. Commun. *474*, 357–363.
- Hany, T.F., Gharehpapagh, E., Kamel, E.M., Buck, A., Himms-Hagen, J., and von Schulthess, G.K. (2002). Brown adipose tissue: a factor to consider in symmetrical tracer uptake in the neck and upper chest region. Eur. J. Nucl. Med. Mol. Imaging *29*, 1393–1398.
- Harmon, J.L., Wills, L.P., McOmish, C.E., Demireva, E.Y., Gingrich, J.A., Beeson, C.C., and Schnellmann, R.G. (2016). 5-HT2 receptor regulation of mitochondrial genes: Unexpected pharmacological effects of agonists and antagonists. J. Pharmacol. Exp. Ther. *357*, 1–9.
- Harrison, R.K. (2016). Phase II and phase III failures: 2013-2015. Nat. Rev. Drug Discov. *15*, 817–818.
- Hedlund, P.B., Danielson, P.E., Thomas, E.A., Slanina, K., Carson, M.J., and Sutcliffe, J.G. (2003). No hypothermic response to serotonin in 5-HT7 receptor knockout mice. Proc. Natl. Acad. Sci. U. S. A. *100*, 1375–1380.
- Heim, T., and Hull, D. (1966). The blood flow and oxygen consumption of

brown adipose tissue in the new-born rabbit. J. Physiol. *186*, 42–55.
- Henry, J.P., Sagné, C., Bedet, C., and Gasnier, B. (1998). The vesicular monoamine transporter: From chromaffin granule to brain. Neurochem. Int. *32*, 227–246.
- Hill, J.E., Makky, K., Shrestha, L., Hillard, C.J., and Gasser, P.J. (2011). Natural and synthetic corticosteroids inhibit uptake2-mediated transport in CNS neurons. Physiol. Behav. *104*, 306–311.
- Himms-Hagen, J., Erickson, J.C., Hollopeter, G., Palmiter, R.D., Pelleymounter, M.A., Cullen, M.J., Baker, M.B., Hecht, R., Winters, D., Boone, T., et al. (1997). On raising energy expenditure in ob/ob mice. Science (80-.). *276*, 1132–1133.
- Hinney, A., Barth, N., Ziegler, A., Von Prittwitz, S., Hamann, A., Hennighausen, K., Pirke, K.M., Heils, A., Rosenkranz, K., Roth, H., et al. (1997). Serotonin transporter gene-linked polymorphic region: Allele distributions in relationship to body weight and in anorexia nervosa. Life Sci. *61*.
- Hodges, M.R., Tattersall, G.J., Harris, M.B., McEvoy, S.D., Richerson, D.N., Deneris, E.S., Johnson, R.L., Chen, Z.F., and Richerson, G.B. (2008). Defects in breathing and thermoregulation in mice with near-complete absence of central serotonin neurons. J. Neurosci. *28*, 2495–2505.
- Holmes, A., Yang, R.J., Murphy, D.L., and Crawley, J.N. (2002). Evaluation of antidepressant-related behavioral responses in mice lacking the serotonin transporter. Neuropsychopharmacology *27*, 914–923.
- Homberg, J.R., La Fleur, S.E., and Cuppen, E. (2010). Serotonin transporter deficiency increases abdominal fat in female, but not male rats. Obesity *18*, 137–145.
- Hoyer, D., Clarke, D.E., Fozard, J.R., Hartig, P.R., Martin, G.R., Mylecharane, E.J., Saxena, P.R., and Humphrey, P.P. (1994). International Union of Pharmacology classification of receptors for 5-hydroxytryptamine (Serotonin). Pharmacol. Rev. *46*, 157–203.
- Huang, D.W., Sherman, B.T., and Lempicki, R.A. (2009a). Systematic and integrative analysis of large gene lists using DAVID bioinformatics resources. Nat. Protoc. *4*, 44–57.
- Huang, D.W., Sherman, B.T., and Lempicki, R.A. (2009b). Bioinformatics enrichment tools: Paths toward the comprehensive functional analysis of large gene lists. Nucleic Acids Res. *37*, 1–13.
- Huether, G., Hajak, G., Reimer, A., Poeggeler, B., Blömer, M., Rodenbeck, A., and Rüther, E. (1992). The metabolic fate of infused l-tryptophan in men: possible clinical implications of the accumulation of circulating tryptophan and tryptophan metabolites. Psychopharmacology (Berl). *109*, 422–432.
- Humphrey, J.H., and Jaques, R. (1954). The histamine and serotonin content of the platelets and polymorphonuclear leucocytes of various species. J.

Physiol. *124*, 305–310.
- Huttunen, P., Hirvonen, J., and Kinnula, V. (1981). The occurrence of brown adipose tissue in outdoor workers. Eur. J. Appl. Physiol. Occup. Physiol. *46*, 339–345.
- Ikegami, R., Shimizu, I., Sato, T., Yoshida, Y., Hayashi, Y., Suda, M., Katsuumi, G., Li, J., Wakasugi, T., Minokoshi, Y., et al. (2018). Gamma-Aminobutyric Acid Signaling in Brown Adipose Tissue Promotes Systemic Metabolic Derangement in Obesity. Cell Rep. *24*, 2827-2837.e5.
- Ioannides-Demos, L.L., Proietto, J., Tonkin, A.M., and McNeil, J.J. (2006). Safety of drug therapies used for weight loss and treatment of obesity. Drug Saf. *29*, 277–302.
- Isidor, M.S., Winther, S., Basse, A.L., Petersen, M.C.H., Cannon, B., Nedergaard, J., and Hansen, J.B. (2016). An siRNA-based method for efficient silencing of gene expression in mature brown adipocytes. Adipocyte *5*, 175–185.
- Jaggar, M., Weisstaub, N., Gingrich, J.A., and Vaidya, V.A. (2017). 5-HT2A receptor deficiency alters the metabolic and transcriptional, but not the behavioral, consequences of chronic unpredictable stress. Neurobiol. Stress *7*, 89–102.
- Jespersen, N.Z., Larsen, T.J., Peijs, L., Daugaard, S., Homøe, P., Loft, A., de Jong, J., Mathur, N., Cannon, B., Nedergaard, J., et al. (2013). A classical brown adipose tissue mRNA signature partly overlaps with brite in the supraclavicular region of adult humans. Cell Metab. *17*, 798–805.
- Jimenez, M., Léger, B., Canola, K., Lehr, L., Arboit, P., Seydoux, J., Russell, A.P., Giacobino, J.P., Muzzin, P., and Preitner, F. (2002). B1/B2/B3-Adrenoceptor Knockout Mice Are Obese and Cold-Sensitive But Have Normal Lipolytic Responses To Fasting. FEBS Lett. *530*, 37–40.
- Jin, U.H., Lee, S.O., Sridharan, G., Lee, K., Davidson, L.A., Jayaraman, A., Chapkin, R.S., Alaniz, R., and Safe, S. (2014). Microbiome-derived tryptophan metabolites and their aryl hydrocarbon receptor-dependent agonist and antagonist activities. Mol. Pharmacol. *85*, 777–788.
- Jones, L.H. (2016). An industry perspective on drug target validation. Expert Opin. Drug Discov. *11*, 623–625.
- Kalinovich, A. V., de Jong, J.M.A., Cannon, B., and Nedergaard, J. (2017). UCP1 in adipose tissues: two steps to full browning. Biochimie *134*, 127–137.
- Kampert, J.B., Blair, S.N., Barlow, C.E., and Kohl, H.W. (1996). Physical activity, physical fitness, and all-cause and cancer mortality: A prospective study of men and women. Ann. Epidemiol. *6*, 452–457.
- Kanarek, R.B., and Dushkin, H. (1988). Peripheral serotonin administration selectively reduces fat intake in rats. Pharmacol. Biochem. Behav. *31*, 113–122.
- Kazak, L., Chouchani, E.T., Jedrychowski, M.P., Erickson, B.K., Shinoda,

K., Cohen, P., Vetrivelan, R., Lu, G.Z., Laznik-Bogoslavski, D., Hasenfuss, S.C., et al. (2015). A Creatine-Driven Substrate Cycle Enhances Energy Expenditure and Thermogenesis in Beige Fat. Cell *163*, 643–655.

- Khera, R., Murad, M.H., Chandar, A.K., Dulai, P.S., Wang, Z., Prokop, L.J., Loomba, R., Camilleri, M., and Singh, S. (2016). Association of pharmacological treatments for obesity withweight loss and adverse events a systematic review and meta-analysis. JAMA - J. Am. Med. Assoc. *315*, 2424–2434.
- Kim, H.J., Kim, J.H., Noh, S., Hur, H.J., Sung, M.J., Hwang, J.T., Park, J.H., Yang, H.J., Kim, M.S., Kwon, D.Y., et al. (2011). Metabolomic analysis of livers and serum from high-fat diet induced obese mice. J. Proteome Res. *10*, 722–731.
- Kingma, B., Frijns, A., and Lichtenbelt, W.V.M. (2012). The thermoneutral zone: Implications for metabolic studies. Front. Biosci. - Elit. *4 E*, 1975–1985.
- Kinoshita, M., Ono, K., Horie, T., Nagao, K., Nishi, H., Kuwabara, Y., Takanabe-Mori, R., Hasegawa, K., Kita, T., and Kimura, T. (2010). Regulation of adipocyte differentiation by activation of serotonin (5-HT) receptors 5-HT2AR and 5-HT2CR and involvement of microRNA-448-mediated repression of KLF5. Mol. Endocrinol. *24*, 1978–1987.
- Klepac, K., Kilić, A., Gnad, T., Brown, L.M., Herrmann, B., Wilderman, A., Balkow, A., Glöde, A., Simon, K., Lidell, M.E., et al. (2016). The G q signalling pathway inhibits brown and beige adipose tissue. Nat. Commun. *7*, 10895.
- Koe, B.K., and Weissman, A. (1966). p-Chlorophenylalanine: a specific depletor of brain serotonin. J. Pharmacol. Exp. Ther. *154*, 499–516.
- Kondo, M., Yoshida, T., Nakanishi, T., and Yoshimura, M. (1992). Beta-3 adrenergic agonist, BRL-26830A, and alpha/beta blocker, arotinolol, markedly increase regional blood flow in the brown adipose tissue in anesthetized rats. Jpn. Circ. J. *56*, 936–942.
- Kontani, Y., Wang, Y., Kimura, K., Inokuma, K.I., Saito, M., Suzuki-Miura, T., Wang, Z., Sato, Y., Mori, N., and Yamashita, H. (2005). UCP1 deficiency increases susceptibility to diet-induced obesity with age. Aging Cell *4*, 147–155.
- Kopecky, J., Clarke, G., Enerbäck, S., Spiegelman, B., and Kozak, L.P. (1995). Expression of the mitochondrial uncoupling protein gene from the aP2 gene promoter prevents genetic obesity. J. Clin. Invest. *96*, 2914–2923.
- Kopecký, J., Hodný, Z., Rossmeisl, M., Syrový, I., and Kozak, L.P. (1996). Reduction of dietary obesity in aP2-Ucp transgenic mice: Physiology and adipose tissue distribution. Am. J. Physiol. - Endocrinol. Metab. *270*, E768–E775.
- Kozak, L.P. (2010). Brown Fat and the Myth of Diet-Induced Thermogenesis. Cell Metab. *11*, 263–267.

- Krief, S., Lonnqvist, F., Raimbault, S., Baude, B., Van Spronsen, A., Arner, P., Strosberg, A.D., Ricquier, D., and Emorine, L.J. (1993). Tissue distribution of β3-adrenergic receptor mRNA in man. J. Clin. Invest. *91*, 344–349.
- Krishnan, S., Ding, Y., Saedi, N., Choi, M., Sridharan, G. V., Sherr, D.H., Yarmush, M.L., Alaniz, R.C., Jayaraman, A., and Lee, K. (2018). Gut Microbiota-Derived Tryptophan Metabolites Modulate Inflammatory Response in Hepatocytes and Macrophages. Cell Rep. *23*, 1099–1111.
- Krstic, J., Reinisch, I., Schupp, M., Schulz, T.J., and Prokesch, A. (2018). P53 functions in adipose tissue metabolism and homeostasis. Int. J. Mol. Sci. *19*.
- Kruk, Z.L. (1973). Dopamine and 5-hydroxytryptamine inhibit feeding in rats. Nat. New Biol. *246*, 52–53.
- Kulke, M.H., O'Dorisio, T., Phan, A., Bergsland, E., Law, L., Banks, P., Freiman, J., Frazier, K., Jackson, J., Yao, J.C., et al. (2014). Telotristat etiprate, a novel serotonin synthesis inhibitor, in patients with carcinoid syndrome and diarrhea not adequately controlled by octreotide. Endocr. Relat. Cancer *21*, 705–714.
- Van Der Lans, A.A.J.J., Hoeks, J., Brans, B., Vijgen, G.H.E.J., Visser, M.G.W., Vosselman, M.J., Hansen, J., Jörgensen, J.A., Wu, J., Mottaghy, F.M., et al. (2013). Cold acclimation recruits human brown fat and increases nonshivering thermogenesis. J. Clin. Invest. *123*, 3395–3403.
- Lee, P., Smith, S., Linderman, J., Courville, A.B., Brychta, R.J., Dieckmann, W., Werner, C.D., Chen, K.Y., and Celi, F.S. (2014). Temperature-acclimated brown adipose tissue modulates insulin sensitivity in humans. Diabetes *63*, 3686–3698.
- Leibel, R.L., Rosenbaum, M., and Hirsch, J. (1995). Changes in energy expenditure resulting from altered body weight. N. Engl. J. Med. *332*, 621–628.
- Lemstra, M., Bird, Y., Nwankwo, C., Rogers, M., and Moraros, J. (2016). Weight loss intervention adherence and factors promoting adherence: a meta-analysis. Patient Prefer. Adherence *10*, 1547–1559.
- Lesurtel, M., Graf, R., Aleil, B., Walther, D.J., Tian, Y., Jochum, W., Gachet, C., Bader, M., and Clavien, P.A. (2006). Platelet-derived serotonin mediates liver regeneration. Science (80-.). *312*, 104–107.
- Lewis, M.T., Lujan, H.L., Tonson, A., Wiseman, R.W., and DiCarlo, S.E. (2019). Obesity and inactivity, not hyperglycemia, cause exercise intolerance in individuals with type 2 diabetes: Solving the obesity and inactivity versus hyperglycemia causality dilemma. Med. Hypotheses *123*, 110–114.
- Li, Y., Fromme, T., Schweizer, S., Schöttl, T., and Klingenspor, M. (2014). Taking control over intracellular fatty acid levels is essential for the analysis of thermogenic function in cultured primary brown and brite/beige

adipocytes. EMBO Rep. *15*, 1069–1076.
- Li, Y., Hu, N., Yang, D., Oxenkrug, G., and Yang, Q. (2017). Regulating the balance between the kynurenine and serotonin pathways of tryptophan metabolism. FEBS J. *284*, 948–966.
- Li, Z., Chalazonitis, A., Huang, Y.Y., Mann, J.J., Margolis, K.G., Yang, Q.M., Kim, D.O., Côté, F., Mallet, J., and Gershon, M.D. (2011). Essential roles of enteric neuronal serotonin in gastrointestinal motility and the development/survival of enteric dopaminergic neurons. J. Neurosci. *31*, 8998–9009.
- Lindblad, L.E., Shepherd, J.T., and Vanhoutte, P.M. (1984). Cooling Augments Platelet-Induced Contraction of Peripheral Arteries of the Dog. Proc. Soc. Exp. Biol. Med. *176*, 119–122.
- Liu, L., Su, X., Quinn, W.J., Hui, S., Krukenberg, K., Frederick, D.W., Redpath, P., Zhan, L., Chellappa, K., White, E., et al. (2018). Quantitative Analysis of NAD Synthesis-Breakdown Fluxes. Cell Metab. *27*, 1067-1080.e5.
- Liu, Q., Yang, Q., Sun, W., Vogel, P., Heydorn, W., Yu, X.Q., Hu, Z., Yu, W., Jonas, B., Pineda, R., et al. (2008). Discovery and characterization of novel tryptophan hydroxylase inhibitors that selectively inhibit serotonin synthesis in the gastrointestinal tract. J. Pharmacol. Exp. Ther. *325*, 47–55.
- Liu, X., Rossmeisl, M., McClaine, J., and Kozak, L.P. (2003). Paradoxical resistance to diet-induced obesity in UCP1-deficient mice. J. Clin. Invest. *111*, 399–407.
- Loh, R.K.C., Formosa, M.F., Eikelis, N., Bertovic, D.A., Anderson, M.J., Barwood, S.A., Nanayakkara, S., Cohen, N.D., La Gerche, A., Reutens, A.T., et al. (2018). Pioglitazone reduces cold-induced brown fat glucose uptake despite induction of browning in cultured human adipocytes: a randomised, controlled trial in humans. Diabetologia *61*, 220–230.
- Lonsdale, J., Thomas, J., Salvatore, M., Phillips, R., Lo, E., Shad, S., Hasz, R., Walters, G., Garcia, F., Young, N., et al. (2013). The Genotype-Tissue Expression (GTEx) project. Nat. Genet. *45*, 580–585.
- Lopez-Vilchez, I., Diaz-Ricart, M., White, J.G., Escolar, G., and Galan, A.M. (2009). Serotonin enhances platelet procoagulant properties and their activation induced during platelet tissue factor uptake. Cardiovasc. Res. *84*, 309–316.
- Lowell, B.B., S-Susulic, V., Hamann, A., Lawitts, J.A., Himms-Hagen, J., Boyer, B.B., Kozak, L.P., and Flier, J.S. (1993). Development of obesity in transgenic mice after genetic ablation of brown adipose tissue. Nature *366*, 740–742.
- Ma, S.W.Y., and Foster, D.O. (1986). Uptake of glucose and release of fatty acids and glycerol by rat brown adipose tissue in vivo. Can. J. Physiol. Pharmacol. *64*, 609–614.
- Malyszko, J., Urano, T., Knofler, R., Taminato, A., Yoshimi, T., Takada,

Y., and Takada, A. (1994). Daily variations of platelet aggregation in relation to blood and plasma serotonin in diabetes. Thromb. Res. *75*, 569–576.

- Van Marken Lichtenbelt, W.D., Vanhommerig, J.W., Smulders, N.M., Drossaerts, J.M.A.F.L., Kemerink, G.J., Bouvy, N.D., Schrauwen, P., and Teule, G.J.J. (2009). Cold-activated brown adipose tissue in healthy men. N. Engl. J. Med. *360*, 1500–1508.
- Martin, C.K., Redman, L.M., Zhang, J., Sanchez, M., Anderson, C.M., Smith, S.R., and Ravussin, E. (2011). Lorcaserin, a 5-HT2C receptor agonist, reduces body weight by decreasing energy intake without influencing energy expenditure. J. Clin. Endocrinol. Metab. *96*, 837–845.
- Masson, J., Emerit, M.B., Hamon, M., and Darmon, M. (2012). Serotonergic signaling: Multiple effectors and pleiotropic effects. Wiley Interdiscip. Rev. Membr. Transp. Signal. *1*, 685–713.
- Masters, E.M. (1972). Monoamine oxidase activity in cultured brown fat cells. Exp. Cell Res. *71*, 372–376.
- McAllister, E.J., Dhurandhar, N. V., Keith, S.W., Aronne, L.J., Barger, J., Baskin, M., Benca, R.M., Biggio, J., Boggiano, M.M., Eisenmann, J.C., et al. (2009). Ten putative contributors to the obesity epidemic. Crit. Rev. Food Sci. Nutr. *49*, 868–913.
- McGlashon, J.M., Gorecki, M.C., Kozlowski, A.E., Thirnbeck, C.K., Markan, K.R., Leslie, K.L., Kotas, M.E., Potthoff, M.J., Richerson, G.B., and Gillum, M.P. (2015). Central Serotonergic Neurons Activate and Recruit Thermogenic Brown and Beige Fat and Regulate Glucose and Lipid Homeostasis. Cell Metab. *21*, 692–705.
- McKinney, J., Knappskog, P.M., and Haavik, J. (2005). Different properties of the central and peripheral forms of human tryptophan hydroxylase. J. Neurochem. *92*, 311–320.
- Melnyk, A., Harper, M.E., and Himms-Hagen, J. (1997). Raising at thermoneutrality prevents obesity and hyperphagia in BAT-ablated transgenic mice. Am. J. Physiol. *272*.
- Miller, W.C., Koceja, D.M., and Hamilton, E.J. (1997). A meta-analysis of the past 25 years of weight loss research using diet, exercise or diet plus exercise intervention. Int. J. Obes. *21*, 941–947.
- Mina, A.I., LeClair, R.A., LeClair, K.B., Cohen, D.E., Lantier, L., and Banks, A.S. (2018). CalR: A Web-Based Analysis Tool for Indirect Calorimetry Experiments. Cell Metab. *28*, 656-666.e1.
- Morrison, S.F., Madden, C.J., and Tupone, D. (2014). Central neural regulation of brown adipose tissue thermogenesis and energy expenditure. Cell Metab. *19*, 741–756.
- Mory, G., Combes-George, M., and Nechad, M. (1984). Localization of serotonin and dopamine in the brown adipose tissue of the rat and their variations during cold exposure. Biol. Cell *48*, 159–166.

- Mössner, R., Simantov, R., Marx, A., Lesch, K.P., and Seif, I. (2006). Aberrant accumulation of serotonin in dopaminergic neurons. Neurosci. Lett. *401*, 49–54.
- Mota, C.M.D., Branco, L.G.S., Morrison, S.F., and Madden, C.J. (2020). Systemic serotonin inhibits brown adipose tissue sympathetic nerve activity via a GABA input to the dorsomedial hypothalamus, not via 5HT1A receptor activation in raphe pallidus. Acta Physiol. *228*.
- Mottillo, E.P., Bloch, A.E., Leffs, T., and Granneman, J.G. (2012). Lipolytic products activate peroxisome proliferator-activated receptor (PPAR) α and δ in brown adipocytes to match fatty acid oxidation with supply. J. Biol. Chem. *287*, 25038–25048.
- Mottillo, E.P., Balasubramanian, P., Lee, Y.H., Weng, C., Kershaw, E.E., and Granneman, J.G. (2014). Coupling of lipolysis and de novo lipogenesis in brown, beige, and white adipose tissues during chronic β3-adrenergic receptor activation. J. Lipid Res. *55*, 2276–2286.
- Müller, N., and Schwarz, M.J. (2007). The immune-mediated alteration of serotonin and glutamate: Towards an integrated view of depression. Mol. Psychiatry *12*, 988–1000.
- Müller, H.K., Kragballe, M., Fjorback, A.W., and Wiborg, O. (2014). Differential regulation of the serotonin transporter by vesicle-associated membrane protein 2 in cells of neuronal versus non-neuronal origin. PLoS One *9*.
- Murphy, D.L., and Lesch, K.P. (2008). Targeting the murine serotonin transporter: Insights into human neurobiology. Nat. Rev. Neurosci. *9*, 85–96.
- Nagano, J., Shimizu, M., Hara, T., Shirakami, Y., Kochi, T., Nakamura, N., Ohtaki, H., Ito, H., Tanaka, T., Tsurumi, H., et al. (2013). Effects of Indoleamine 2,3-Dioxygenase Deficiency on High-Fat Diet-Induced Hepatic Inflammation. PLoS One *8*, e73404.
- Nakamura, K., and Morrison, S.F. (2007). Central efferent pathways mediating skin cooling-evoked sympathetic thermogenesis in brown adipose tissue. Am. J. Physiol. - Regul. Integr. Comp. Physiol. *292*, R127--36.
- Namkung, J., Shong, K.E., Kim, H., Oh, C.M., Park, S., and Kim, H. (2018). Inhibition of serotonin synthesis induces negative hepatic lipid balance. Diabetes Metab. J. *42*, 233–243.
- Narboux-Nême, N., Sagné, C., Doly, S., Diaz, S.L., Martin, C.B.P., Angenard, G., Martres, M.P., Giros, B., Hamon, M., Lanfumey, L., et al. (2011). Severe serotonin depletion after conditional deletion of the vesicular monoamine transporter 2 gene in serotonin neurons: Neural and behavioral consequences. Neuropsychopharmacology *36*, 2538–2550.
- Nedergaard, J., and Cannon, B. (2013). UCP1 mRNA does not produce heat. Biochim. Biophys. Acta - Mol. Cell Biol. Lipids *1831*, 943–949.

- Nedergaard, J., Bengtsson, T., and Cannon, B. (2011). New powers of brown fat: Fighting the metabolic syndrome. Cell Metab. *13*, 238–240.
- Ng, M., Fleming, T., Robinson, M., Thomson, B., Graetz, N., Margono, C., Mullany, E.C., Biryukov, S., Abbafati, C., Abera, S.F., et al. (2014). Global, regional, and national prevalence of overweight and obesity in children and adults during 1980-2013: A systematic analysis for the Global Burden of Disease Study 2013. Lancet *384*, 766–781.
- Nirengi, S., Yoneshiro, T., Sugie, H., Saito, M., and Hamaoka, T. (2015). Human brown adipose tissue assessed by simple, noninvasive near-Infrared time-resolved spectroscopy. Obesity *23*, 973–980.
- Nonogaki, K., Strack, A.M., Dallman, M.F., and Tecott, L.H. (1998). Leptin-independent hyperphagia and type 2 diabetes in mice with a mutated serotonin 5-HT(2C) receptor gene. Nat. Med. *4*, 1152–1156.
- Nonogaki, K., Nozue, K., Takahashi, Y., Yamashita, N., Hiraoka, S., Kumano, H., Kuboki, T., and Oka, Y. (2007). Fluvoxamine, a selective serotonin reuptake inhibitor, and 5-HT 2C receptor inactivation induce appetite-suppressing effects in mice via 5-HT1B receptors. Int. J. Neuropsychopharmacol. *10*, 675–681.
- Ntziachristos, V., Pleitez, M.A., Aime, S., and Brindle, K.M. (2019). Emerging Technologies to Image Tissue Metabolism. Cell Metab. *29*, 518–538.
- O'Neill, H.M., Maarbjerg, S.J., Crane, J.D., Jeppesen, J., Jørgensen, S.B., Schertzer, J.D., Shyroka, O., Kiens, B., Van Denderen, B.J., Tarnopolsky, M.A., et al. (2011). AMP-activated protein kinase (AMPK) β1β2 muscle null mice reveal an essential role for AMPK in maintaining mitochondrial content and glucose uptake during exercise. Proc. Natl. Acad. Sci. U. S. A. *108*, 16092–16097.
- Ogawa, T., Sugidachi, A., Tanaka, N., Fujimoto, K., and Asai, F. (2002). Pharmacological profiles of R-96544, the active form of a novel 5-HT2A receptor antagonist R-102444. Eur. J. Pharmacol. *457*, 107–114.
- Oguri, Y., Fujita, Y., Abudukadier, A., Ohashi, A., Goto, T., Furuya, F., Obara, A., Fukushima, T., Matsuo, N., Kim, M., et al. (2017). Tetrahydrobiopterin activates brown adipose tissue and regulates systemic energy metabolism. JCI Insight *2*.
- Oh, C.M., Namkung, J., Go, Y., Shong, K.E., Kim, K., Kim, H., Park, B.Y., Lee, H.W., Jeon, Y.H., Song, J., et al. (2015). Regulation of systemic energy homeostasis by serotonin in adipose tissues. Nat. Commun. *6*, 6794.
- Oh, C.M., Park, S., and Kim, H. (2016). Serotonin as a new therapeutic target for diabetes mellitus and obesity. Diabetes Metab. J. *40*, 89–98.
- Ohara-Imaizumi, M., Kim, H., Yoshida, M., Fujiwara, T., Aoyagi, K., Toyofuku, Y., Nakamichi, Y., Nishiwaki, C., Okamura, T., Uchida, T., et al. (2013). Serotonin regulates glucose-stimulated insulin secretion from pancreatic β cells during pregnancy. Proc. Natl. Acad. Sci. U. S. A. *110*,

19420–19425.
- Ojeda-Rodríguez, A., Morell-Azanza, L., Azcona-Sanjulián, M.C., Martínez, J.A., Ramírez, M.J., Marti del Moral, A., Rendo-Urteaga, T., and Chueca, M. (2018). Disminución de los niveles de serotonina tras una intervención de estilo de vida en niños obesos: Asociación con glucosa y medidas antropométricas. Nutr. Hosp. *35*, 279–285.
- Oldendorf, W.H. (1971). Brain uptake of radiolabeled amino acids, amines, and hexoses after arterial injection. Am. J. Physiol. *221*, 1629–1639.
- Olsen, J.M., Sato, M., Dallner, O.S., Sandström, A.L., Pisani, D.F., Chambard, J.C., Amri, E.Z., Hutchinson, D.S., and Bengtsson, T. (2014). Glucose uptake in brown fat cells is dependent on mTOR complex 2-promoted GLUT1 translocation. J. Cell Biol. *207*, 365–374.
- Ootsuka, Y., and Blessing, W.W. (2006). Thermogenesis in brown adipose tissue: Increase by 5-HT2A receptor activation and decrease by 5-HT1A receptor activation in conscious rats. Neurosci. Lett. *395*, 170–174.
- Ootsuka, Y., Blessing, W.W., and Nalivaiko, E. (2008). Selective blockade of 5-HT2A receptors attenuates the increased temperature response in brown adipose tissue to restraint stress in rats. Stress *11*, 125–133.
- Ortiz, J., and Artigas, F. (1992). Effects of monoamine uptake inhibitors on extracellular and platelet 5-hydroxytryptamine in rat blood: different effects of clomipramine and fluoxetine. Br. J. Pharmacol. *105*, 941–946.
- Osuide, G., Wambebe, C., and Bodhankar, S. (1984). Effect of some serotoninergic agents on the rectal temperature of the domestic fowl (gallus domesticus). Neuropharmacology *23*, 1407–1414.
- Palego, L., Betti, L., Rossi, A., and Giannaccini, G. (2016). Tryptophan biochemistry: Structural, nutritional, metabolic, and medical aspects in humans. J. Amino Acids *2016*, 8952520.
- Pan, Y., Gembom, E., Peng, W., Lesch, K.P., Mossner, R., and Simantov, R. (2001). Plasticity in serotonin uptake in primary neuronal cultures of serotonin transporter knockout mice. Dev. Brain Res. *126*, 125–129.
- Paulik, M.A., Buckholz, R.G., Lancaster, M.E., Dallas, W.S., Hull-Ryde, E.A., Weiel, J.E., and Lenhard, J.M. (1998). art%3A10.1023%2FA%3A1011993019385.pdf. Pharm. Res. *15*, 944–949.
- Paulmann, N., Grohmann, M., Voigt, J.P., Bert, B., Vowinckel, J., Bader, M., Skelin, M., Jevšek, M., Fink, H., Rupnik, M., et al. (2009). Intracellular serotonin modulates insulin secretion from pancreatic β-cells by protein serotonylation. PLoS Biol. *7*, e1000229.
- Pear, W.S., Nolan, G.P., Scott, M.L., and Baltimore, D. (1993). Production of high-titer helper-free retroviruses by transient transfection. Proc. Natl. Acad. Sci. U. S. A. *90*, 8392–8396.
- Pérez, V., Gilaberte, I., Faries, D., Alvarez, E., and Artigas, F. (1997). Randomised, double-blind, placebo-controlled trial of pindolol in combination with fluoxetine antidepressant treatment. Lancet *349*, 1594–

1597.
- Petrassi, M., Barber, R., Be, C., Beach, S., Cox, B., D'Souza, A.M., Duggan, N., Hussey, M., Fox, R., Hunt, P., et al. (2017). Identification of a novel allosteric inhibitory site on tryptophan hydroxylase 1 enabling unprecedented selectivity over all related hydroxylases. Front. Pharmacol. *8*, 240.
- Pirzgalska, R.M., Seixas, E., Seidman, J.S., Link, V.M., Sánchez, N.M., Mahú, I., Mendes, R., Gres, V., Kubasova, N., Morris, I., et al. (2017). Sympathetic neuron-associated macrophages contribute to obesity by importing and metabolizing norepinephrine. Nat. Med. *23*, 1309–1318.
- Pollock, J.D., and Rowland, N. (1981). Peripherally administered serotonin decreases food intake in rats. Pharmacol. Biochem. Behav. *15*, 179–183.
- Popa, M., Stefănescu, A.M., and Dumitriu, L. (1989). Low level of urinary 5-hydroxyindole acetic acid (5 HIAA) in obese children having concomitantly high 3-methoxy-4-hydroxyphenyl glycol (MHPG) excretion. Endocrinologie *27*, 29–34.
- Quay, W.B. (1963). Effect of Dietary Phenylalanine and Tryptophan on Pineal and Hypothalamic Serotonin Levels. Proc. Soc. Exp. Biol. Med. *114*, 718–721.
- Rahman, M.K., Toshiharu, N., and Takeshi, K. (1981). Aromatic l-amino acid decarboxylase activity in central and peripheral tissues and serum of rats with l-dopa and l-5-hydroxytryptophan as substrates. Biochem. Pharmacol. *30*, 645–649.
- Rami, M., Guillamat-Prats, R., Rinne, P., Salvermoser, M., Ring, L., Bianchini, M., Blanchet, X., Megens, R.T.A., Döring, Y., Walzog, B., et al. (2018). Chronic intake of the selective serotonin reuptake inhibitor fluoxetine enhances atherosclerosis. Arterioscler. Thromb. Vasc. Biol. *38*, 1007–1019.
- Ravussin, Y., Gutman, R., Leduc, C.A., and Leibel, R.L. (2013). Estimating energy expenditure in mice using an energy balance technique. Int. J. Obes. *37*, 399–403.
- Raymond, C.S., and Soriano, P. (2007). High-efficiency FLP and ΦC31 site-specific recombination in mammalian cells. PLoS One *2*.
- Richardson-Jones, J.W., Craige, C.P., Guiard, B.P., Stephen, A., Metzger, K.L., Kung, H.F., Gardier, A.M., Dranovsky, A., David, D.J., Beck, S.G., et al. (2010). 5-HT1A Autoreceptor Levels Determine Vulnerability to Stress and Response to Antidepressants. Neuron *65*, 40–52.
- Rosen, E.D., and Spiegelman, B.M. (2014). What we talk about when we talk about fat. Cell *156*, 20–44.
- Rossi, F., Miggiano, R., Ferraris, D.M., and Rizzi, M. (2019). The synthesis of kynurenic acid in mammals: An updated kynurenine aminotransferase structural KATalogue. Front. Mol. Biosci. *6*.
- Roth, B.L. (2007). Focus on research: Drugs and valvular heart disease. N.

Engl. J. Med. *356*, 6–9.
- Roth, B.L. (2012). NIMH PDSP - Assay Protocol Book Version II.
- Rothman, R.B., Baumann, M.H., Savage, J.E., Rauser, L., McBride, A., Hufeisen, S.J., and Roth, B.L. (2000). Evidence for possible involvement of 5-HT(2B) receptors in the cardiac valvulopathy associated with fenfluramine and other serotonergic medications. Circulation *102*, 2836–2841.
- Rothwell, N.J., and Stock, M.J. (1979). A role for brown adipose tissue in diet-induced thermogenesis. Nature *281*, 31–35.
- Rozenblit-Susan, S., Chapnik, N., and Froy, O. (2018). Serotonin prevents differentiation into brown adipocytes and induces transdifferentiation into white adipocytes. Int. J. Obes. *42*, 704–710.
- Ryerson, A.B., Eheman, C.R., Altekruse, S.F., Ward, J.W., Jemal, A., Sherman, R.L., Henley, S.J., Holtzman, D., Lake, A., Noone, A.M., et al. (2016). Annual Report to the Nation on the Status of Cancer, 1975-2012, featuring the increasing incidence of liver cancer. Cancer *122*, 1312–1337.
- Saito, M., Okamatsu-Ogura, Y., Matsushita, M., Watanabe, K., Yoneshiro, T., Nio-Kobayashi, J., Iwanaga, T., Miyagawa, M., Kameya, T., Nakada, K., et al. (2009). High incidence of metabolically active brown adipose tissue in healthy adult humans: Effects of cold exposure and adiposity. Diabetes *58*, 1526–1531.
- Sangkuhl, K., Klein, T.E., and Altman, R.B. (2009). Selective serotonin reuptake inhibitors pathway. Pharmacogenet. Genomics *19*, 907–909.
- Schindler, R. (1959). The conversion of 14C-labelled tryptophan to 5-hydroxytryptamine by neoplastic mast cells. Biochem. Pharmacol. *1*, 323–327.
- Schmitt, A., Mössner, R., Gossmann, A., Fischer, I.G., Gorboulev, V., Murphy, D.L., Koepsell, H., and Lesch, K.P. (2003). Organic cation transporter capable of transporting serotonin is up-regulated in serotonin transporter-deficient mice. J. Neurosci. Res. *71*, 701–709.
- Schreiber, R., Diwoky, C., Schoiswohl, G., Feiler, U., Wongsiriroj, N., Abdellatif, M., Kolb, D., Hoeks, J., Kershaw, E.E., Sedej, S., et al. (2017). Cold-Induced Thermogenesis Depends on ATGL-Mediated Lipolysis in Cardiac Muscle, but Not Brown Adipose Tissue. Cell Metab. *26*, 753-763.e7.
- Seretis, K., Goulis, D.G., Koliakos, G., and Demiri, E. (2015a). Short- and Long-Term Effects of Abdominal Lipectomy on Weight and Fat Mass in Females: a Systematic Review. Obes. Surg. *25*, 1950–1958.
- Seretis, K., Goulis, D.G., Koliakos, G., and Demiri, E. (2015b). The effects of abdominal lipectomy in metabolic syndrome components and insulin sensitivity in females: A systematic review and meta-analysis. Metabolism. *64*, 1640–1649.
- Serretti, A., and Mandelli, L. (2010). Antidepressants and body weight: A

comprehensive review and meta-analysis. J. Clin. Psychiatry *71*, 1259–1272.

- Shaw, K., Gennat, H., O'Rourke, P., and Del Mar, C. (2006). Exercise for overweight or obesity. Cochrane Database Syst. Rev.
- Shih, J.C., Chen, K., and Ridd, M.J. (1999). Monoamine Oxidase: From Genes to Behavior. Annu. Rev. Neurosci. *22*, 197–217.
- Shin, H., Ma, Y., Chanturiya, T., Cao, Q., Wang, Y., Kadegowda, A.K.G., Jackson, R., Rumore, D., Xue, B., Shi, H., et al. (2017). Lipolysis in Brown Adipocytes Is Not Essential for Cold-Induced Thermogenesis in Mice. Cell Metab. *26*, 764-777.e5.
- Sibon, D., Coman, T., Rossignol, J., Lamarque, M., Kosmider, O., Bayard, E., Fouquet, G., Rignault, R., Topçu, S., Bonneau, P., et al. (2019). Enhanced Renewal of Erythroid Progenitors in Myelodysplastic Anemia by Peripheral Serotonin. Cell Rep. *26*, 3246-3256.e4.
- Sinh, V., and Ootsuka, Y. (2019). Blockade of 5-HT2A receptors inhibits emotional hyperthermia in mice. J. Physiol. Sci. *69*, 1097–1102.
- Siraganian, R.P. (2003). Mast cell signal transduction from the high-affinity IgE receptor. Curr. Opin. Immunol. *15*, 639–646.
- Sjoerdsma, A., Smith, T.E., Stevenson, T.D., and Udenfriend, S. (1955). Metabolism of 5-Hydroxytryptamine (Serotonin) by Monoamine Oxidase. Proc. Soc. Exp. Biol. Med. *89*, 36–38.
- Smith, R.E., and Horwitz, B.A. (1969). Brown fat and thermogenesis. Physiol. Rev. *49*, 330–425.
- Smith, B.M., Smith, J.M., Tsai, J.H., Schultz, J.A., Gilson, C.A., Estrada, S.A., Chen, R.R., Park, D.M., Prieto, E.B., Gallardo, C.S., et al. (2008). Discovery and structure-activity relationship of (1R)-8-chloro-2,3,4,5-tetrahydro-1-methyl-1H-3-benzazepine (Lorcaserin), a selective serotonin 5-HT2C receptor agonist for the treatment of obesity. J. Med. Chem. *51*, 305–313.
- Smith, S.R., Prosser, W.A., Donahue, D.J., Morgan, M.E., Anderson, C.M., and Shanahan, W.R. (2009). Lorcaserin (APD356), a selective 5-HT 2C agonist, reduces body weight in obese men and women. Obesity *17*, 494–503.
- Soloveva, V., Graves, R.A., Rasenick, M.M., Spiegelman, B.M., and Ross, S.R. (1997). Transgenic Mice Overexpressing the β1-Adrenergic Receptor in Adipose Tissue Are Resistant to Obesity. Mol. Endocrinol. *11*, 27–38.
- Song, W., Luo, Q., Zhang, Y., Zhou, L., Liu, Y., Ma, Z., Guo, J., Huang, Y., Cheng, L., Meng, Z., et al. (2019). Organic cation transporter 3 (Oct3) is a distinct catecholamines clearance route in adipocytes mediating the beiging of white adipose tissue. PLoS Biol. *17*.
- Sookoian, S., Gianotti, T.F., Gemma, C., Burguẽo, A., and Pirola, C.J. (2008). Contribution of the functional 5-HTTLPR variant of the SLC6A4 gene to obesity risk in male adults. Obesity *16*, 488–491.

- Steiner, G., and Evans, S. (1976). Effect of serotonin on brown adipose tissue and on its sympathetic neurons. Am. J. Physiol. *231*, 34–39.
- Stock, K., and Westermann, E.O. (1963). Concentration of Norepinephrine, Serotonin, and Histamine, and of Amine-Metabolizing Enzymes in Mammalian Adipose Tissue. J. Lipid Res. *4*, 297–304.
- Stott, D.J., Saniabadi, A.R., Hosie, J., Lowe, G.D.O., and Ball, S.G. (1988). The effects of the 5 HT2 antagonist ritanserin on blood pressure and serotonin-induced platelet aggregation in patients with untreated essential hypertension. Eur. J. Clin. Pharmacol. *35*, 123–129.
- Stunes, A.K., Reseland, J.E., Hauso, O., Kidd, M., Tømmerås, K., Waldum, H.L., Syversen, U., and Gustafsson, B.I. (2011). Adipocytes express a functional system for serotonin synthesis, reuptake and receptor activation. Diabetes, Obes. Metab. *13*, 551–558.
- Sugimoto, Y., Yamada, J., and Horisaka, K. (1991). Activation of peripheral serotonin2 receptors induces hypothermia in mice. Life Sci. *48*, 419–423.
- Sumara, G., Sumara, O., Kim, J.K., and Karsenty, G. (2012). Gut-derived serotonin is a multifunctional determinant to fasting adaptation. Cell Metab. *16*, 588–600.
- Susulic, V.S., Frederich, R.C., Lawitts, J., Tozzo, E., Kahn, B.B., Harper -, M.E., Himms-Hagen, J., Flier, J.S., and Lowell, B.B. (1995). Targeted disruption of the β3-adrenergic receptor gene. J. Biol. Chem. *270*, 29483–29492.
- Szasz, R., and Dale, G.L. (2002). Thrombospondin and fibrinogen bind serotonin-derivatized proteins on COAT-platelets. Blood *100*, 2827–2831.
- Tai, T.A.C., Jennermann, C., Brown, K.K., Oliver, B.B., MacGinnitie, M.A., Wilkison, W.O., Roger Brown, H., Lehmann, J.M., Kliewer, S.A., Morris, D.C., et al. (1996). Activation of the nuclear receptor peroxisome proliferator-activated receptor γ promotes brown adipocyte differentiation. J. Biol. Chem. *271*, 29909–29914.
- Tanabe, M., and Corporation, P. (2012). Summary of Product Characteristics - ANPLAG ® Tablets. *2012*.
- Tate, C.M., and Geliebter, A. (2017). Intragastric Balloon Treatment for Obesity: Review of Recent Studies. Adv. Ther. *34*, 1859–1875.
- Tecott, L.H. (2007). Serotonin and the Orchestration of Energy Balance. Cell Metab. *6*, 352–361.
- Thomas, D.M., Bouchard, C., Church, T., Slentz, C., Kraus, W.E., Redman, L.M., Martin, C.K., Silva, A.M., Vossen, M., Westerterp, K., et al. (2012). Why do individuals not lose more weight from an exercise intervention at a defined dose? an energy balance analysis. Obes. Rev. *13*, 835–847.
- Thomsen, W.J., Grottick, A.J., Menzaghi, F., Reyes-Saldana, H., Espitia, S., Yuskin, D., Whelan, K., Martin, M., Morgan, M., Chen, W., et al. (2008). Lorcaserin, a novel selective human 5-hydroxytryptamine2C agonist: In vitro and in vivo pharmacological characterization. J. Pharmacol. Exp. Ther.

325, 577–587.

- Thorogood, A., Mottillo, S., Shimony, A., Filion, K.B., Joseph, L., Genest, J., Pilote, L., Poirier, P., Schiffrin, E.L., and Eisenberg, M.J. (2011). Isolated aerobic exercise and weight loss: A systematic review and meta-analysis of randomized controlled trials. Am. J. Med. *124*, 747–755.
- Tian, X.Y., Ganeshan, K., Hong, C., Nguyen, K.D., Qiu, Y., Kim, J., Tangirala, R.K., Tonotonoz, P., and Chawla, A. (2016). Thermoneutral Housing Accelerates Metabolic Inflammation to Potentiate Atherosclerosis but Not Insulin Resistance. Cell Metab. *23*, 165–178.
- Tschöp, M.H., Speakman, J.R., Arch, J.R.S., Auwerx, J., Brüning, J.C., Chan, L., Eckel, R.H., Farese, R. V., Galgani, J.E., Hambly, C., et al. (2012). A guide to analysis of mouse energy metabolism. Nat. Methods *9*, 57–63.
- U.S. Food and Drug Administration (2020). FDA requests the withdrawal of the weight-loss drug Belviq, Belviq XR (lorcaserin) from the market: Potential risk of cancer outweights the benefits.
- Üçeyler, N., Schütt, M., Palm, F., Vogel, C., Meier, M., Schmitt, A., Lesch, K.P., Mössner, R., and Sommer, C. (2010). Lack of the serotonin transporter in mice reduces locomotor activity and leads to gender-dependent late onset obesity. Int. J. Obes. *34*, 701–711.
- Uldry, M., Yang, W., St-Pierre, J., Lin, J., Seale, P., and Spiegelman, B.M. (2006). Complementary action of the PGC-1 coactivators in mitochondrial biogenesis and brown fat differentiation. Cell Metab. *3*, 333–341.
- Vallerand, A.L., Perusse, F., and Bukowiecki, L.J. (1990). Stimulatory effects of cold exposure and cold acclimation on glucose uptake in rat peripheral tissues. Am. J. Physiol. - Regul. Integr. Comp. Physiol. *259*, R1043–R1049.
- Vanover, K.E., Weiner, D.M., Makhay, M., Veinbergs, I., Gardell, L.R., Lameh, J., Del Tredici, A.L., Piu, F., Schiffer, H.H., Ott, T.R., et al. (2006). Pharmacological and behavioral profile of N-(4-fluorophenylmethyl)-N-(1-methylpiperidin-4-yl)-N′-(4-(2-methylpropyloxy)phenylmethyl) carbamide (2R,3R)-dihydroxybutanedioate (2:1) (ACP-103), a novel 5-hydroxytryptamine2A receptor inverse agonist. J. Pharmacol. Exp. Ther. *317*, 910–918.
- Villarroya, F., and Vidal-Puig, A. (2013). Beyond the sympathetic tone: The new brown fat activators. Cell Metab. *17*, 638–643.
- Virtanen, K.A., Lidell, M.E., Orava, J., Heglind, M., Westergren, R., Niemi, T., Taittonen, M., Laine, J., Savisto, N.J., Enerbäck, S., et al. (2009). Functional brown adipose tissue in healthy adults. N. Engl. J. Med. *360*, 1518–1525.
- Virtue, S., and Vidal-Puig, A. (2013). Assessment of brown adipose tissue function. Front. Physiol. *4*.
- Visentin, V., Prévot, D., Marti, L., and Carpéné, C. (2003). Inhibition of rat fat cell lipolysis by monoamine oxidase and semicarbazide-sensitive amine

oxidase substrates. Eur. J. Pharmacol. *466*, 235–243.
- Vogel, C., and Marcotte, E.M. (2012). Insights into the regulation of protein abundance from proteomic and transcriptomic analyses. Nat. Rev. Genet. *13*, 227–232.
- Wacker, D., Wang, S., McCorvy, J.D., Betz, R.M., Venkatakrishnan, A.J., Levit, A., Lansu, K., Schools, Z.L., Che, T., Nichols, D.E., et al. (2017). Crystal Structure of an LSD-Bound Human Serotonin Receptor. Cell *168*, 377-389.e12.
- Waku, T., Shiraki, T., Oyama, T., Maebara, K., Nakamori, R., and Morikawa, K. (2010). The nuclear receptor PPARγ individually responds to serotonin-and fatty acid-metabolites. EMBO J. *29*, 3395–3407.
- Walther, D.J., Peter, J.U., Bashammakh, S., Hörtnagl, H., Voits, M., Fink, H., and Bader, M. (2003a). Synthesis of serotonin by a second tryptophan hydroxylase isoform. Science (80-.). *299*, 76.
- Walther, D.J., Peter, J.U., Winter, S., Höltje, M., Paulmann, N., Grohmann, M., Vowinckel, J., Alamo-Bethencourt, V., Wilhelm, C.S., Ahnert-Hilger, G., et al. (2003b). Serotonylation of Small GTPases Is a Signal Transduction Pathway that Triggers Platelet α-Granule Release. Cell *115*, 851–862.
- Ward, Z.J., Bleich, S.N., Cradock, A.L., Barrett, J.L., Giles, C.M., Flax, C., Long, M.W., and Gortmaker, S.L. (2019). Projected U.S. state-level prevalence of adult obesity and severe obesity. N. Engl. J. Med. *381*, 2440–2450.
- Watanabe, H., Akasaka, D., Ogasawara, H., Sato, K., Miyake, M., Saito, K., Takahashi, Y., Kanaya, T., Takakura, I., Hondo, T., et al. (2010). Peripheral serotonin enhances lipid metabolism by accelerating bile acid turnover. Endocrinology *151*, 4776–4786.
- Watanabe, H., Nakano, T., Saito, R., Akasaka, D., Saito, K., Ogasawara, H., Minashima, T., Miyazawa, K., Kanaya, T., Takakura, I., et al. (2016). Serotonin improves high fat diet induced obesity in mice. PLoS One *11*, e0147143.
- Watts, S.W. (2016). Oh, the places you'll go! My many colored serotonin (apologies to Dr. Seuss). Am. J. Physiol. - Hear. Circ. Physiol. *311*, H1225–H1233.
- Watts, S.W., Morrison, S.F., Davis, R.P., and Barman, S.M. (2012). Serotonin and blood pressure regulation. Pharmacol. Rev. *64*, 359–388.
- Weir, G., Ramage, L.E., Akyol, M., Rhodes, J.K., Kyle, C.J., Fletcher, A.M., Craven, T.H., Wakelin, S.J., Drake, A.J., Gregoriades, M.L., et al. (2018). Substantial Metabolic Activity of Human Brown Adipose Tissue during Warm Conditions and Cold-Induced Lipolysis of Local Triglycerides. Cell Metab. *27*, 1348-1355.e4.
- Weiss, E.P., Racette, S.B., Villareal, D.T., Fontana, L., Steger-May, K., Schechtman, K.B., Klein, S., Ehsani, A.A., and Holloszy, J.O. (2007). Lower extremity muscle size and strength and aerobic capacity decrease

with caloric restriction but not with exercise-induced weight loss. J. Appl. Physiol. *102*, 634–640.

- Welzel, T.M., Graubard, B.I., Quraishi, S., Zeuzem, S., Davila, J.A., El-Serag, H.B., and McGlynn, K.A. (2013). Population-attributable fractions of risk factors for hepatocellular carcinoma in the United States. Am. J. Gastroenterol. *108*, 1314–1321.
- Weng, R., Shen, S., Tian, Y., Burton, C., Xu, X., Liu, Y., Chang, C., Bai, Y., and Liu, H. (2015). Metabolomics Approach Reveals Integrated Metabolic Network Associated with Serotonin Deficiency. Sci. Rep. *5*, 11864.
- Westerterp, K.R. (2017). Doubly labelled water assessment of energy expenditure: principle, practice, and promise. Eur. J. Appl. Physiol. *117*, 1277–1285.
- Weyer, C., Tataranni, P.A., Snitker, S., Danforth, E., and Ravussin, E. (1998). Increase in insulin action and fat oxidation after treatment with CL 316,243, a highly selective β3-adrenoceptor agonist in humans. Diabetes *47*, 1555–1561.
- Whitaker-Azmitia, P.M. (1999). The discovery of serotonin and its role in neuroscience. Neuropsychopharmacology *21*, 2S-8S.
- Whiting, D.R., Guariguata, L., Weil, C., and Shaw, J. (2011). IDF Diabetes Atlas: Global estimates of the prevalence of diabetes for 2011 and 2030. Diabetes Res. Clin. Pract. *94*, 311–321.
- Williams, E.G., and Auwerx, J. (2015). The Convergence of Systems and Reductionist Approaches in Complex Trait Analysis. Cell *162*, 23–32.
- Williams, E.G., Mouchiroud, L., Frochaux, M., Pandey, A., Andreux, P.A., Deplancke, B., and Auwerx, J. (2014). An Evolutionarily Conserved Role for the Aryl Hydrocarbon Receptor in the Regulation of Movement. PLoS Genet. *10*, e1004673.
- Worth, C.L., Kreuchwig, F., Tiemann, J.K.S., Kreuchwig, A., Ritschel, M., Kleinau, G., Hildebrand, P.W., and Krause, G. (2017). GPCR-SSFE 2.0 - A fragment-based molecular modeling web tool for Class A G-protein coupled receptors. Nucleic Acids Res. *45*, W408–W415.
- Wu, T., Gao, X., Chen, M., and Van Dam, R.M. (2009). Long-term effectiveness of diet-plus-exercise interventions vs. diet-only interventions for weight loss: A meta-analysis: Obesity Management. Obes. Rev. *10*, 313–323.
- Wu, X., Kekuda, R., Huang, W., Fei, Y.J., Leibach, F.H., Chen, J., Conway, S.J., and Ganapathy, V. (1998). Identity of the organic cation transporter OCT3 as the extraneuronal monoamine transporter (uptake2) and evidence for the expression of the transporter in the brain. J. Biol. Chem. *273*, 32776–32786.
- Wurtman, J.J., and Wurtman, R.J. (1977). Fenfluramine and fluoxetine spare protein consumption while suppressing caloric intake by rats. Science

(80-.). *198*, 1178–1180.

- Xu, Y., Jones, J.E., Kohno, D., Williams, K.W., Lee, C.E., Choi, M.J., Anderson, J.G., Heisler, L.K., Zigman, J.M., Lowell, B.B., et al. (2008). 5-HT2CRs Expressed by Pro-Opiomelanocortin Neurons Regulate Energy Homeostasis. Neuron *60*, 582–589.
- Yabut, J.M., Desjardins, E.M., Chan, E.J., Day, E.A., Leroux, J.M., Wang, B., Crane, E.D., Wong, W., Morrison, K.M., Crane, J.D., et al. (2020). Genetic deletion of mast cell serotonin synthesis prevents the development of obesity and insulin resistance. Nat. Commun. *11*, 463.
- Yang, Y., and Balcarcel, R.R. (2003). 24-Well Plate Spectrophotometric Assay for Preliminary Screening of Metabolic Activity. Assay Drug Dev. Technol. *1*, 461–468.
- Ye, L., Wu, J., Cohen, P., Kazak, L., Khandekar, M.J., Jedrychowski, M.P., Zeng, X., Gygi, S.P., and Spiegelman, B.M. (2013). Fat cells directly sense temperature to activate thermogenesis. Proc. Natl. Acad. Sci. U. S. A. *110*, 12480–12485.
- Yoshimura, K., Hiroshige, T., and Itoh, S. (1969a). Lipolytic action of serotonin in brown adipose tissue in vitro. Jpn. J. Physiol. *19*, 176–186.
- Yoshimura, K., Hiroshige, T., and Itoh, S. (1969b). Role of serotonin in the thermogenesis of rat brown adipose tissue. Jpn. J. Physiol. *19*, 791–800.
- Young, R.L., Lumsden, A.L., Martin, A.M., Schober, G., Pezos, N., Thazhath, S.S., Isaacs, N.J., Cvijanovic, N., Sun, E.W.L., Wu, T., et al. (2018). Augmented capacity for peripheral serotonin release in human obesity. Int. J. Obes. *42*, 1880–1889.
- Yuasa, H.J., Ball, H.J., Ho, Y.F., Austin, C.J.D., Whittington, C.M., Belov, K., Maghzal, G.J., Jermiin, L.S., and Hunt, N.H. (2009). Characterization and evolution of vertebrate indoleamine 2, 3-dioxygenases. IDOs from monotremes and marsupials. Comp. Biochem. Physiol. - B Biochem. Mol. Biol. *153*, 137–144.
- Yusuf, S., Hawken, S., Ôunpuu, S., Dans, T., Avezum, A., Lanas, F., McQueen, M., Budaj, A., Pais, P., Varigos, J., et al. (2004). Effect of potentially modifiable risk factors associated with myocardial infarction in 52 countries (the INTERHEART study): case-control study. Lancet *364*, 937–952.
- Zelkas, L., Raghupathi, R., Lumsden, A.L., Martin, A.M., Sun, E., Spencer, N.J., Young, R.L., and Keating, D.J. (2015). Serotonin-secreting enteroendocrine cells respond via diverse mechanisms to acute and chronic changes in glucose availability. Nutr. Metab. *12*.
- Zha, W., Ho, H.T.B., Hu, T., Hebert, M.F., and Wang, J. (2017). Serotonin transporter deficiency drives estrogen-dependent obesity and glucose intolerance. Sci. Rep. *7*, 1137.
- Zhang, X., Beaulieu, J.M., Sotnikova, T.D., Gainetdinov, R.R., and Caron, M.G. (2004). Tryptophan hydroxylase-2 controls brain serotonin synthesis.

Science (80-.). *305*, 217.
- Zhang, X., Wang, X., Yin, H., Zhang, L., Feng, A., Zhang, Q.X., Lin, Y., Bao, B., Hernandez, L.L., Shi, G.P., et al. (2019). Functional Inactivation of Mast Cells Enhances Subcutaneous Adipose Tissue Browning in Mice. Cell Rep. *28*, 792-803.e4.
- Zhu, H.J., Appel, D.I., Gründemann, D., Richelson, E., and Markowitz, J.S. (2012). Evaluation of organic cation transporter 3 (SLC22A3) inhibition as a potential mechanism of antidepressant action. Pharmacol. Res. *65*, 491–496.
- Zingaretti, M.C., Crosta, F., Vitali, A., Guerrieri, M., Frontini, A., Cannon, B., Nedergaard, J., and Cinti, S. (2009). The presence of UCP1 demonstrates that metabolically active adipose tissue in the neck of adult humans truly represents brown adipose tissue. FASEB J. *23*, 3113–3120.
- Zucker, M.B., Friedman, B.K., and Rapport, M.M. (1954). Identification and Quantitative Determination of Serotonin (5-hydroxy-tryptamine) in Blood Platelets. Proc. Soc. Exp. Biol. Med. *85*, 282–285.

21 Supporting Data

21.1 Supporting data for Figure 4

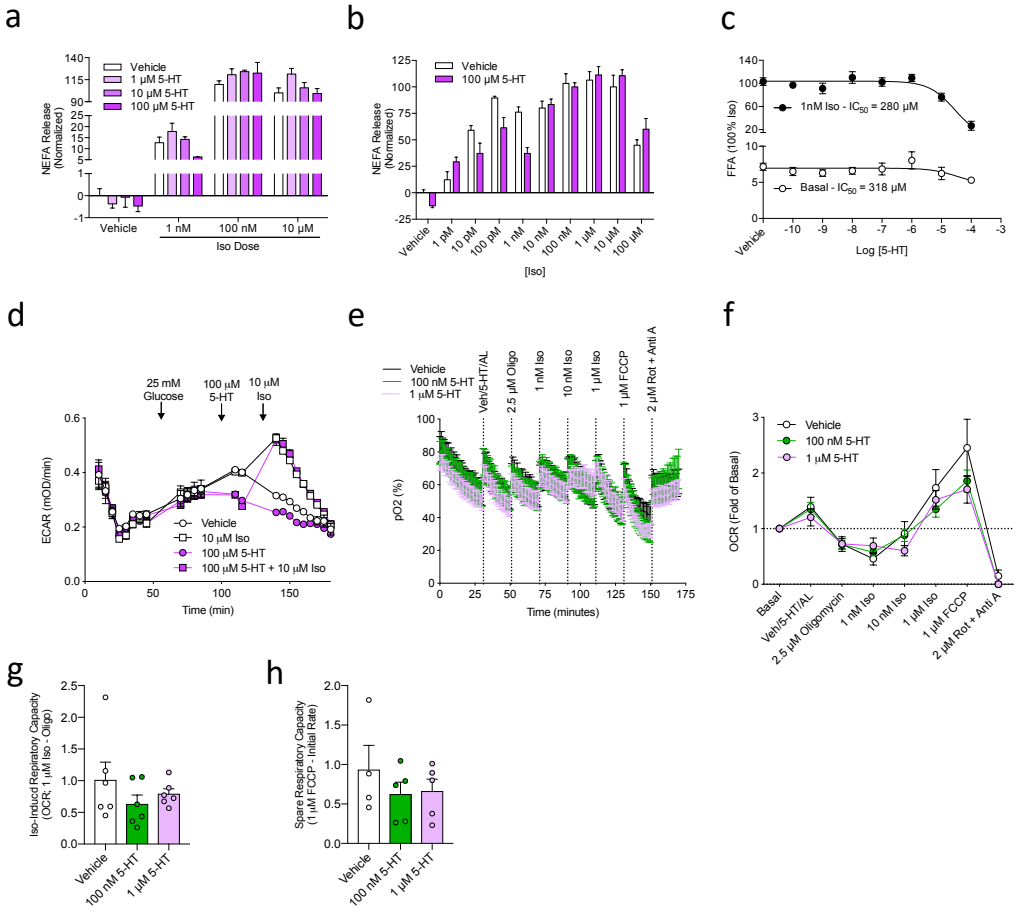

Figure S4- 1 Additional data related to Figure 4. a and b, Normalized NEFA release data from Figure 4b and Figure 4c (n = 1 independent experiment performed in 3 replicates – error bars represent within experiment error), respectively. c, 5-HT dose response on isoproterenol stimulated FFA release (n = 1 performed in 5 replicates – error bars represent within experiment error; from Dr. Emilio Mottillo). d, Time course of ECAR in response to different stimuli (n = 1 independent experiment performed in 5 replicates – error bars represent within experiment error; related to Figure 4d). e, Time course of pO2 in BAs in response to indicated treatments (n = 1 performed in 6 replicates – error bars represent within experiment error). f, OCR of BAs in response to indicated treatments and calculated from data presented in e (n = 1 performed in 6 replicates – error bars represent within experiment error). g, Iso-induced respiratory capacity in BAs under different 5-HT

concentrations (n = 1 performed in 6 replicates – error bars represent within experiment error). f, Spare respiratory capacity in BAs under different 5-HT concentrations (n = 1 performed in 4-5 replicates – error bars represent within experiment error).

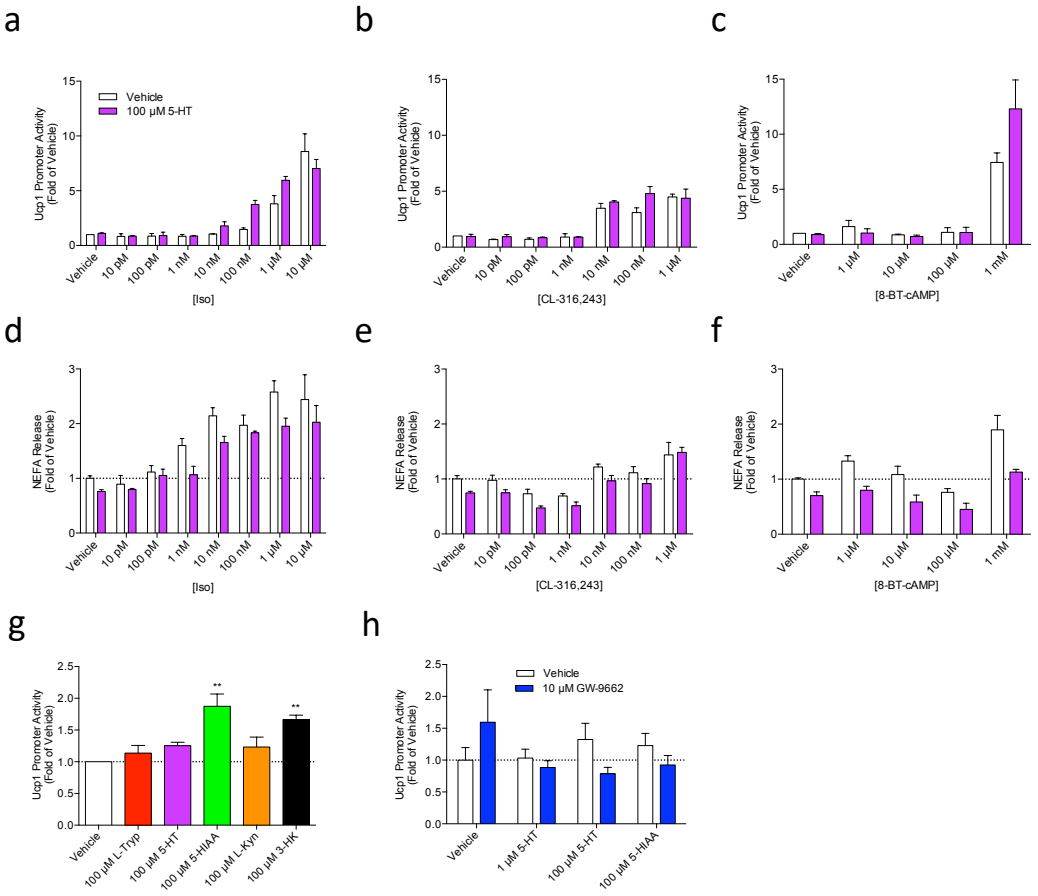

Figure S4- 2 In combination with high dose 5-HT and adrenergic stimuli, 5-HT increases Ucp1 promoter activity likely via the 5-HT metabolite 5-HIAA and its PPARy agonist activity. a-c, *Ucp1* promoter activity in BAs in response to 100 µM 5-HT and Isoproterenol (a), CL-316,243 (b) and 8-BT-cAMP (c; n = 1 independent experiment performed with 3 technical replicates – error bars represent within experiment error). d-f, NEFA levels in media from samples treated as in a-c. g, *Ucp1* promoter activity in response to various 5-HT and tryptophan metabolites (n = 3 independent experiments performed with 3 replicates). f, *Ucp1* promoter activity in response to 5-HT and 5-HIAA in combination with the PPARy antagonist – GW-9662 (n = 1 independent experiment performed in 3 replicates – error bars represent within experiment error). Data related to Figure 4.

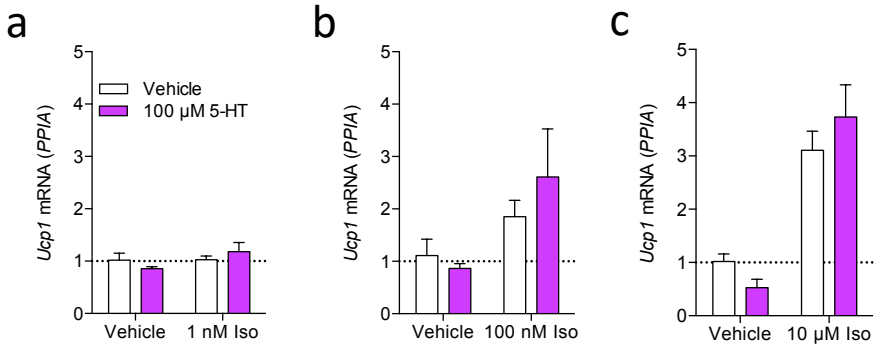

Figure S4- 3 High dose 5-HT increases *Ucp1* mRNA expression in BAs in combination with adrenergic stimuli. a-b, *Ucp1* mRNA levels in response to 100 µM 5-HT followed by 1 nM (a), 100 nM (b) or 10 µM (c) isoproterenol (n = 1 independent experiment performed in 3 replicates – error bars represent within experiment error). Data related to Figure 4.

21.2 Supporting data for Figure 5.

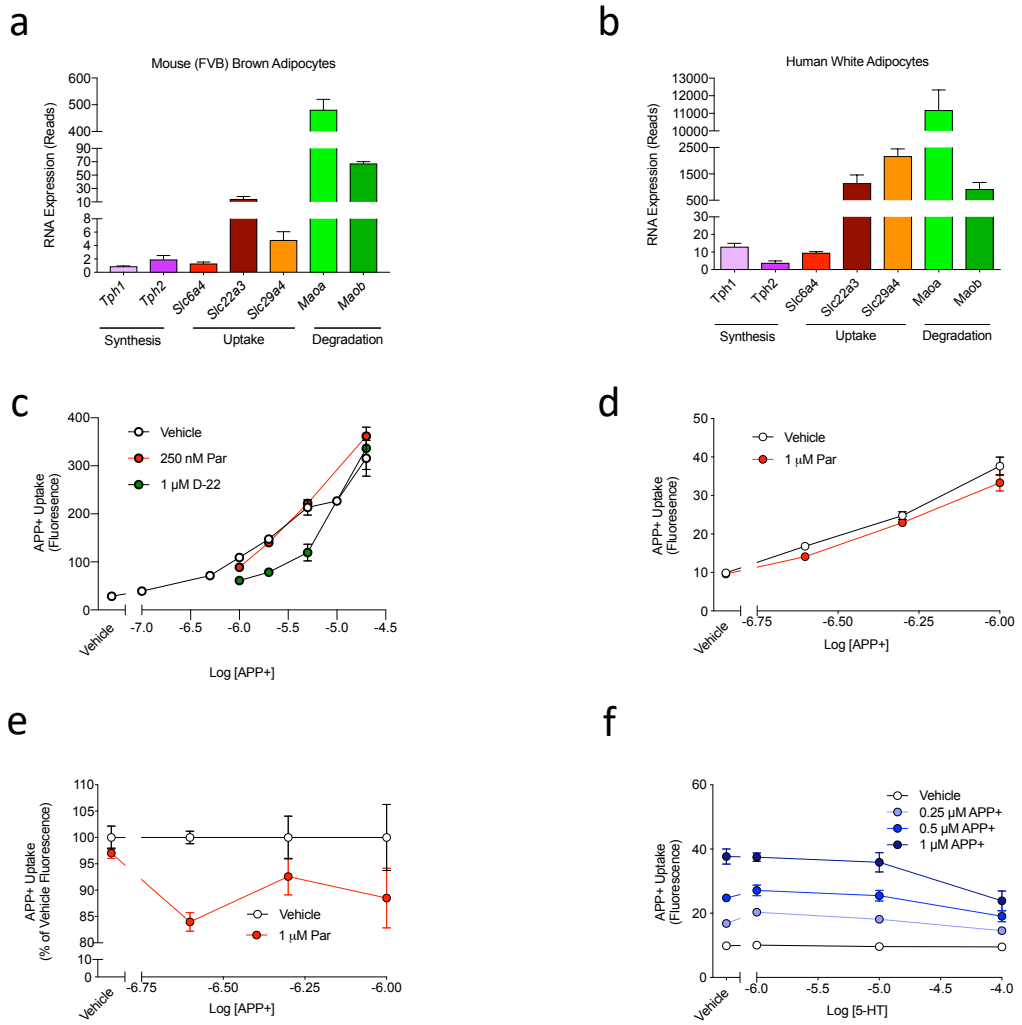

Figure S5- 1 Supporting information for Figure 5Figure 5. 5-HT transporter and metabolism genes are expressed in mouse and human brown adipocytes. a, *Slc6a4* mRNA expression in immortalized *Slc6a4*$^{+/+}$ *and Sl6a4*$^{-/-}$ BA progenitors after differentiation (n = 1 independent experiment performed in triplicate – error bars represent within experiment error). b and c, Expression of 5-HT synthesis, uptake/transport and degradation gene mRNAs in mouse BAs. (n = 1 independent experiment performed in triplicate – error bars represent within experiment error) and human BAs (data is obtained from BAs from 5 different subjects), respectively. Bars represent mean ± S.E.M. Additional data is included in Figure S5- 1, Figure S5- 2, Figure S5- 3, Figure S5- 4, Figure S5- 5 and Table S5- 1. **showing 5-HT transporter and metabolism gene expression and active 5-HT analog uptake in BAs.** a, RNA-Seq RNA expression analysis of serotonin synthesis, uptake and

degradation genes *in vitro* differentiated FVB mouse brown adipocytes (n = 1 independent experiment performed in 6 replicates – error bars represent within experiment error). b, RNA-Seq RNA expression analysis of serotonin synthesis, uptake and degradation genes *in vitro* differentiated primary human white adipocytes (n = 5 individuals – error bars represent s.e.m.). c, APP+ fluorescence in response to an SSRI (Par; Paroxetine) and an OCT3/PMAT inhibitor (D-22; Decynium-22) with different concentrations of APP+ (n = 1 independent experiment performed in 3 replicates – error bars represent within experiment error). d, APP+ fluorescence in response to a high dose of Paroxetine with different concentrations of APP+ (n = 1 independent experiment performed in 3 replicates – error bars represent within experiment error). e, data from d presented as percentage of vehicle (n = 1 independent experiment performed in 3 replicates – error bars represent within experiment error). f, APP+ fluorescence in different concentrations of competing 5-HT (n = 1 independent experiment performed in 3 replicates – error bars represent within experiment error). Data related to Figure 5

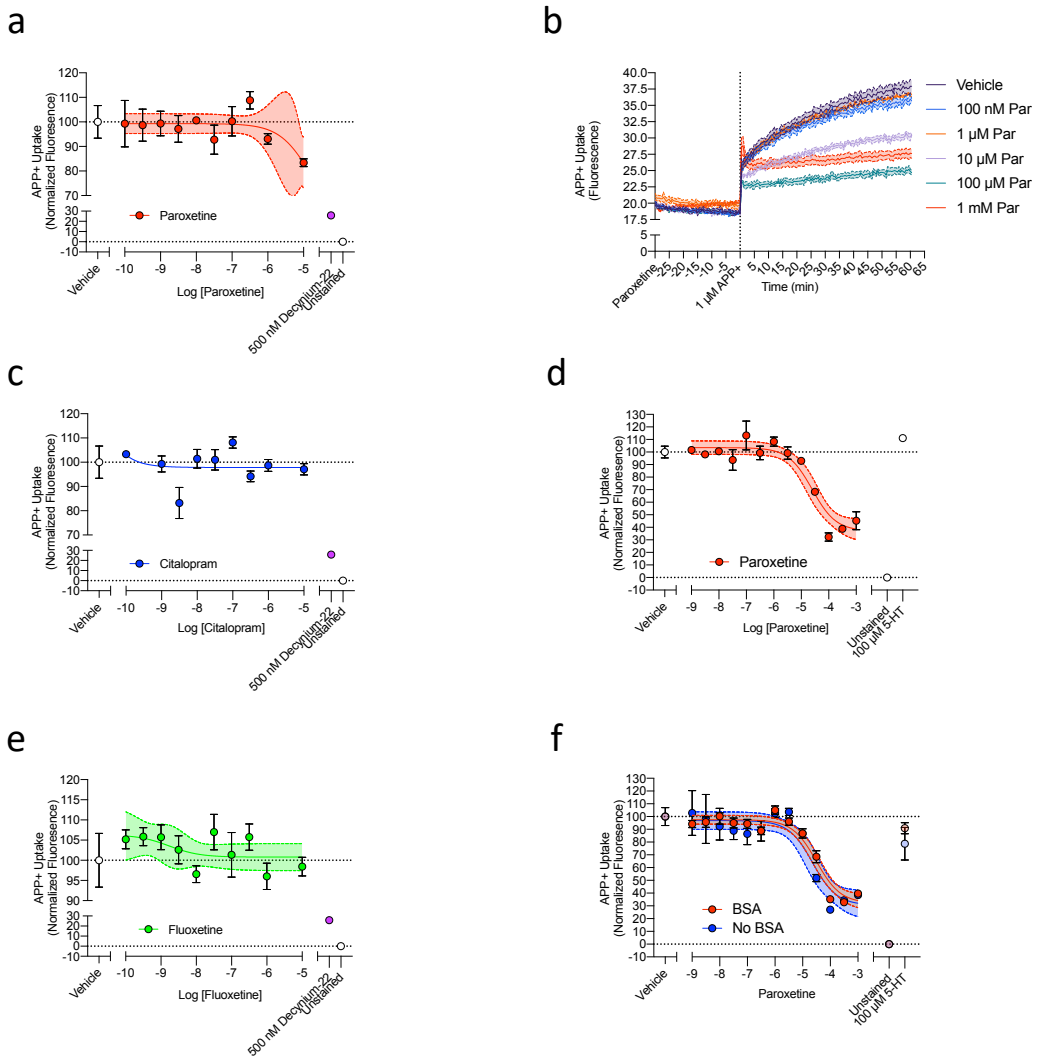

Figure S5- 2 SSRIs do not block 5-HT analog transport at doses specific to SERT (*Slc6a4*) but at high doses may block transport via PMAT or Oct3. a, 1 µM APP+ fluorescence in response to clinical circulating concentrations of Paroxetine (n = 3 independent experiments performed in 2-6 replicates – error bars represent s.e.m. between experiments and shaded region represents 95% confidence interval of non-linear regression fit). b, Sample time course of APP+ fluorescence in response to different concentrations of Paroxetine (Par; shaded region represents area within 1 s.e.m.). c and e, 1 µM APP+ fluorescence in response to Citalopram (c) and Fluoxetine (e; n = 1 independent experiment each performed in 3 replicates – error bars represent s.e.m. within experiments and shaded region represents 95% confidence interval of non-linear regression fit. d, 1 µM APP+ fluorescence in response to high concentrations of Paroxetine (n = 3 independent experiments performed in 3 replicates – error bars represent s.e.m. between experiments and

shaded region represents 95% confidence interval of non-linear regression fit). f, 1 μM APP+ fluorescence in response to high concentrations of Paroxetine with or without BSA (n = 3 independent experiments performed in 3 replicates – error bars represent s.e.m. between experiments and shaded region represents 95% confidence interval of non-linear regression fit). All calculated constants for non-linear regression fits are summarized in Table S5- 1. Data related to Figure 5.

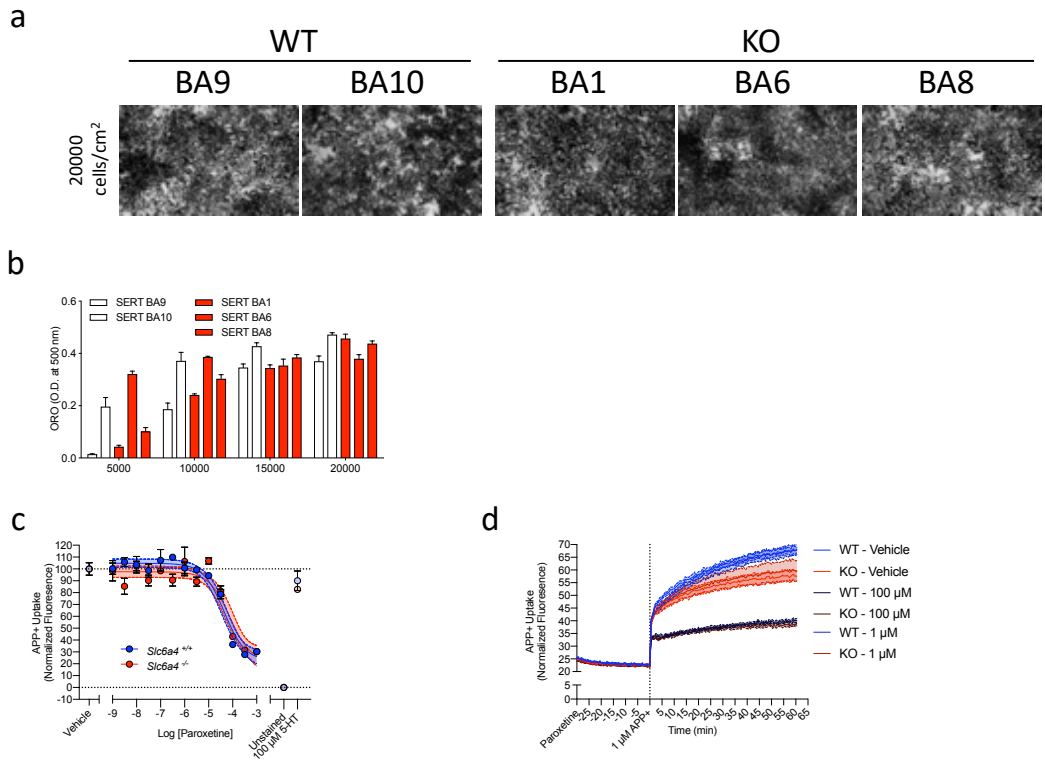

Figure S5- 3 *Slc6a4*$^{-/-}$ BAs accumulate lipid, transport 5-HT analogs and high doses of Paroxetine (an SSRI) inhibit non-SERT *(Slc6a4)* mediated transport (likely PMAT and Oct3). a, Images of pre-adipocytes from *Slc6a4*$^{+/+}$ (WT) and *Slc6a4*$^{-/-}$ (KO) differentiated for 9 days and stained with Oil Red O. b, Quantification of eluted Oil Red O (ORO) stain from a (1 individual experiment performed in triplicate – error bars represent within experiment s.e.m.). c, 1 µM APP+ fluorescence in response to high concentrations of Paroxetine in *Slc6a4*$^{+/+}$ or *Slc6a4*$^{-/-}$ BAs (n = 3 independent experiments performed in 3 replicates – error bars represent s.e.m. between experiments and shaded region represents 95% confidence interval of non-linear regression fit). d, Representative time course of APP+ uptake for select concentrations of Paroxetine from c (shaded region represents area within 1 s.e.m.). All calculated constants for non-linear regression fits are summarized in Table S5- 1. Data related to Figure 5.

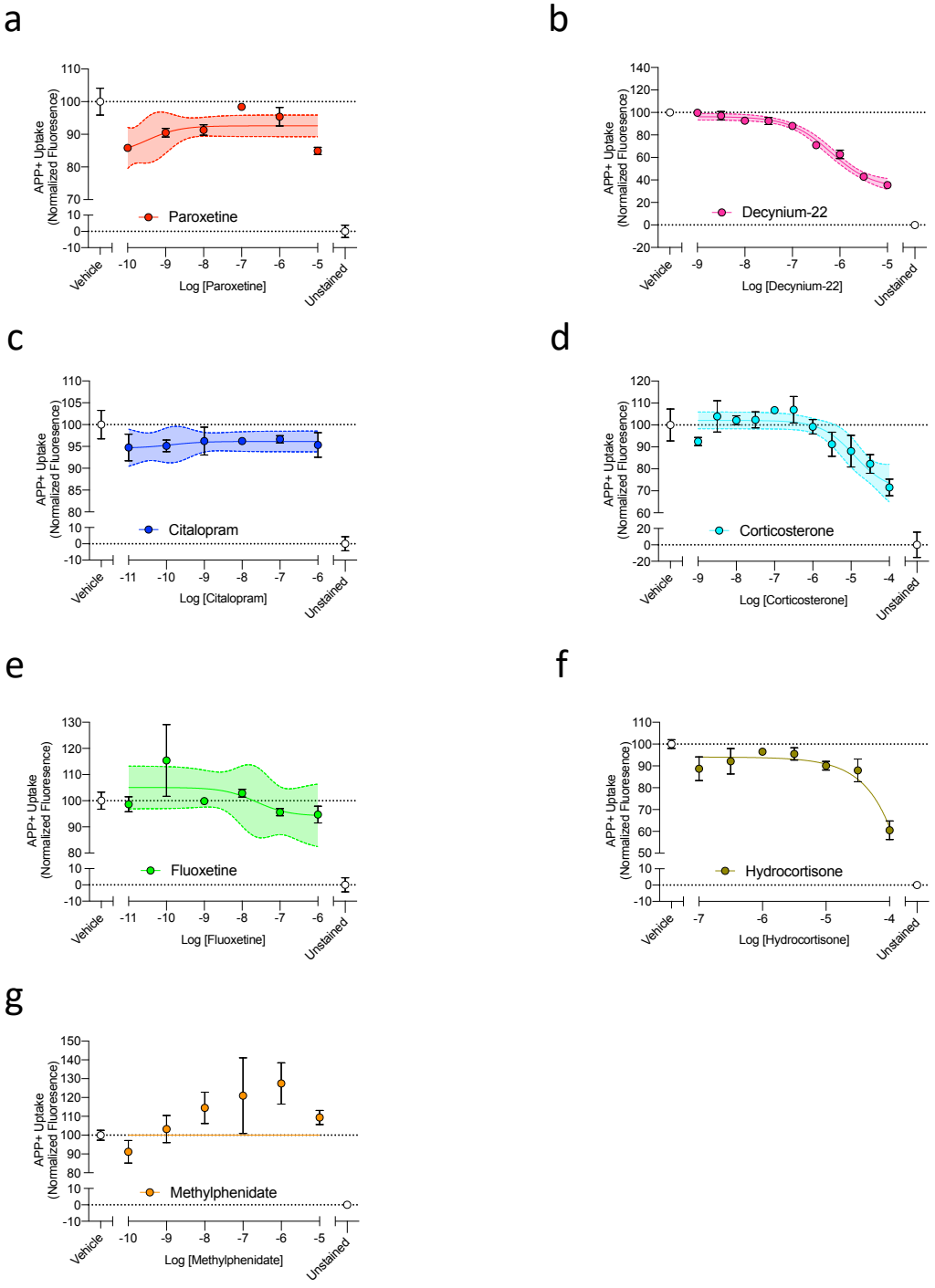

Figure S5- 4 Transport of 5-HT analogs at high doses are mediated by PMAT or Oct3 and not DAT or NET. High doses are doses presumably facilitated by non-SERT mechanisms and inhibited by Decynium-22, Corticosterone and Hydrocortisone but not Methylphenidate. a-g, 20 µM APP+ fluorescence in

response to clinical circulating concentrations of Paroxetine (a), Decynium-22 (b), Citalopram (c), Cortisone (d), Fluoxetine (e), Hydrocortisone (f) and Methylphenidate (g; n = 3-4 independent experiments performed in 2-3 replicates – error bars represent s.e.m. between experiments and shaded region represents 95% confidence interval of non-linear regression fit; except g: N = 1 independent experiment performed in triplicate – error bars represent within experiment error). All calculated constants for non-linear regression fits are summarized in Table S5-1. Data related to Figure 5.

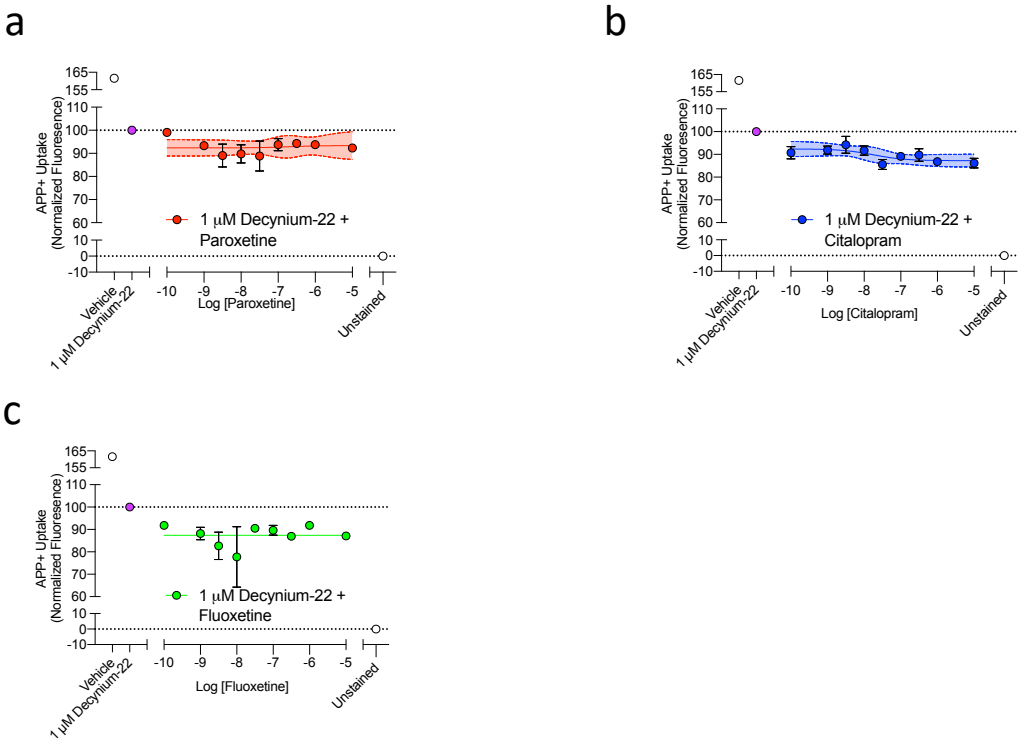

Figure S5- 5 SSRIs had no additional transport inhibitory activity above that inhibited by Decynium-22, inferring undetectable/minimal SERT activity *(Slc6a4)*. a, 20 μM APP+ fluorescence in response to clinical circulating concentrations of Paroxetine (n = 1 independent experiment performed in 3 replicates – error bars represent error within experiments and shaded region represents 95% confidence interval of non-linear regression fit). All calculated constants for non-linear regression fits are summarized in Table S5- 1. Data related to Figure 5.

Drug/Condition	Target (Gene)	Mean Reported Ki [Number of Studies] (nM)[1]	N [Tech. replicates/ experiment]	Mean IC_{50} (μM) [95% C.I.][5]	$LogIC_{50}$ (M)	Percent Inhibition (i.e. Span)	R^2
1 μM APP+							
Paroxetine (1 nM - 1 mM)	SERT (Slc6a4)	0.504 ± 0.227 [20]	3 [2-6]	21.625 ± 6.942	-4.728 ± 0.18	60.53 ± 3.1	0.89 ± 0.03
Paroxetine (100 pM - 10 μM)	SERT (Slc6a4)	0.504 ± 0.227 [20]	1 [3]	15.31 [Undeterminable]	-4.815	40.56	0.24
Citalopram (100 pM - 10 μM)	SERT (Slc6a4)	6.305 ± 1.763 [27]	1 [3]	Ambiguous	Ambiguous	Ambiguous	Ambiguous
Fluoxetine (100 pM - 10 μM)	SERT (Slc6a4)	17.289 ± 8.06 [35]	1 [3]	0.00169 [Undeterminable]	-8.771	5.56	0.10
Slc6a4$^{+/+}$ + Paroxetine (1 nM – 1 mM)	SERT (Slc6a4)	0.504 ± 0.227 [20]	3 [2-6]	45.4 ± 7.546	-4.355 ± 0.073	72.9 ± 4.74	0.89 ± 0.03
Slc6a4$^{-/-}$ + Paroxetine (1 nM – 1 mM)	SERT (Slc6a4)	0.504 ± 0.227 [20]	3 [3-6]	72.207 ± 26.456	-4.221 ± 0.2	70.16 ± 14.46	0.78 ± 0.05
2 μM APP+							
Methylphenidate	NET (*Slc6a2*) DAT (*Slc6a3*)	660 [1] 93.3 ± 24.849 [10]	1 [3]	0.000241 [Undeterminable]	-9.618 [Undeterminable]	14.88	0.25
Decynium-22	OCT3 (*Slc22a3*) PMAT (*Slc29a4*)	90 ± 10 [7][2] 100 ± 17.32 [3][3]	1 [3]	0.109 [0.036-0.323]	-6.962	79.14	0.86
20 μM APP+							
Paroxetine	SERT (*Slc6a4*)	0.504 ± 0.227 [20]	3 [2-3]	0.013 ± 0.008	-8.353 ± 0.583	21.33 ± 19.53	0.48 ± 0.15
Citalopram	SERT (*Slc6a4*)	6.305 ± 1.763 [27]	3 [3][4]	0.000221 ± 0.000089	-9.696 ± 0.187	0.67 ± 2.23	0.03 ± 0
Fluoxetine	SERT (*Slc6a4*)	17.289 ± 8.06 [35]	3 [2-3][4]	0.057025 ± 0.033735	-7.338 ± 0.296	1593.46 ± 1582.54	0.41 ± 0.25
Methylphenidate	NET (*Slc6a2*) DAT (*Slc6a3*)	660 [1] 93.3 ± 24.849 [10]	1 [3]	Ambiguous	Ambiguous	Ambiguous	Ambiguous
Decynium-22	OCT3 (*Slc22a3*) PMAT (*Slc29a4*)	90 ± 10 [7][2] 100 ± 17.32 [3][3]	3 [3]	1.11 ± 0.234	-5.978 ± 0.106	87.66 ± 12.15	0.97 ± 0.01
Hydrocortisone	OCT3 (*Slc22a3*)	Unavailable	4 [3][4]	586.1 ± 585.95	-5.787 ± 1.579	124.47 ± 118.4	0.47 ± 0.22
Corticocsterone	OCT3 (*Slc22a3*)	290 ± 40 [7][2]	4 [2-3]	11.027 ± 2.279	-4.979 ± 0.102	33.89 ± 1.92	0.81 ± 0.1
Decynium-22 + Paroxetine	SERT (*Slc6a4*) OCT3 (*Slc22a3*) PMAT (*Slc29a4*)	See above	1 [3]	1.927×10^{-7} [Undeterminable]	-6.715	-0.9977	0.0043
Decynium-22 + Citalopram	SERT (*Slc6a4*) OCT3 (*Slc22a3*) PMAT (*Slc29a4*)	See above	1 [3]	1.79×10^{-8} [Undeterminable]	-7.748	5.161	0.23
Decynium-22 + Fluoxetine	SERT (*Slc6a4*) OCT3 (*Slc22a3*) PMAT (*Slc29a4*)	See above	1 [3]	Ambiguous	Ambiguous	Ambiguous	Ambiguous

Table S5- 1 Summary of 5-HT analog transport pharmacological data from previous reports and Figure S5- 2 to Figure S5- 5. [1]Ki Database [2]Mean IC50 ± S.E.M. [number of experiments] in response to 25 nM MPP+ from https://www.ncbi.nlm.nih.gov/pmc/articles/PMC1573414/ [3]Mean Ki ± S.E.M. [number of experiments] from http://www.jbc.org/content/279/48/50042.full [4]Calculations have 1 less experiment because 1 experiment had interrupted/ambiguous curve fit [5]For conditions with only 1 individual experiment, 95% C.I. from curve fitting is shown instead of S.E.M. Data related to Figure 5.

21.3 Supporting data for Figure 6

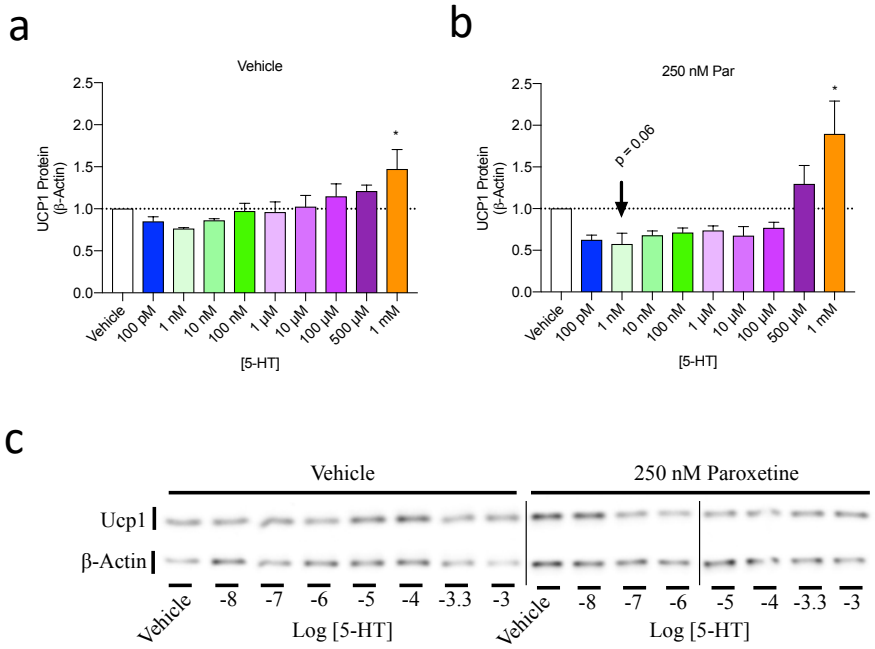

Figure S6- 1 5-HT may decrease UCP1 protein levels via a cell membrane receptor mediated mechanism. a-b, UCP1 protein expression in BAs treated bidaily with 5-HT for 8 days post-differentiation (defined as 9 days post-induction) in combination with vehicle (a) or 250 nM Paroxetine (Par; b; n = 2-5 independent experiments, performed in 2-3 replicates – error represents error between experiments). c, Representative western blot of UCP1 protein levels from a and b (note: doses below 10 nM were run on separate gels and are not shown). Data is related to Figure 6.

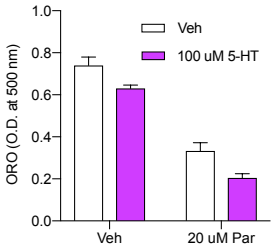

Figure S6- 2 High dose 5-HT and high dose SSRI impairs BA lipid accumulation in an additive manner. Eluted Oil Red O stain from BAs incubated with 100 μM 5-HT and 20 μM Par during differentiation (n = 1 independent experiment performed in 3 replicates – error bars represent error within experiment). Data related to Figure 6.

21.4 Supporting data for Figure 8

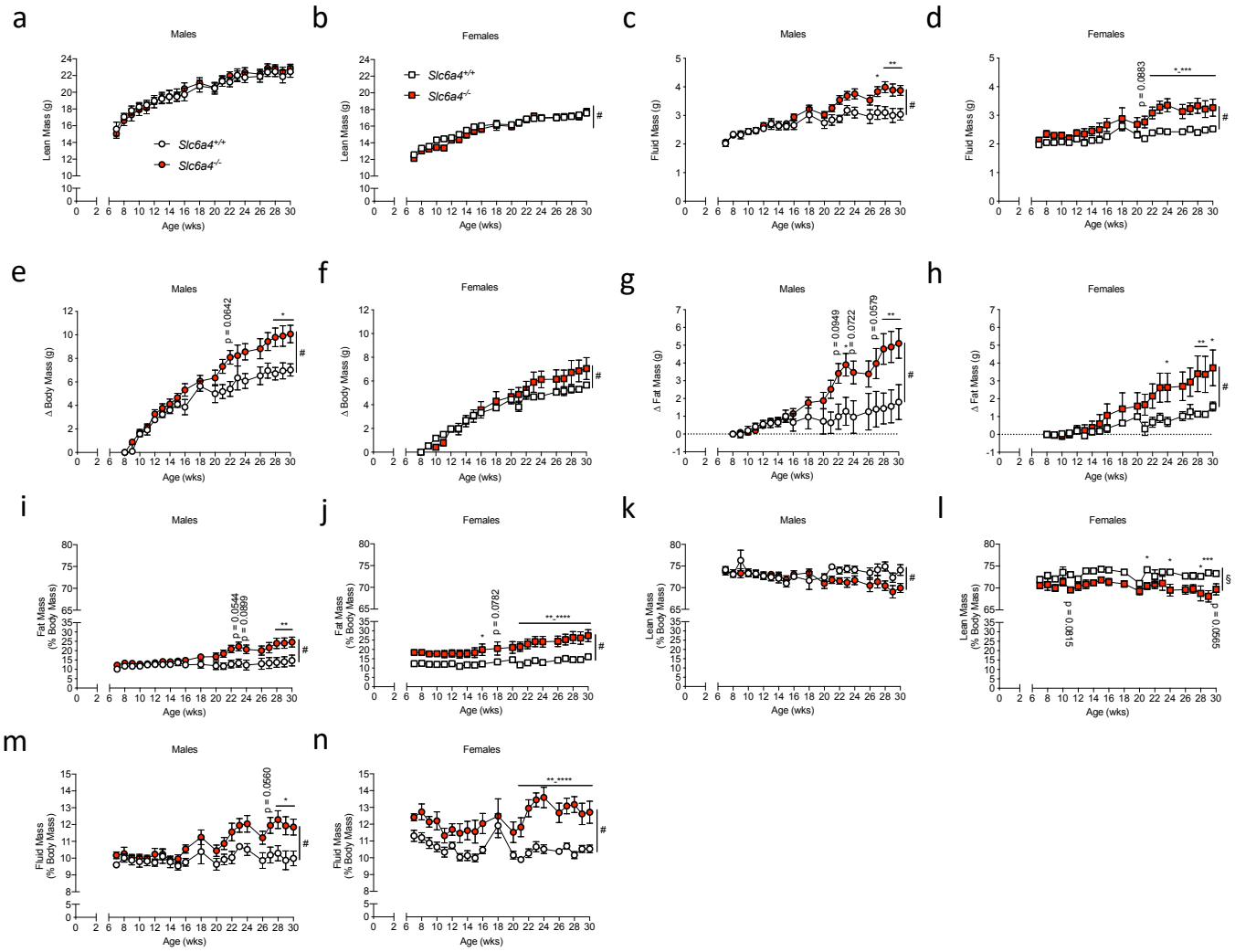
a
Males
Lean Mass (g)
Slc6a4+/+
Slc6a4-/-
Age (wks)
b
Females
Lean Mass (g)
Slc6a4+/+
Slc6a4-/-
Age (wks)
c
Males
Fluid Mass (g)
Age (wks)
d
Females
p = 0.0883
Fluid Mass (g)
Age (wks)
e
Males
p = 0.0642
Δ Body Mass (g)
Age (wks)
f
Females
Δ Body Mass (g)
Age (wks)
g
Males
p = 0.0949
p = 0.0722
p = 0.0579
Δ Fat Mass (g)
Age (wks)
h
Females
Δ Fat Mass (g)
Age (wks)
i
Males
p = 0.0544
p = 0.0899
Fat Mass (% Body Mass)
Age (wks)
j
Females
p = 0.0782
Fat Mass (% Body Mass)
Age (wks)
k
Males
Lean Mass (% Body Mass)
Age (wks)
l
Females
p = 0.0816
p = 0.0665
Lean Mass (% Body Mass)
Age (wks)
m
Males
p = 0.0560
Fluid Mass (% Body Mass)
Age (wks)
n
Females
Fluid Mass (% Body Mass)
Age (wks)

Figure S8- 1 Additional body composition measurements of *Slc6a4*$^{-/-}$ and *Slc6a4*$^{+/+}$ mice. a-b, Lean mass of male (a; n = 5-9) and female (b; n = 6-8) *Slc6a4*$^{-/-}$ and *Slc6a4*$^{+/+}$ mice. c-d, Fluid mass of male (a; n = 5-9) and female (b; n = 6-8) *Slc6a4*$^{-/-}$ and *Slc6a4*$^{+/+}$ mice. e-f, Change in body mass of male (a; n = 5-9) and female (b; n = 6-8) *Slc6a4*$^{-/-}$ and *Slc6a4*$^{+/+}$ mice. g-h, Change in fat mass of male (a; n = 5-9) and female (b; n = 6-8) *Slc6a4*$^{-/-}$ and *Slc6a4*$^{+/+}$ mice. i-j, Fat mass as a percentage of body mass of male (a; n = 5-9) and female (b; n = 6-8) *Slc6a4*$^{-/-}$ and *Slc6a4*$^{+/+}$ mice. k-l, Lean mass as a percentage of body mass of male (a; n = 5-9) and female (b; n = 6-8) *Slc6a4*$^{-/-}$ and *Slc6a4*$^{+/+}$ mice. m-n, Fluid mass as a percentage of body mass of male (a; n = 5-9) and female (b; n = 6-8) *Slc6a4*$^{-/-}$ and *Slc6a4*$^{+/+}$ mice. Points indicate mean and error bars indicate s.e.m. § = genotype effect and # = overall interaction effect as determined by 2-way ANOVA. * indicates significant effect as assessed by Bonferroni *post-hoc* test. Data related to Figure 8.

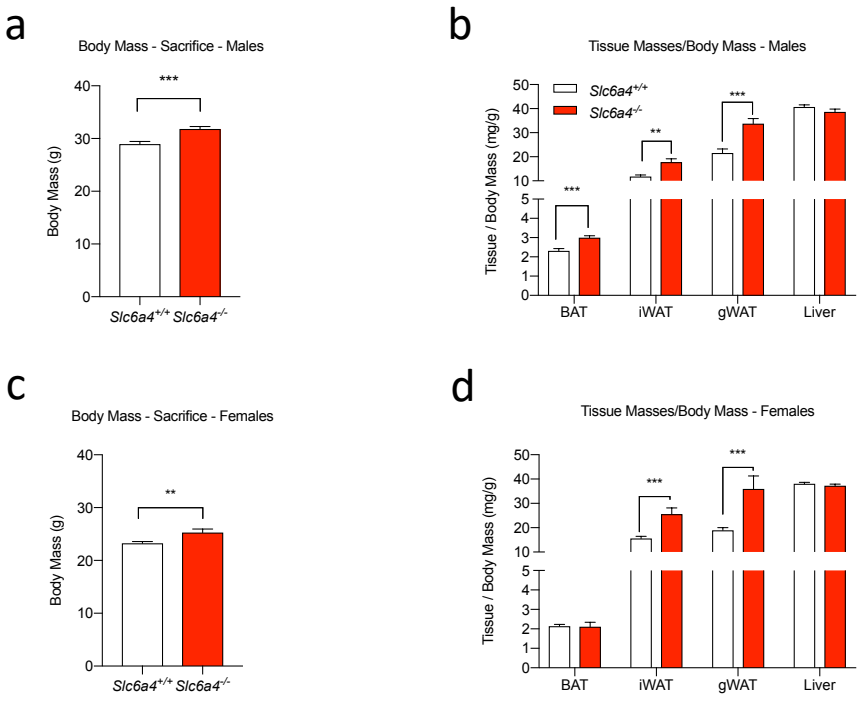

Figure S8- 2 Body masses and tissue masses corrected to body mass at sacrifice are higher in *Slc6a4*$^{+/+}$ and *Slc6a4*$^{-/-}$ mice. a-d, body mass and tissue masses corrected to body mass in males (a-b; n = 14-20) and females (c-d; n = 9-16). Bars indicate mean values and error bars indicate s.e.m. * indicates significance as determined by t-test. Data is related to Figure 8.

21.5 Supporting Data for Figure 9

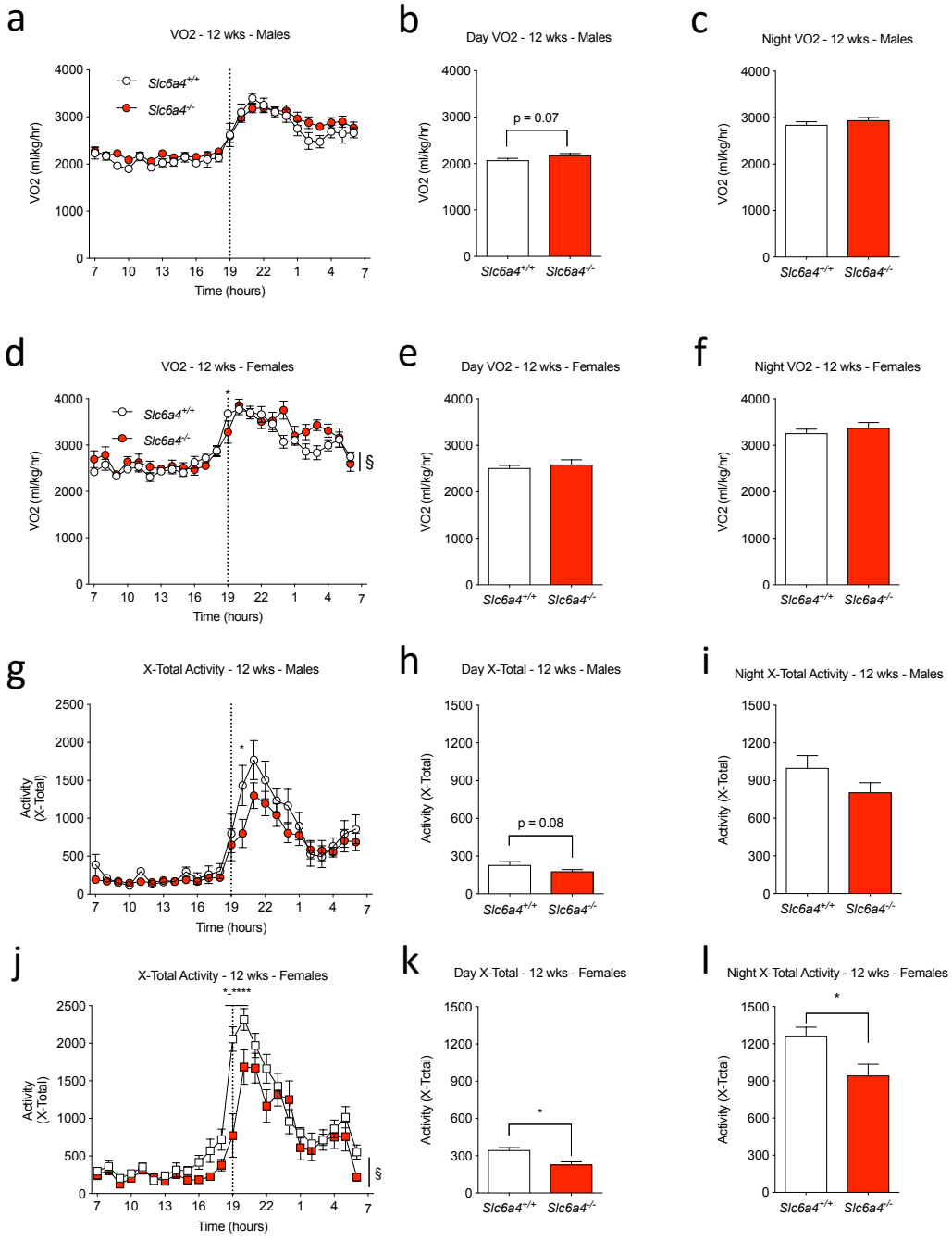

Figure S9- 1 *Slc6a4*$^{-/-}$ have similar absolute oxygen consumption rates but reduced x-total activity levels at 12 weeks of age. a-c, Body mass corrected oxygen consumption over 24 hours (a), the average during the day (b) and the average during the night (c) in male *Slc6a4*$^{+/+}$ and *Slc6a4*$^{-/-}$ mice at 12 weeks of age

(n = 6-11). d-f, same as a-c but in female mice (n = 5-9). g-i, X-Total activity over 24 hours (g), the average during the day (h) and the average during the night (i) in male *Slc6a4*$^{+/+}$ and *Slc6a4*$^{-/-}$ mice at 12 weeks of age (n = 6-11). j-l, same as g-i but in female mice (n = 5-9). All bars represent average values within group and error bars indicate s.e.m. § = overall genotype effect as determined by 2-way ANOVA. * indicates significant effect as assessed by Bonferroni *post-hoc* tests in ANOVA tests or significance determined by t-test. Data is related to Figure 9.

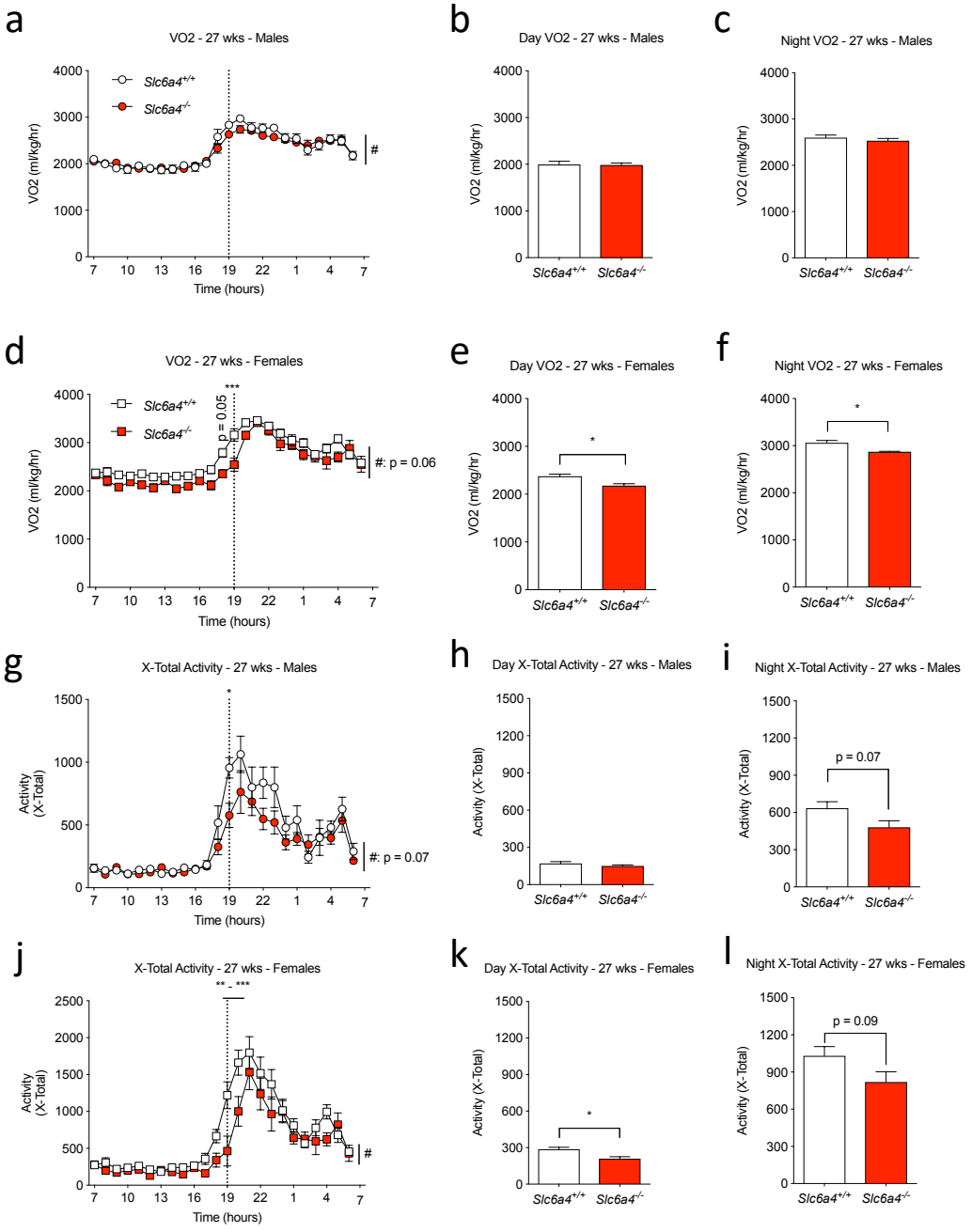

Figure S9- 2 Body mass corrected oxygen consumption and x-axis total activity are lower in *Slc6a4*$^{-/-}$ versus *Slc6a4*$^{+/+}$ mice at 27 weeks of age. a-f, 24-hour oxygen consumption (a and d), average oxygen consumption during the day (b and e) or night period (c and f) in male (a-c; n = 9-16) and female (d-f; n = 7-14) mice. g-l, 24-hour X-total activity (g and j), average X-total activity during the day (h and k) and night period (i and l) in male (g-i; n = 8-15) and female (j-l; n = 7-14) mice. # = overall interaction effect as determined by 2-way ANOVA. All bars represent

average values within group and error bars indicate s.e.m. * indicates significant effect as assessed by Bonferroni *post-hoc* tests in ANOVA tests or significance determined by t-test. Data is related to Figure 9.

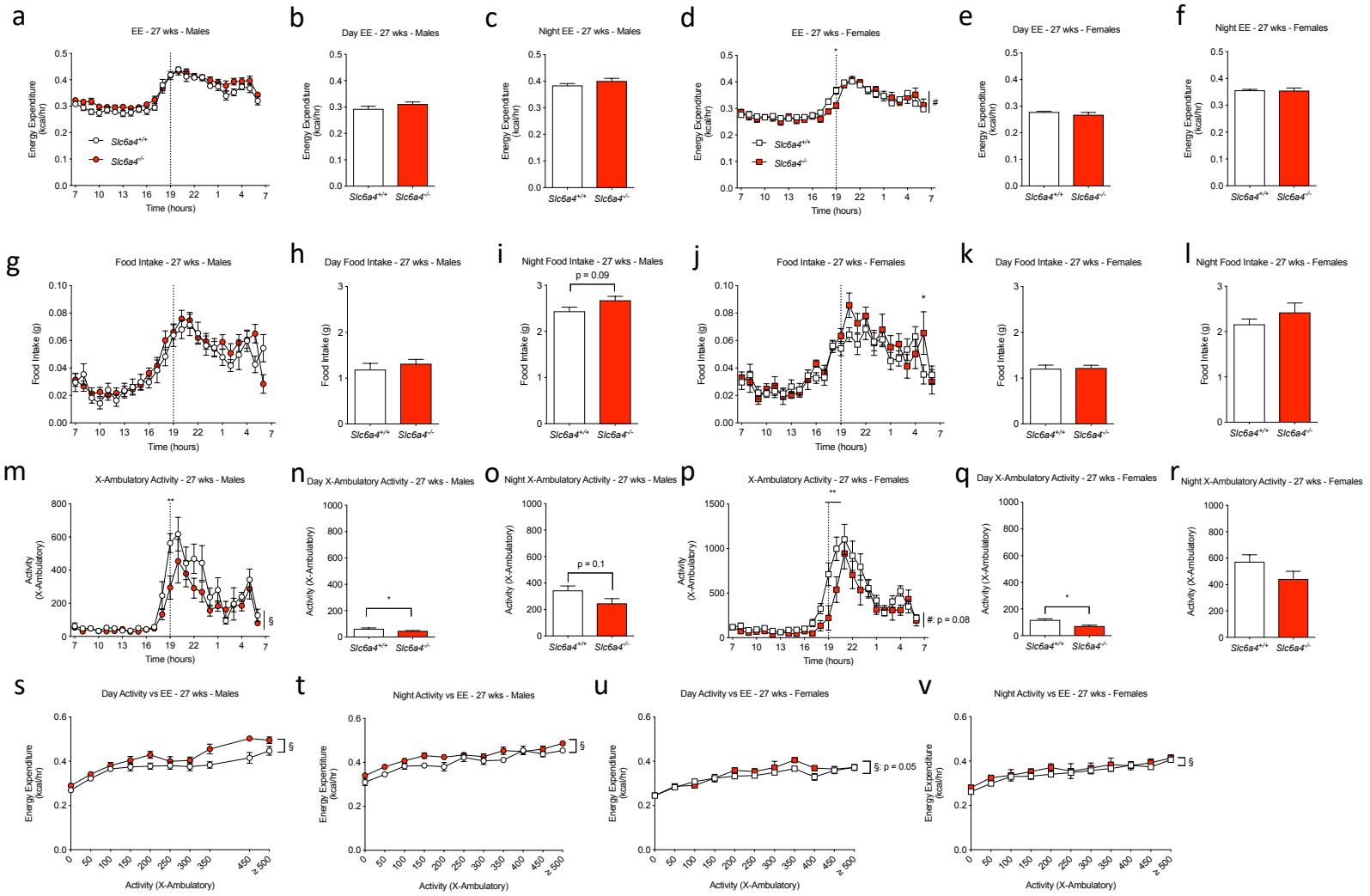
a
EE - 27 wks - Males
Energy Expenditure (kcal/hr)
Slc6a4+/+
Slc6a4-/-
Time (hours)
b
Day EE - 27 wks - Males
c
Night EE - 27 wks - Males
d
EE - 27 wks - Females
#
e
Day EE - 27 wks - Females
f
Night EE - 27 wks - Females
g
Food Intake - 27 wks - Males
Food Intake (g)
h
Day Food Intake - 27 wks - Males
i
Night Food Intake - 27 wks - Males
p = 0.09
j
Food Intake - 27 wks - Females
k
Day Food Intake - 27 wks - Females
l
Night Food Intake - 27 wks - Females
m
X-Ambulatory Activity - 27 wks - Males
Activity (X-Ambulatory)
§
n
Day X-Ambulatory Activity - 27 wks - Males
o
Night X-Ambulatory Activity - 27 wks - Males
p = 0.1
p
X-Ambulatory Activity - 27 wks - Females
#: p = 0.08
q
Day X-Ambulatory Activity - 27 wks - Females
r
Night X-Ambulatory Activity - 27 wks - Females
s
Day Activity vs EE - 27 wks - Males
t
Night Activity vs EE - 27 wks - Males
u
Day Activity vs EE - 27 wks - Females
§: p = 0.05
v
Night Activity vs EE - 27 wks - Females

Figure S9- 3 Food intake tends to be higher, daily activity lower and higher energy expenditure (EE) per level of activity in *Slc6a4*$^{+/+}$ and *Slc6a4*$^{-/-}$ mice at 27 weeks of age. a-f, EE over a 24-hour period (a and d), average during the day (b and e) and night period (c and f) in male (a-c; n = 9-16) and female (d-f; n = 7-14) mice. g-l, Food intake over a 24-hour period (g and j), average during the day (h and k) and night period (i and l) in male (a-c; n = 9-16) and female (g-i; n = 7-12) mice. m-r, X-Ambulatory activity over a 24-hour period (m and p), average during the day (n and q) and night period (o and r) in male (m-o; n = 8-15) and female (p-r; n = 7-14) mice. s-v, EE per level of activity during the day (s and u) and night (t and v) period in male (s-t; n = 8-15) and female (u-v; n = 7-13) mice. All bars represent average values within group and error bars indicate s.e.m. § = genotype effect and # = overall interaction effect as determined by 2-way ANOVA. * indicates significant effect as assessed by Bonferroni *post-hoc* tests in ANOVA tests or significance determined by t-test. Data is related to Figure 9.

21.6 Supporting Data for Figure 10

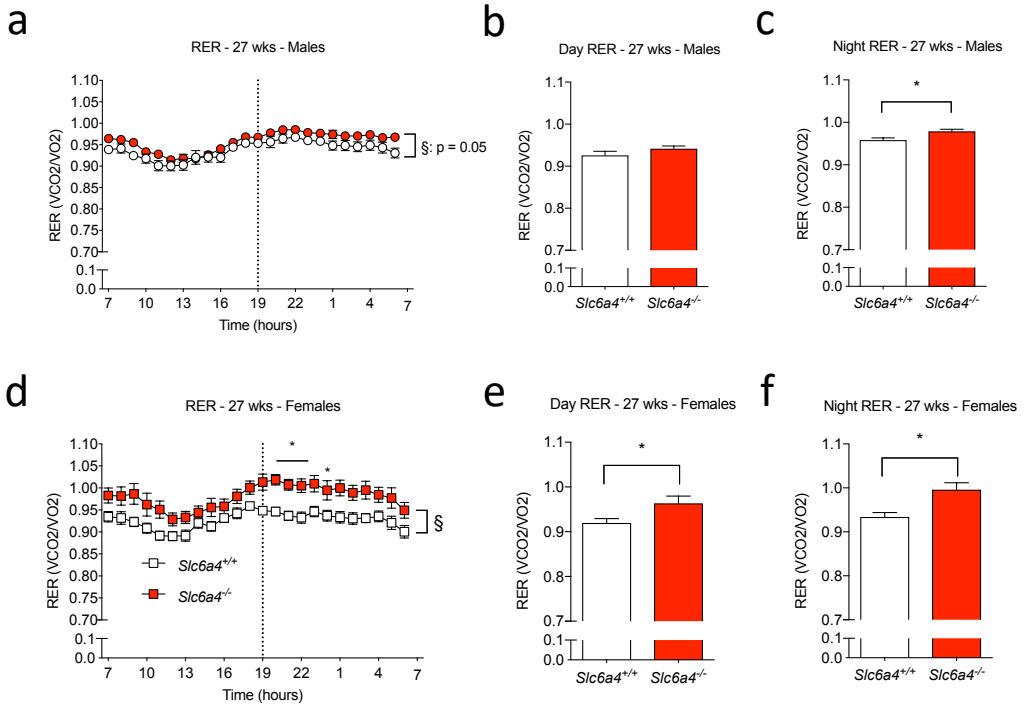

Figure S10- 1 RER is elevated in male and female *Slc6a4*$^{+/+}$ and *Slc6a4*$^{-/-}$ mice at 27 weeks of age. a-f, RER over a 24-hour period (a and d), average RER during day (b and e) and night (c and f) in male (a-c; n = 8-15) and female (d-f; n = 7-14) mice. § = genotype effect as determined by 2-way ANOVA. All bars represent average values within group and error bars indicate s.e.m. * indicates significant effect as assessed by Bonferroni *post-hoc* tests in ANOVA tests or significance determined by t-test. Data is related to Figure 10

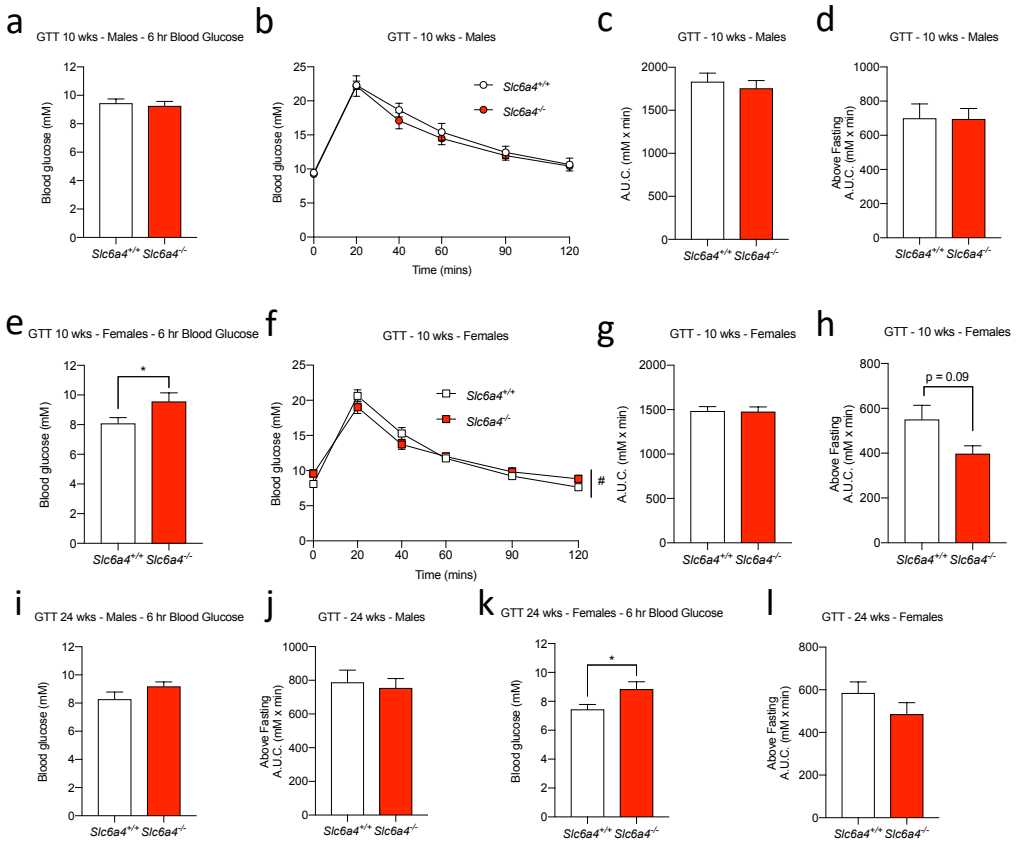

Figure S10- 2 Glucose homeostasis is slightly altered in female *Slc6a4*$^{-/-}$ mice at 10 weeks of age. a, 6 hour fasting blood glucose in 10-week-old male (n = 5-12) mice. b-d, Glucose tolerance test time course (b), a.u.c. (c) and a.u.c. above fasting (d; n = 5-12) in male mice. e, 6 hour fasting blood glucose in 10-week-old female mice (n = 6-9). f-h, Glucose tolerance test time course (f), a.u.c. (g) and a.u.c. above fasting (h; n = 6-9) in 10-week-old female mice. i-l, fasting blood glucose (I and k) and a.u.c. (j and l) above fasting in 24-week-old male (i-j; n = 15-21) and female (k-l; n = 9-16) mice. § = genotype effect and # = overall interaction effect as determined by 2-way ANOVA. All bars represent average values within group and error bars indicate s.e.m. * indicates significant effect as assessed by Bonferroni *post-hoc* tests in ANOVA tests or significance determined by t-test. Data is related to Figure 10.

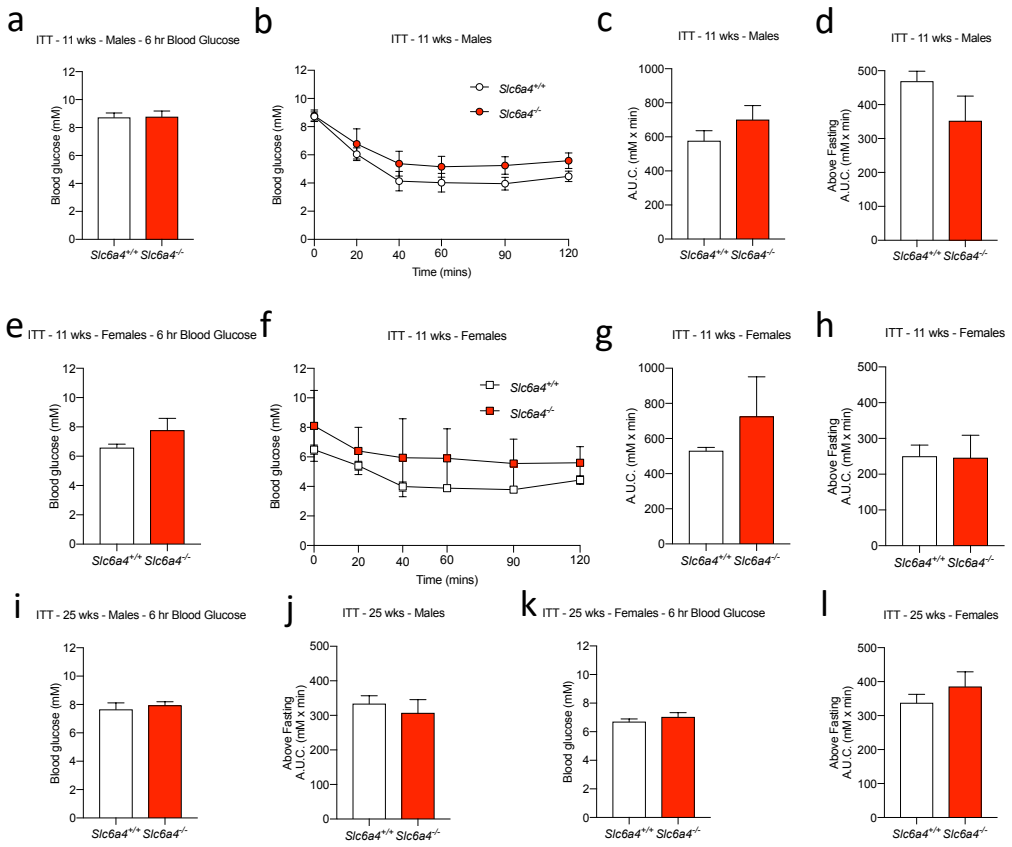

Figure S10- 3 Insulin sensitivity is unaltered in *Slc6a4*$^{-/-}$ mice. a, 6 hour fasting blood glucose in 11-week-old male (n = 5-12) mice. b-d, Insulin tolerance test time course (b), a.u.c. (c) and a.u.c. above fasting (d; n = 5-12) in male mice. e, 6 hour fasting blood glucose in 11-week-old female mice (n = 5-8). f-h, Insulin tolerance test time course (f), a.u.c. (g) and a.u.c. above fasting (h; n = 5-8) in 11-week-old female mice. i-l, fasting blood glucose (I and k) and a.u.c. (j and l) above fasting in 24-week-old male (i-j; n = 16-21) and female (k-l; n = 9-15) mice. § = genotype effect and # = overall interaction effect as determined by 2-way ANOVA. All bars represent average values within group and error bars indicate s.e.m. * indicates significant effect as assessed by Bonferroni post-hoc tests in ANOVA tests or significance determined by t-test. Data is related to Figure 10.

21.7 Supporting data for Figure 11

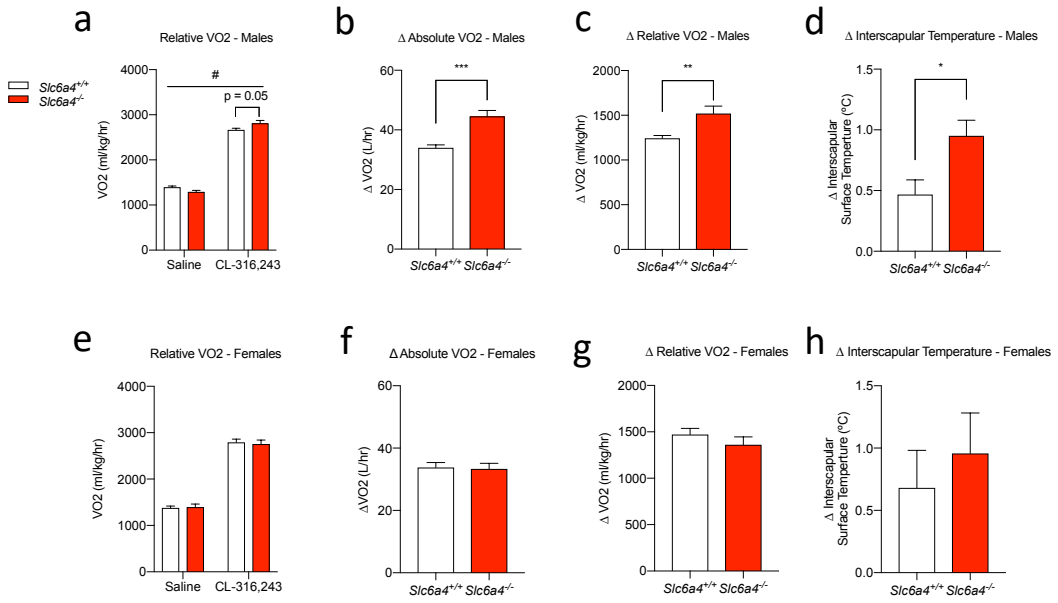

Figure S11- 1 Additional thermography values for *Slc6a4*$^{-/-}$ mice. a-d, Relative VO2 values (a), change in absolute VO2 (b), relative VO2 (c) and interscapular surface temperature (d; n = 15-18) in male mice. e-h, Relative VO2 values (e), change in absolute VO2 (f), relative VO2 (g) and interscapular surface temperature (h; n = 9-14) in female mice. All bars represent average values within group and error bars indicate s.e.m. # = overall interaction effect as determined by 2-way ANOVA. * indicates significant effect as assessed by Bonferroni *post-hoc* tests in ANOVA tests or significance determined by t-test. Data is related to Figure 11.

21.8 Supporting data for Figure 12

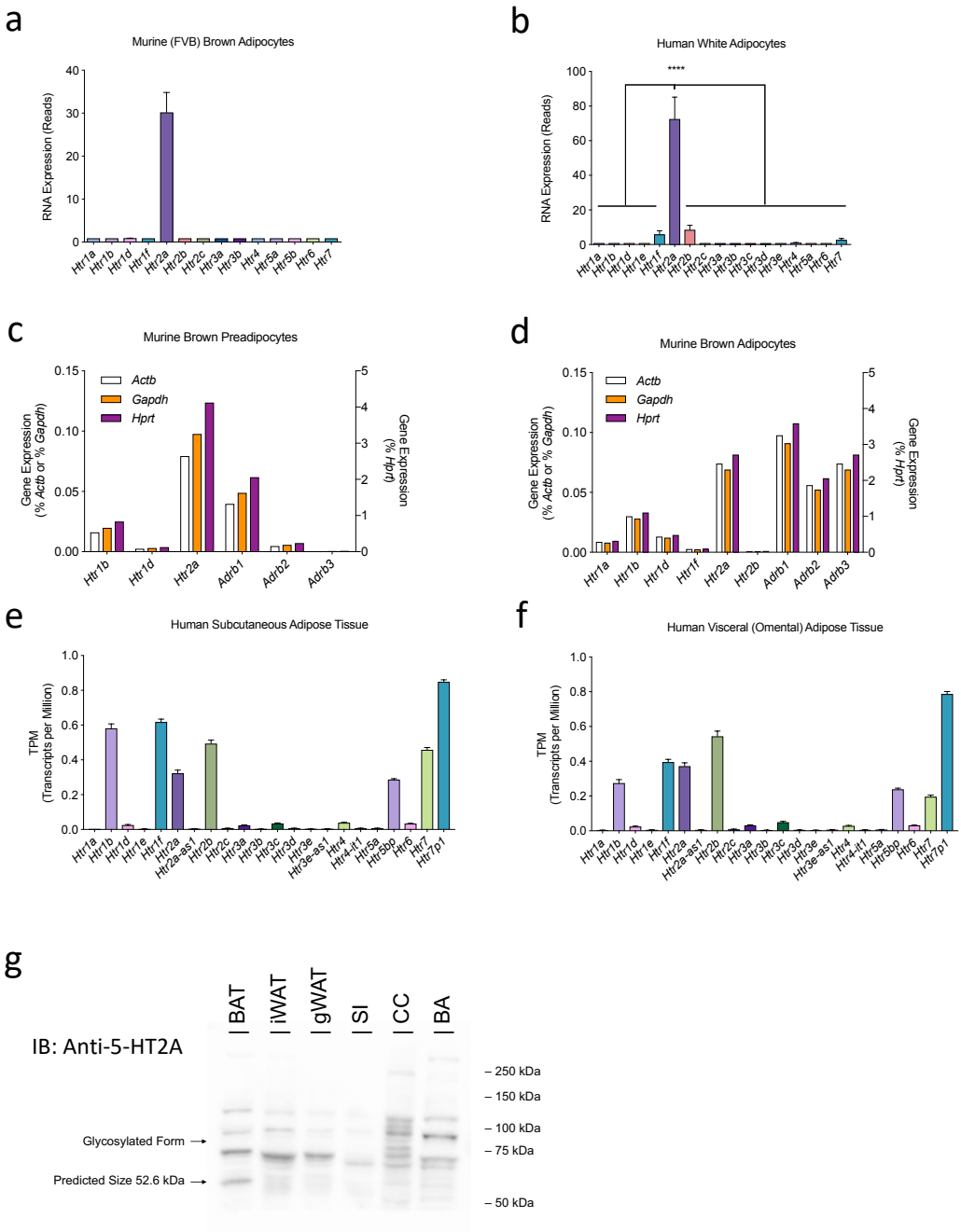

Figure S12- 1 Expression of 5-HT receptors in preadipocytes, brown adipocytes, white adipocytes and white adipose tissue. a-b, 5-HT receptor mRNA expression levels, as assessed by RNA-seq, in differentiated BAs from FVB mice (a; n = 1 independent experiment performed in 5 replicates, error bars

represent within experiment error) or human-derived differentiated BAs (b; n = 5 different participants, error bars represent between participants). a-d Graph of adapted data from supplementary tables of Klepac et al., (2016) showing detected 5-HT- and β-adrenergic receptors corrected to various housekeeping gene expression in murine preadipocytes (c) and differentiated preadipocytes (d). e-f, Gene expression levels of 5-HT receptors in human subcutaneous (e; n = 368) and visceral (f; n = 234) white adipose tissue from the GTExPortal (bars represent means and error bars are s.e.m. between individuals). g, Western blot using antibody against 5-HT2A - BAT: brown adipose tissue; iWAT: inguinal white adipose tissue; gWAT: gonadal white adipose tissue; SI: small intestine; CC: corpus callosum; BA: cultured brown adipocytes. * indicates significant effect as assessed by Bonferroni *post-hoc* tests in 1-way ANOVA test. This data is related to Figure 12.

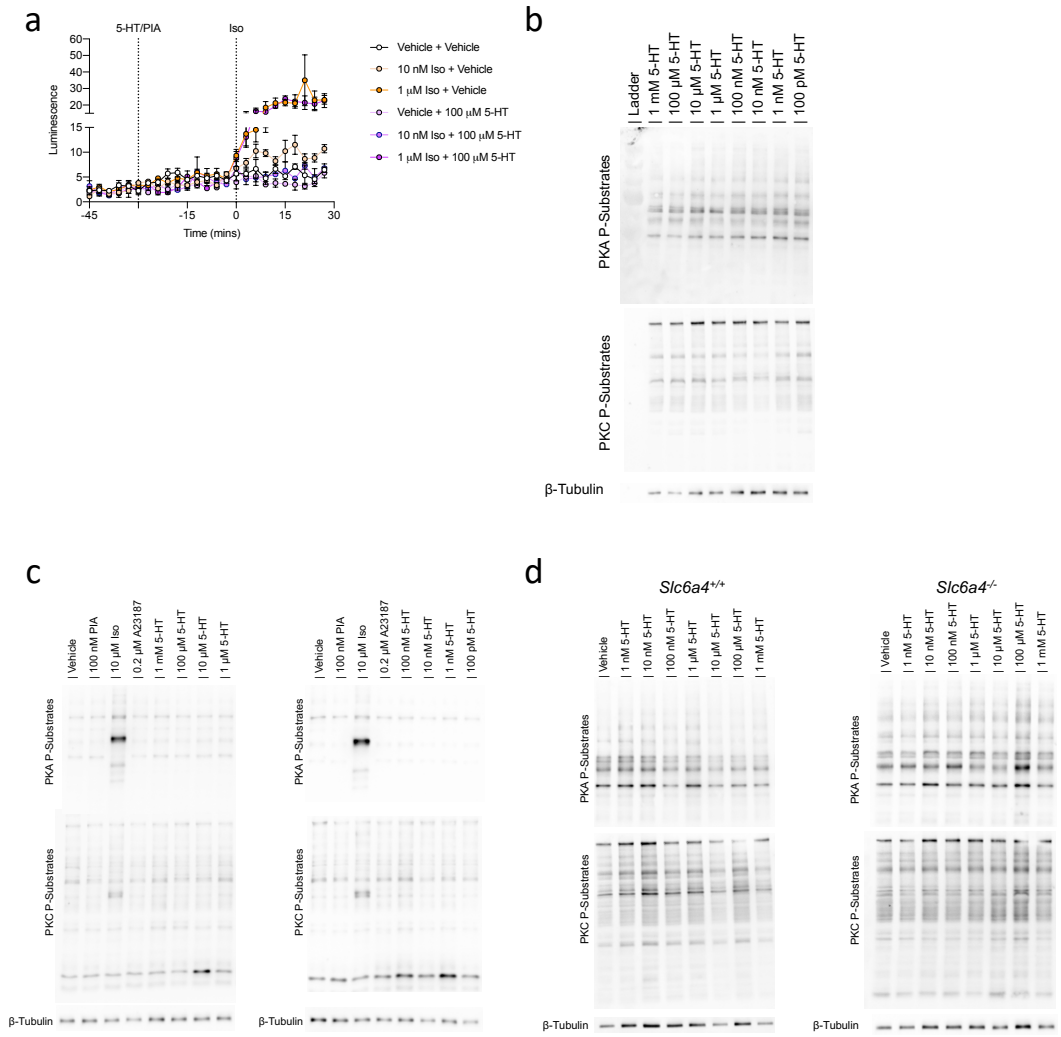

Figure S12- 2 Gs- and Gi- coupled 5-HT receptors are not active at physiological levels of 5-HT in mouse BAs. a, Representative time course of cAMP reporter luminescence in BAs stably expressing pGloSensor-22F in response to different concentrations of Iso and high concentrations of 5-HT (n = 3 independent experiments performed in 3 replicates; error bars represent error between experiments). b, Protein Kinase A (PKA) substrate phosphorylation in response to an acute treatment with different doses of 5-HT as determined by western blot. c-d, PKA and PKC substrate phosphorylation in response to an acute treatment with 5-HT in BAs from FVB mice (c) and in BAs from *Slc6a4*$^{+/+}$ and *Slc6a4*$^{-/-}$ mice (d). This data is related to Figure 12.

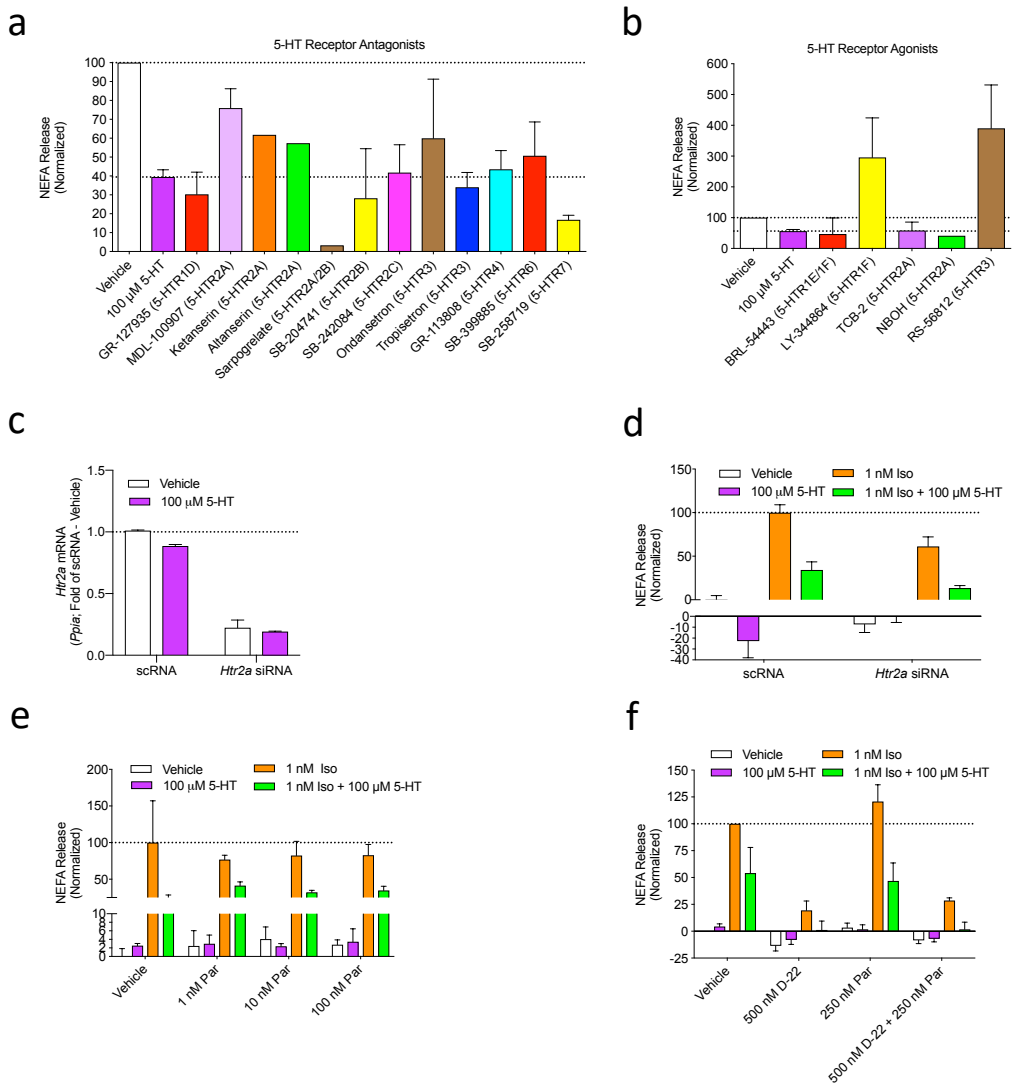

Figure S12- 3 No 5-HT receptor antagonist or 5-HT transporter inhibitor tested prevented the inhibition of lipolysis by high dose 5-HT. a, Select NEFA release assays in BAs with 10 nM antagonist treatments in combination with 100 µM 5-HT and 1 nM Iso (n = 1-3 for antagonists performed in 2-3 replicates). Full dose responses are available in Figure S12- 4. b, Select NEFA release assays in BAs of various 5-HT receptor agonists (1 µM) in the presence of 1 nM Iso (n = 1-3 for agonists performed in 2-3 replicates). Full dose responses are available in Figure S12- 5. c, Validation of *Htr2a* mRNA reduction by *Htr2a* siRNA with qPCR analysis of *Htr2a* mRNA levels in BAs (n = 2 performed in 3 replicates). d, NEFA release in BAs with reduced *Htr2a* mRNA (n = 1 independent experiment performed in triplicate – error bars represent within experiment error). e, NEFA release in BAs treated with different doses of Par (n = 1 independent experiment performed in triplicate – error bars represent within experiment error). f, NEFA release in BAs treated with Par (an SSRI), D-22 (a PMAT/OCT3 inhibitor) and in

combination (n = 1 independent experiment performed in triplicate – error bars represent within experiment error). All bars represent means with error bars representing S.E.M. This data is related to Figure 12.

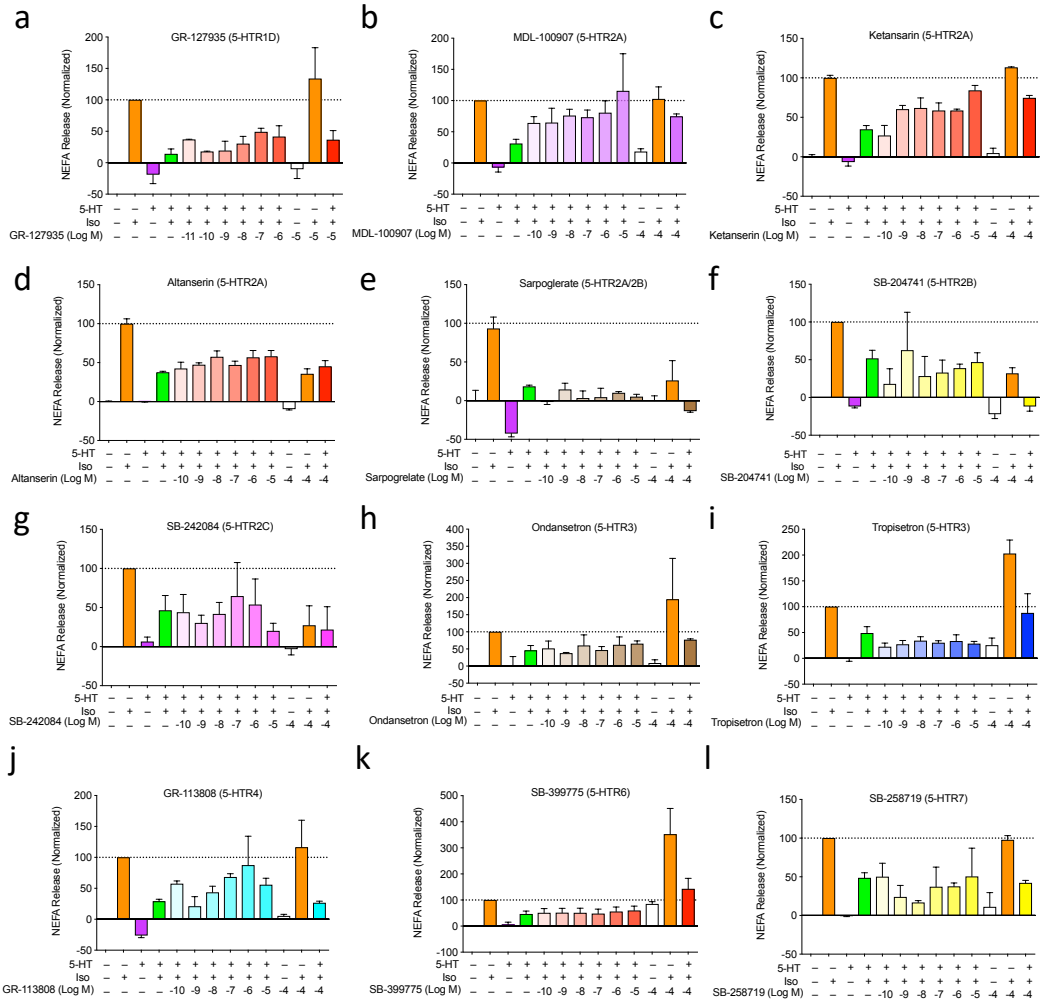

Figure S12- 4 Full dose responses of 5-HT receptor antagonists on NEFA release from BAs. Data is expanded version of Figure 12a. a-l, NEFA release assays in BAs with indicated antagonist treatments in combination with 100 µM 5-HT and 1 nM Iso (n = 1-3 for antagonists performed in 2-3 replicates) response is normalized to vehicle and 1 nM Iso treatment. This data is related to Figure 12**.**

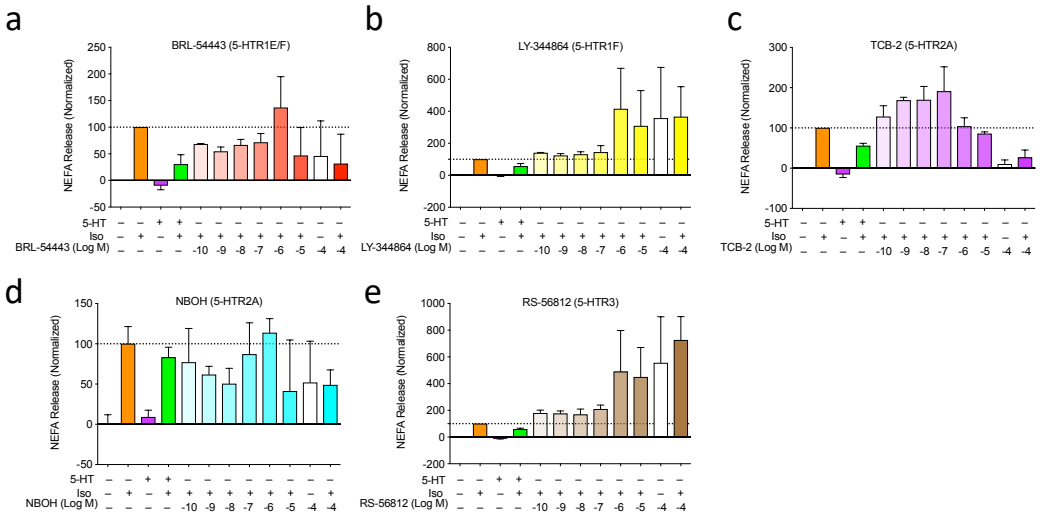

Figure S12- 5 Full dose responses of 5-HT receptor agonists on NEFA release from BAs. a-e, NEFA release assays in BAs of various 5-HT receptor agonists in the presence of 1 nM Iso (n = 1-3 for agonists performed in 2-3 replicates). Values are normalized to vehicle and 1 nM Iso treatment. This data is related to Figure 12.

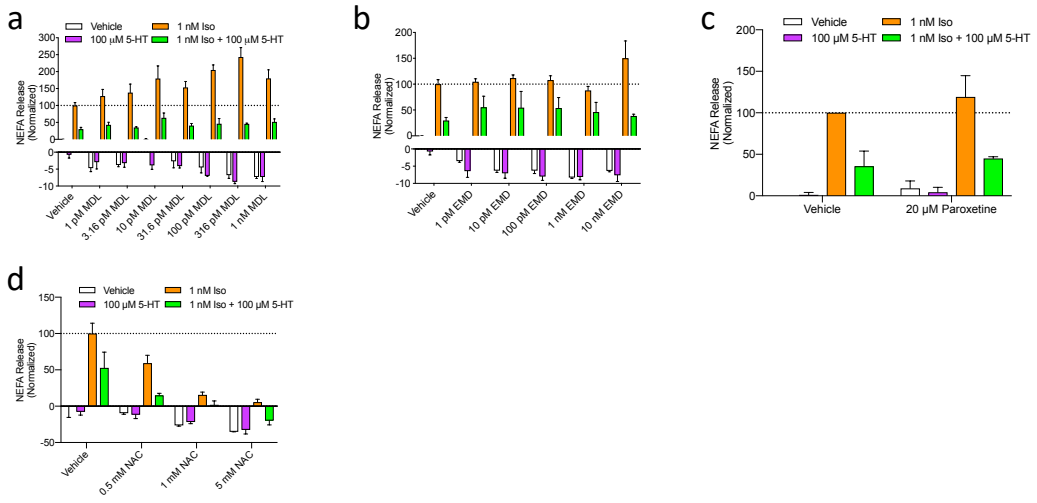

Figure S12- 6 Full dose responses of 5-HT2A receptor antagonists, SSRI (SERT inhibitor) antagonists and ROS scavengers on NEFA release from BAs. a-d, NEFA release normalized to vehicle and 1 nM Iso for BAs treated with indicated treatments of the 5-HT2A antagonists – MDL (MDL-100907; a; n = 1 experiment performed in triplicate – error bars represents within experiment error) and EMD (EMD-281014; b; n = 1 experiment performed in triplicate – error bars represents within experiment error) – Paroxetine (an SSRI; c; n = 1 experiment performed in triplicate – error bars represents within experiment error) and N-acetylcysteine (NAC; d; n = 1 experiment performed in triplicate – error bars represents within experiment error). This data is related to Figure 12.

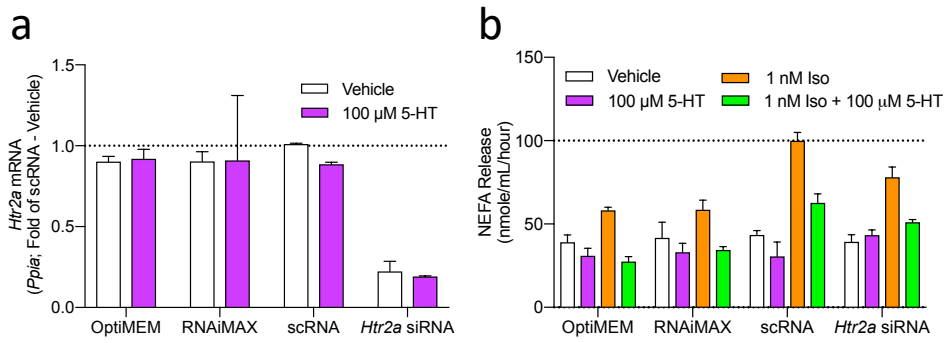

Figure S12- 7 *Htr2a* siRNA transfection of successfully reduces *Htr2a* mRNA levels but does not affect BA NEFA release. a, *Htr2a* mRNA levels in BAs transfected with *Htr2a* siRNA (n = 1 experiment performed in triplicate – error bars represents within experiment error). b, Not normalized, NEFA release from siRNA treated BAs (n = 1 experiment performed in triplicate – error bars represents within experiment error). This data is related to Figure 12**.**

a

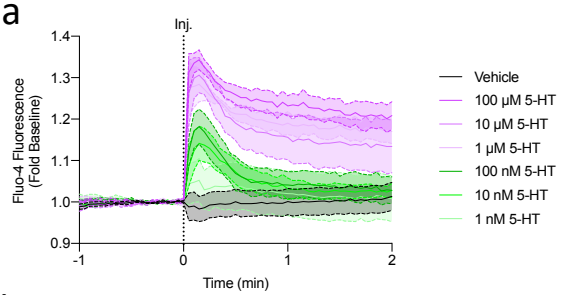

b

Antagonist	Target (gene)	N [Tech. replicates]	Mean IC_{50} (nM)	Fold MDL-100907 IC_{50}	Log IC_{50} (M)	R^2	Published 5-HT2A Ki	Fold MDL-100907 Ki for 5-HT2A
MDL-100907	5-HT2A (*Htr2a*)	3 [3]	0.38 ± 0.04	1	-9.42 ± 0.05	0.55 ± 0.08	1.19 ± 0.27	1
SB-204741	5-HT2B (*Htr2b*)	3 [3]	1771.1 ± 678.05	4622.67	-5.87 ± 0.26	0.46 ± 0.13	7505.94 ± 1439.95	6287.82
SB-242084	5-HT2C (*Htr2c*)	3 [3]	270.69 ± 187.56	706.51	-6.83 ± 0.35	0.59 ± 0.05	504.81 ± 346.33	422.88

c

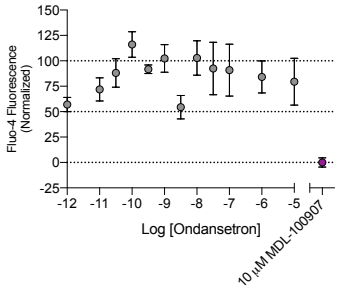

Figure S12- 8 Pharmacological properties of 5-HT2A, 5-HT2B, 5-HT2C and 5-HT3 antagonists in BAs. a, Representative time course of Fluo-4 fluorescence in response to increasing doses of 5-HT (solid lines represent mean response and shaded regions represent error within experiment). b, Table of pharmacological properties of 5-HT2A, 5-HT2B and 5-HT2C antagonists. c, Ondansetron (5-HT3 antagonist) dose response inhibiting 5-HT induced Ca^{2+} peaks (n = 1 performed in 3 replicates, points indicate average response and error bars represent within experiment error). This data is related to Figure 12.

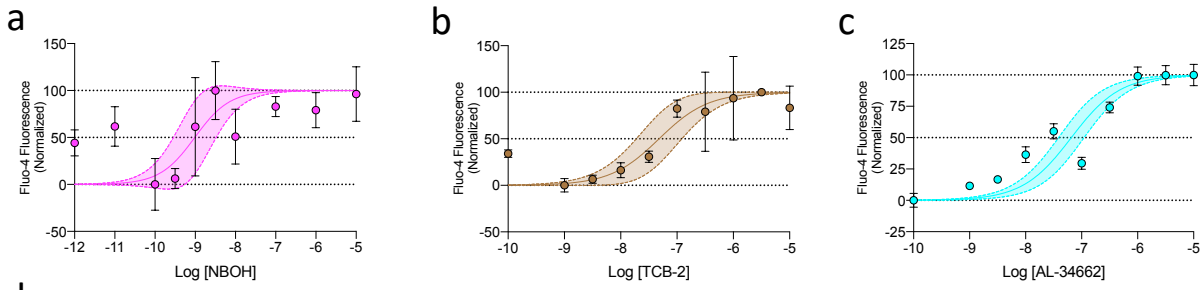

d

Agonist	Target (gene)	N [Tech. replicates]	Mean EC_{50} (nM)	Log IC_{50} (M)	R^2
5-HT	All 5-HTR (All *Htr*)	4 (3)	230.12 ± 124.41	-6.8 ± 0.21	0.68 ± 0.08
NBOH	5-HTR2A (*Htr2a*)	4 (2-3)	22.68 ± 21.55	-8.51 ± 0.49	0.07 ± 0.07
TCB-2	5-HTR2A (*Htr2a*)	4 (2-3)	50.47 ± 31.26	-7.61 ± 0.32	0.55 ± 0.05
AL-34662	Peripheral 5-HTR2A (*Htr2a*)	4 (3)	55.41 ± 9.18	-7.28 ± 0.08	0.75 ± 0.11

Figure S12- 9 Effects of 5-HT2A agonists on BA Ca2+ transient activity. a-c, Fluorescence curves of BAs loaded with Fluo-4 and treated with different doses of 5-HT2A agonists: NBOH-2C-CN (NBOH; a), TCB-2 (b) and AL-34662 (c; n = 4 individual experiments performed in 2-3 replicates – shaded region represents 95% confidence in non-linear curve fit, points represent mean values and error bars are S.E.M.). d, Pharmacological properties of 5-HT2A agonists. This data is related to Figure 12.

a

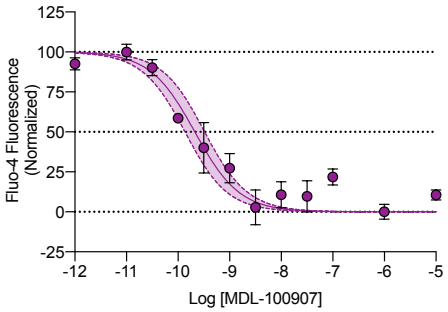

b

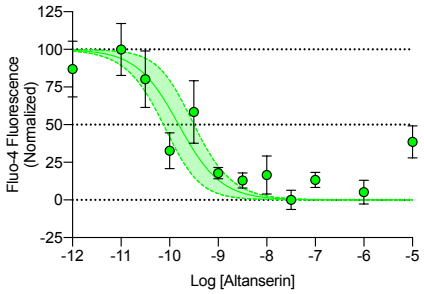

c

Antagonist	N [Tech. replicates]	Mean IC_{50} (nM)	Log IC_{50} (M)	R^2
MDL-100907	3 [3]	0.4 ± 0.19	-9.49 ± 0.19	0.74 ± 0.11
Altanserin	3 [3]	0.22 ± 0.07	-9.69 ± 0.12	0.24 ± 0.18

d

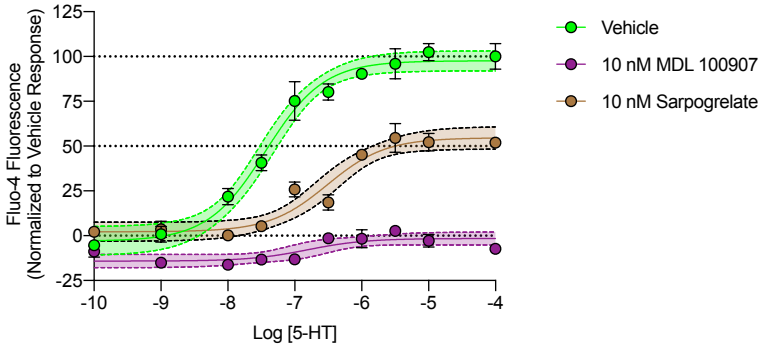

e

Antagonist	N [Tech. replicates]	Mean EC_{50} (nM)	Log EC_{50} (M)	Fold 5-HT EC_{50}	Percent Max. 5-HT Effect (i.e. Span)	R^2
Vehicle (5-HT only)	3 [3-6]	60.08 ± 31.68	-7.43 ± 0.27	1 ± 0	100.11 ± 2.07	0.8 ± 0.06
MDL-100907	3 [3-6]	84.81 ± 38.04	-7.18 ± 0.24	2.66 ± 1.12	26.04 ± 10.3	0.33 ± 0.09
Sarpogrelate	3 [2-6]	240.33 ± 65.12	-6.66 ± 0.15	5.32 ± 2.34	82.44 ± 16	0.91 ± 0.03

Figure S12- 10 Effects of 5-HT2A antagonists on BA Ca^{2+} transient activity. a-b, Representative fluorescence curves of Fluo-4 loaded BAs treated with 5-HT2A antagonists – MDL-100907 (a) and Altanserin (b) followed by 5-HT (n = 3 individual experiments performed in 3 replicates – shaded region represents 95% confidence in non-linear curve fit, points represent mean values and error bars are

S.E.M.). c, Pharmacological properties of 5-HT2A antagonists for blocking 5-HT elicited Ca^{2+} transients in BAs. d, Representative fluorescence curves of Fluo-4 loaded BAs treated with 5-HT2A antagonists – MDL-100907 and Sarpogrelate – in response to a variety of 5-HT concentrations (n = 3 individual experiments performed in 3-6 replicates – shaded region represents 95% confidence in non-linear curve fit, points represent mean values and error bars are S.E.M.). e, Pharmacological properties of 5-HT2A antagonists for blocking Ca^{2+} transients elicited by a wide range of 5-HT doses. This data is related to Figure 12.

Rank	ENSG ID	Gene	VAT r	ScAT r	Mean r
1	ENSG00000183578.5	*Tnfaip8L3*	0.651	0.606	0.6285
2	ENSG00000164106	*Scrg1*	0.599	0.63	0.6145
3	ENSG00000135931	*Armc9*	0.59	0.596	0.593
4	ENSG00000110811	*Leprel2*	0.579	0.587	0.583
5	ENSG00000138080	*Emilin1*	0.607	0.559	0.583
6	ENSG00000185483	*Ror1*	0.627	0.536	0.5815
7	ENSG00000171812	*Col8A2*	0.586	0.563	0.5745
8	ENSG00000128591.11	*Flnc*	0.653	0.496	0.5745
9	ENSG00000104290.6	*Fzd3*	0.607	0.539	0.573
10	ENSG00000089472.12	*Heph*	0.547	0.597	0.572
11	ENSG00000214050.3	*Fbxo16*	0.536	0.599	0.5675
12	ENSG00000235162.4	*C12Orf75*	0.606	0.517	0.5615
13	ENSG00000134247	*Ptgfrn*	0.576	0.547	0.5615
14	ENSG00000187955.7	*Col14A1*	0.548	0.57	0.559
15	ENSG00000141756	*Fkbp10*	0.51	0.606	0.558
16	ENSG00000125675	*Gria3*	0.512	0.6	0.556
17	ENSG00000169515	*Ccdc8*	0.571	0.535	0.553
18	ENSG00000117069	*St6Galnac5*	0.484	0.62	0.552
19	ENSG00000166557.8	*Tmed3*	0.491	0.608	0.5495
20	ENSG00000144057.11	*St6Gal2*	0.571	0.526	0.5485
21	ENSG00000144649.4	*Fam198A*	0.548	0.543	0.5455
22	ENSG00000106772	*Prune2*	0.632	0.452	0.542
23	ENSG00000166444	*St5*	0.552	0.53	0.541
24	ENSG00000154175	*Abi3Bp*	0.478	0.602	0.54
25	ENSG00000152556.11	*Pfkm*	0.547	0.533	0.54
26	ENSG00000151067	*Cacna1C*	0.584	0.496	0.54
27	ENSG00000169071	*Ror2*	0.565	0.513	0.539
28	ENSG00000159164.5	*Sv2A*	0.538	0.537	0.5375
29	ENSG00000072195	*Speg*	0.521	0.552	0.5365
30	ENSG00000103710.6	*Rasl12*	0.503	0.569	0.536
31	ENSG00000111674	*Eno2*	0.595	0.474	0.5345
32	ENSG00000197380	*Dact3*	0.538	0.53	0.534
33	ENSG00000184194.5	*Gpr173*	0.479	0.586	0.5325
34	ENSG00000143515.12	*Atp8B2*	0.447	0.612	0.5295
35	ENSG00000165995.14	*Cacnb2*	0.556	0.502	0.529
36	ENSG00000160469	*Brsk1*	0.461	0.596	0.5285
37	ENSG00000149557	*Fez1*	0.548	0.508	0.528
38	ENSG00000242902.1	*Rp11-309L24.2*	0.623	0.433	0.528
39	ENSG00000143847	*Ppfia4*	0.511	0.545	0.528
40	ENSG00000107130.6	*Ncs1*	0.667	0.381	0.524
41	ENSG00000102230	*Pcyt1B*	0.558	0.49	0.524
42	ENSG00000055118	*Kcnh2*	0.565	0.483	0.524
43	ENSG00000112208	*Bag2*	0.513	0.533	0.523
44	ENSG00000077942.13	*Fbln1*	0.493	0.549	0.521
45	ENSG00000138696.6	*Bmpr1B*	0.592	0.449	0.5205
46	ENSG00000108091.10	*Ccdc6*	0.553	0.486	0.5195
47	ENSG00000186310	*Nap1L3*	0.478	0.559	0.5185
48	ENSG00000164484.7	*Tmem200A*	0.504	0.532	0.518
49	ENSG00000050165	*Dkk3*	0.525	0.507	0.516
50	ENSG00000182492	*Bgn*	0.504	0.526	0.515

Table S12- 1 Top 50 genes positively correlated with *Htr2a* mRNA expression in both human visceral (VAT) and subcutaneous (ScAT) adipose tissue depots. Data obtained from the GTExPortal dataset. Full list available upon request. This data is related to Figure 12.

Rank	ENSG ID	Gene	VAT r	ScAT r	Mean r
1	ENSG00000182118.5	*Fam89A*	-0.507	-0.54	-0.5235
2	ENSG00000122378.9	*Fam213A*	-0.546	-0.499	-0.5225
3	ENSG00000176485.6	*Pla2G16*	-0.522	-0.503	-0.5125
4	ENSG00000079435	*Lipe*	-0.518	-0.503	-0.5105
5	ENSG00000132170.15	*Pparg*	-0.527	-0.477	-0.502
6	ENSG00000271738	*Rp11-137H2.6*	-0.499	-0.493	-0.496
7	ENSG00000165269	*Aqp7*	-0.506	-0.474	-0.49
8	ENSG00000132376	*Inpp5K*	-0.484	-0.494	-0.489
9	ENSG00000186205.8	*March1*	-0.503	-0.475	-0.489
10	ENSG00000186466	*Aqp7P1*	-0.515	-0.445	-0.48
11	ENSG00000184811.3	*Tusc5*	-0.522	-0.437	-0.4795
12	ENSG00000158571.6	*Pfkfb1*	-0.514	-0.443	-0.4785
13	ENSG00000245848.2	*Cebpa*	-0.508	-0.447	-0.4775
14	ENSG00000187288.6	*Cidec*	-0.511	-0.444	-0.4775
15	ENSG00000135447	*Ppp1R1A*	-0.452	-0.499	-0.4755
16	ENSG00000221290.1	*Mir1182*	-0.463	-0.487	-0.475
17	ENSG00000255108.1	*Ap006621.8*	-0.499	-0.447	-0.473
18	ENSG00000176720.3	*Bok*	-0.479	-0.459	-0.469
19	ENSG00000175445	*Lpl*	-0.473	-0.461	-0.467
20	ENSG00000177666.11	*Pnpla2*	-0.496	-0.437	-0.4665
21	ENSG00000213904	*Lipe-As1*	-0.499	-0.434	-0.4665
22	ENSG00000135604.9	*Stx11*	-0.465	-0.466	-0.4655
23	ENSG00000134463.10	*Echdc3*	-0.489	-0.442	-0.4655
24	ENSG00000157617.12	*C2Cd2*	-0.44	-0.488	-0.464
25	ENSG00000185825	*Bcap31*	-0.468	-0.458	-0.463
26	ENSG00000166819.7	*Plin1*	-0.486	-0.439	-0.4625
27	ENSG00000167588	*Gpd1*	-0.494	-0.431	-0.4625
28	ENSG00000174307.5	*Phlda3*	-0.443	-0.476	-0.4595
29	ENSG00000185818.7	*Nat8L*	-0.456	-0.46	-0.458
30	ENSG00000228971	*Rp11-286B14.1*	-0.426	-0.49	-0.458
31	ENSG00000051620	*Hebp2*	-0.451	-0.464	-0.4575
32	ENSG00000131943	*C19Orf12*	-0.477	-0.437	-0.457
33	ENSG00000005249	*Prkar2B*	-0.458	-0.45	-0.454
34	ENSG00000166123.9	*Gpt2*	-0.486	-0.416	-0.451
35	ENSG00000197879	*Myo1C*	-0.457	-0.443	-0.45
36	ENSG00000001084.6	*Gclc*	-0.409	-0.489	-0.449
37	ENSG00000122912	*Slc25A16*	-0.47	-0.428	-0.449
38	ENSG00000267815	*Ctb-191K22.5*	-0.436	-0.46	-0.448
39	ENSG00000126561	*Stat5A*	-0.44	-0.453	-0.4465
40	ENSG00000138207	*Rbp4*	-0.492	-0.401	-0.4465
41	ENSG00000167468	*Gpx4*	-0.445	-0.446	-0.4455
42	ENSG00000184887.9	*Btbd6*	-0.454	-0.437	-0.4455
43	ENSG00000159423	*Aldh4A1*	-0.443	-0.447	-0.445
44	ENSG00000157152	*Syn2*	-0.4	-0.489	-0.4445
45	ENSG00000152465	*Nmt2*	-0.508	-0.38	-0.444
46	ENSG00000169692.8	*Agpat2*	-0.469	-0.417	-0.443
47	ENSG00000228436	*Rp5-864K19.4*	-0.411	-0.474	-0.4425
48	ENSG00000076555	*Acacb*	-0.454	-0.43	-0.442
49	ENSG00000042286	*Aifm2*	-0.438	-0.445	-0.4415
50	ENSG00000111275	*Aldh2*	-0.491	-0.391	-0.441

Table S12- 2 Top 50 genes negatively correlated with *Htr2a* mRNA expression in both human visceral (VAT) and subcutaneous (ScAT) adipose tissue depots. Data obtained from the GTExPortal dataset. Full list available upon request. This data is related to Figure 12.

GO Term	Term Description	Count	%	DAVID p-value	Fold Enrichment	Bonferroni	Benjamini	FDR
GO:0005814	centriole	43	1.45	5.20E-10	2.74	4.66E-07	4.66E-07	8.10E-07
GO:0005925	focal adhesion	92	3.10	3.07E-07	1.69	2.75E-04	1.37E-04	4.78E-04
GO:0005634	nucleus	861	29.05	3.25E-07	1.14	2.91E-04	9.69E-05	5.06E-04
GO:0005737	cytoplasm	823	27.77	3.11E-06	1.13	2.78E-03	6.96E-04	4.85E-03
GO:0030054	cell junction	100	3.37	3.74E-06	1.57	3.35E-03	6.70E-04	5.83E-03
GO:0005654	nucleoplasm	464	15.65	4.71E-06	1.20	4.21E-03	7.02E-04	7.34E-03
GO:0031012	extracellular matrix	70	2.36	7.55E-06	1.70	6.73E-03	9.65E-04	1.18E-02
GO:0005578	proteinaceous extracellular matrix	64	2.16	1.40E-05	1.72	1.24E-02	1.56E-03	2.17E-02
GO:0005813	centrosome	91	3.07	2.37E-05	1.54	2.10E-02	2.35E-03	3.69E-02
GO:0005829	cytosol	535	18.05	3.20E-05	1.16	2.82E-02	2.86E-03	4.98E-02
GO:0005604	basement membrane	26	0.88	4.07E-05	2.37	3.58E-02	3.31E-03	6.34E-02
GO:0005788	endoplasmic reticulum lumen	47	1.59	1.19E-04	1.76	1.01E-01	8.81E-03	1.85E-01
GO:0016020	membrane	364	12.28	1.19E-04	1.19	1.01E-01	8.14E-03	1.85E-01
GO:0005622	intracellular	230	7.76	2.32E-04	1.24	1.87E-01	1.47E-02	3.60E-01
GO:0005581	collagen trimer	27	0.91	2.34E-04	2.11	1.89E-01	1.39E-02	3.63E-01
GO:0005874	microtubule	67	2.26	2.39E-04	1.55	1.93E-01	1.33E-02	3.72E-01
GO:0036038	MKS complex	8	0.27	4.12E-04	4.80	3.08E-01	2.15E-02	6.40E-01
GO:0043234	protein complex	83	2.80	4.16E-04	1.45	3.11E-01	2.05E-02	6.46E-01
GO:0036064	ciliary basal body	27	0.91	6.82E-04	1.98	4.57E-01	3.16E-02	1.06E+00
GO:0005614	interstitial matrix	8	0.27	7.86E-04	4.43	5.05E-01	3.46E-02	1.22E+00
GO:0035869	ciliary transition zone	11	0.37	7.98E-04	3.30	5.10E-01	3.34E-02	1.24E+00

Table S12- 3 GO terms enriched with genes positively correlated with *Htr2a* mRNA expression in WAT. Genes from Table S12- 1 and Table S12- 2 were used for gene ontology analysis. This data is related to Figure 12.

GO Term	Term Description	Count	%	DAVID p-value	Fold Enrichment	Bonferroni	Benjamini	FDR
GO:0005739	mitochondrion	129	15.23	1.93E-20	2.36	9.19E-18	9.19E-18	2.76E-17
GO:0005743	mitochondrial inner membrane	60	7.08	8.26E-16	3.32	3.70E-13	1.85E-13	1.11E-12
GO:0043209	myelin sheath	25	2.95	1.31E-08	4.01	6.24E-06	2.08E-06	1.88E-05
GO:0005759	mitochondrial matrix	38	4.49	2.30E-08	2.84	1.09E-05	2.73E-06	3.29E-05
GO:0005829	cytosol	193	22.79	1.11E-07	1.42	5.28E-05	1.06E-05	1.59E-04
GO:0070062	extracellular exosome	166	19.60	5.18E-07	1.44	2.47E-04	4.11E-05	7.41E-04
GO:0016020	membrane	127	14.99	4.93E-05	1.41	2.32E-02	3.35E-03	7.05E-02
GO:0005789	endoplasmic reticulum membrane	60	7.08	7.65E-05	1.70	3.57E-02	4.54E-03	1.09E-01
GO:0005777	peroxisome	15	1.77	8.59E-05	3.52	4.01E-02	4.53E-03	1.23E-01
GO:0005741	mitochondrial outer membrane	17	2.01	4.07E-04	2.78	1.76E-01	1.92E-02	5.80E-01
GO:0005747	mitochondrial respiratory chain complex I	9	1.06	7.73E-04	4.48	3.08E-01	3.29E-02	1.10E+00
GO:0045254	pyruvate dehydrogenase complex	4	0.47	1.25E-03	16.26	4.47E-01	4.82E-02	1.77E+00
GO:0000502	proteasome complex	9	1.06	2.96E-03	3.66	7.56E-01	1.03E-01	4.15E+00
GO:0008541	proteasome regulatory particle, lid subcomplex	4	0.47	3.28E-03	12.20	7.90E-01	1.06E-01	4.59E+00
GO:0005811	lipid particle	9	1.06	5.36E-03	3.33	9.23E-01	1.57E-01	7.40E+00
GO:0005778	peroxisomal membrane	8	0.94	6.22E-03	3.61	9.49E-01	1.69E-01	8.54E+00
GO:0012505	endomembrane system	12	1.42	7.06E-03	2.57	9.66E-01	1.80E-01	9.63E+00
GO:0005838	proteasome regulatory particle	4	0.47	8.81E-03	8.87	9.85E-01	2.09E-01	1.19E+01
GO:0005737	cytoplasm	243	28.69	1.16E-02	1.14	9.96E-01	2.53E-01	1.54E+01
GO:0048471	perinuclear region of cytoplasm	38	4.49	1.44E-02	1.49	9.99E-01	2.91E-01	1.87E+01

Table S12- 4 GO terms enriched with genes negatively correlated with *Htr2a* mRNA expression in WAT. Genes from Table S12- 1 and Table S12- 2 were used for gene ontology analysis. This data is related to Figure 12.

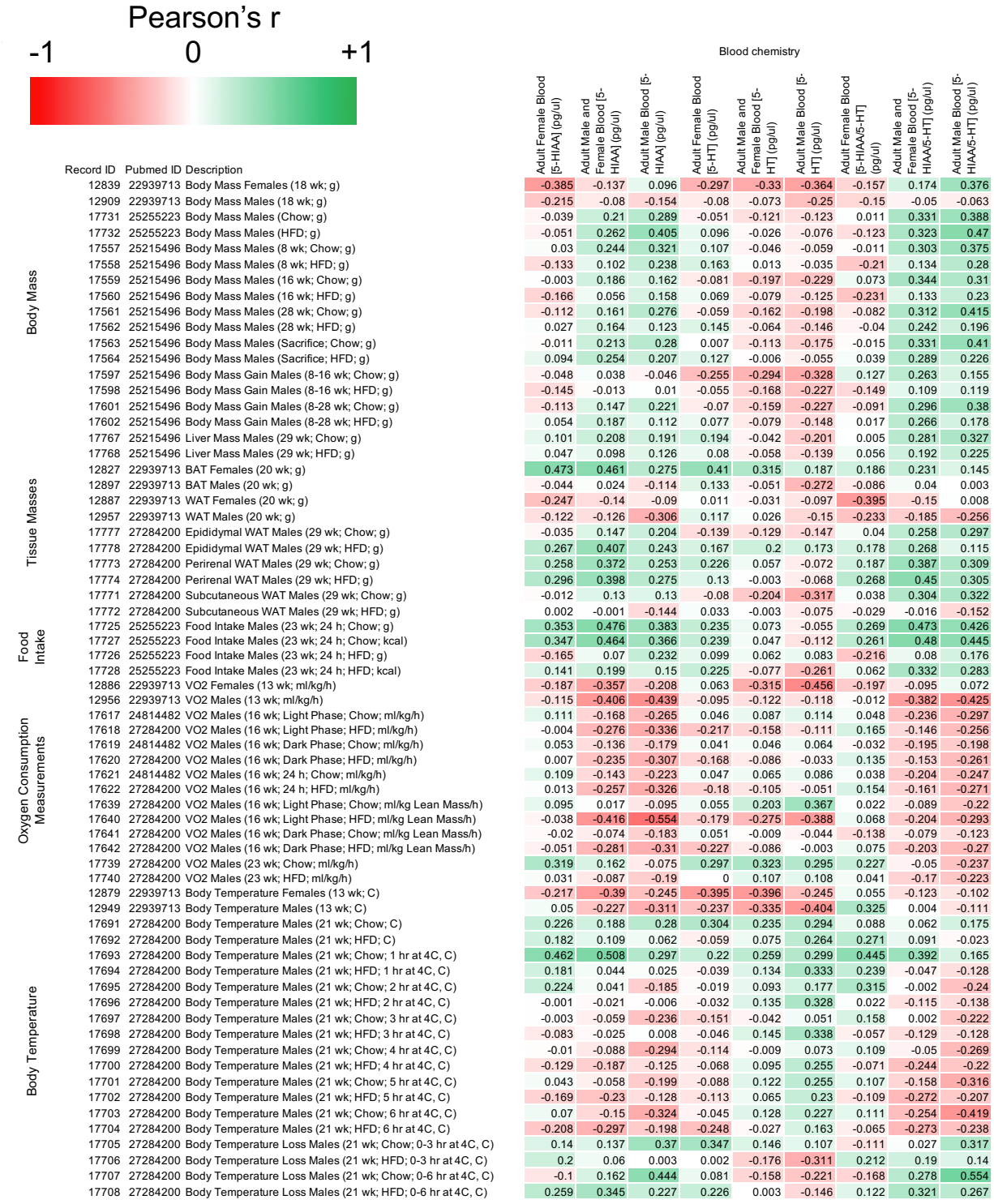

Table S12- 5 Metabolic phenotypes correlated with blood 5-HT parameters in BXD mice. This data is related to Figure 12.

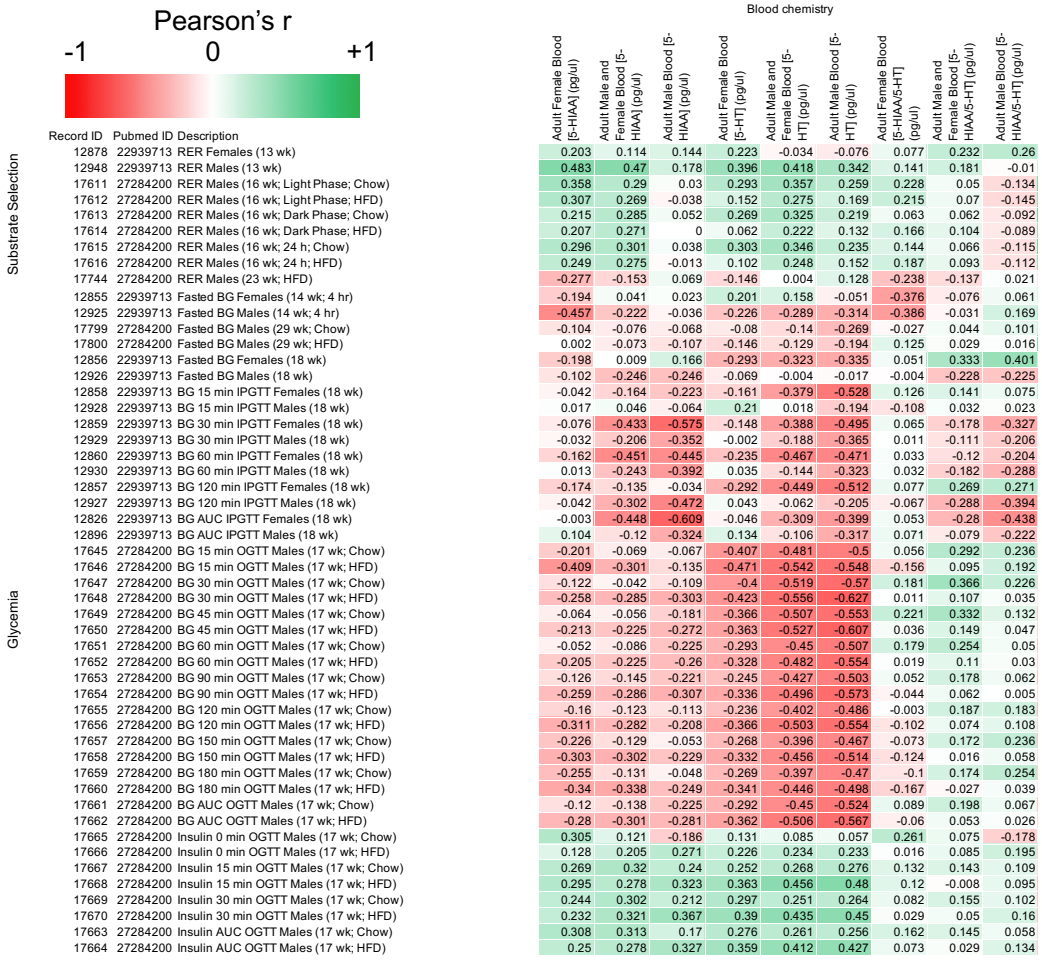

Table S12- 6 Metabolic phenotypes correlated with blood 5-HT parameters in BXD mice continued. This data is related to Figure 12.

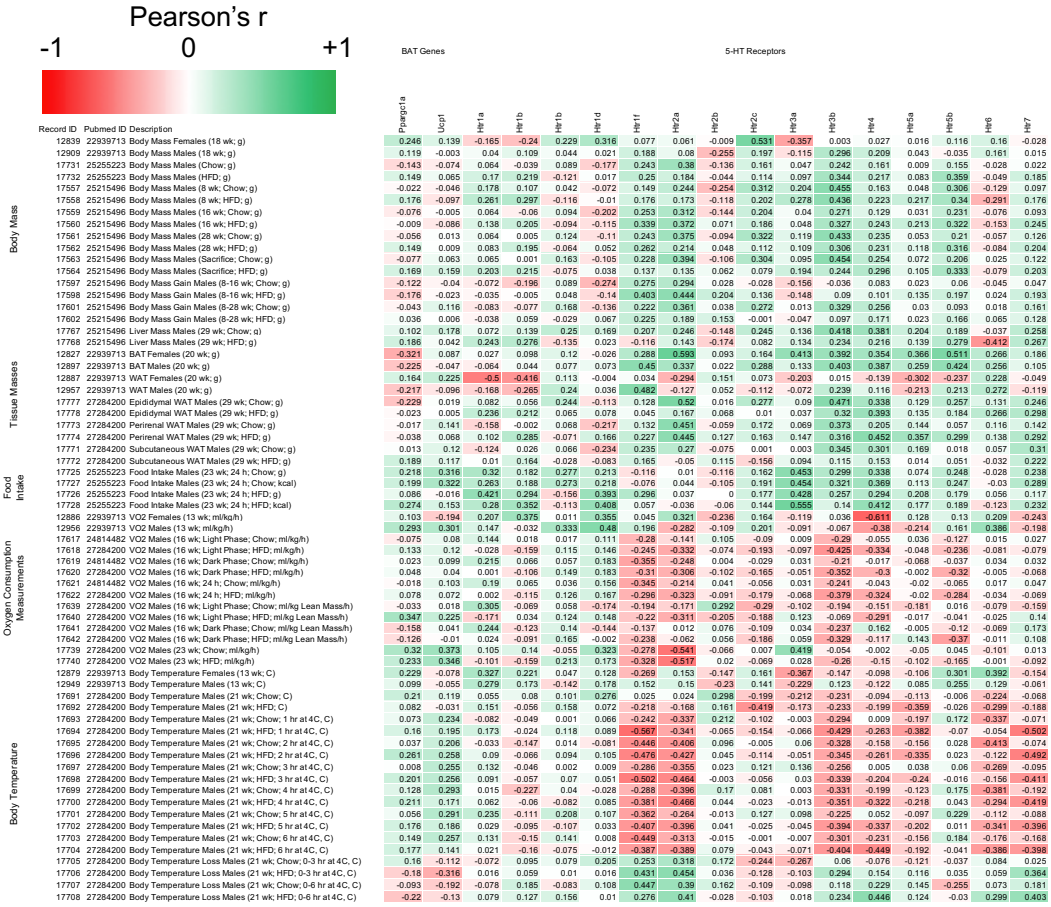

Table S12- 7 Metabolic phenotypes correlated with BAT 5-HT receptor expression in BXD mice. This data is related to Figure 12.

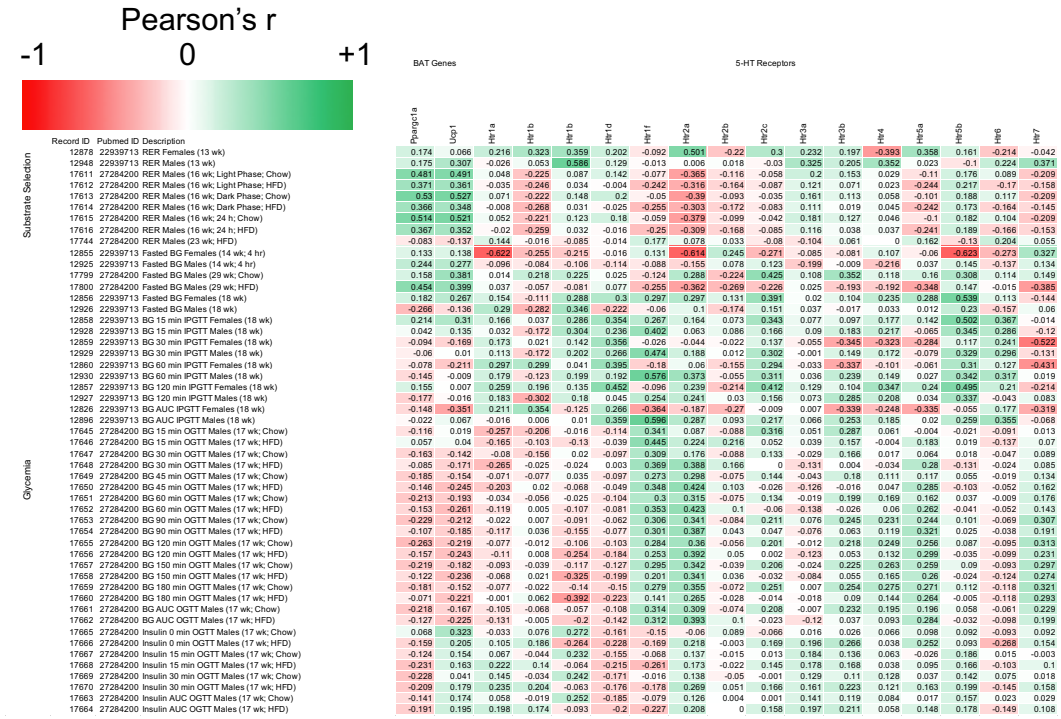

Table S12- 8 Metabolic phenotypes correlated with BAT 5-HT receptor expression in BXD mice continued. This data is related to Figure 12.

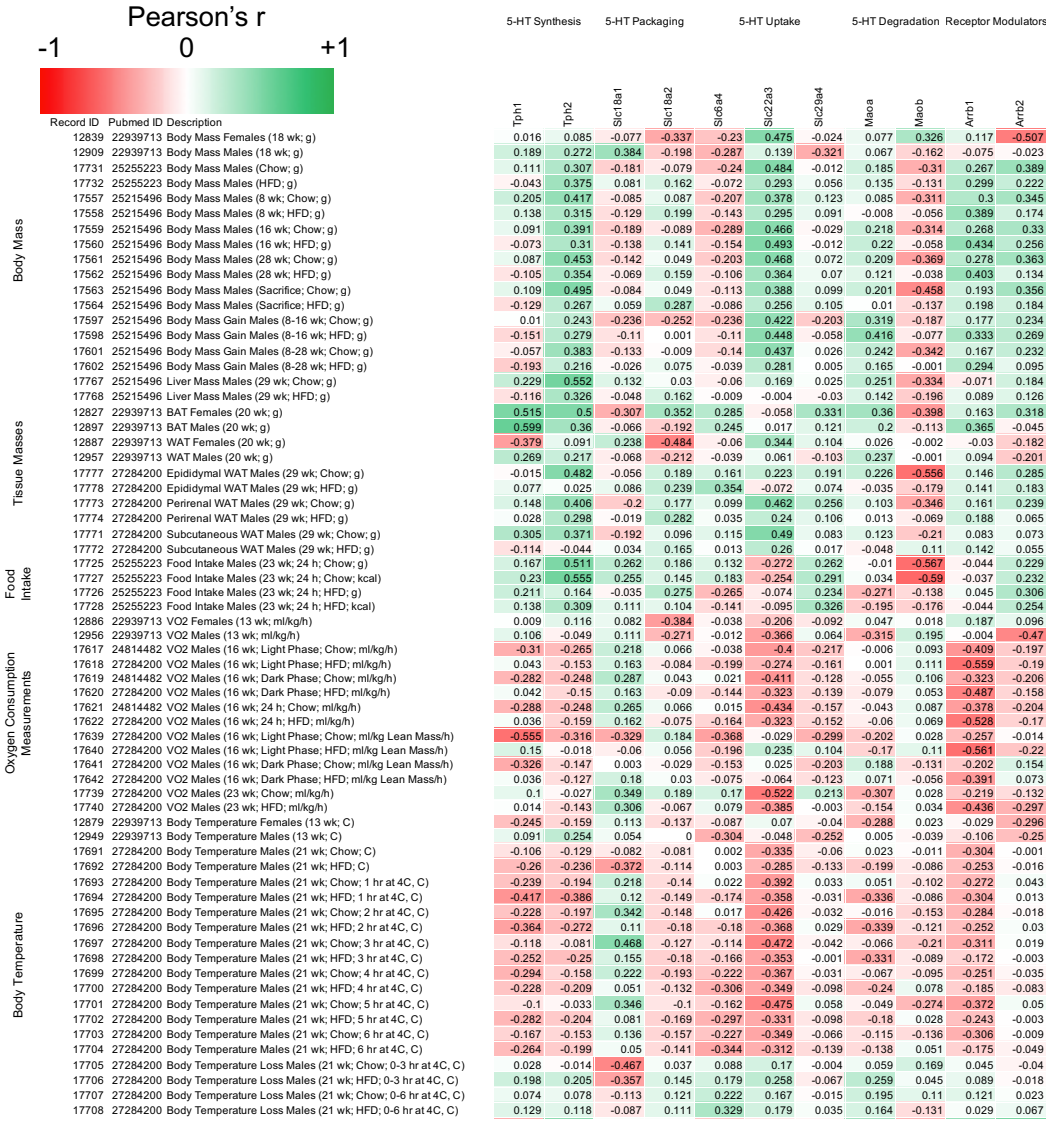

Record ID	Pubmed ID	Description	Tph1	Tph2	Slc18a1	Slc18a2	Slc6a4	Slc22a3	Slc29a4	Maoa	Maob	Arrb1	Arrb2
12839	22939713	Body Mass Females (18 wk; g)	0.016	0.085	-0.077	-0.337	-0.23	0.475	-0.024	0.077	0.326	0.117	-0.507
12909	22939713	Body Mass Males (18 wk; g)	0.189	0.272	0.384	-0.198	-0.287	0.139	-0.321	0.067	-0.162	-0.075	-0.023
17731	25255223	Body Mass Males (Chow; g)	0.111	0.307	-0.181	-0.079	-0.24	0.484	-0.012	0.185	-0.31	0.267	0.389
17732	25255223	Body Mass Males (HFD; g)	-0.043	0.375	0.081	0.162	-0.072	0.293	0.056	0.135	-0.131	0.299	0.222
17557	25215496	Body Mass Males (8 wk; Chow; g)	0.205	0.417	-0.085	0.087	-0.207	0.378	0.123	0.085	-0.311	0.3	0.345
17558	25215496	Body Mass Males (8 wk; HFD; g)	0.138	0.315	-0.129	0.199	-0.143	0.295	0.091	-0.008	-0.056	0.389	0.174
17559	25215496	Body Mass Males (16 wk; Chow; g)	0.091	0.391	-0.189	-0.089	-0.289	0.466	-0.029	0.218	-0.314	0.268	0.33
17560	25215496	Body Mass Males (16 wk; HFD; g)	-0.073	0.31	-0.138	0.141	-0.154	0.493	-0.012	0.22	-0.058	0.434	0.256
17561	25215496	Body Mass Males (28 wk; Chow; g)	0.087	0.453	-0.142	0.049	-0.203	0.468	0.072	0.209	-0.369	0.278	0.363
17562	25215496	Body Mass Males (28 wk; HFD; g)	-0.105	0.354	-0.069	0.159	-0.106	0.364	0.07	0.121	-0.038	0.403	0.134
17563	25215496	Body Mass Males (Sacrifice; Chow; g)	0.109	0.495	-0.084	0.049	-0.113	0.388	0.099	0.201	-0.458	0.193	0.356
17564	25215496	Body Mass Males (Sacrifice; HFD; g)	-0.129	0.267	0.059	0.287	-0.086	0.256	0.105	0.01	-0.137	0.198	0.184
17597	25215496	Body Mass Gain Males (8-16 wk; Chow; g)	0.01	0.243	-0.236	-0.252	-0.236	0.422	-0.203	0.319	-0.187	0.177	0.234
17598	25215496	Body Mass Gain Males (8-16 wk; HFD; g)	-0.151	0.279	-0.11	0.001	-0.11	0.448	-0.058	0.416	-0.077	0.333	0.269
17601	25215496	Body Mass Gain Males (8-28 wk; Chow; g)	-0.057	0.383	-0.133	-0.009	-0.14	0.437	0.026	0.242	-0.342	0.167	0.232
17602	25215496	Body Mass Gain Males (8-28 wk; HFD; g)	-0.193	0.216	-0.026	0.075	-0.039	0.281	0.005	0.165	-0.001	0.294	0.095
17767	25215496	Liver Mass Males (29 wk; Chow; g)	0.229	0.552	0.132	0.03	-0.06	0.169	0.025	0.251	-0.334	-0.071	0.184
17768	25215496	Liver Mass Males (29 wk; HFD; g)	-0.116	0.326	-0.048	0.162	-0.009	-0.004	-0.03	0.142	-0.196	0.089	0.126
12827	22939713	BAT Females (20 wk; g)	0.515	0.5	-0.307	0.352	0.285	-0.058	0.331	0.36	-0.398	0.163	0.318
12897	22939713	BAT Males (20 wk; g)	0.599	0.36	-0.066	-0.192	0.245	0.017	0.121	0.2	-0.113	0.365	-0.045
12887	22939713	WAT Females (20 wk; g)	-0.379	0.091	0.238	-0.484	-0.06	0.344	0.104	0.026	-0.002	-0.03	-0.182
12957	22939713	WAT Males (20 wk; g)	0.269	0.217	-0.068	-0.212	-0.039	0.061	-0.103	0.237	-0.001	0.094	-0.201
17777	27284200	Epididymal WAT Males (29 wk; Chow; g)	-0.015	0.482	-0.056	0.189	0.161	0.223	0.191	0.226	-0.556	0.146	0.285
17778	27284200	Epididymal WAT Males (29 wk; HFD; g)	0.077	0.025	0.086	0.239	0.354	-0.072	0.074	-0.035	-0.179	0.141	0.183
17773	27284200	Perirenal WAT Males (29 wk; Chow; g)	0.148	0.406	-0.2	0.177	0.099	0.462	0.256	0.103	-0.346	0.161	0.239
17774	27284200	Perirenal WAT Males (29 wk; HFD; g)	0.028	0.298	-0.019	0.282	0.035	0.24	0.106	0.013	-0.069	0.188	0.065
17771	27284200	Subcutaneous WAT Males (29 wk; Chow; g)	0.305	0.371	-0.192	0.096	0.115	0.49	0.083	0.123	-0.21	0.083	0.073
17772	27284200	Subcutaneous WAT Males (29 wk; HFD; g)	-0.114	-0.044	0.034	0.165	0.013	0.26	0.017	-0.048	0.11	0.142	0.055
17725	25255223	Food Intake Males (23 wk; 24 h; Chow; g)	0.167	0.511	0.262	0.186	0.132	-0.272	0.262	-0.01	-0.567	-0.044	0.229
17727	25255223	Food Intake Males (23 wk; 24 h; Chow; kcal)	0.23	0.555	0.255	0.145	0.183	-0.254	0.291	0.034	-0.59	-0.037	0.232
17726	25255223	Food Intake Males (23 wk; 24 h; HFD; g)	0.211	0.164	-0.035	0.275	-0.265	-0.074	0.234	-0.271	-0.138	0.045	0.306
17728	25255223	Food Intake Males (23 wk; 24 h; HFD; kcal)	0.138	0.309	0.111	0.104	-0.141	-0.095	0.326	-0.195	-0.176	-0.044	0.254
12886	22939713	VO2 Females (13 wk; ml/kg/h)	0.009	0.116	0.082	-0.384	-0.038	-0.206	-0.092	0.047	0.018	0.187	0.096
12956	22939713	VO2 Males (13 wk; ml/kg/h)	0.106	-0.049	0.111	-0.271	-0.012	-0.366	0.064	-0.315	0.195	-0.004	-0.47
17617	24814482	VO2 Males (16 wk; Light Phase; Chow; ml/kg/h)	-0.31	-0.265	0.218	0.066	-0.038	-0.4	-0.217	-0.006	0.093	-0.409	-0.197
17618	27284200	VO2 Males (16 wk; Light Phase; HFD; ml/kg/h)	0.043	-0.153	0.163	-0.084	-0.199	-0.274	-0.161	0.001	0.111	-0.559	-0.19
17619	24814482	VO2 Males (16 wk; Dark Phase; Chow; ml/kg/h)	-0.282	-0.248	0.287	0.043	0.021	-0.411	-0.128	-0.055	0.106	-0.323	-0.206
17620	27284200	VO2 Males (16 wk; Dark Phase; HFD; ml/kg/h)	0.042	-0.15	0.163	-0.09	-0.144	-0.323	-0.139	-0.079	0.053	-0.487	-0.158
17621	24814482	VO2 Males (16 wk; 24 h; Chow; ml/kg/h)	-0.288	-0.248	0.265	0.066	0.015	-0.434	-0.157	-0.043	0.087	-0.378	-0.204
17622	27284200	VO2 Males (16 wk; 24 h; HFD; ml/kg/h)	0.036	-0.159	0.162	-0.075	-0.164	-0.323	-0.152	-0.06	0.069	-0.528	-0.17
17639	27284200	VO2 Males (16 wk; Light Phase; Chow; ml/kg Lean Mass/h)	-0.555	-0.316	-0.329	0.184	-0.368	-0.029	-0.299	-0.202	0.028	-0.257	-0.014
17640	27284200	VO2 Males (16 wk; Light Phase; HFD; ml/kg Lean Mass/h)	0.15	-0.018	-0.06	0.056	-0.196	0.235	0.104	-0.17	0.11	-0.561	-0.22
17641	27284200	VO2 Males (16 wk; Dark Phase; Chow; ml/kg Lean Mass/h)	-0.326	-0.147	0.003	-0.029	-0.153	0.025	-0.203	0.188	-0.131	-0.202	0.154
17642	27284200	VO2 Males (16 wk; Dark Phase; HFD; ml/kg Lean Mass/h)	0.036	-0.127	0.18	0.03	-0.075	-0.064	-0.123	0.071	-0.056	-0.391	0.073
17739	27284200	VO2 Males (23 wk; Chow; ml/kg/h)	0.1	-0.027	0.349	0.189	0.17	-0.522	0.213	-0.307	0.028	-0.219	-0.132
17740	27284200	VO2 Males (23 wk; HFD; ml/kg/h)	0.014	-0.143	0.306	-0.067	0.079	-0.385	-0.003	-0.154	0.034	-0.436	-0.297
12879	22939713	Body Temperature Females (13 wk; C)	-0.245	-0.159	0.113	-0.137	-0.087	0.07	-0.04	-0.288	0.023	-0.029	-0.296
12949	22939713	Body Temperature Males (13 wk; C)	0.091	0.254	0.054	0	-0.304	-0.048	-0.252	0.005	-0.039	-0.106	-0.25
17691	27284200	Body Temperature Males (21 wk; Chow; C)	-0.106	-0.129	-0.082	-0.081	0.002	-0.335	-0.06	0.023	-0.011	-0.304	-0.001
17692	27284200	Body Temperature Males (21 wk; HFD; C)	-0.26	-0.236	-0.372	-0.114	0.003	-0.285	-0.133	-0.199	-0.086	-0.253	-0.016
17693	27284200	Body Temperature Males (21 wk; Chow; 1 hr at 4C, C)	-0.239	-0.194	0.218	-0.14	0.022	-0.392	0.033	0.051	-0.102	-0.272	0.043
17694	27284200	Body Temperature Males (21 wk; HFD; 1 hr at 4C, C)	-0.417	-0.386	0.12	-0.149	-0.174	-0.358	-0.031	-0.336	-0.086	-0.304	0.013
17695	27284200	Body Temperature Males (21 wk; Chow; 2 hr at 4C, C)	-0.228	-0.197	0.342	-0.148	0.017	-0.426	-0.032	-0.016	-0.153	-0.284	-0.018
17696	27284200	Body Temperature Males (21 wk; HFD; 2 hr at 4C, C)	-0.364	-0.272	0.11	-0.18	-0.18	-0.368	0.029	-0.339	-0.121	-0.252	0.03
17697	27284200	Body Temperature Males (21 wk; Chow; 3 hr at 4C, C)	-0.118	-0.081	0.468	-0.127	-0.114	-0.472	-0.042	-0.066	-0.21	-0.311	0.019
17698	27284200	Body Temperature Males (21 wk; HFD; 3 hr at 4C, C)	-0.252	-0.25	0.155	-0.18	-0.166	-0.353	-0.001	-0.331	-0.089	-0.172	-0.003
17699	27284200	Body Temperature Males (21 wk; Chow; 4 hr at 4C, C)	-0.294	-0.158	0.222	-0.193	-0.222	-0.367	-0.031	-0.067	-0.095	-0.251	-0.035
17700	27284200	Body Temperature Males (21 wk; HFD; 4 hr at 4C, C)	-0.228	-0.209	0.051	-0.132	-0.306	-0.349	-0.098	-0.24	0.078	-0.185	-0.083
17701	27284200	Body Temperature Males (21 wk; Chow; 5 hr at 4C, C)	-0.1	-0.033	0.346	-0.1	-0.162	-0.475	0.058	-0.049	-0.274	-0.372	0.05
17702	27284200	Body Temperature Males (21 wk; HFD; 5 hr at 4C, C)	-0.282	-0.204	0.081	-0.169	-0.297	-0.331	-0.098	-0.18	0.028	-0.243	-0.003
17703	27284200	Body Temperature Males (21 wk; Chow; 6 hr at 4C, C)	-0.167	-0.153	0.136	-0.157	-0.227	-0.349	-0.066	-0.115	-0.136	-0.306	-0.009
17704	27284200	Body Temperature Males (21 wk; HFD; 6 hr at 4C, C)	-0.264	-0.199	0.05	-0.141	-0.344	-0.312	-0.139	-0.138	0.051	-0.175	-0.049
17705	27284200	Body Temperature Loss Males (21 wk; Chow; 0-3 hr at 4C, C)	0.028	-0.014	-0.467	0.037	0.088	0.17	-0.004	0.059	0.169	0.045	-0.04
17706	27284200	Body Temperature Loss Males (21 wk; HFD; 0-3 hr at 4C, C)	0.198	0.205	-0.357	0.145	0.179	0.258	-0.067	0.259	0.045	0.089	-0.018
17707	27284200	Body Temperature Loss Males (21 wk; Chow; 0-6 hr at 4C, C)	0.074	0.078	-0.113	0.121	0.222	0.167	-0.015	0.195	0.11	0.121	0.023
17708	27284200	Body Temperature Loss Males (21 wk; HFD; 0-6 hr at 4C, C)	0.129	0.118	-0.087	0.111	0.329	0.179	0.035	0.164	-0.131	0.029	0.067

Table S12- 9 Metabolic phenotypes correlated with BAT 5-HT related genes in BXD mice. This data is related to Figure 12.

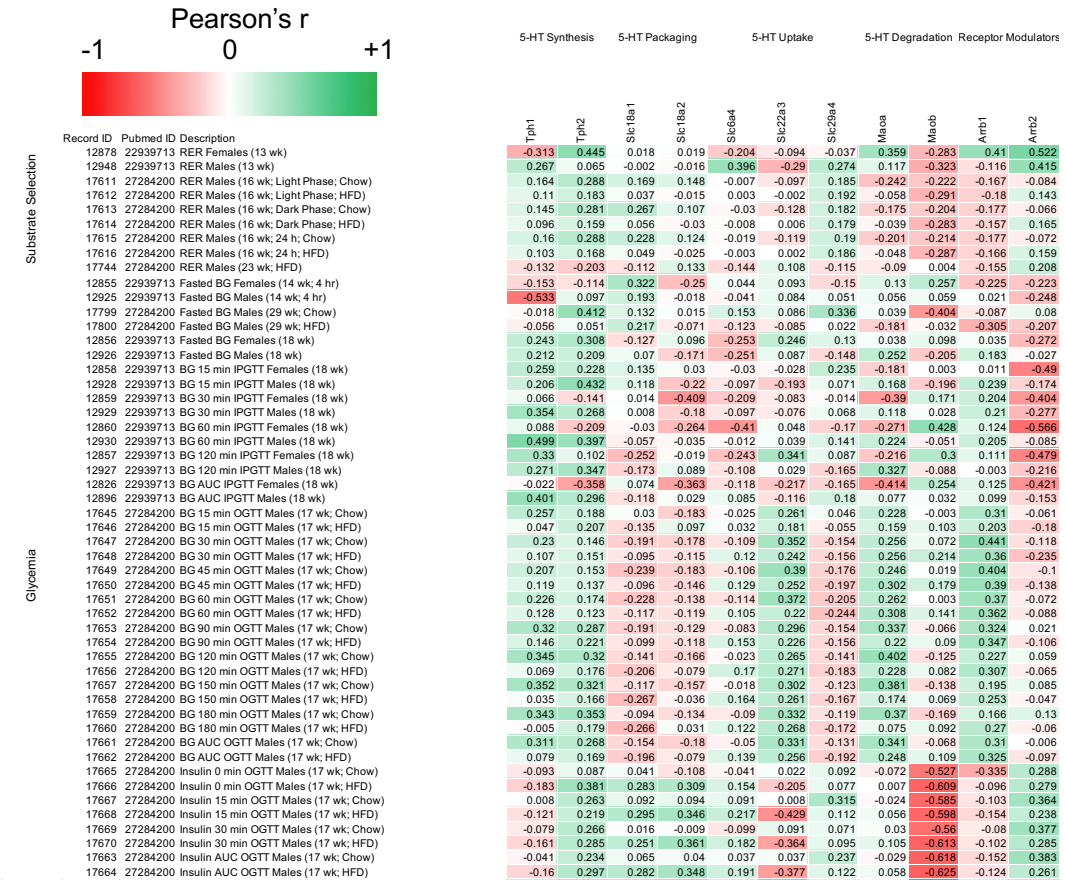

Tph1	Tph2	Slc18a1	Slc18a2	Slc6a4	Slc22a3	Slc29a4	Maoa	Maob	Arrb1	Arrb2
-0.313	0.445	0.018	0.019	-0.204	-0.094	-0.037	0.359	-0.283	0.41	0.522
0.267	0.065	-0.002	-0.016	0.396	-0.29	0.274	0.117	-0.323	-0.116	0.415
0.164	0.288	0.169	0.148	-0.007	-0.097	0.185	-0.242	-0.222	-0.167	-0.084
0.11	0.183	0.037	-0.015	0.003	-0.002	0.192	-0.058	-0.291	-0.18	0.143
0.145	0.281	0.267	0.107	-0.03	-0.128	0.182	-0.175	-0.204	-0.177	-0.066
0.096	0.159	0.056	-0.03	-0.008	0.006	0.179	-0.039	-0.283	-0.157	0.165
0.16	0.288	0.228	0.124	-0.019	-0.119	0.19	-0.201	-0.214	-0.177	-0.072
0.103	0.168	0.049	-0.025	-0.003	0.002	0.186	-0.048	-0.287	-0.166	0.159
-0.132	-0.203	-0.112	0.133	-0.144	0.108	-0.115	-0.09	0.004	-0.155	0.208
-0.153	-0.114	0.322	-0.25	0.044	0.093	-0.15	0.13	0.257	-0.225	-0.223
-0.533	0.097	0.193	-0.018	-0.041	0.084	0.051	0.056	0.059	0.021	-0.248
-0.018	0.412	0.132	0.015	0.153	0.086	0.336	0.039	-0.404	-0.087	0.08
-0.056	0.051	0.217	-0.071	-0.123	-0.085	0.022	-0.181	-0.032	-0.305	-0.207
0.243	0.308	-0.127	0.096	-0.253	0.246	0.13	0.038	0.098	0.035	-0.272
0.212	0.209	0.07	-0.171	-0.251	0.087	-0.148	0.252	-0.205	0.183	-0.027
0.259	0.228	0.135	0.03	-0.03	-0.028	0.235	-0.181	0.003	0.011	-0.49
0.206	0.432	0.118	-0.22	-0.097	-0.193	0.071	0.168	-0.196	0.239	-0.174
0.066	-0.141	0.014	-0.409	-0.209	-0.083	-0.014	-0.39	0.171	0.204	-0.404
0.354	0.268	0.008	-0.18	-0.097	-0.076	0.068	0.118	0.028	0.21	-0.277
0.088	-0.209	-0.03	-0.264	-0.41	0.048	-0.17	-0.271	0.428	0.124	-0.566
0.499	0.397	-0.057	-0.035	-0.012	0.039	0.141	0.224	-0.051	0.205	-0.085
0.33	0.102	-0.252	-0.019	-0.243	0.341	0.087	-0.216	0.3	0.111	-0.479
0.271	0.347	-0.173	0.089	-0.108	0.029	-0.165	0.327	-0.088	-0.003	-0.216
-0.022	-0.358	0.074	-0.363	-0.118	-0.217	-0.165	-0.414	0.254	0.125	-0.421
0.401	0.296	-0.118	0.029	0.085	-0.116	0.18	0.077	0.032	0.099	-0.153
0.257	0.188	0.03	-0.183	-0.025	0.261	0.046	0.228	-0.003	0.31	-0.061
0.047	0.207	-0.135	0.097	0.032	0.181	-0.055	0.159	0.103	0.203	-0.18
0.23	0.146	-0.191	-0.178	-0.109	0.352	-0.154	0.256	0.072	0.441	-0.118
0.107	0.151	-0.095	-0.115	0.12	0.242	-0.156	0.256	0.214	0.36	-0.235
0.207	0.153	-0.239	-0.183	-0.106	0.39	-0.176	0.246	0.019	0.404	-0.1
0.119	0.137	-0.096	-0.146	0.129	0.252	-0.197	0.302	0.179	0.39	-0.138
0.226	0.174	-0.228	-0.138	-0.114	0.372	-0.205	0.262	0.003	0.37	-0.072
0.128	0.123	-0.117	-0.119	0.105	0.22	-0.244	0.308	0.141	0.362	-0.088
0.32	0.287	-0.191	-0.129	-0.083	0.296	-0.154	0.337	-0.066	0.324	0.021
0.146	0.221	-0.099	-0.118	0.153	0.226	-0.156	0.22	0.09	0.347	-0.106
0.345	0.32	-0.141	-0.166	-0.023	0.265	-0.141	0.402	-0.125	0.227	0.059
0.069	0.176	-0.206	-0.079	0.17	0.271	-0.183	0.228	0.082	0.307	-0.065
0.352	0.321	-0.117	-0.157	-0.018	0.302	-0.123	0.381	-0.138	0.195	0.085
0.035	0.166	-0.267	-0.036	0.164	0.261	-0.167	0.174	0.069	0.253	-0.047
0.343	0.353	-0.094	-0.134	-0.09	0.332	-0.119	0.37	-0.169	0.166	0.13
-0.005	0.179	-0.266	0.031	0.122	0.268	-0.172	0.075	0.092	0.27	-0.06
0.311	0.268	-0.154	-0.18	-0.05	0.331	-0.131	0.341	-0.068	0.31	-0.006
0.079	0.169	-0.196	-0.079	0.139	0.256	-0.192	0.248	0.109	0.325	-0.097
-0.093	0.087	0.041	-0.108	-0.041	0.022	0.092	-0.072	-0.527	-0.335	0.288
-0.183	0.381	0.283	0.309	0.154	-0.205	0.077	0.007	-0.609	-0.096	0.279
0.008	0.263	0.092	0.094	0.091	0.008	0.315	-0.024	-0.585	-0.103	0.364
-0.121	0.219	0.295	0.346	0.217	-0.429	0.112	0.056	-0.598	-0.154	0.238
-0.079	0.266	0.016	-0.009	-0.099	0.091	0.071	0.03	-0.56	-0.08	0.377
-0.161	0.285	0.251	0.361	0.182	-0.364	0.095	0.105	-0.613	-0.102	0.285
-0.041	0.234	0.065	0.04	0.037	0.037	0.237	-0.029	-0.618	-0.152	0.383
-0.16	0.297	0.282	0.348	0.191	-0.377	0.122	0.058	-0.625	-0.124	0.261

Table S12- 10 Metabolic phenotypes correlated with BAT 5-HT related genes in BXD mice continued. This data is related to Figure 12.

21.9 Supporting Data for Figure 13

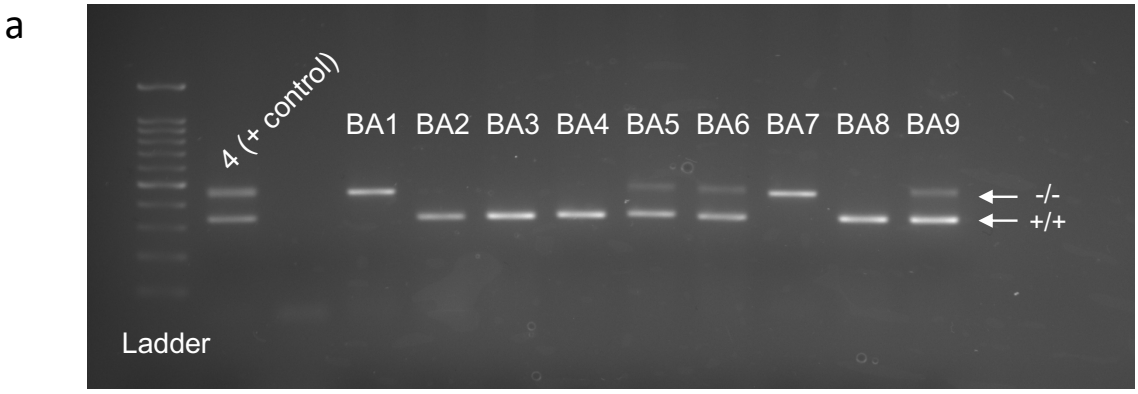

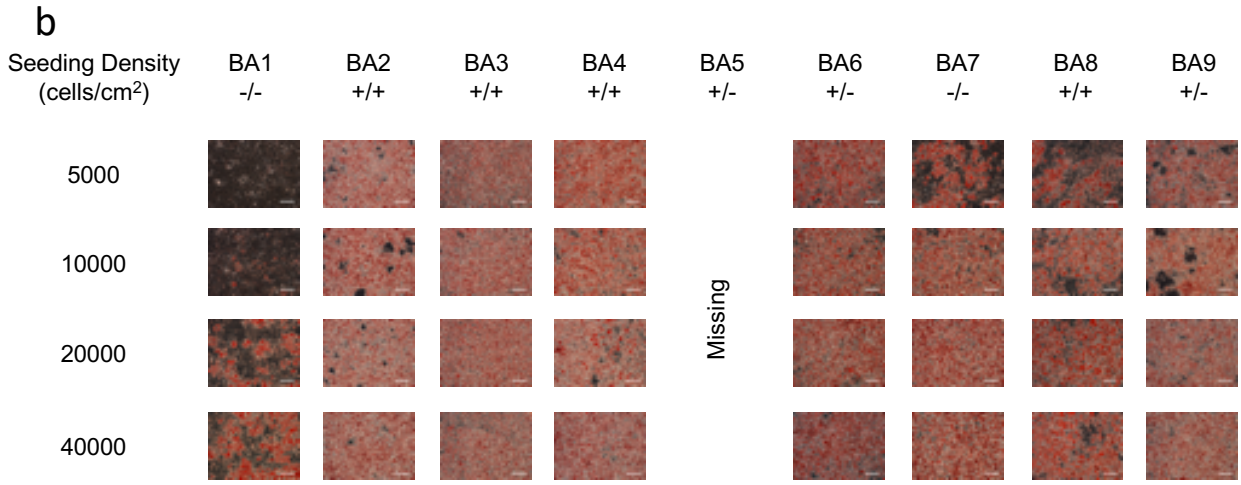

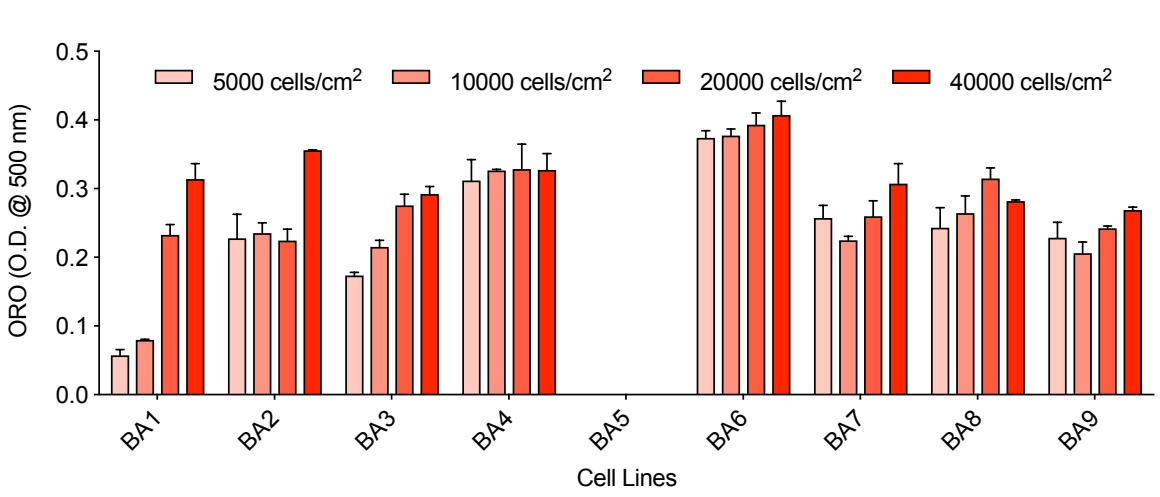

Figure S13- 1 Validation of *Htr2a*$^{-/-}$ BA progenitor cell line generation and subsequent differentiation. a, Genotyping of mice used for cell line generation. b, Representative images of immortalized and differentiated BA progenitors seeded at different densities and stained for lipid accumulation with Oil Red O (ORO). c, Elution of ORO from cells differentiated as noted in b (n = 1 independent experiment performed in triplicate for each cell line, bars represent average response and error bars are within experiment S.E.M.). Data is related to Figure 13.

a

Genotype	N [Tech. replicates]	Mean EC_{50} (nM)	Log EC_{50} (M)	Percent Max. 5-HT Effect (i.e. Span)	R^2
Htr2a$^{+/+}$	3 [3]	177.73 ± 47.47	-6.78 ± 0.11	123.07 ± 11.21	0.86 ± 0.07
Htr2a$^{-/-}$	3 [3]	193498.29 ± 193100.99	-6.17 ± 1.71	-24.9 ± 38.49	0.14 ± 0.08

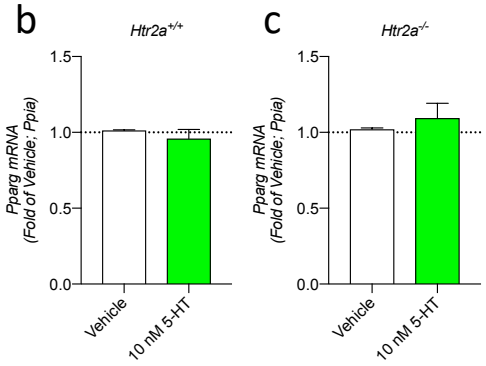

Figure S13- 2 Additional data in *Htr2a*$^{-/-}$ BAs. a, Calculated pharmacological properties of 5-HT Ca^{2+} response in *Htr2a*$^{+/+}$ and *Htr2a*$^{-/-}$ BAs. b-c, qPCR measurements of *Pparg* mRNA levels in *Htr2a*$^{+/+}$ (a) and *Htr2a*$^{-/-}$ (c) BAs treated with vehicle or 10 nM 5-HT for 4 hours (n = 3 independent experiments performed in 2-3 replicates – error bars represents S.E.M. between experiments). Data is related to Figure 13.

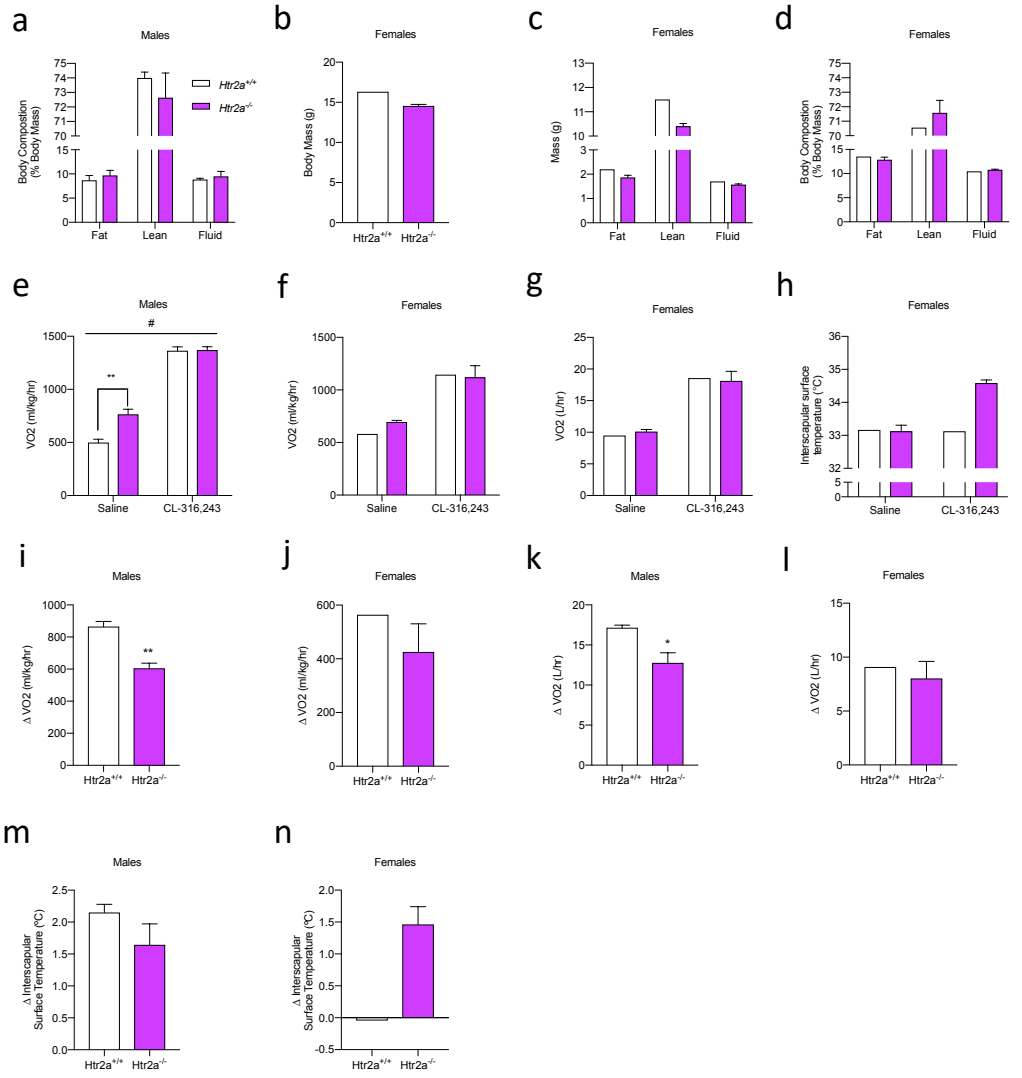

Figure S13- 3 Additional body composition and thermography data from *Htr2a*$^{+/+}$ and *Htr2a*$^{-/-}$ mice. a, Tissue masses as a percentage of body mass in male *Htr2a*$^{+/+}$ and *Htr2a*$^{-/-}$ mice (n = 3-4 mice). b-d, Body mass (b) and tissue masses (c-d) from female *Htr2a*$^{+/+}$ and *Htr2a*$^{-/-}$ mice (n = 1-3 mice). e-f, Oxygen consumption rates relative to total body mass in male (e; n = 3-4 mice) and female (f; n = 1-3 mice) *Htr2a*$^{+/+}$ and *Htr2a*$^{-/-}$ mice in response to CL-316,243. g-h, Absolute oxygen consumption rates (g) and interscapular surface temperature (h) in female *Htr2a*$^{+/+}$ and *Htr2a*$^{-/-}$ mice (n = 1-3 mice) treated with CL-316,243. i-l, Difference in relative (i and j) and absolute (k and l) oxygen consumption rates between saline and CL-316,243 treated male (i and k; n = 3-4 mice) and female (j and l; n = 1-3 mice) *Htr2a*$^{+/+}$ and *Htr2a*$^{-/-}$ mice. m-n, Difference in interscapular surface temperature between saline and CL-316,243 in male (m; n = 3-4 mice) and female (n; n = 1-3 mice) *Htr2a*$^{+/+}$ and *Htr2a*$^{-/-}$ mice. Data is related to Figure 13.

21.10 Supporting Data for Figure 14

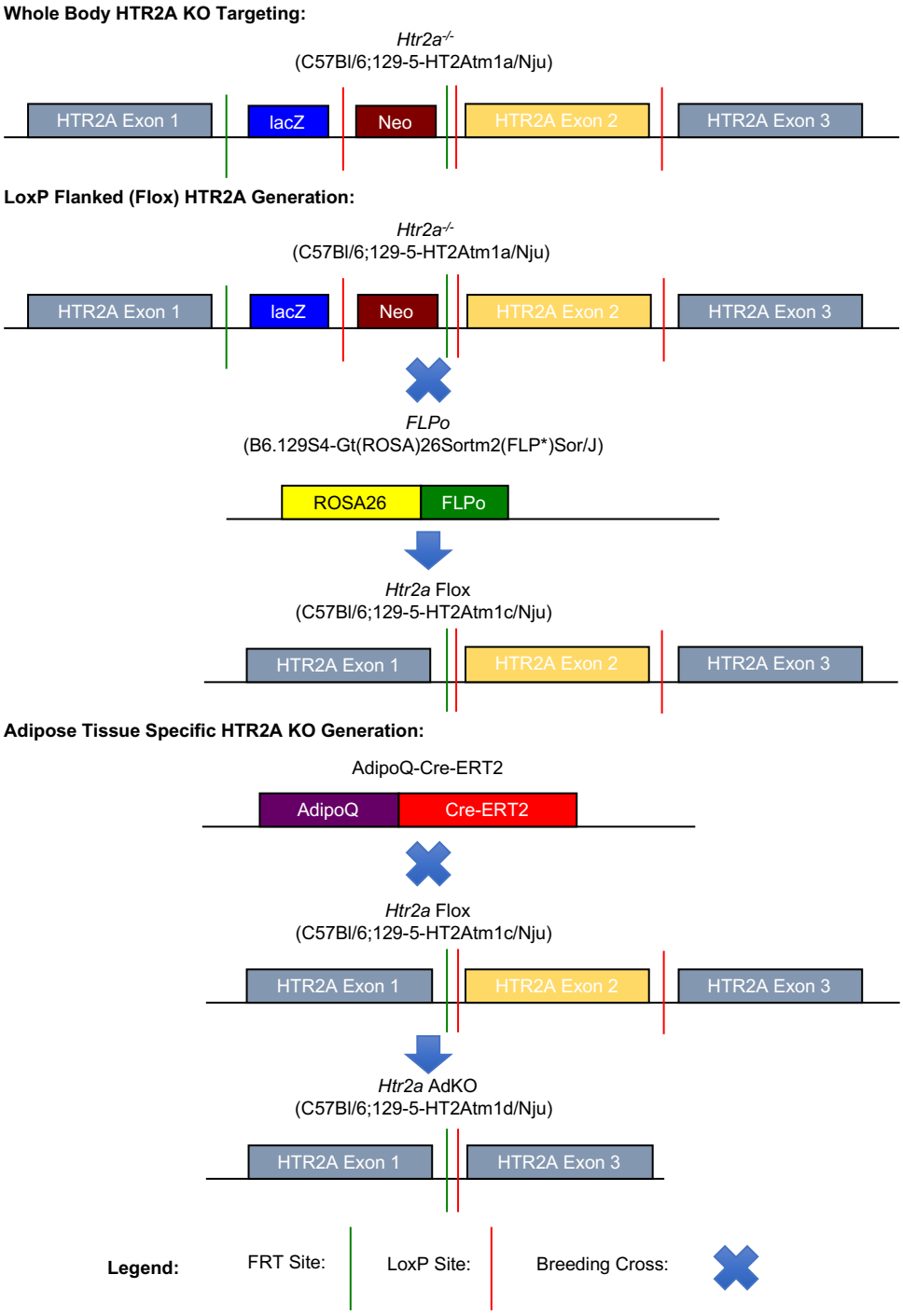

Figure S14- 1 Breeding schematic for generation of *Htr2a* AdKO mice. Breeding schema is related to Figure 14.

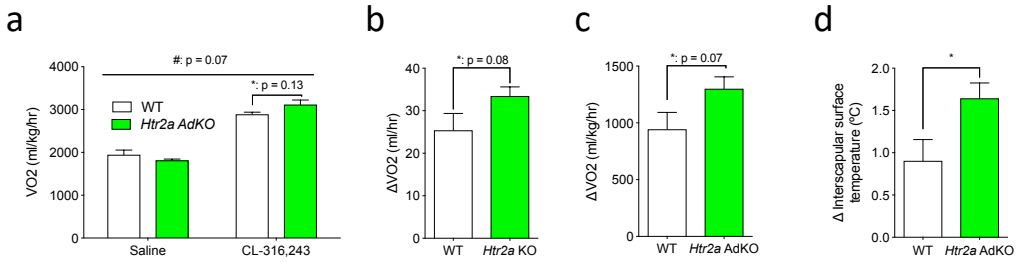

Figure S14- 2 Additional thermography data for *Htr2a* AdKO mice. a, Relative-oxygen consumption response to CL-316,243 in WT and *Htr2a* AdKO mice (n = 6-8 mice). b-c, Change in absolute (b) and relative (c) oxygen consumption levels in response to CL-316,243 (n = 6-8 mice). d, Change in interscapular surface temperature in response to CL-316,243 (n = 6-8 mice). Data is related to Figure 14.

21.11 Supporting Data for Figure 15

Compound	*Dose*	*Connectivity Score*	*Mechanism of Action*
Pazopanib	10 μM	0.562	Tyrosine kinase inhibitor
Andostenol	10 μM	0.5543	Inverse agonist of nuclear receptor subfamily 1, group I, member 3
BX-912	10 μM	0.5538	PDK1 inhibitor
RS-17053	10 μM	0.543	a1 Adrenergic receptor antagonist
U-0126	10 μM	0.5421	MEK 1/2 inhibitor
Ruxolitinib	10 μM	0.522	JAK 1/2 inihibitor
PP-2	10 μM	0.5071	Src inhibitor
IKK-16	10 μM	0.5043	Inhibitor of IkB kinase
Irbesartan	10 μM	0.5011	Angiotensin II receptor antagonist
SYK-inhibitor	10 μM	0.4975	Syk Inhibitor
Altanserin	10 μM	0.4873	Htr2a receptor antagonist
Lysergol	10 μM	0.4856	Naturally occuring weak Htr2a agonist
Midostaurin	10 μM	0.4845	Inhibitor of calcium or diacylglycerol-dependent isoforms of protein kinase C
BAS-02859604	10 μM	0.4837	
NVP-TAE684	10 μM	0.4809	ALK inhibitor
Pimozide	10 μM	0.485	Htr7, D2, D3 and D4 antagonist
Lavendustin-c	10 μM	0.4749	Inhibitor of EGFR, src and CAMK2a
SNS-314	10 μM	0.4674	Inhibits Aurora Kinase A/B/C
Isoxicam	10 μM	0.4672	COX1 and COX2 Inhibitor
SA-425500	10 μM	0.467	
NTNCB	10 μM	0.4657	NPY Y5 antagonist with some affinity for D2
Nortriptyline	10 μM	0.4647	Inhibitor of NET and Htr2a
Oxybuprocaine	10 μM	0.4624	Inhibits sodium channel protein type 10 subunit alpha
SU-11274	10 μM	0.4623	c-Met inhibitor
Methyllidocaine	10 μM	0.4622	
Calcifediol	10 μM	0.4613	Precursor to Vitamin D
LY-303511	10 μM	0.4575	Inhibits PI3K
ST-4029010	10 μM	0.4549	
Fluvastatin	10 μM	0.4534	HMG-CoA Reductase Inhibitor

Table S15- 1 Full list of compounds predicted to elicit gene signatures similar to BAs. Compounds are related to Figure 15.

a

Antagonist	N [Tech. replicates]	Mean IC_{50} (nM)	Log IC_{50} (M)	R^2
Xylamidine	3 [3-4]	7.53 ± 5.69	-8.4 ± 0.34	0.89 ± 0.02

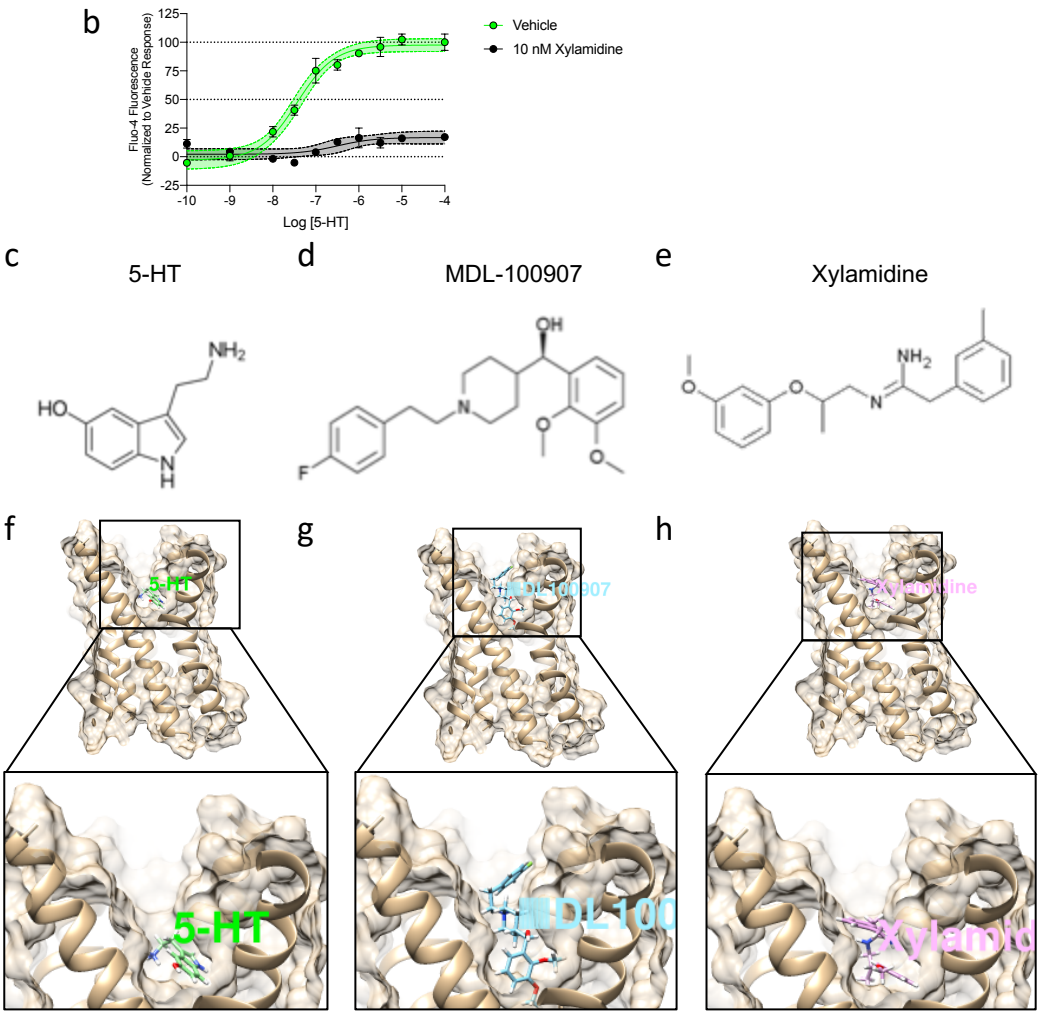

Figure S15- 1 Additional data regarding Xylamidine's pharmacological properties and 5-HT2A binding. a, Pharmacological properties of Xylamidine inhibition of 5-HT-elicited Ca^{2+} transients in BAs. b, Representative curve of Ca^{2+} transients in response to a range of 5-HT doses and in the absence or presence of 10 nM Xylamidine in BAs. c-e, Chemical structure of 5-HT2A ligands – including 5-HT (c), MDL-100907 (d) and Xylamidine (e). f-h, Visual representation of homology-based predicted 5-HT2A structure and top docking formation of 5-HT2A ligands – including 5-HT (f), MDL-100907 (g) and Xylamidine (h). i, Predicted docking values of top docking formation of different ligands for binding the 5-HT2A receptor. Data is related to Figure 15**.**

a

Drug	Activity	Pa/Pi
Xylamidine	5 Hydroxytryptamine 2A antagonist	281
MDL-100907	5 Hydroxytryptamine 2A antagonist	189.5
Ketanserin	5 Hydroxytryptamine 2A antagonist	172.5
TCB-2	5 Hydroxytryptamine 2A antagonist	51.75
Pruvanserin	5 Hydroxytryptamine 2A antagonist	36.8
DOI	5 Hydroxytryptamine 2A antagonist	31.54545455
Serotonin	5 Hydroxytryptamine 2A antagonist	2.452380952
AL-34662	5 Hydroxytryptamine 2A antagonist	1.428571429

b

Drug	Activity	Pa/Pi
DOI	5 Hydroxytryptamine 2A agonist	840
AL-34662	5 Hydroxytryptamine 2A agonist	827
Serotonin	5 Hydroxytryptamine 2A agonist	184
TCB-2	5 Hydroxytryptamine 2A agonist	55.75
NBOH-2C-CN	5 Hydroxytryptamine 2A agonist	17.9
Pruvanserin	5 Hydroxytryptamine 2A agonist	2.34482759
Metformin	5 Hydroxytryptamine 2A agonist	2.11111111

c

Drug	Activity	Pa/Pi
Xylamidine	5 Hydroxytryptamine 2 antagonist	201
MDL-100907	5 Hydroxytryptamine 2 antagonist	185.75
Ketanserin	5 Hydroxytryptamine 2 antagonist	182.25
Pruvanserin	5 Hydroxytryptamine 2 antagonist	34.63636364
DOI	5 Hydroxytryptamine 2 antagonist	26.69230769
TCB-2	5 Hydroxytryptamine 2 antagonist	20.86666667
AL-34662	5 Hydroxytryptamine 2 antagonist	3.155555556
Serotonin	5 Hydroxytryptamine 2 antagonist	2.259259259

d

Drug	Activity	Pa/Pi
DOI	5 Hydroxytryptamine 2 agonist	165
AL-34662	5 Hydroxytryptamine 2 agonist	158
TCB-2	5 Hydroxytryptamine 2 agonist	71.5
Serotonin	5 Hydroxytryptamine 2 agonist	14.875

e

Drug	Activity	Pa/Pi
Naftidrofuryl	Ulceration	958
BW501c	Hypomagnesemia	160.6
Ketanserin	QT interval prolongation	93.375
Sarpogrelate	Miotic	83.125
MDL-100907	Torsades de pointes	51.5
Pruvanserin	Choreoathetosis	38.625
Xylamidine	Palpitation	13

Table S15- 2 Way2Drug predicted pharmacological properties of various 5-HT2A ligands. a, Predicted 5-HT2A antagonist activities. b, Predicted 5-HT2A agonist activities. c, Predicted 5-HT2 antagonist activities. d, Predicted 5-HT2 agonist activities. e, Top predicted adverse effects of each 5-HT2A antagonist examined. Pa = Predicted activation activity; Pi = Predicted inhibitory activity. Data is related to Figure 15.

Drug	Xylamidine	MDL-100907	Ketanserin	Pruvanserin	Sarpogrelate	Naftidrofuryl	BW501c67	LP533401	Canagliflozin	Metformin	Rosiglitazone	Sitagliptin
BBB	0.21	1.22	0.02	1.78	0.11	0.19	0.04	0.08	0.24	0.58	0.01	0.03
Caco2	31.95	55.68	23.81	29.34	43.33	57.19	20.99	19.26	6.42	21.08	28.62	21.68
HIA	96.18	96.12	96.79	94.17	99.21	98.02	95.24	97.42	90.36	30.43	97.45	97.05
MDCK	43.37	1.22	0.13	0.28	0.05	11.02	1.39	0.04	2.28	81.89	2.08	0.23
Plasma_Protein_Binding	76.77	82.77	78.75	66.67	82.21	85.16	53.26	97.42	90.41	42.27	91.10	54.32

Table S15- 3 ADMET predictions from PreADMET for various 5-HT2A antagonists, TPH inhibitors, and anti-diabetes drugs. BBB values > 2.0, 0.1-0.2 and < 0.1 indicate high, moderate and low predicted BBB penetration. To evaluate intestinal absorption predictions of Caco2 and MDCK cell line permeability and predicted HIA absorption were completed. For Caco2 and MDCK predictions scores of > 70, 4-70 and < 4 indicate high, moderate and low permeability respectively. For HIA predictions, scores of 70-100, 20-70 and 0-20 indicate high, moderate and poor absorption, respectively. Predictions of plasma protein binding is used to predict the availability of a drug for target engagement. Scores for Plasma Protein Binding > 90% indicate strong binding and thus low availability for target engagement. To further evaluate 5-HT2A/5-HT receptor antagonists of interest (i.e. Xylamidine, Ketanserin, Saprogrelate, Naftidrofuryl and BW501c67) other compounds with known clinical efficacy were also analyzed and used for comparison. MDL-100907 and Pruvanserin are 5-HT2A antagonists with known central activity. LP-533401 is a TPH inhibitor though to have minimal BBB penetration and poor bioavailability (specifically oral to plasma transmission). Additionally, antidiabetic drugs such as Canagliflozin (a SGLT2 inhibitor), Metformin (a primarily liver active insulin sensitizer with rapid excretion and some weight reducing effects), Rosiglitazone (a PPARɣ agonist) and Sitagliptin (a DPP-4 inhibitor). No weight-loss drugs were used for comparison as no current weight-loss drugs are thought to act peripherally to increase EE. BBB = Blood brain barrier. HIA – Human intestinal absorption. MDCK = Madin-Darby Canine Kidney cells penetration. Data is related to Figure 15.

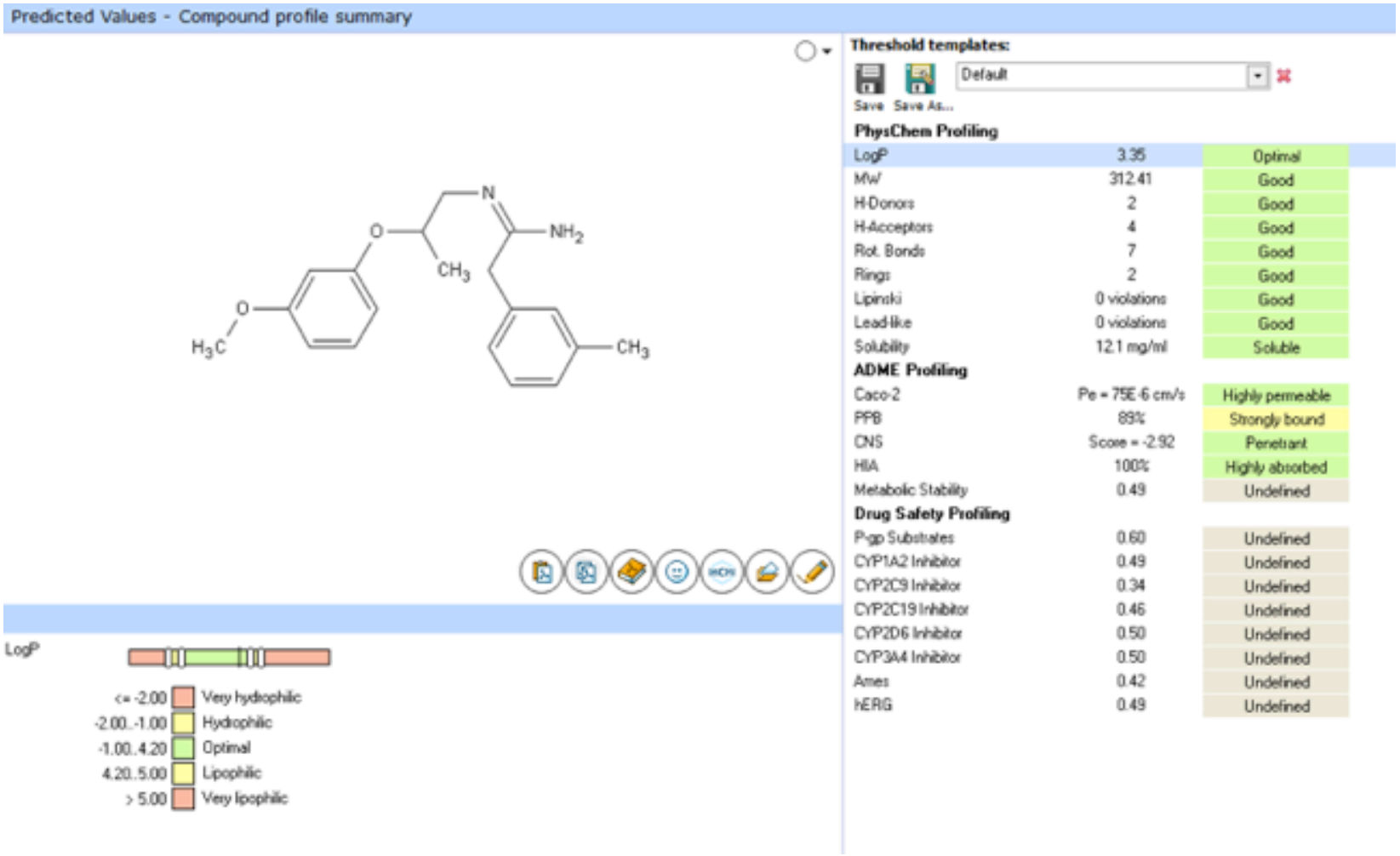

Figure S15- 2 ACD Labs Percepta predicted properties of Xylamidine. Data is related to Figure 15.

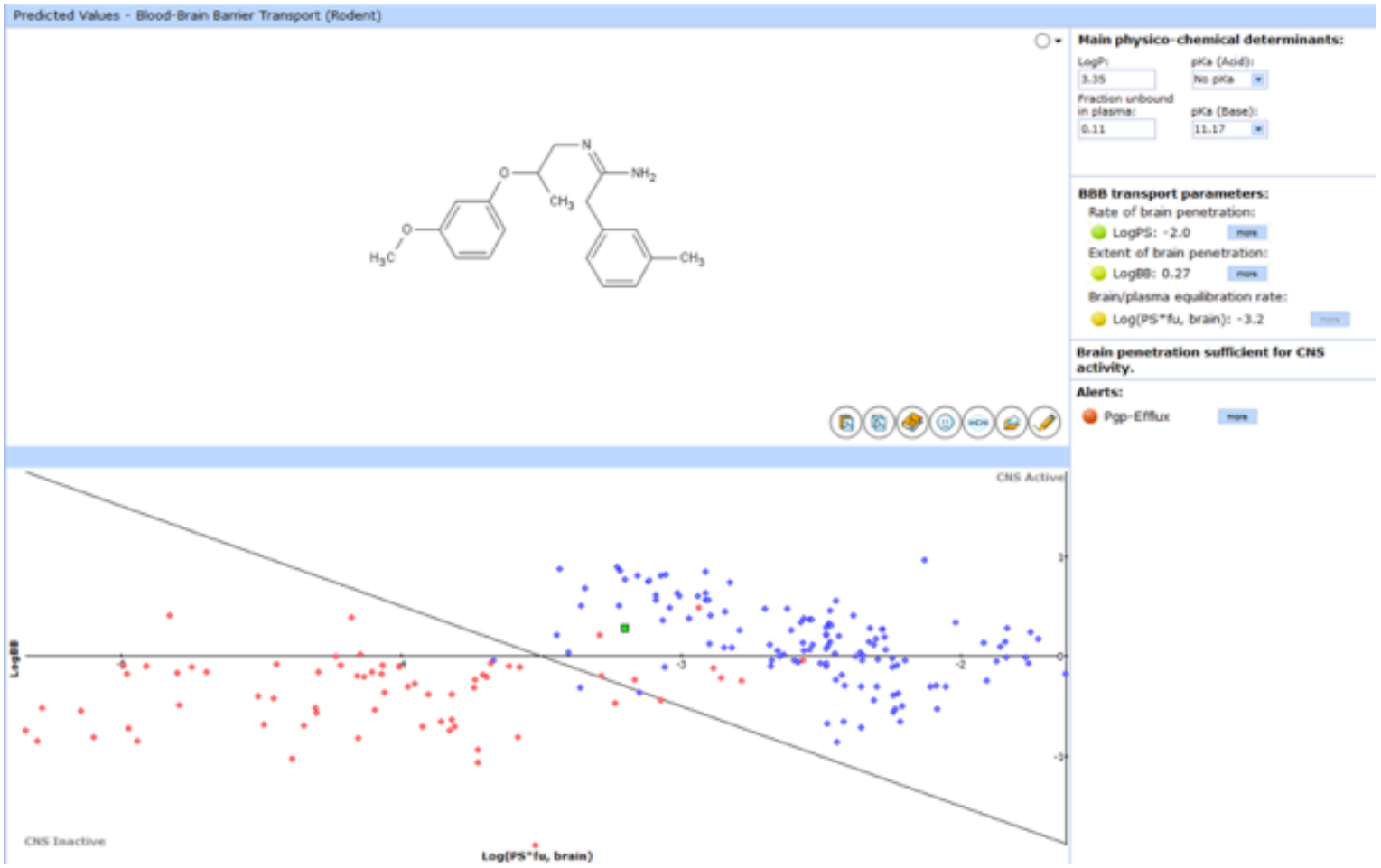

Figure S15- 3 ACD Labs Percepta predicted blood brain barrier permeability of Xylamidine. Xylamidine indicated by green box. Values in the lower left quadrant are predicted to be CNS inactive. Data is related to Figure 15.

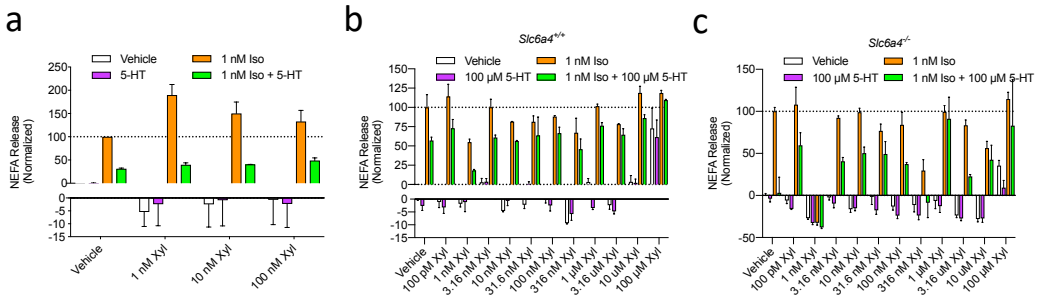

Figure S15- 4 Xylamidine does not attenuate high dose 5-HT inhibition of NEFA release. a, Normalized NEFA release from BAs treated with different doses of Xylamidine (Xyl) in combination with 100 µM 5-HT and 1 nM Iso (n = 1 independent experiment performed with 3 replicates – error bars represent within experiment error). b-c, Normalized NEFA release from *Slc6a4*$^{+/+}$ (b) and *Slc6a4*$^{-/-}$ (c) BAs treated with different doses of Xylamidine, 100 µM 5-HT and 1 nM Iso (n = 1 independent experiment performed with 3 replicates – error bars represent within experiment error). Data is related to Figure 15.

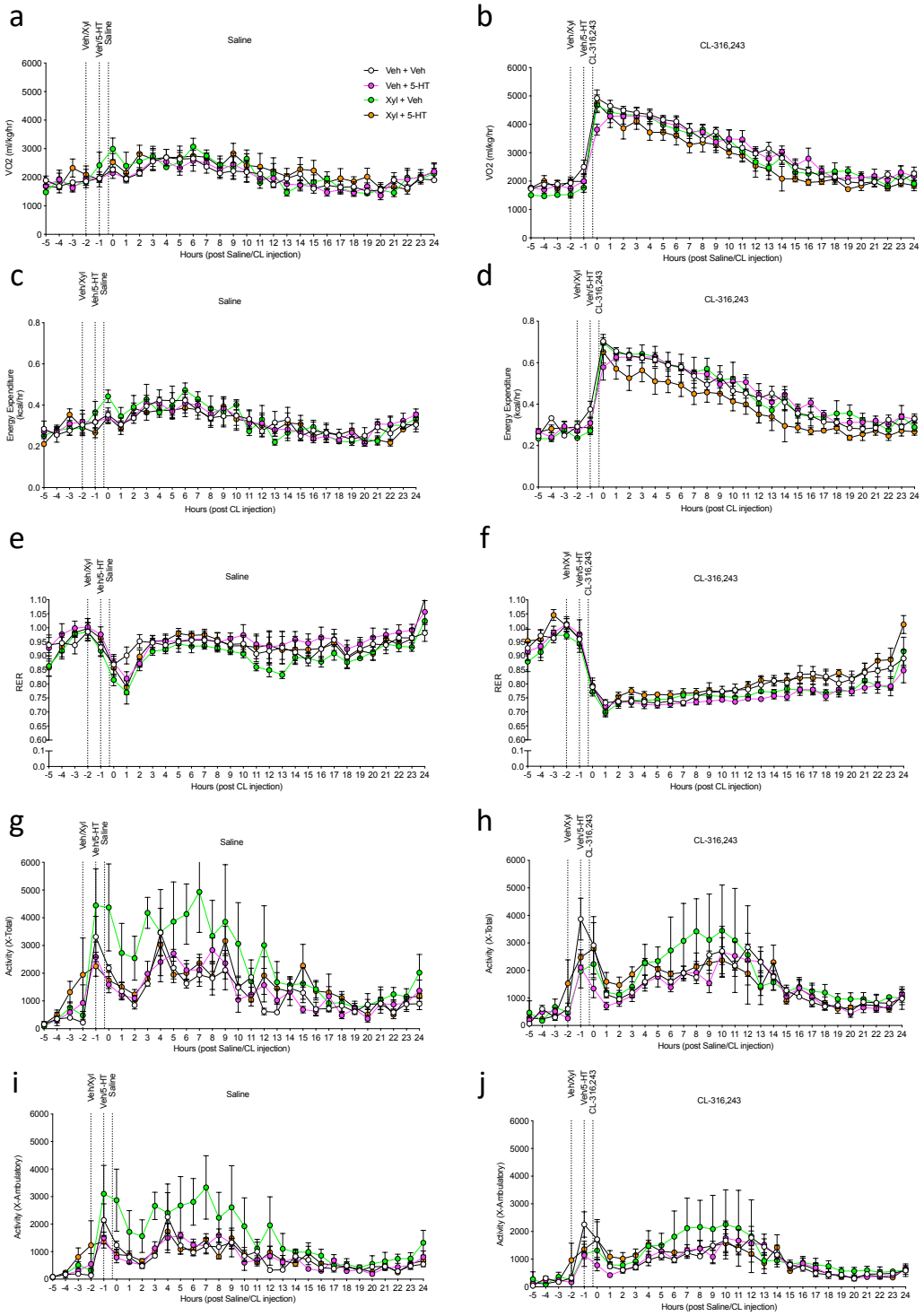

Figure S15- 5 Full time courses of respiratory gas analysis and activity levels following acute 5-HT injection in combination with Xylamidine and/or CL-316,243. a-d, Oxygen consumption rates relative to body mass (b-d) and energy expenditure rates (c-d) in saline (a and c) or CL-316,243 (b and d) treated mice. e-

f, Respiratory exchange ratio (RER) in saline (e) and CL-316,243 (f) treated mice. g-h, Total (g and h) and ambulatory (i and j) activity levels in mice treated with saline (g and i) or CL-316,243 (h and j). For all graphs n = 4 mice, points indicate mean and error bars indicate S.E.M. Data is related to Figure 15.

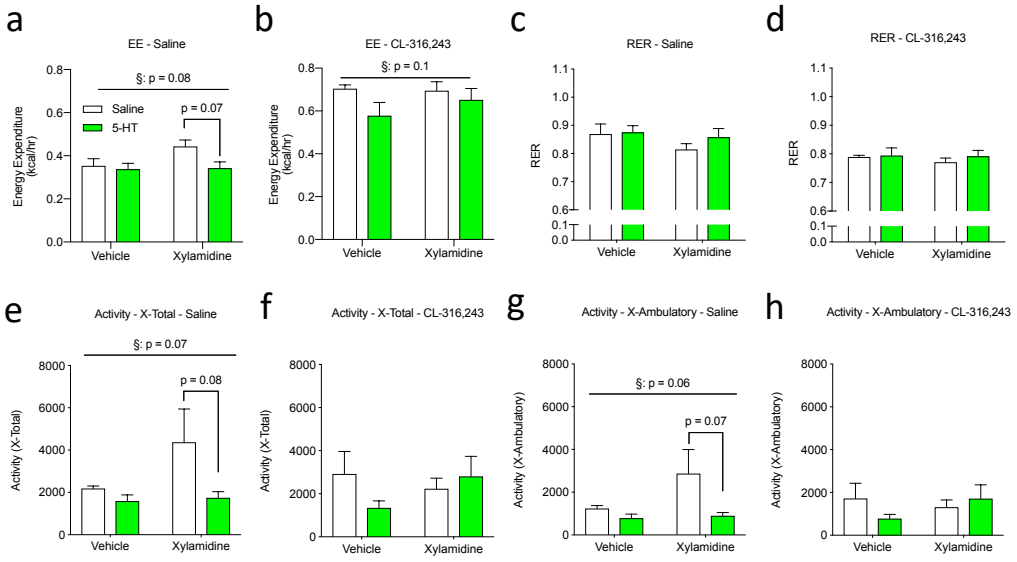

Figure S15- 6 Comparison of respiratory gas analysis and activity levels following acute 5-HT injection in combination with Xylamidine and/or CL-316,243 20 minutes post-injection. a-b, Average energy expenditure rates in saline (a) and CL-316,243 (b) treated animals. c-d, Respiratory exchange ratio (c-d), total activity (e-f), and ambulatory activity levels (g-h) in mice treated with saline (c, e and g) or CL-316,243 (d, f and h) treated animals. For all graphs n = 4 mice, points indicate mean and error bars indicate S.E.M. § = Effect of 5-HT treatment by 2-way ANOVA, individual p-values are from Bonferroni *post-hoc* tests. Data is related to Figure 15.

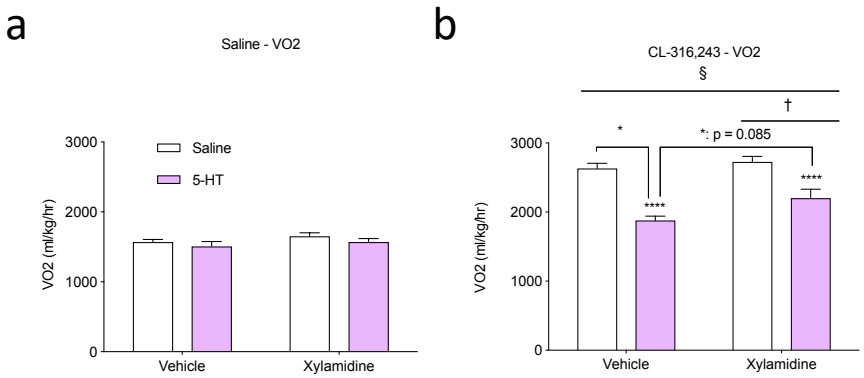

Figure S15- 7 Oxygen consumption rates of anaesthetized mice at 30ºC injected acutely with 0.1 mg/kg 5-HT IP and Xylamidine. a, Oxygen consumption rates corrected to body mass in mice injected with Xylamidine and/or 5-HT (n = 10-12 mice/group). b, Oxygen consumption rates corrected to body mass in mice treated with Xylamidine and/or 5-HT followed by CL-316,243 (n = 10-12 mice/group). § = Effect of 5-HT and † = effect of Xylamidine by 2-Way ANOVA. * indicates significance by Bonferroni *post-hoc* test. This data is related to Figure 15.

21.12 Supporting Data for Figure 16

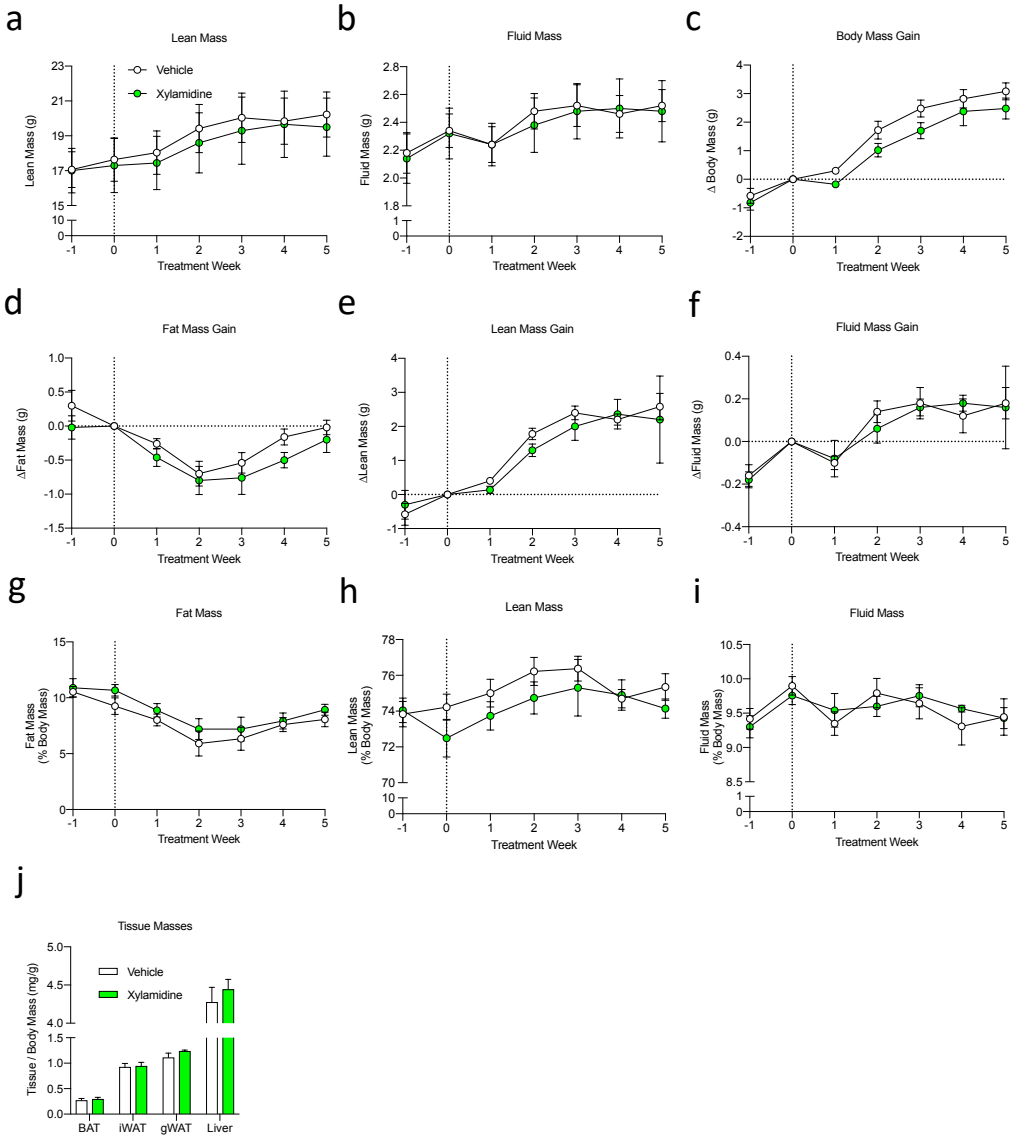

Figure S16- 1 Additional body composition measures for chow-fed mice treated with Xylamidine daily. a-b, Lean (a) and fluid (b) mass assessed over time. c-f, Gain in body mass (c), fat mass (d), lean mass (e) and fluid mass (f) over time. g-i, Fat (g), lean (h), and fluid (i) mass over time as a percentage of total body mass. j, Tissue masses at harvest as a fraction of total body mass. For all graphs, n = 5 mice/group. Additional data related to Figure 16.

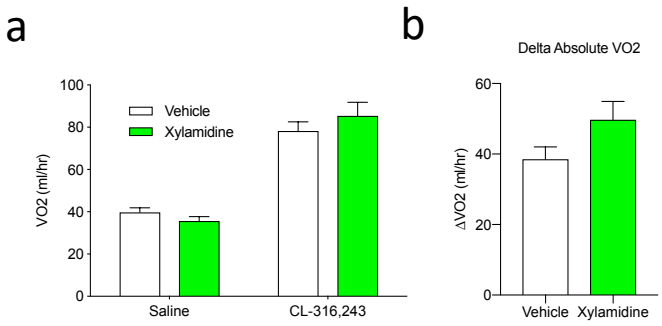

Figure S16- 2 Additional thermography data for Xylamidine treated chow-fed mice. a-b, Absolute oxygen consumption rates (a) and difference between saline and CL-316,243 induced oxygen consumption rates (b) in Vehicle and Xylamidine treated mice. For all graphs, n = 5 mice/group. Additional data related to Figure 16.

21.13 Supporting Data for Figure 17

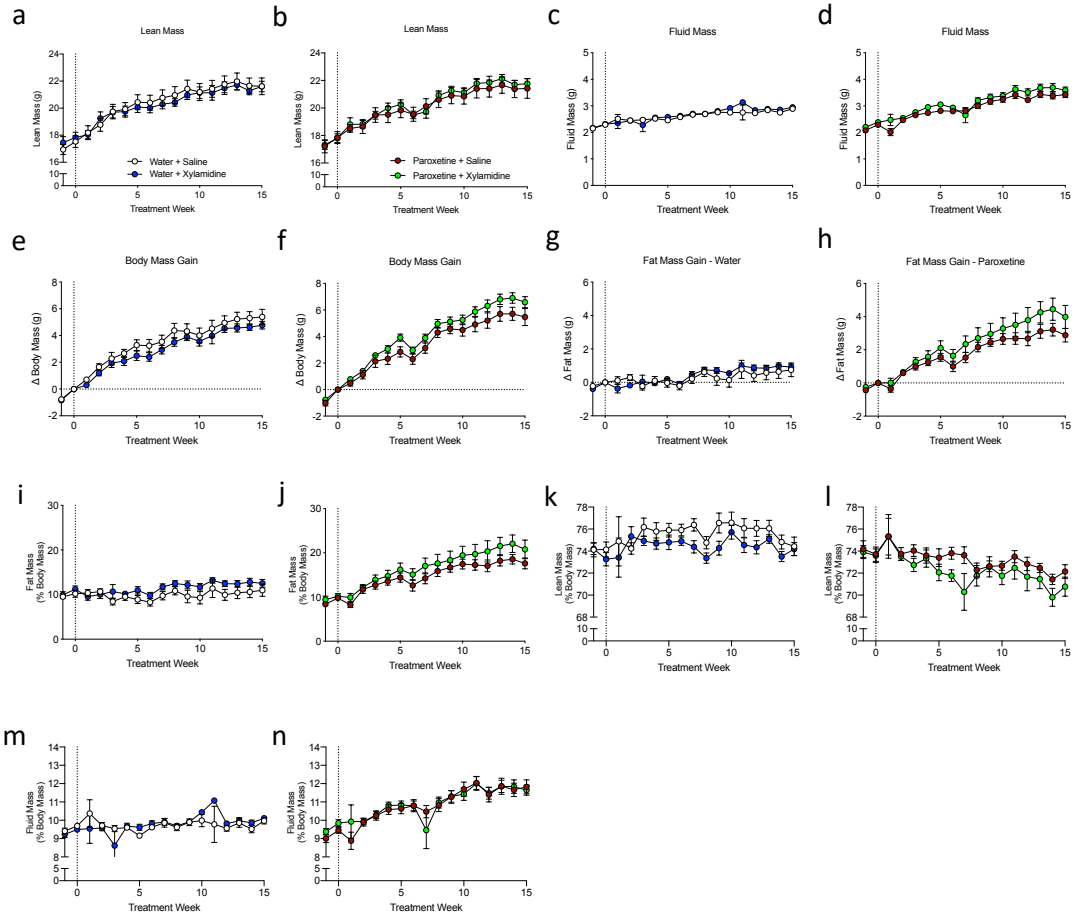

Figure S17- 1 Additional body composition measurements of mice fed Paroxetine and treated with Xylamidine. a-d, Lean (a-b) and fluid (c-d) mass of mice on water (a and c) or Paroxetine (b and d). e-h, Gain in body mass (e-f) and fat mass (g-h) from start of normal water (e and g) or Paroxetine feeding (f and h) in combination with Xylamidine-treatment. i-n, Fat (i-j), lean (k-l) and fluid (m-n) masses corrected to total body mass. For all graphs, n = 9-10 mice/group. Data related to Figure 17.

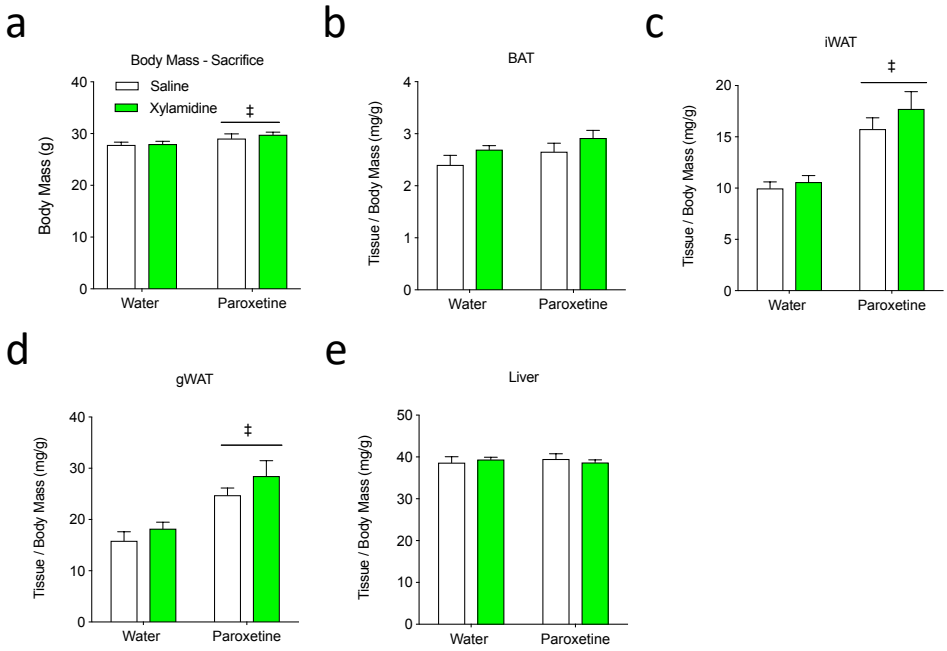

Figure S17- 2 Tissue masses at sacrifice in mice fed Paroxetine and treated daily with Xylamidine. a, Body mass at sacrifice. b-d, Brown (b), inguinal white (c) and gonadal white (d) adipose tissue masses at sacrifice corrected to total body mass. e, Liver mass at sacrifice corrected to total body mass. For all graphs, n = 9-10 mice/group and ‡ = overall effect of Paroxetine treatment by 2-way ANOVA. Additional data related to for Figure 17.

21.14 Supporting Data for Figure 18

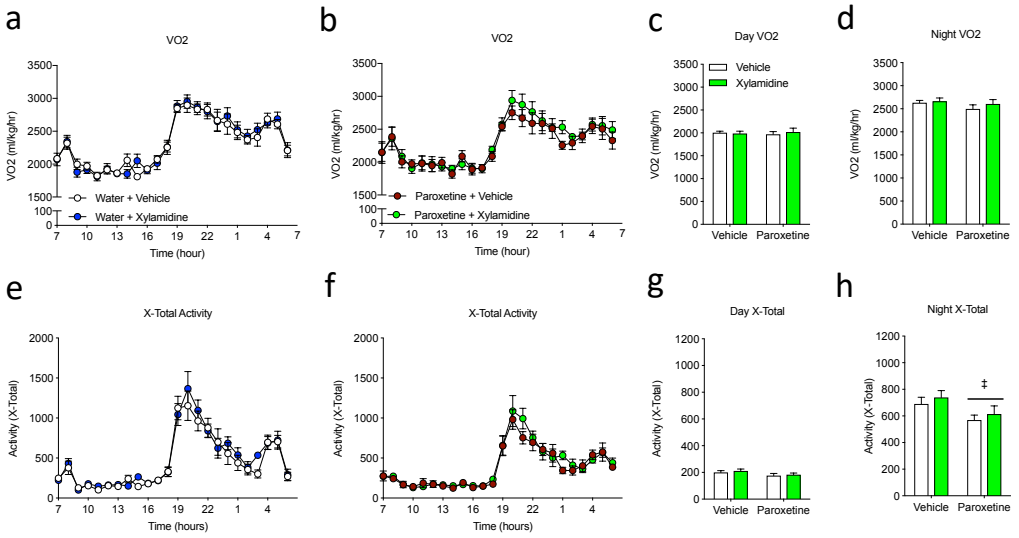

Figure S18- 1 Additional respiratory and activity level measurements from Paroxetine fed and Xylamidine treated mice. a-b, Hourly rate of oxygen consumption in water- (a) or Paroxetine- (b) fed mice treated with Xylamidine. c-d, Average oxygen consumption rates throughout the day (c) and night (d). e-f, Total activity levels in water- (e) and Paroxetine (f) fed mice treated with Xylamidine. g-h, Average total activity levels during the day (g) and night (h). For all graphs, n = 7-9 mice/group and ‡ = overall effect of Paroxetine treatment by 2-way ANOVA. Additional data for Figure 18.

21.15 Supporting Data for Figure 19

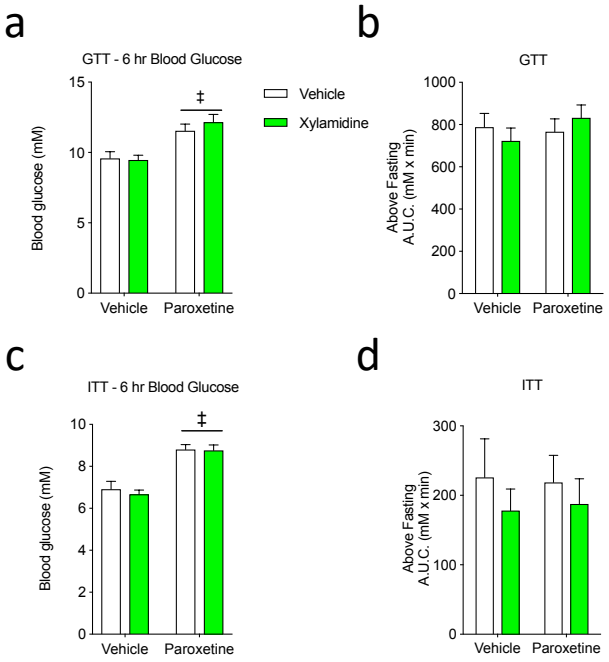

Figure S19- 1 Additional GTT and ITT data for Paroxetine-fed and Xylamidine-treated mice. a and c, 6 hour fasting blood glucose during GTT (a) and ITT (c). b and d, A.U.C. corrected for differences in fasting blood glucose during GTT (b) and ITT (d). For all graphs, n = 8-10 mice/group and ‡ = overall effect of Paroxetine treatment by 2-way ANOVA. Data related to for Figure 19.

21.16 Supporting Data for Figure 20

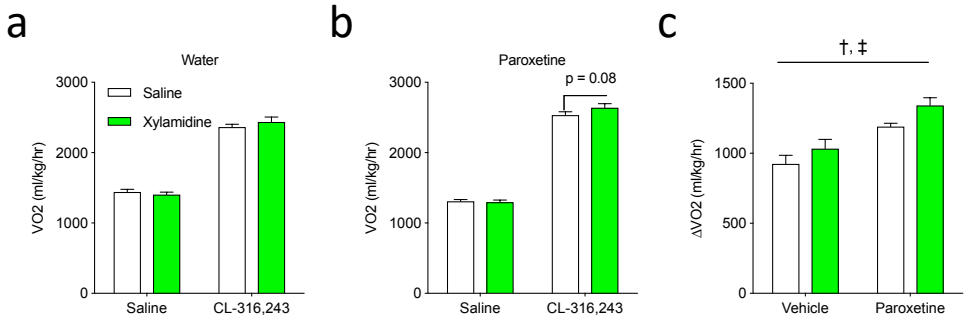

Figure S20- 1 Additional thermography data for Paroxetine-fed and Xylamidine-treated mice. a-b, Rate of oxygen consumption corrected to body mass in water- (a) and Paroxetine- (b) fed mice treated with Xylamidine in response to saline or CL-316,243 treatment. c, Change in relative oxygen consumption rates between saline and CL-316,243 treatments. For all graphs, n = 9-10 mice/group, † = overall effect of Xylamidine and ‡ = overall effect of Paroxetine treatment by 2-way ANOVA. Data related to Figure 20.